APAE-42(Vol. II)

REACTORS—POWER

DESIGN ANALYSIS OF A PREPACKAGED NUCLEAR POWER PLANT (1000 eKW). VOLUME II. REACTOR DESIGN ANALYSIS

February 1, 1959

Alco Products, Inc.
Schenectady, New York

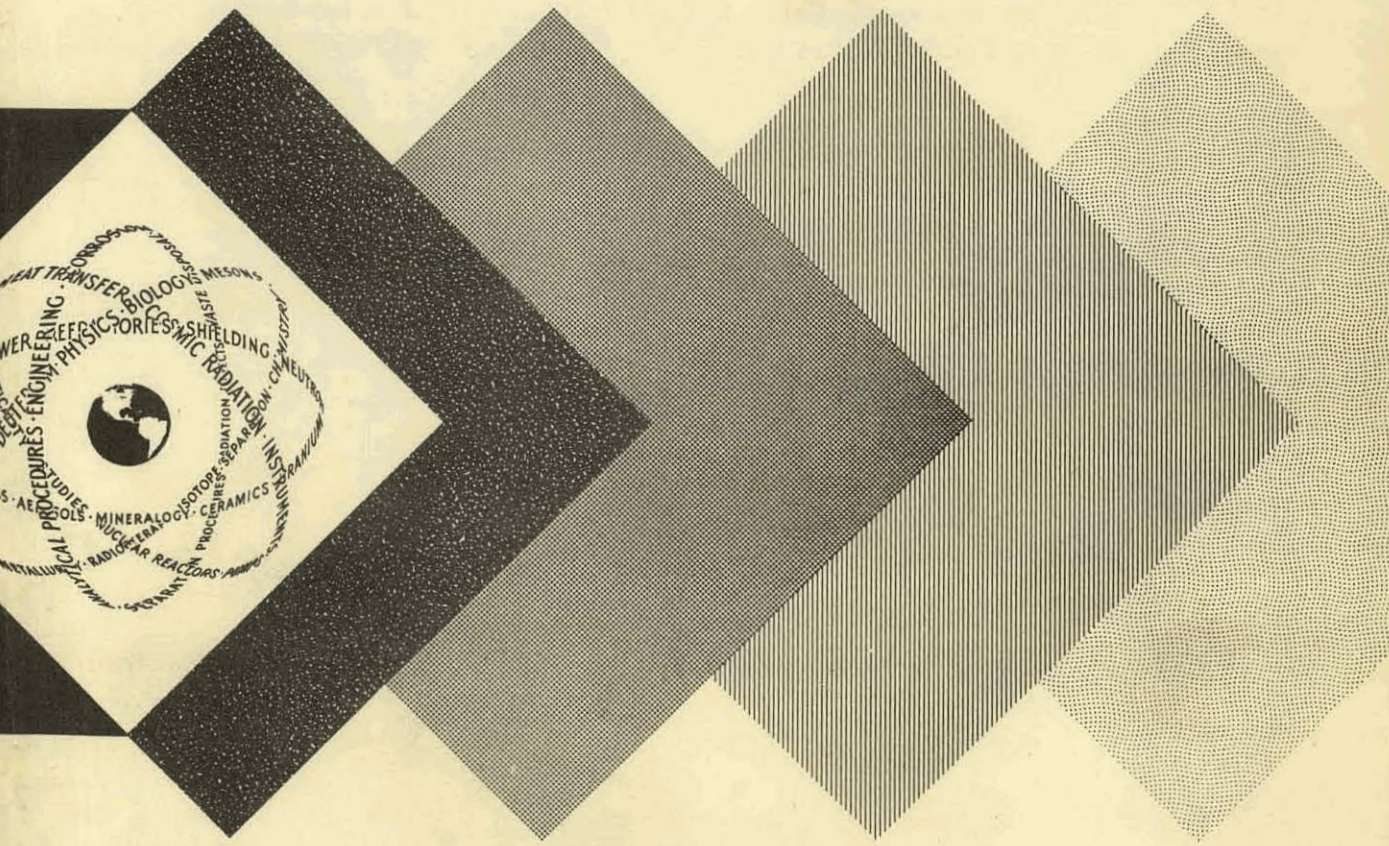

UNITED STATES ATOMIC ENERGY COMMISSION
Technical Information Service

DISCLAIMER

Consolidation of this material into compact form to permit economical, direct reproduction has resulted in multiple folios for some pages, e.g., 10–12, 27–29, etc.

LEGAL NOTICE

This report has been reproduced directly from the best available copy.

Printed in USA. This report consists of 2 volumes, total price $7.00. Available from the Office of Technical Services, Department of Commerce, Washington 25, D. C.

AEC Technical Information Service Extension
Oak Ridge, Tennessee

APAE-42

DESIGN ANALYSIS

OF A

PREPACKAGED NUCLEAR POWER PLANT

(1000 eKW)

VOLUME II

REACTOR DESIGN ANALYSIS

ISSUED FEBRUARY 1, 1959

Work performed under Contract No. DA-44-009-Eng-3638

Alco Products, Inc.
Post Office Box 414
Schenectady, N. Y.

THIS PAGE

WAS INTENTIONALLY

LEFT BLANK

Volume II

1000 eKW SKID MOUNTED
REACTOR DESIGN ANALYSIS

MASTER INDEX

CHAPTER

TABLE OF CONTENTS

TABLE OF CONTENTS (Continued)

TABLE OF CONTENTS (Continued)

TABLE OF CONTENTS (Continued)

TABLE OF CONTENTS (Continued)

TABLE OF CONTENTS (Continued)

TABLE OF CONTENTS (Continued)

TABLE OF CONTENTS (Continued)

TABLE OF CONTENTS (Continued)

TABLE OF CONTENTS (Continued)

TABLE OF CONTENTS (Continued)

LIST OF FIGURES

CHAPTER A: CORE DESIGN ANALYSIS

LIST OF FIGURES (CONTINUED)

LIST OF FIGURES (CONTINUED)

LIST OF FIGURES (CONTINUED)

LIST OF TABLES

CHAPTER A: CORE DESIGN ANALYSIS

CHAPTER B: SHIELDING DESIGN ANALYSIS

LIST OF TABLES (CONTINUED)

LIST OF TABLES (CONTINUED)

LIST OF TABLES (CONTINUED)

A. CORE DESIGN ANALYSIS

1.0 CONTRACT DESIGN REQUIREMENTS

The core design requirements are set forth in the general objective and project guide lines. The general objective for this project requires that the core be of the APPR type and be adaptable to skid mounting of the primary system. The project guide lines call for following items that affect core design:

a. System reliability with minimum down time for refueling.

b. Minimum installed capital cost at a remote site.

c. Utilization of proven technology.

d. Availability for procurement by January 1, 1959.

e. Minimum personnel requirements for operation and maintenance.

f. Minimum of one year between refueling when operating at full power.

1.1 Comparison with APPR-1 and 1a design requirements

The contract requirements for this design are not inconsistent in any way with those for the APPR-1[1] and 1-a [2] reactor cores. By relaxing design requirements the contractor is able to make improvements in core design and operating philosophy that are of benefit to the military.

2.0 COMPARISON WITH 10 Mw SKID-MOUNTED CORE DESIGN ANALYSIS

Core configuration and core operating temperatures for the 6.5 megawatt skid-mounted reactor is identical to those for the 10 megawatt reactor described in APAE 39. Hence, the core design analysis for the 6.5 megawatt reactor of this report follows quite closely that given in APAE 39.

Differences exist only where flux levels are concerned. Where appropriate, values are scaled down by a factor equal to the ratio of the power levels $\left(\frac{6.5}{10}\right)$. A more complex consideration involves the reactivity gain due to less xenon poisoning in the 6.5 MW core. However, modified two group analysis revealed that this reactivity difference for equilibrium xenon at zero MWYR amounts to only 0.4%. As core burnout increases, the difference becomes even smaller. Values of K_{eff} for the two reactors for various fractional burnups are given in Table 2-1. These values are based on a uniform burnup computation.

(1) APAE-10 Vol. 1, Phase 3 Design Analysis for the Army Package Power Reactor.

(2) APAE-17, Vol.1, Phase 3 of the report Army Package Power Reactor Field Unit #1, APPR-1a

Table 2-1

Reactivity Comparison Between 6.5 Mw and 10 Mw Cores

(Uniform burnup comparison)

Per Cent Burnout	K_{eff} 6.5 Mw Core	10 Mw Core
0	1.055744	1.051258
5	1.052396	1.048611
10	1.053523	1.050534
15	1.050607	1.048573
20	1.043938	1.042993

The differences in xenon effect on reactivity between the 6.5 Mw and 10 Mw reactors are shown to be quite small. Hence, alterations of the core design analysis of APAE 39 as mentioned above will not include reactivity values.

2.1 Core and reflector configurations

The core array selected for the skid mounted APPR is the basic 7 x 7 array of the APPR-1 with 3 elements missing in each corner which results in a core of 37 fuel elements. In this manner a reduction in effective core diameter is obtained of approximately 2 inches. The arrangement of the 32 fixed elements, 5 control rod fuel element, and 5 absorber sections in the core support structure and control rod baskets is very similar to that of the APPR-1 which has proven itself from all standpoints.

The reflector configuration originally envisioned for the skid mounted APPR (See APAE 33, Drawing AEL-335) employed a minimum water reflector followed by the reactor vessel. No thermal shielding was to be employed. It was intended to employ a solid stainless steel reactor vessel because of the high fast neutron flux on the reactor vessel. As will be discussed in Shielding Design Analysis, Section 5.0, the heating in this vessel resulted in too high thermal stresses. It then became necessary to investigate the addition of thermal shielding which resulted in an increased diameter of the stainless steel vessel. A configuration employing a large thickness of thermal shielding (practically a stainless steel reflector) resulted in a stainless steel vessel whose inside diameter was not significantly smaller than that of the carbon steel vessel. The inside diameter of the shield was such as to permit adequate water to be placed between it and the reactor vessel to reduce the fast neutron flux to a level such that the total integrated nvt over a 20-year life was not a problem. The basic characteristics of the reactor core together with a comparison with APPR-1, Core I are given in Section 2.3.

2.2 APPR-1 core I and core II characteristics.

The project guide lines are consistent with the core design developed

in "APAE-33, 2000 Kw skid mounted APPR power plant". The core design proposed in AE-33 employed 32 fixed fuel elements of APPR-1 Core I or Core II specifications and 5 control rod fuel elements of APPR-1 Core II specifications and 5 boron absorber sections of APPR-1 Core I specifications. It is felt that this core configuration, as will be proven in the design analysis, meets all the project guide lines, such as utilization of proven technology, minimum of one year core life and minimum installed cost. By employing APPR-1 fuel elements in this core the installation becomes capable of receiving fuel elements of improved technology as they are developed for the APPR family.

2.3 Dimensional and material tabulation

All core dimensions and material for the Skid Mounted Reactor are listed in Table 2-2. Data for the APPR-1 core is also listed to supply the reader with a comparison between the two cores. All experimental information is marked with an asterisk (*).

Table 2-2

Comparison of Skid Mounted Core and APPR-1

("Hot" means 512°F in Skid Core, 440°F in APPR-1 Core)

	Skid Mounted	APPR-1
Configuration	7 x 7 - 3 elements in each corner missing - 37 elements	7 x 7 - corners missing - 45 elements
Equivalent diameter - in.	20.16	22.20
Active core height - in.	22.0	22.0
No. of fixed elements	32	38
No. of control rod elements	5	7
Material content of core		
U^{235} - kg.	18.49	22.50
B^{10} - gm.	16.66	19.52
SS - kg.	172.10	208.92
H_2O (68°F) - kg.	91.54	111.08
Fixed element		
U^{235} - gm.	515.16	515.16
B^{10} - gm.	0.464	0.446
Control Rod element		
U^{235} - gm.	401.12	417.76
B^{10} - gm.	0.362	0.363
Control Rod Absorber Section		
B^{10} - gm.	56.4	56.4
Volume in core - cc		
SS UO_2, B_4C	23,907	29,095
H_2O	91,195	110,894
Total	115,102	139,989

Table 2-2 (Cont'd)

Configuration	Skid Mounted 7 x 7 - 3 elements in each corner missing - 37 elements	APPR-1 7 x 7 - corners missing - 45 elements
Fuel elements		
Fuel plate meat - rectangular flat UO_2 - SS - B_4C		
Fuel plate clad - type 304L stainless steel		
Meat thickness - in.		
Fixed element	0.020	0.020
Control Rod element	0.020	0.020
Meat width - in.		
Fixed element	2.500	2.500
Control Rod element	2.281	2.281
Active length - in.		
Fixed element	22.0	22.0
Control Rod element	21.125	22.0
Cladding - in.		
Fixed element	0.005	0.005
Control Rod element	0.005	0.005
Fuel Plates per element		
Fixed element	18	18
Control Rod element	16	16
Water gap between plates - in.		
Fixed element	0.133	0.133
Control Rod element	0.133	0.133
Fuel plate meat composition - wt.%		
UO_2	25.032	25.98
B_4C	0.134	0.14
SS	78.834	73.88

Control Rods

Type - square stainless steel basket containing absorber section and control rod fuel element (7/8" Europium flux suppressor at top of meat-1gm Eu).

Absorber section - four plates welded into a square tube.

Composition - boron enriched in B^{10} isotope dispersed in iron and clad with type 304L stainless steel.

Travel-22 in.

Weight of one rod - 55 lb.

Table 2-2 (Cont'd)

Configuration	Skid Mounted 7 x 7 - 3 elements in each corner missing - 37 elements	APPR-1 7 x 7 - corners missing - 45 elements
"Hot" means 512°F in Skid core, 440°F in APPR-1 core. * means experimental data.		
Initial reactivities - $\%\rho$		
Cold - 68°F - no xenon	14.11	15.35*
Hot - no xenon	7.65	10.37*
Hot - eq. xenon	5.15	8.15*
Initial bank positions - inches from bottom		
Cold - 68°F - no xenon	5.0	3.7*
Hot - no xenon	9.7	6.8*
Hot - eq. xenon	11.6	8.3*
Power - peak to average, hot, clean		
0 MWYR		
Radial	1.46	1.49
Axial	1.65	1.71
Average Thermal neutron flux $\left(\frac{\text{neutrons}}{\text{cm}^2 - \text{sec.}}\right)$		
0 MWYR	1.09×10^{13}	1.36×10^{13}
Expected total energy release - MWYR	10	15*
Average fuel burnup	(10 MWYR)	(15 MWYR)
	26%	32%
Maximum fuel burnup	49%	75%
Composition of core at end of life		
U-235 left - Kg.	13.7	15.3
Original B-10 left - gms.	3.0	2.3
Maximum burnup of control rod material	27%	43%
Temperature coefficient		
Cold - 68°F	-0.22×10^{-4}	-0.22×10^{-4}*
Hot -	-3.4×10^{-4}	-2.2×10^{-4}*
Pressure Coeficient	$/3.1 \times 10^{-6}$ (1750psia)	$/2.1 \times 10^{-6}$ (1200psia)
Five rod bank worth - $\%\rho$		
Cold - 68°F	19.9	19.0
Hot	19.5	19.2
Center rod worth - $\%\rho$		
Cold - 68°F	4.5	4.1
Hot	4.0	4.1

Table 2-2 (Cont'd)

Configuration	Skid Mounted 7 x 7 - 3 elements in each corner missing - 37 elements	APPR-1 7 x 7 - corners missing - 45 elements
Radial Reflector savings - S_r - cm.		
Cold - 68°F	6.117207	6.180821
Hot	8.248812	7.797679
Axial reflector savings - S_z - cm.		
Cold - 68°F	6.030801	5.109191
Hot	7.978338	6.103367
Radial buckling - B_r^2 - cm^{-2}		
Cold - 68°F	0.005747	0.004895
Hot	0.005046	0.004465
Axial buckling - B^2_z - cm^{-2}		
Cold - 68°F	0.002138	0.002259
Hot	0.001913	0.002129
Total Buckling - B_T2 - cm^{-2}		
Cold - 68°F	0.007885	0.007154
Hot	0.006959	0.006954

3.0 APPR-1 MEASURED CORE CHARACTERISTICS

Because of the fact that the skid mounted APPR employs 37 APPR-1 fuel elements the measurements made on the APPR-1 core employing 45 fuel elements are of particular significance. It is expected that the principal effect of employing 37 rather than 45 fuel elements is to reduce the reactivity of the core throughout lifetime. In addition, there will be some increase in temperature coefficient due to the reduced core size.

3.1 Bank position

The 5 rod bank position in the APPR-1 has been measured under a wide range of conditions. These are -

70°F	No Xenon
440°F	No Xenon
442°F	Equilibrium Xenon
442°F	Peak Xenon

The results of these measurements through 7 MWYR of core life are shown in Fig. 3-1 (Fig. 2A Progress Report #5, Task VII). It would be expected that the 5 rod bank position for the skid mounted reactor would be further withdrawn at room temperature because of the lower core reactivity

and higher rod worth and would be further withdrawn at operating temperature due to the same reasons together with the higher operating temperature (512° F vs 440°F).

3.2 Control rod worth

The 5 rod bank worth has been measured under a variety of conditions in the ZPE and at Ft. Belvoir. The measurements at Ft. Belvoir provide a comparison between the room temperature calibrations made in the ZPE and calibrations made at operating temperature. A summary of all the measurements is contained in Fig. 3-2. (Fig. 3D Progress Report #6) (11). It would be expected that the 5 rod bank calibration for the skid mounted APPR would not differ significantly from that in Fig. 3-2.

3.3 Stuck rod positions

With rods A&B* fully withdrawn and considered stationary, the most reactive condition with a single stuck rod is that of an excentric rod stuck in its fully withdrawn position. The case of having the centerline rod stuck in its fully withdrawn position is less reactive.

Fig. 3-3 (Fig. 5C Progress Report #5) shows the critical position of the partially withdrawn rod as a function of lifetime. From calibrations of the critical rods and their position, the reactivity in the core can be determined if the partially withdrawn rod is completely withdrawn. This result is shown in Fig. 3-4 (Fig. 5D). It would be expected that the critical position of the partially withdrawn rod in the skid mounted APPR would be further out than that of the APPR-1. It should be noted that if APPR-1 Core II boron loading as specified in APAE 32 (7) can be employed, then the skid mounted APPR could be made sub-critical with one rod stuck full out.

3.4 Temperature coefficient

The temperature coefficient has been measured in the APPR-1 during the course of core burnout. This data is shown plotted in Fig. 3-5 (Fig. 1A Progress Report #6). Two effects would be present in the skid mounted APPR that would tend to increase the temperature coefficient. These are reduced core size and higher operating temperature. The effect of core size has been investigated in ZPE II and can be used in interpreting this change.

3.5 Pressure coefficient

Pressure coefficient as measured in the APPR-1 is shown in Fig. 3-6 (Fig. 1A Progress Report #1).

3.6 Startup count rate

The startup count rate is being measured in the APPR-1 during the course of core burnout. The count rate ranges from 3 to 5 counts per second with the beryllium photoeutron block installed in the APPR-1.

*Rods A&B are close packed control rods in APPR-1 and are not present in the skid core.

3.7 Conclusions

It is apparent from the wealth of experimental data available on the APPR-1 core that the characteristics of the skid mounted core can be predicted with high precision. This fact should place the core performance on a firm basis.

4.0 SKID-MOUNTED CORE CHARACTERISTICS

The basis for determining the Skid Mounted Core Characteristics is through calculation and comparison with the APPR-1 and zero power measurements.

The analytical model used in the Skid-Mounted Core calculation is one which was used in the analysis of the Zero Power Experiments (6) and the APPR-1, (7).

4.1 Method for establishing - calculation and experiment

4.1.1 Calculational model

The basic model uses two neutron-energy group diffusion theory as defined by the equations:

$$-D_f \nabla^2 \phi_f (r,z) + \Sigma_r \phi_f (r,z) = k_{th} \Sigma_{th}^a \phi_{th} (r,z) + (1-p)\, k_f \Sigma_r \phi_f (r,z)$$

$$-D_{th} \nabla^2 \phi_{th}(r,z) + \Sigma_{th}^a \phi_{th}(r,z) = p \Sigma_r \phi_f (r,z)$$

The definitions of the symbols are given at the end of the report. Assuming separability of the radial (r) and axial (z) dimensions, the solution to these equations can be obtained from various codes for digital computers (1). The Valprod (2) and Windowshade (3) codes, written for the IBM-650 digital computer, were used to solve the multiregion diffusion equations in the radial and axial directions. The output of the codes include reactivity (K_{eff}), normalized power, and normalized thermal and fast flux distributions. In the Windowshade code, a uniform absorption cross-section simulating a bank of control rods can be specified. The code then adjusts the rod bank to the critical position.

4.1.2 Thermal constants - 68°F and 512°F

Since the Skid Mounted core contains APPR-1 type elements, the thermal group constants for the cold (68°F) core were abstracted from APAE 27 (6). Constants for the homogenized hot (512°F) core were prepared by the P-3 code (5). Neutron cross sections for each material were evaluated at a hardened energy of 0.0597 ev and the thermal cutoff was taken at 0.248 ev. The P-3 code solves the one velocity transport equation to the third spherical harmonic approximation for plate type elements. Table 4-1 shows hot and cold Skid Mounted constants compared to APPR-1 constants.

Fig. 3-1

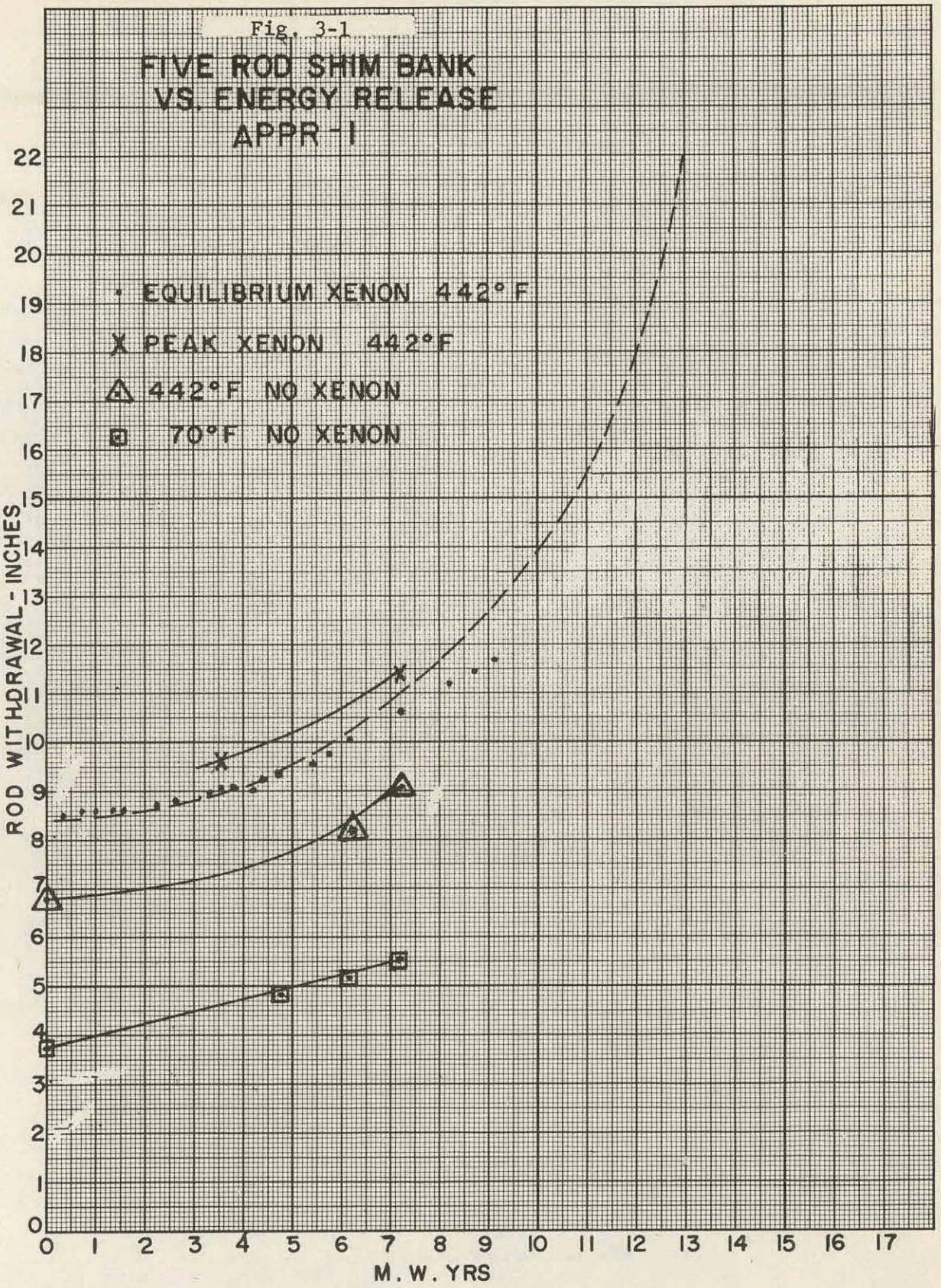
FIVE ROD SHIM BANK
VS. ENERGY RELEASE
APPR-1
• EQUILIBRIUM XENON 442°F
X PEAK XENON 442°F
△ 442°F NO XENON
⊡ 70°F NO XENON
ROD WITHDRAWAL - INCHES
0 1 2 3 4 5 6 7 8 9 10 11 12 13 14 15 16 17 18 19 20 21 22
0 1 2 3 4 5 6 7 8 9 10 11 12 13 14 15 16 17
M.W.YRS

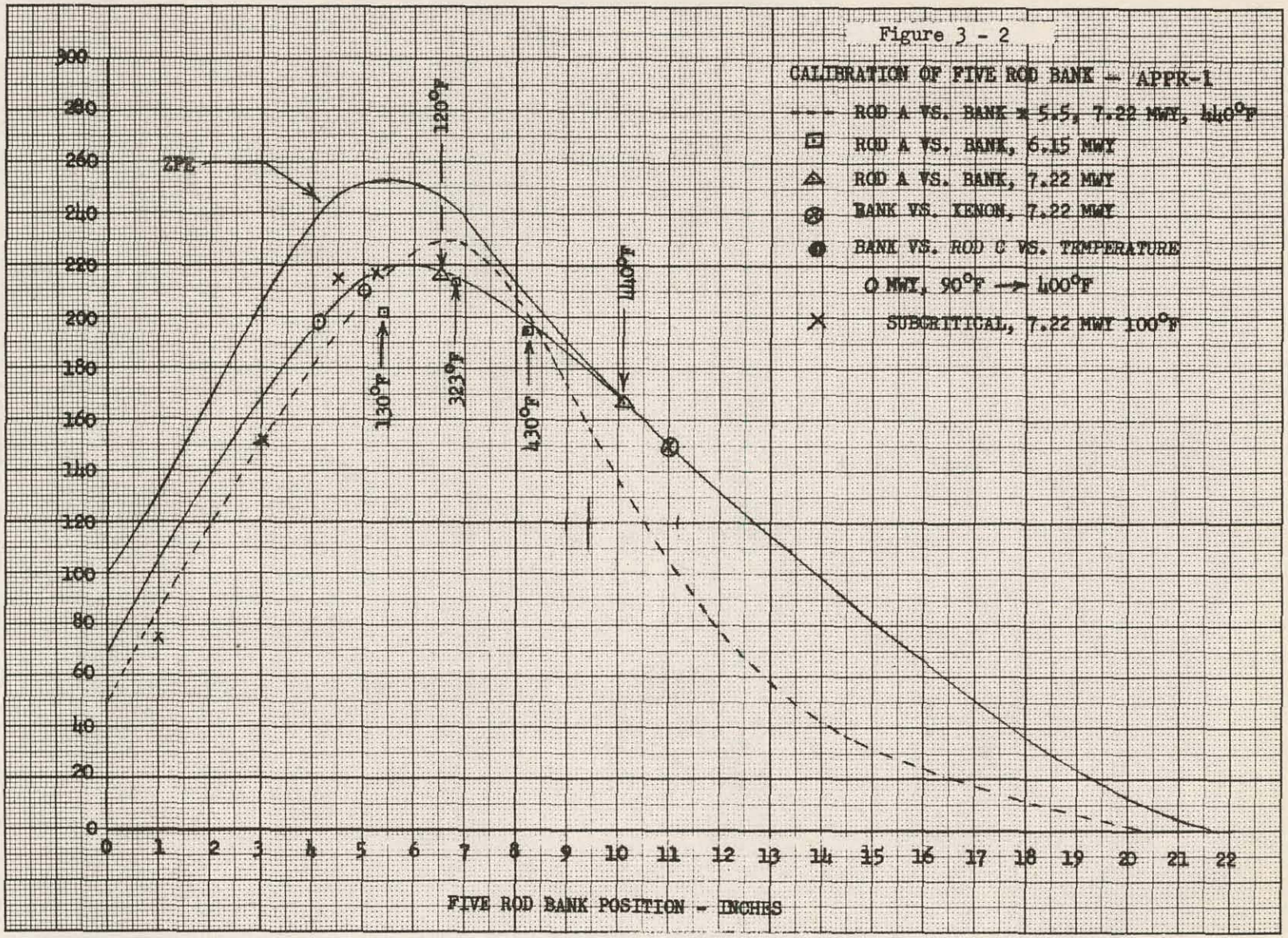
Figure 3 - 2
CALIBRATION OF FIVE ROD BANK — APPR-1
ROD A VS. BANK @ 5.5, 7.22 MWT, 440°F
ROD A VS. BANK, 6.15 MWT
ROD A VS. BANK, 7.22 MWT
BANK VS. XENON, 7.22 MWT
BANK VS. ROD C VS. TEMPERATURE
0 MWT, 90°F → 400°F
SUBCRITICAL, 7.22 MWT 100°F
ZPL
120°F
130°F
323°F
430°F
400°F
REACTIVITY - CENTS PER INCH
FIVE ROD BANK POSITION - INCHES

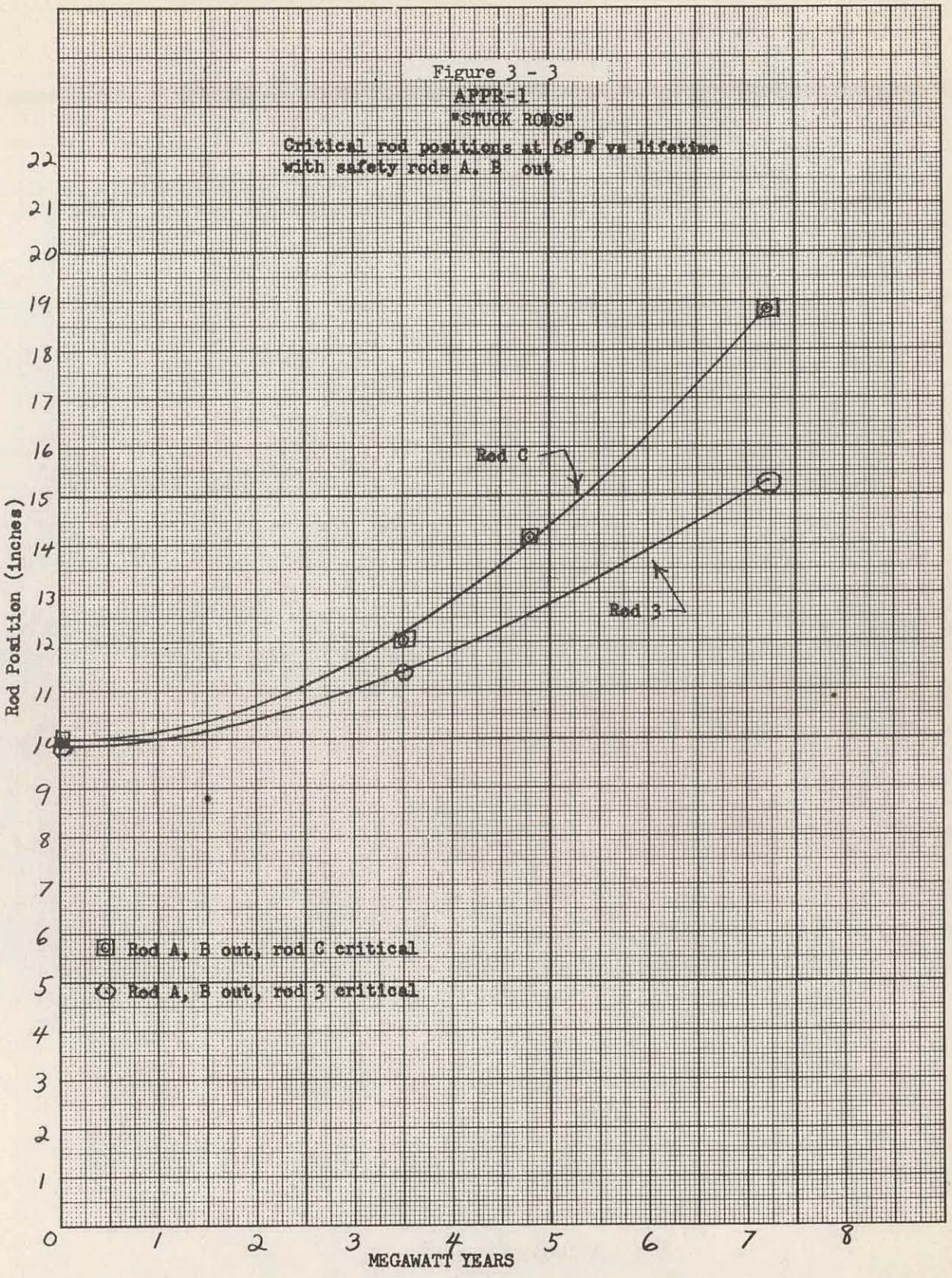
Figure 3 - 3
APPR-1
"STUCK RODS"
Critical rod positions at 68°F vs lifetime
with safety rods A, B out
Rod Position (inches)
MEGAWATT YEARS
Rod C
Rod 3
Rod A, B out, rod C critical
Rod A, B out, rod 3 critical

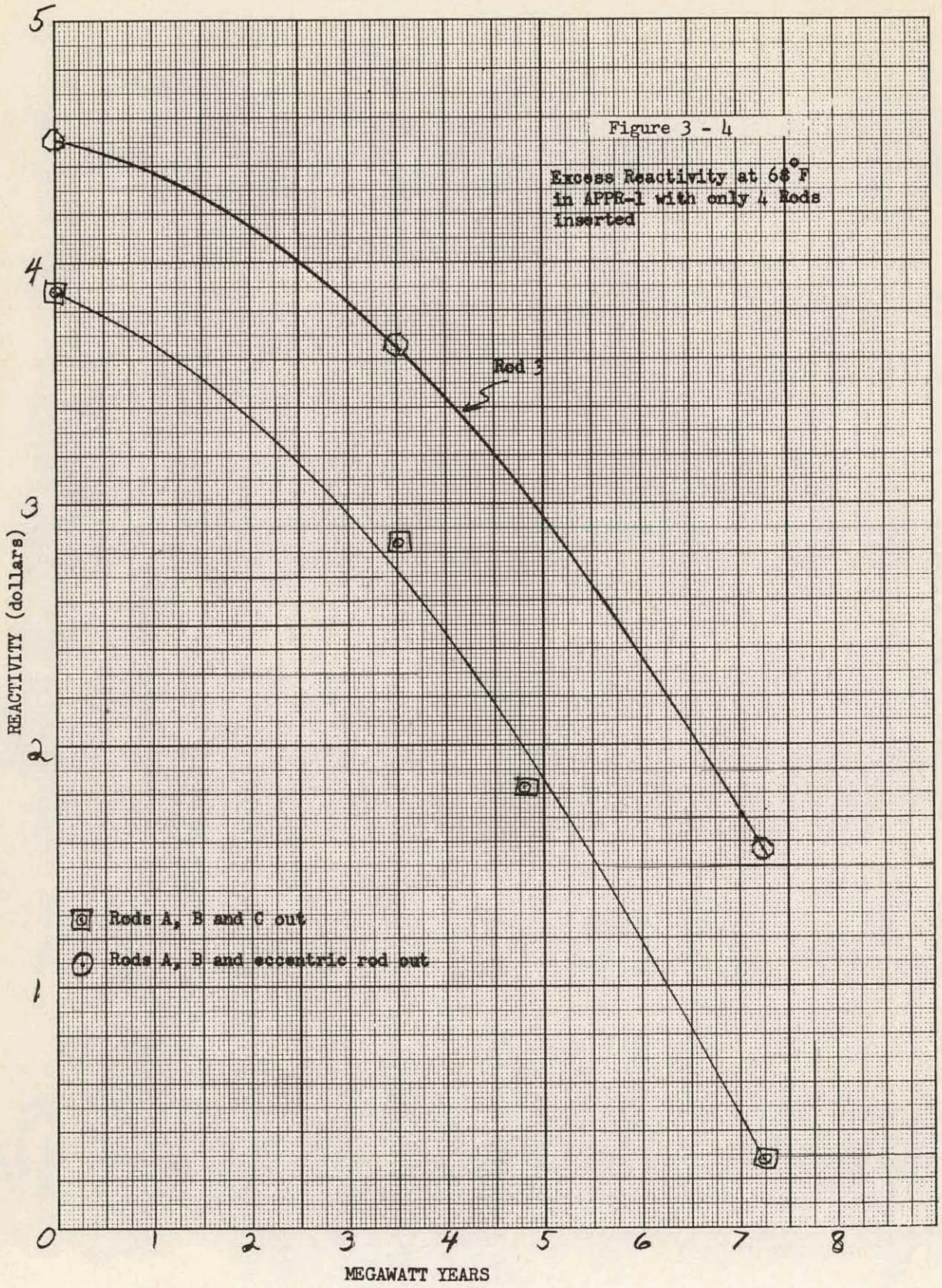
Figure 3 - 4
Excess Reactivity at 68°F in APPR-1 with only 4 Rods inserted
Rod 3
Rods A, B and C out
Rods A, B and eccentric rod out
REACTIVITY (dollars)
MEGAWATT YEARS
0
1
2
3
4
5
6
7
8

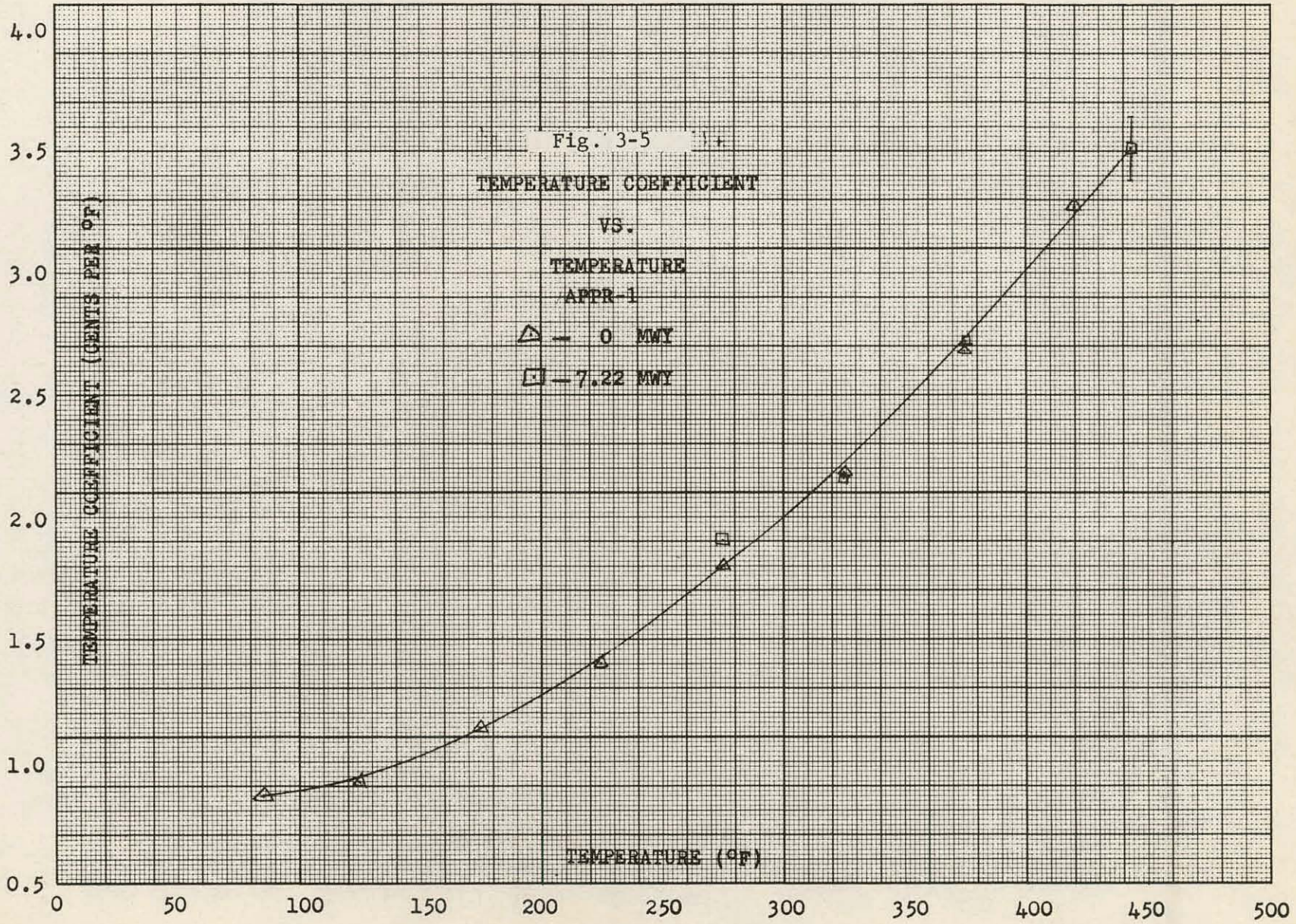
Fig. 3-5
TEMPERATURE COEFFICIENT
VS.
TEMPERATURE
APPR-1
△ — 0 MWY
□ — 7.22 MWY
TEMPERATURE COEFFICIENT (CENTS PER °F)
TEMPERATURE (°F)
4.0
3.5
3.0
2.5
2.0
1.5
1.0
0.5
0
50
100
150
200
250
300
350
400
450
500

Fig. 3-6

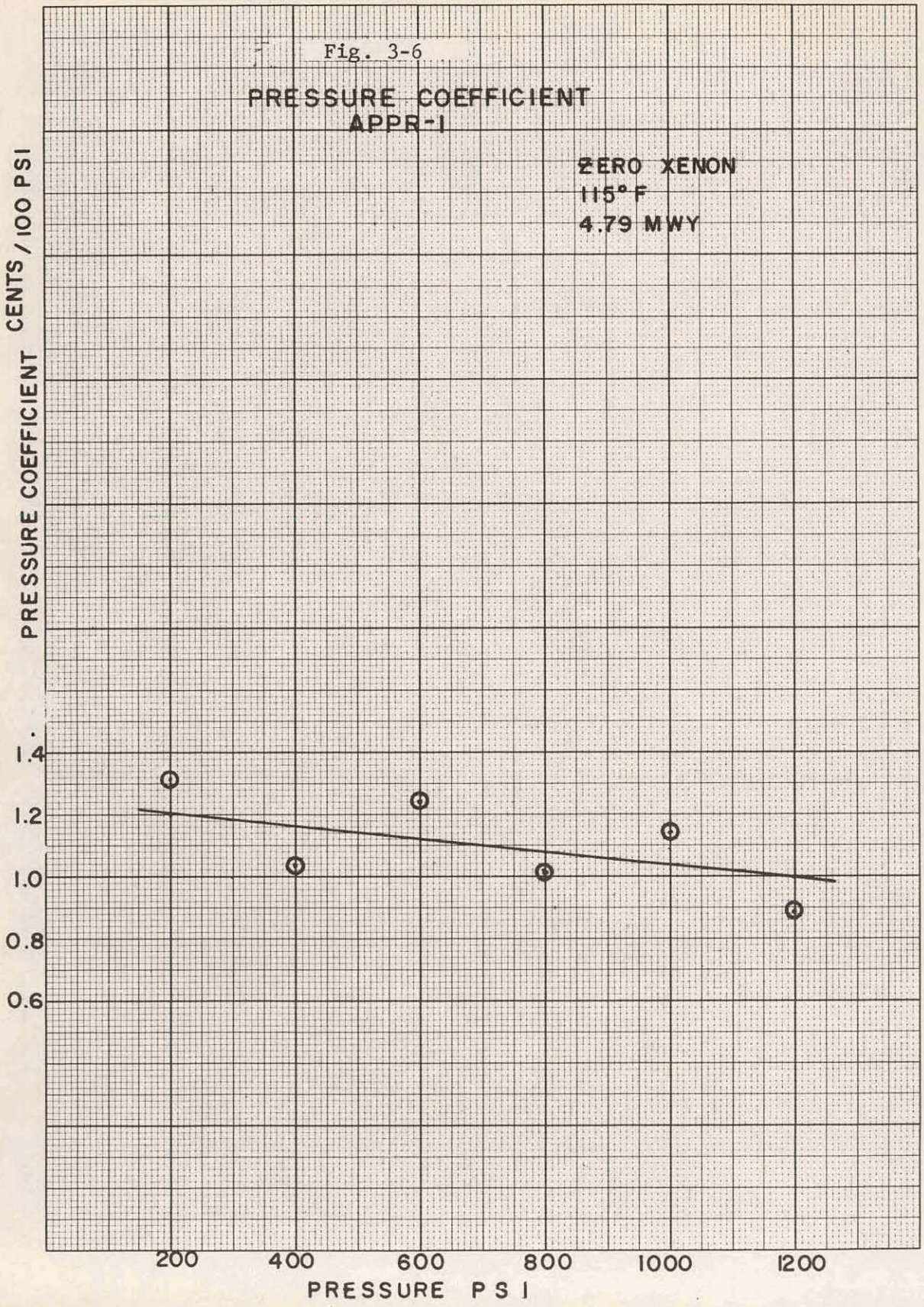
PRESSURE COEFFICIENT
APPR-1
ZERO XENON
115° F
4.79 MWY
PRESSURE COEFFICIENT CENTS / 100 PSI
1.4
1.2
1.0
0.8
0.6
200
400
600
800
1000
1200
PRESSURE PSI

Table 4-1

Constants-Skid Mounted and APPR-1

Fixed Elements

	Skid	APPR-1	Skid	APPR-1
	Cold (68°F)	Cold (68°F)	Hot (512°F)	Hot (440°F)
τ	32.403796	32.3788	48.438042	42.9631
D_f	1.321181	1.321185	1.565798	1.491955
Σ_f^a	0.010286	0.01102	0.009287	0.010867
g'	0.898091	0.898091	0.938302	0.933348
$\nu\Sigma_f^f$	0.013235	0.014181	0.011910	0.013921
p	0.747733	0.747790	0.712723	0.729024
k_f	1.286758	1.286817	1.282469	1.280967
Σ_{th}^a	0.266734	0.266863	0.200244	0.207138
$\nu\Sigma_{th}^f$	0.405789	0.405789	0.309479	0.317149
k_{th}	1.521326	1.520589	1.545509	1.53110
D_{th}	0.170539	0.170538	0.267920	0.245022
Σ_{xe}^a	--------	--------	0.006776	0.006272
$\Sigma_{SUB.}^a$	0.005289	0.007846	0.003785	0.006131
Σ_p	0.095242	0.088263	0.073065	0.07756

CONTROL ROD FUEL ELEMENTS

	Skid Cold (68°F)	Skid Hot (512°F)
τ	32.763697	48.462583
D_f	1.288348	1.510167
Σ_r^r	0.039322	0.031162
Σ_f^a	0.009254	0.008411
$\nu\Sigma_f^f$	0.010876	0.009798
p	0.764649	0.730070
k_f	1.175275	1.164865
Σ_{th}^a	0.223360	0.169193
$\nu\Sigma_{th}^f$	0.310757	0.241486
k_{th}	1.391283	1.427281
D_{th}	0.180707	0.275669
L^2	0.809039	1.629316
Σ^s	2.003930	1.387063
Σ^{tr}	1.844579	1.209179

REFLECTOR PROPERTIES (PURE WATER)

	Skid Cold (68°F)	APPR-1 Cold (68°F)	Skid Hot (512°F)	APPR-1 Hot (440°F)
D_{th}	0.14340	0.172304	0.297171	0.264866
D_f	1.671769	1.596015	2.154495	1.893739
Σ_{th}^a	0.019470	0.016960	0.009849	0.011052
τ	34.9638	33.6945	57.373705	47.5034
p	0.985556	0.987116	0.986647	0.988482

4.1.3 Fast constants - 68°F and 512°F

Constants for the fast group were also obtained from machine calculations. The Muft - III code (4) prepares the fast group constants using the P-1 Selengut-Goertzel approximation for slowing down of neutrons in hydrogenous mixtures.

4.1.4 Substitution effect

Of the 37 APPR-1 type fuel elements, 5 are movable control rod fuel elements. These elements contain less uranium and more stainless steel than the fixed elements. The effect of substituting control rod elements for fixed elements can be approximated by weighting the effect at the center of the core by a J_o^2 (μr) Bessel function where μ is the radial buckling. The effect of the center control rod fuel element on reactivity is found by running two Valprod calculations, one of which contains a control rod fuel element region at the centerline. The multiplication constant, K_{eff}, for the Skid-Mounted core can then be found from the equalities:

$$K_{eff} = K_{eff}^{F.E.} - \Delta K_{eff} \quad -N\ (\Delta K_{eff}) \times J_o^2\ (\mu r)$$

where $\Delta K_{eff} = K_{eff}^{F.E.} - K_{eff}$ (F.E. with central control rod fuel element)

N = no. of rods excluding central rod.

F.E. = fixed fuel elements

It is assumed that the effect of substituting a control rod fuel element for a fixed element changes only the thermal absorption cross-section,

$$\Sigma_{th}^{a} = \Sigma_{th}^{a}\ (F.E.) \neq \Sigma_{SUB.}^{a}$$

4.1.5 Model orrection

Reactivity calculations using this analytical approach are different from measured values in the APPR-1 reactor. To compensate for this expected difference between calculation and measurement, a "model" correction is applied to the calculated reactivity of the Skid-Mounted Reactor.

4.2 Core reactivity at 68°F

Using the model described in Section 4.1, the effective multiplication of the Skid Mounted Core at 68°F was calculated to be 1.1653. This result was obtained from a Valprod calculation of a core composed of fixed fuel elements at a temperature of 68°F. The constants for this calculation are listed in Table 4-1.

The substitution effect for a central control rod fuel element was found by running a Valprod calculation with a cylindrical control rod fuel element at the center of the core. For this case, K_{eff} decreased to 1.1594. The substitution effect for all five elements is then:

$$\Delta K_{eff} = 0.0059$$

$$K_{eff} \text{ (actual core)} = 1.1594 - 4\, J_o^2\, (\mu r)\, \Delta K_{eff}$$

$$= 1.1594 - 4\,(0.49673)\,(0.0059) = 1.1594 - 0.0117$$

$$= 1.1477$$

This correction has reduced the reactivity to 1.1477 or 12.87%ρ.

The measured cold reactivity for APPR-1 is 1.81% higher than the calculated value. (See APAE-27, (6) Pg. 48 and 49, APAE-32, (7) Pg. 49,50,56, 73). This difference is almost constant for a variety of core configurations ranging from 1.6 to 2.6%ρ). In all cases the measured reactivity was greater than the calculated reactivity. Thus, the Skid Mounted core should have an excess reactivity of about 14.98% at 68°F.

The measured reactivity of the APPR-1 is 15.35%ρ. This implies that the difference in reactivity between the Skid Mounted and APPR-1 is only 0.67%ρ.

Measurements were made on the zero power experimental core (10) of the position of the five rod bank vs. number of elements in the core. The bank moved 1.7" further in, going from 37 to 45 elements, which corresponds to a reactivity change of 2.57% using the best available rod worth data (1). However, these cores had two additional control rod elements present. In the Skid Mounted core, they are replaced by fixed elements. This difference amounts to 0.75%ρ. Therefore, we can infer from this experimental data that the Skid Mounted Reactor has a reactivity of 13.53%ρ or 1.82%ρ less than the APPR-1. In the interpretation of this experiment, the assumption was made that the rod worth does not change from 45 to 37 elements. There is probably a slight increase in rod worth in the 37 element core (about 0.9%ρ for the total five rod bank).

A difference of 1.15% exists between the two predicted reactivities. We will say, therefore, that the reactivity of the Skid Mounted core at 68°F is 14.11%$\rho \pm$ 0.58%ρ.

4.3 Control rod worth

The worth of the central control rod and the bank of five rods were calculated using the Scram Code (8) for the IBM 650. This code solves a one velocity diffusion equation for a bare reactor with a ring of black absorbing shells including a shell placed at the center of the core. At 68°F, the calculated worth of the bank is 19.9%ρ ; at 512°F, it is 19.5%ρ. A homogeneous thermal poison cross section for the rod bank can then be defined as:

$$\Sigma_p = \Sigma_a \text{ rods in } \_ \Sigma_a \text{ mixed element core}$$

This poison cross section is used to predict the critical rod bank position. The calculated worth of the center rod alone is 4.5% ρ at 68°F and 4.0% ρ at 512°F.

Experimental measurements on the APPR-1 Zero Power Reactor (9), Pg. 44 and 45, show a center rod worth of 4.0% ρ for a boron-steel poisoned core, and 4.8% ρ for a stainless steel poisoned core at 68°F. The integrated worth of the entire bank is 18.2% ρ (11). This is fairly good agreement as it is expected that the rod worth will be larger in the Skid Mounted Core. These experimental measurements (11) indicate no change in rod worth with changes in temperature.

4.4 Core reactivity and bank position

The hot (512°F), clean reactivity for the skid mounted core with fixed elements was calculated using the "Valprod" code (2). The constants used are listed in Table 4-1. The substitution effect reduced the reactivity from 8.4% ρ with all fixed fuel elements to 7.12% ρ with five control rod fuel elements. In APPR-1, this calculational model was 0.53% ρ too low. Therefore, the hot clean reactivity of the skid core is about 7.65% ρ.

In the hot (512°F) equilibrium xenon condition, the reactivity decreased to 4.9% ρ at 0 MWYR.

A "model" correction of 0.30% ρ brings the reactivity up 5.2% ρ for this case. This will be the maximum reactivity for the equilibrium xenon condition since the core will lose reactivity with burnup.

The uniform and one shot burnout models were the same as those used in the APPR-1 burnout calculations (12). All equations can be found in this reference. Calculated core parameters as functions of uranium burnup are plotted in Fig. 4-1 a,b,c. The reactivity for uniform burnup can then be calculated from the two group bare equivalent core equation,

$$K_{eff} = \frac{K_{thP}}{(1 + B_T^2 \tau)\ (1 + L^2 B_T^2)} + \frac{K_f (1-p)}{(1 + B_T 2 \tau)}$$

The results are plotted in Fig. 4-2.

For the non-uniform burnup, the core was divided into seven radial regions and burned out in five time steps with an average flux for each region. The "Nub I" code (12) was used to burn up these regions. Reactivity results were identical with uniform case up to 8.5 MWYR. The initial case was at hot, equilibrium xenon, 0 MWYR. The flux distribution was kept constant but the magnitude of the fluxes varied with burnup.

In the axial direction, the core was divided into five regions and burned out in five time steps using the same assumptions applied to the radial burnout. The initial case was at hot, equilibrium xenon, 0 MWYR, with the rods at the critical position (11.6" out). At each time step, the "Windowshade" code (3) was utilized in finding the critical rod bank position. A comparison between this calculation and APPR-1 results is found in Figure 4-3.

The excess reactivity can then be determined from rod worth measurements on the APPR-1. The rod worth per inch of the five rod bank is plotted in reference (11), and reproduced in Figure 3-2. It is assumed that the rod worth curve for the skid mounted APPR would not be significantly larger than for the APPR-1. The excess reactivity curve for the axial non-uniform burnout is plotted in Fig. 4-2 as is the curve for uniform burnout. If the APPR-1 non-uniform correction (12) were applied to the uniform burnout curve the predicted lifetime would be less. This can be expected since the non-uniformity is greater in the APPR-1. The initial rod bank position in the APPR-1 is 8.3" out of the core. This distorts the axial flux distribution much more than in the skid mounted core.

The lifetime of the skid mounted APPR should be about 10 $\pm$ 1 MWYR and will exceed the requirement to run for one year at 6.5 MW. The maximum fuel burnup for a region of the core is 49% for the center region. The maximum reactivity will occur at the beginning of life before the xenon builds up to the equilibrium condition.

4.5 Stuck rod criticality

In the Skid-Mounted core, the maximum reactivity will occur at the beginning of core life in the cold (68°F), clean condition. If the core can be shut down by any four rods of the five rod bank at this time, then those four rods should be able to shut down the core at any time. The stuck rod condition will not be as severe as in APPR-1 because of the smaller core size and increased rod worth.

Due to the flux perturbations that occur when a rod is stuck out, analytical techniques are not successful in predicting the core criticality. For instance, when one side rod is stuck out, that side of the core becomes essentially a slab reactor, and the flux shift to that side of the core increases the worth of the rod considerably. Fortunately, there is good experimental data from the APPR-1 core (13) showing the reactivity of the core with a side rod or center rod stuck out. Fig. 4-4 shows the excess reactivity of the APPR-1 and Skid Mounted cores for these cases. The rod worths for the Skid Mounted core are assumed to be the same as the APPR-1, but the initial reactivity is smaller by about 1.25%ρ. Since the initial Skid reactivity is close to that of the APPR-1, the core will not shut down with a rod stuck all the way out. However, additional experimental data from the APPR-1 (10) shows the core to be critical with the center rod stuck out 9.98". The worth of this rod in the range is 50.6¢ per inch. Therefore, the critical position of the center rod in the Skid core would be 14.5" out. The APPR-1 core is critical with a side rod out 9.84" where the rod is worth 65¢ per inch. In the Skid core, the rod should make the core critical about 13 inches out. This is verified in Figure 4-5, reproduced from reference (13). These positions are above the equilibrium xenon operating condition where the rod bank is initially withdrawn 11.6". However, if a rod were stuck while overriding xenon, the core might not shut down.

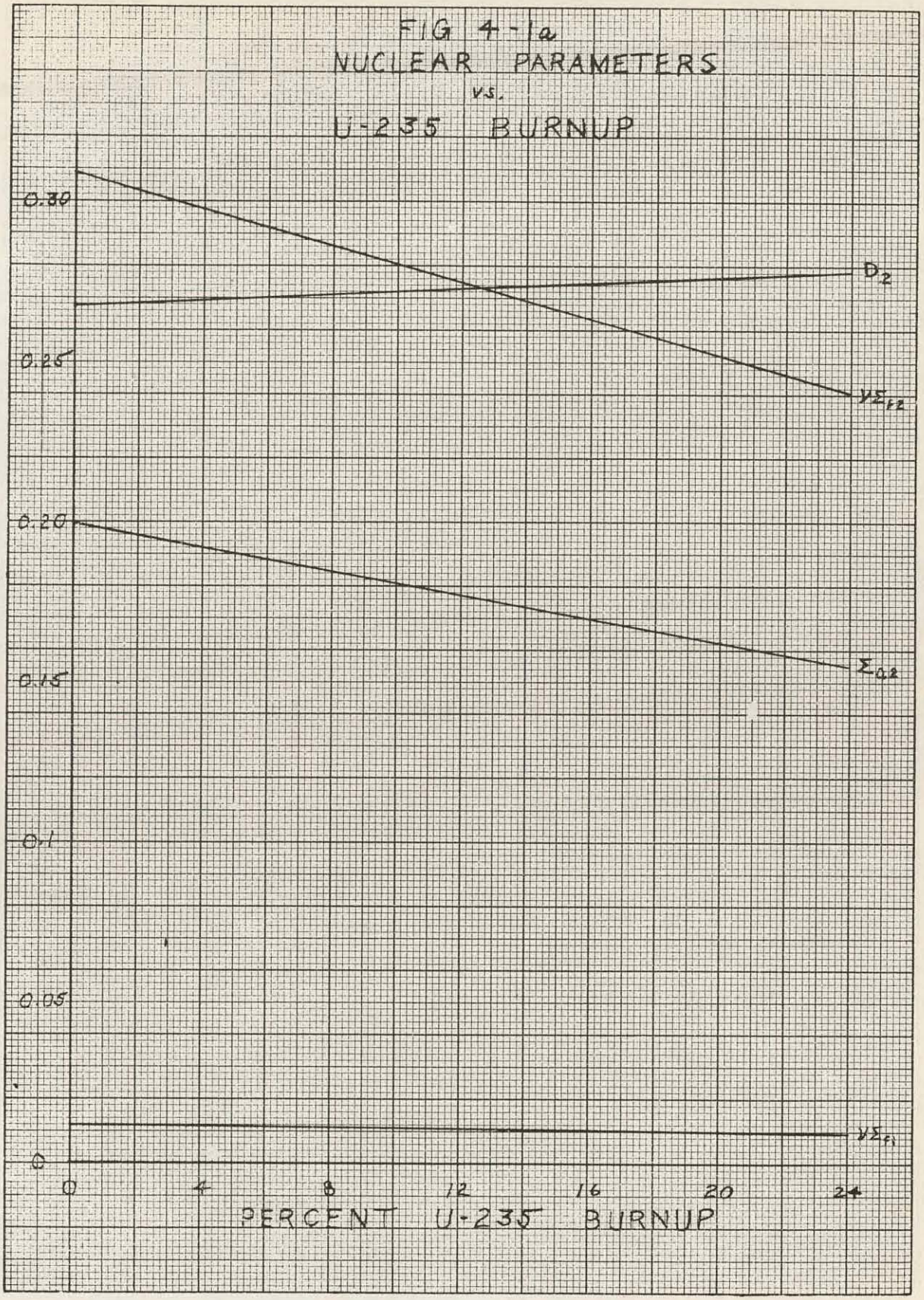
FIG 4-1a
NUCLEAR PARAMETERS
VS.
U-235 BURNUP
0.30
0.25
0.20
0.15
0.1
0.05
0
D_2
$\nu\Sigma_{f2}$
Σ_{a2}
$\nu\Sigma_{f1}$
0
4
8
12
16
20
24
PERCENT U-235 BURNUP

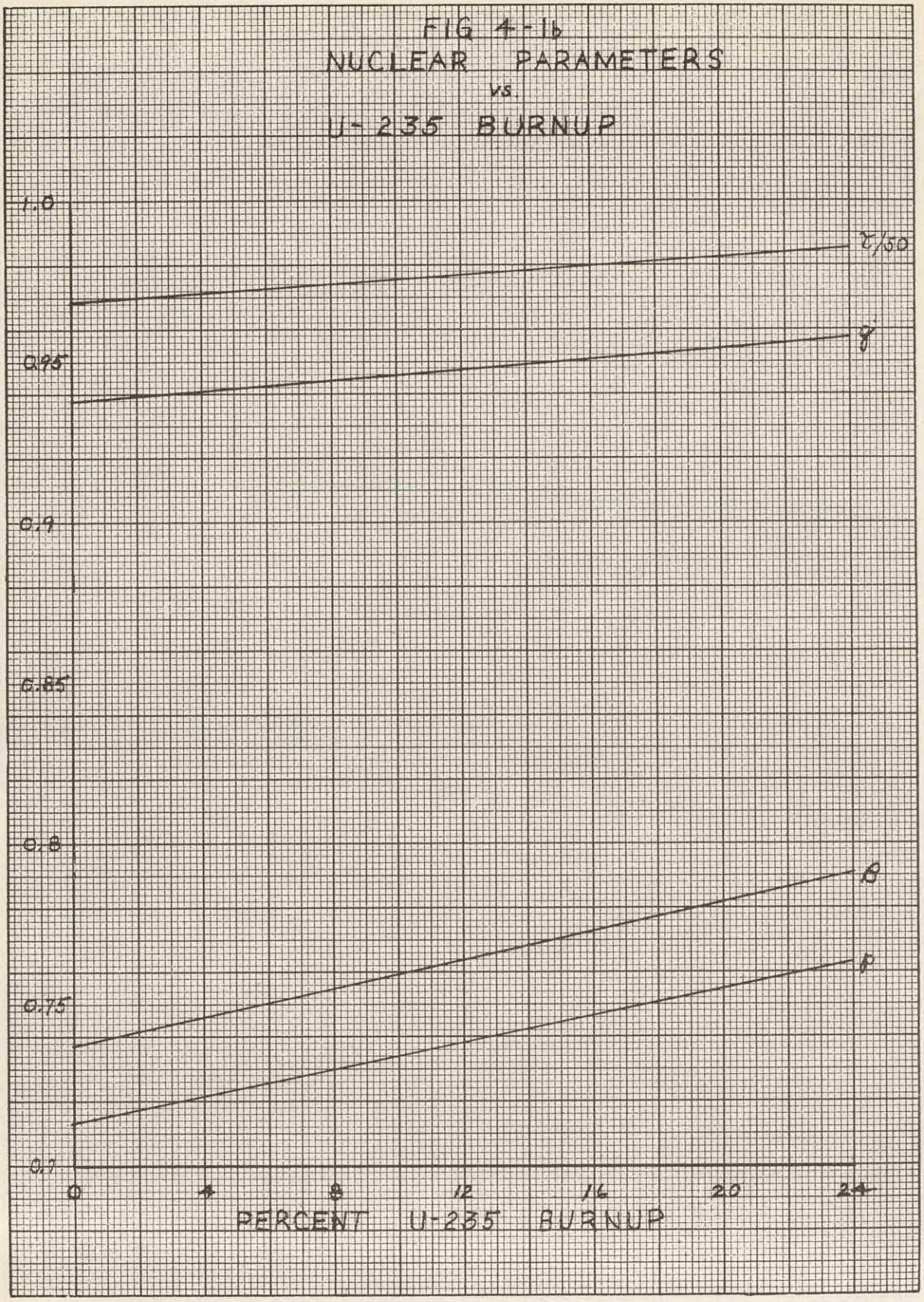
FIG 4-16
NUCLEAR PARAMETERS
vs.
U-235 BURNUP
1.0
0.95
0.9
0.85
0.8
0.75
0.7
0
4
8
12
16
20
24
PERCENT U-235 BURNUP
γ/50
g
δ
p

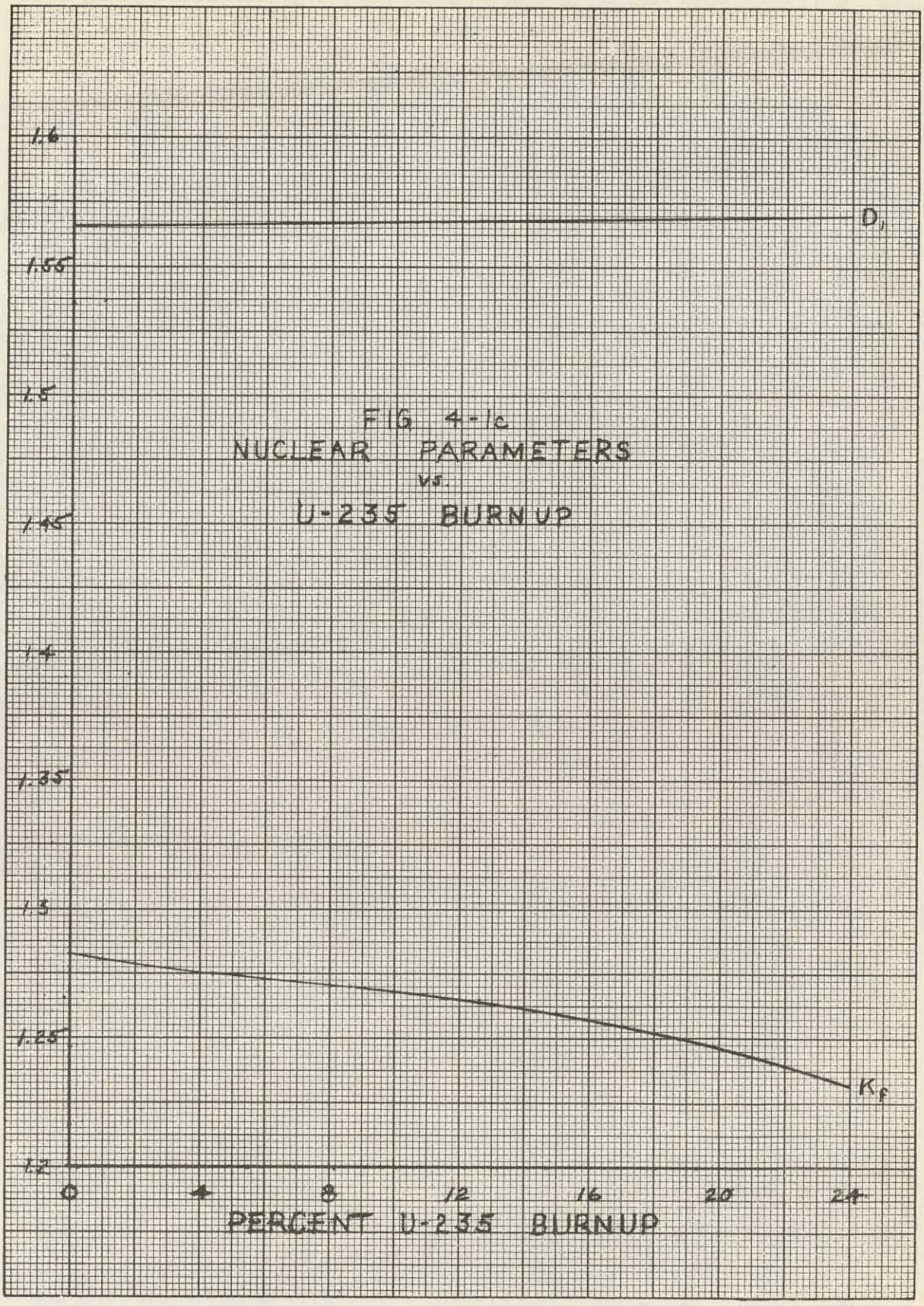

FIG 4-1c
NUCLEAR PARAMETERS
vs.
U-235 BURNUP

The injection of boric acid into the skid mounted core will be necessary to insure complete shutdown in the event of some stuck control rod conditions.

The skid core will shut down with one rod stuck in the equilibrium xenon operating bank position. In the unlikely event of one rod stuck all the way out of the core, the core will not shut down at 68°F with the remaining four rods. The worst case is with one side rod stuck out. In this case, the side of the core becomes a slab reactor, and the flux shift to that side increases the worth of the side rod considerably. About 15 out of the 37 elements form this slab. The excess reactivity can be found from the experimental worth of this rod. (See Fig. 3-4 or Fig. 4-4). Subtracting the difference between the skid and APPR-1 cores, about 1.75% k, the excess reactivity is 1.55% k or $2.12. Since the worth of B-10 to be injected is 70¢ per gm, about 3 grams of boron -10 would be needed in that side of the core. Assuming homogeneous injection of the boron,

$$\frac{37}{15} \times 3 = 7.4 \text{ grams } B^{10}$$

needed in entire core. A total of 9 gms of B^{10} was specified for the core to account for any experimental inaccuracies.

4.6 Control rod burnup

The fraction burnup in the control rod bank is defined as the total number of absorptions in the rods per original atom density of absorber, i.e., $B = \frac{A \text{ total}}{N_o}$, where N_o is the atom density of absorber times the volume of absorber in the core at the average bank position. The assumption is made that all the excess neutrons ($k_{ex} = K_{eff} - 1$) were absorbed in the control rod absorber material.

$$A \text{ total} = P \delta \nu k_{ex} t$$

where

p = power = 6.5×10^6 watts

δ = fissions/watt-sec. = 3.24×10^{10}

$\nu = \frac{\text{neutrons}}{\text{fission}} = 2.46$

k_{ex} = average excess multiplication = 0.05

t = lifetime of core = 4.85×10^7 sec.

If the average bank position is 6" into the core, $N_o = N_B10$ total rod atoms x 6/22 = 4.63×10^{24} atoms in core.

N_B10 total rod atoms = 16.985×10^{24}

$$A \text{ total} = 1.257 \times 10^{24}$$

The maximum fractional burnup is then 0.27. Thus, the amount of original B^{10} absorber left over 10 MWYR is 3.37×10^{24} atoms for an average rod insertion of 6". The average burnup for the entire length of the rods would be 7.4%.

This amount of burnup is a less serious problem than in APPR-1 since the maximum fractional burnup in the APPR-1 is estimated to be 0.37. However, irradiation of APPR-1 rods will be examined and the results will be applicable to the control rods in the Skid Mounted Reactor. After 9 MWYR of operation in the APPR-1, there has been no malfunctioning of the rods due to control rod burnup. This is almost equal to the core lifetime of the skid. However, removal of the control rods from the reactor may present a problem.

4.7 Temperature and pressure coefficients

The temperature coefficient of the Skid Mounted core was primarily based upon extrapolation of existing experimental data. The Zero Power Experiment (9) predicts a temperature coefficient, at the operating temperature of 512°F, of -3.1×10^{-4} $\frac{\Delta k}{\delta F}$. Measurements on the APPR-1 (11) reactor predict the same values of 512°F although the curve is of a slightly different shape. Fig. 4-6 is a reproduction of the experimental curves which also show a rise in the temperature coefficient for a 32 element core. The skid mounted core will therefore have a temperature coefficient of about -3.4×10^{-4} at the operating temperature of 512°F.

The integral of this curve is -7.3% k for the 37 element core from 68°F to 512°F. This number can be checked from available rod bank data (11). In APPR-1 the rod bank is 3.7" out; at 440°F it is at 6.6". Extrapolating this curve to 512°F, the rods would be 8.2" out. This corresponds to 7.0% k and would be slightly higher in the Skid core due to increased rod worth. This is excellent agreement, and, together with the knowledge of the cold (68°F) reactivity of the Skid, should determine the hot (512°F), clean reactivity.

As expected, measurements of the pressure coefficient (24,25) show this to be smaller than the temperature coefficient by at least a factor of 100. In the Skid Mounted reactor, it is estimated to be $\neq 3.1 \times 10^{-6}$ $\frac{\Delta k}{\text{psia}}$ at 512°F and 1750 psi operating pressure. (See Fig. 4-7)

5.0 FLUX AND POWER DISTRIBUTION

Power distributions on the Skid Mounted reactor were obtained for the Thermal Analysis section for determination of the coolant flow rate in each element. Power peaking at the edge of the core was not expected to be a problem because of the placement of the 2" thick stainless steel thermal shield only an average of 1 2/3" from the edge of the core. However, different reflector configurations were examined for effects on the power distribution, flux distributions, and reactivity of the Skid Mounted Core.

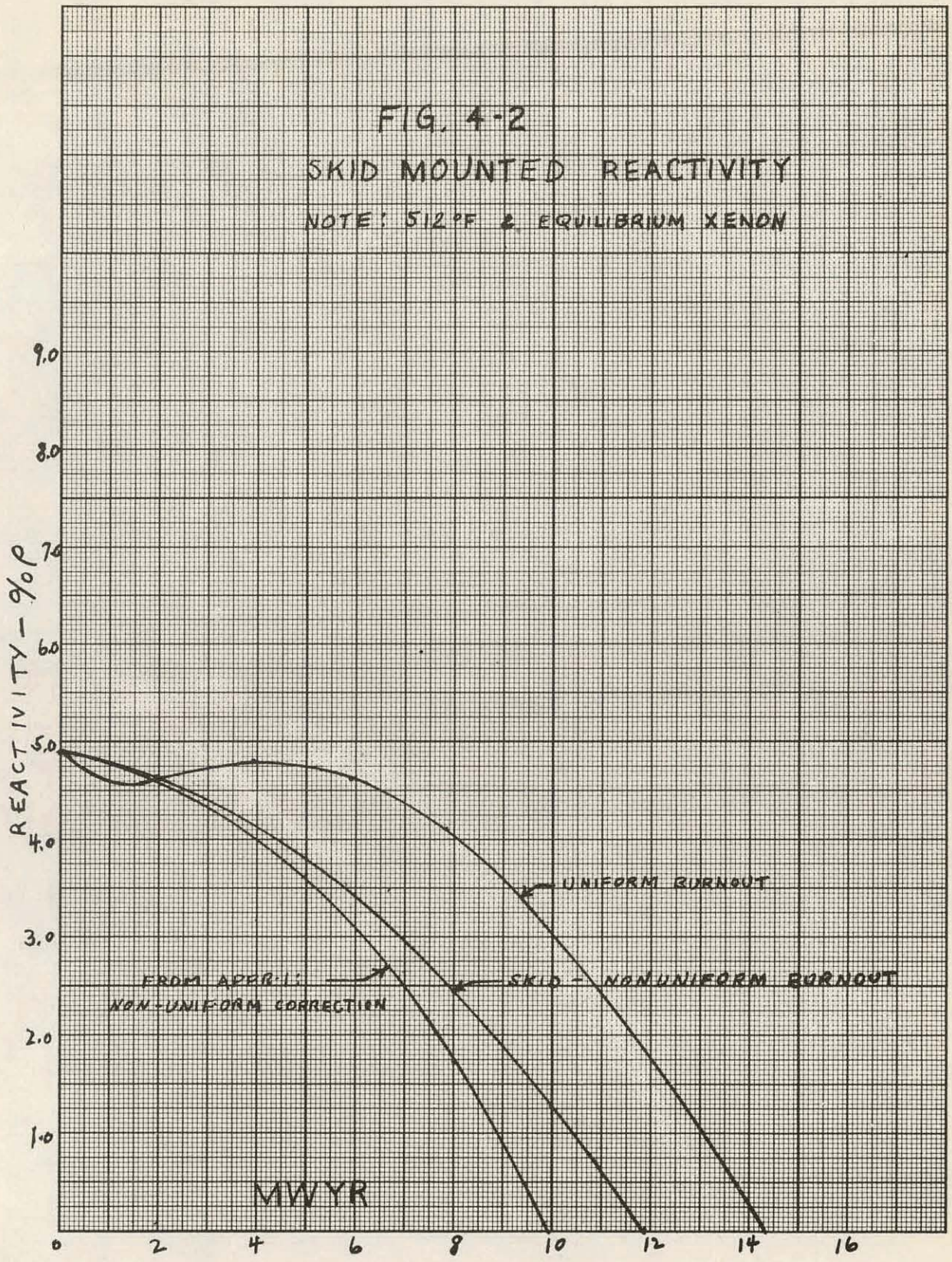
FIG. 4-2
SKID MOUNTED REACTIVITY
NOTE: 512°F & EQUILIBRIUM XENON
REACTIVITY - %ρ
9.0
8.0
7.0
6.0
5.0
4.0
3.0
2.0
1.0
0
2
4
6
8
10
12
14
16
MWYR
UNIFORM BURNOUT
SKID - NONUNIFORM BURNOUT
FROM APP'L'S NON-UNIFORM CORRECTION

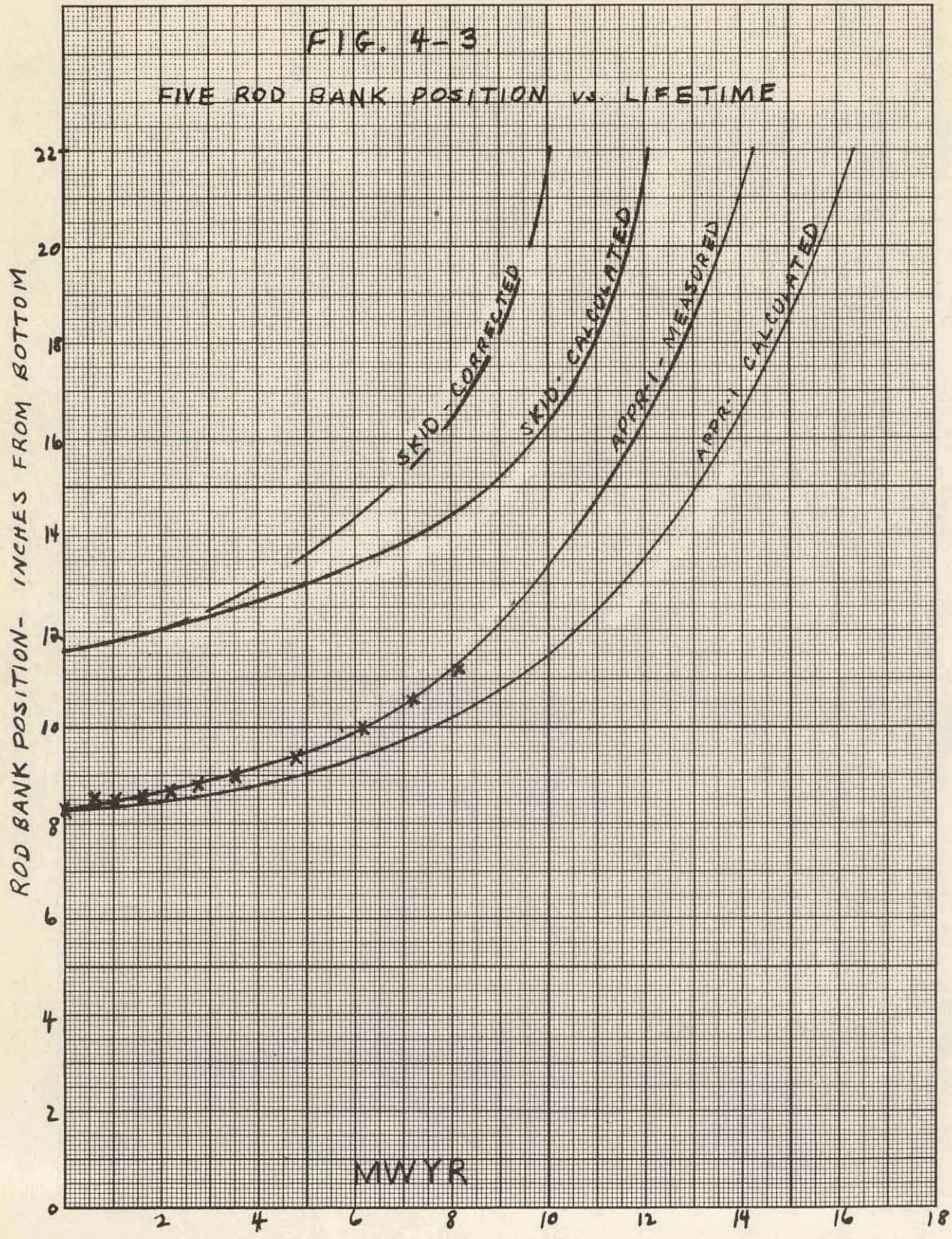
FIG. 4-3
FIVE ROD BANK POSITION vs. LIFETIME
ROD BANK POSITION- INCHES FROM BOTTOM
0
2
4
6
8
10
12
14
16
18
20
22
MWYR
SKID - CORRECTED
SKID - CALCULATED
APPR-1 - MEASURED
APPR-1 CALCULATED

FIG. 4-4

EXCESS REACTIVITY AT 68°F
WITH 4 RODS INSERTED.

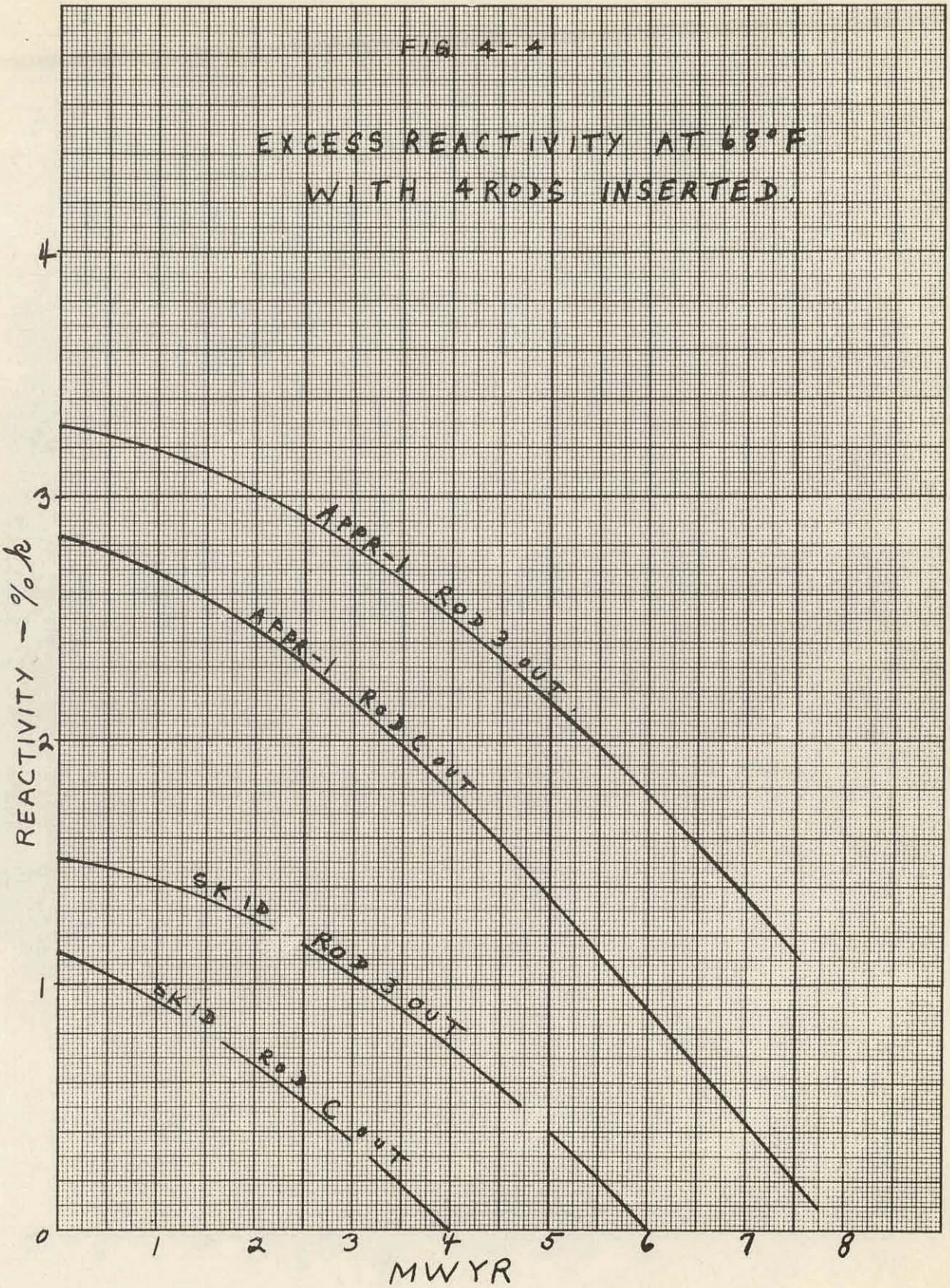

FIG. 4-5

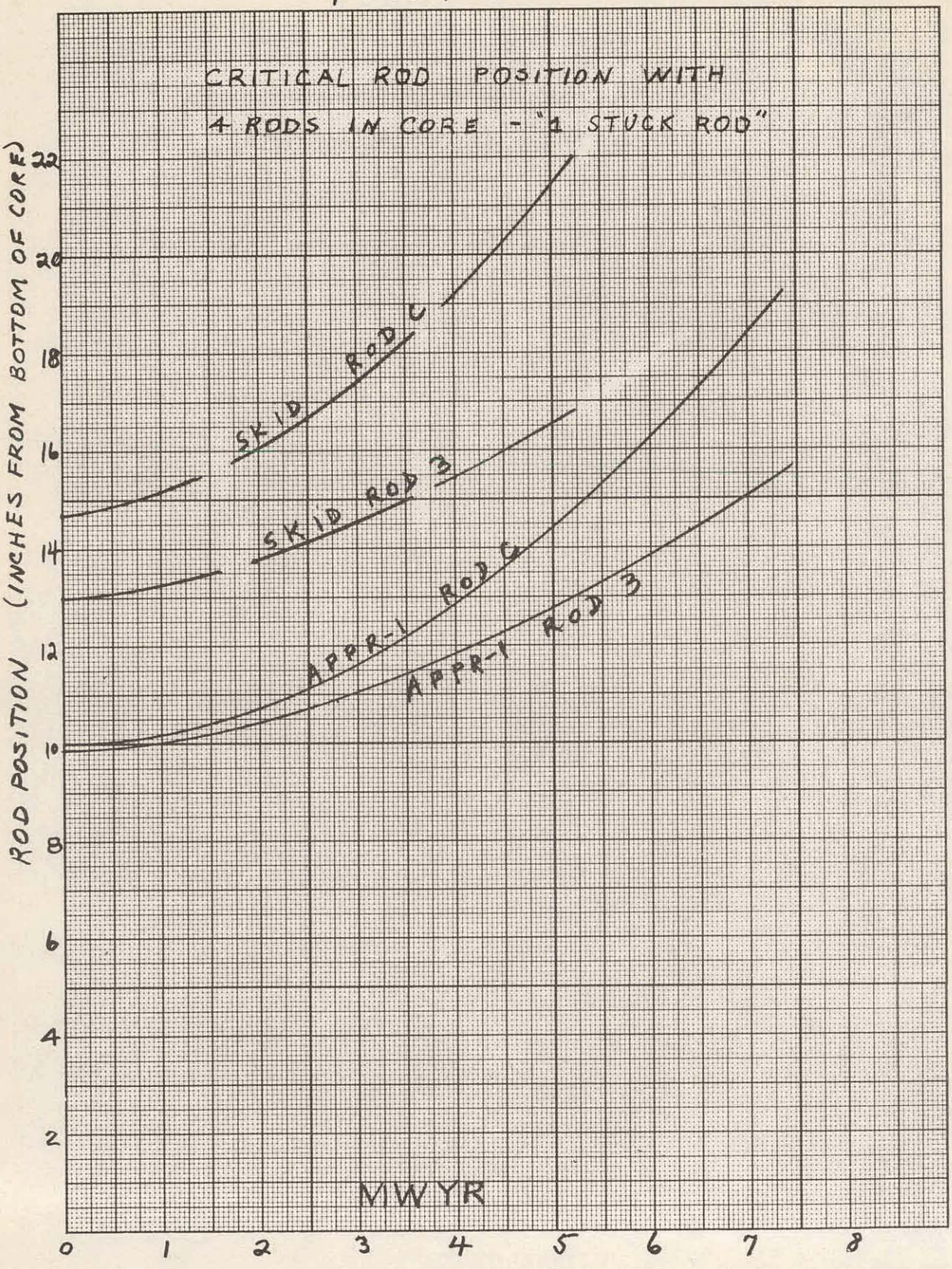
CRITICAL ROD POSITION WITH
4 RODS IN CORE - "1 STUCK ROD"
ROD POSITION (INCHES FROM BOTTOM OF CORE)
SKID ROD C
SKID ROD 3
APPR-1 ROD C
APPR-1 ROD 3
MWYR
0
1
2
3
4
5
6
7
8
2
4
6
8
10
12
14
16
18
20
22

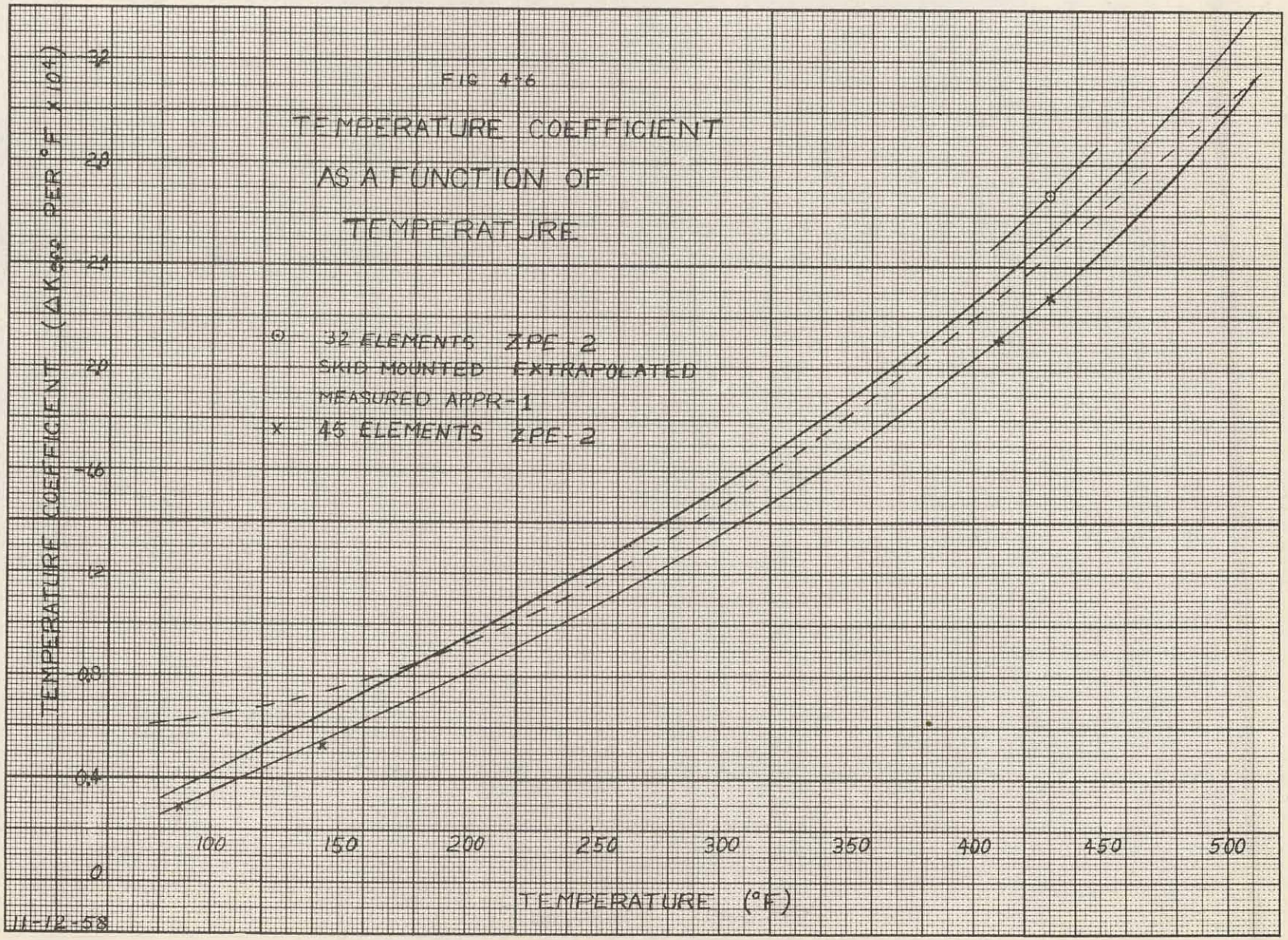
FIG 4-6
TEMPERATURE COEFFICIENT
AS A FUNCTION OF
TEMPERATURE
⊙ 32 ELEMENTS ZPE-2
SKID MOUNTED EXTRAPOLATED
MEASURED APPR-1
× 45 ELEMENTS ZPE-2
TEMPERATURE COEFFICIENT (ΔK/K PER °F X 10⁴)
32
2.8
2.4
2.0
1.6
1.2
0.8
0.4
0
100
150
200
250
300
350
400
450
500
TEMPERATURE (°F)
11-12-58

FIG. 4-7

PRESSURE COEFFICIENT Vs. TEMPERATURE

(FROM TABLES BY TSU AND BEECHER)

○ FROM APAE 18

△ APPR-1 CORE MEASUREMENTS - TASK III

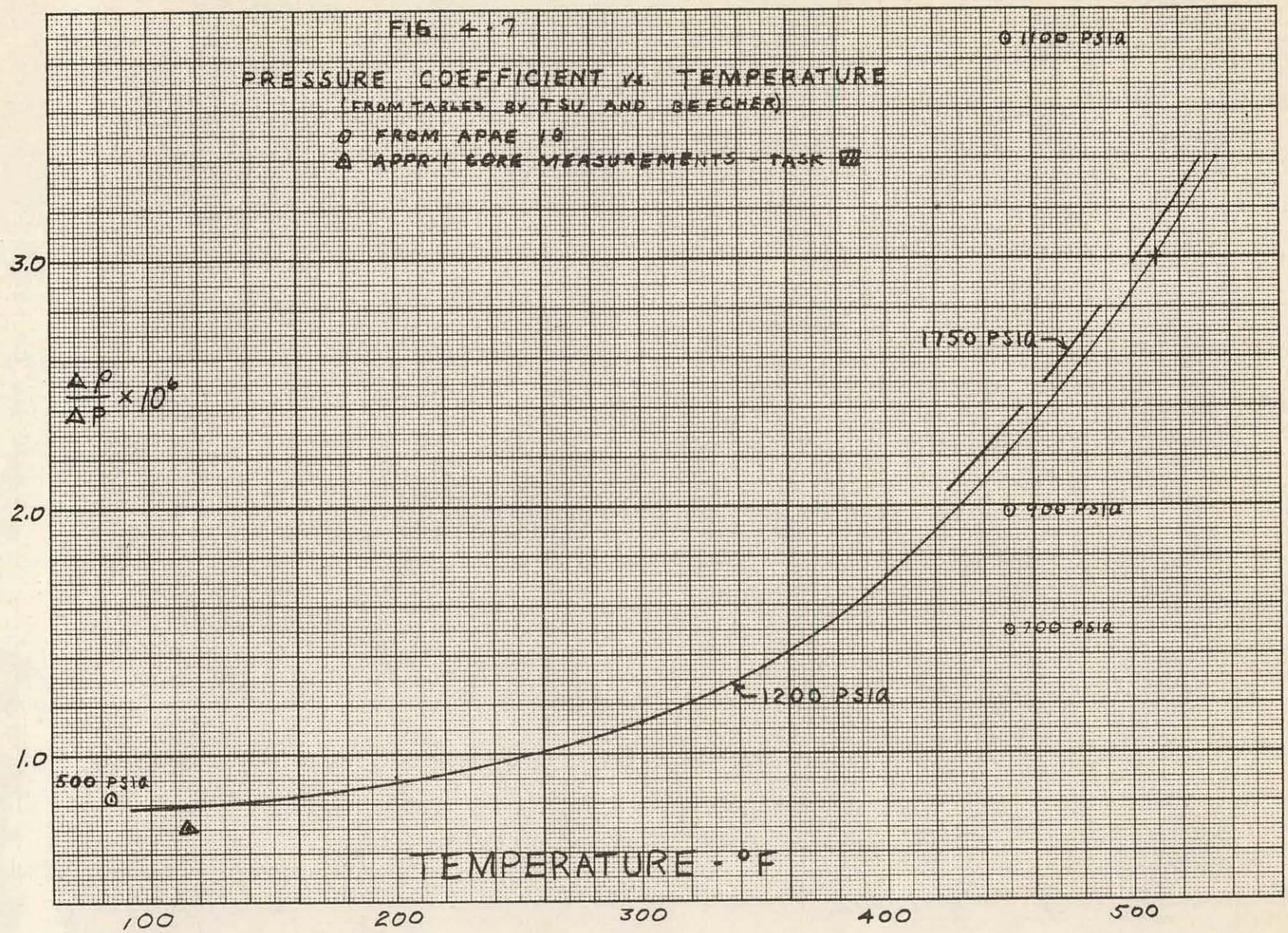

Fast and thermal flux distributions through the primary shield were graphed to show the flux level at various positions in the shield and in the pressure vessel. These calculations helped to set the inner diameter of the pressure vessel andlocation of the various neutron reading instruments in the primary shield.

5.1 Power distribution calculations and experiments

The Valprod code, written for the IBM 650 digital computer, was utilized in determining thermal and fast flux distributions through the primary shield. The code also finds the power distribution and reactivity of the core by solving the two group, multiregion diffusion equationsin one dimension. Material constants were calculated by the MUFT III and P-3 codes.

Experimental flux data is not available on a 37 element core. However, there is radial flux data for 32 and 45 element cores with water reflectors. As seen on Pgs. 78, 79 and 80 of APAE-27 (6), agreement between calculated thermal fluxes and experimental data is excellent. Since the power generation is almost directly proportional to the thermal flux in the core, we can expect the Valprod code to also predict the radial power distribution accurately.

In the axial direction, power distributions with bank of control rods inserted into the core were obtained by assuming the bank could be replaced by a homogeneous thermal absorption cross section (Σ_p). A one dimensional, two group code, the Windowshade code, iterates for the position at which the insertion of this Σ_p will result in a critical core. The most adverse power distributions occur at the beginning of full power operation because the rod bank is at its deepest penetration and the lower part of the core provides most of the power generation as shown in Fig. 5-1 and 5-2. The radial peak to average is 1.46. The axial center peak to average is 1.65; however, this improves as the rods are withdrawn.

5.2 Flux distribution

As the uranium in the core burns up, the rod bank must be moved out to compensate for the reactivity decrease. This helps flatten the axial thermal flux distribution; however, the magnitude of the flux increases. The power level is a function of the flux times the fission cross-section. In order to maintain a constant power level, the flux increases as the fission cross-section decreases due to uranium burnup. Therefore, the magnitude of the fluxes will be largest at the end of core life (10 MWYR). Fig. 5-3 and 5-4 show the radial and axial thermal flux distributions at 0 MWYR and at 8 MWYR at operating temperature (512°F).

Fig. 5-5 shows the radial thermal flux distribution for an infinite water reflector and for a 1 2/3" water gap followed by a 2" thick stainless steel thermal shield. The thermal shield depresses the thermal flux peak at the edge of the core considerably since steel does not scatter thermal neutrons back into the core as effectively as water and is a greater thermal neutron absorber. Reflector properties of stainless steel can be found in APAE-27. (6)

5.3 Flux at chamber position

In order to determine the flux level in the primary shield rings for instrumentation and dosage purposes, radial flux distributions were calculated. The average thermal flux in the core is about 1.09×10^{13} at the beginning of core life for 6.5 MW operation. This increases to a maximum of 1.5×10^{13} after 10 MWYR. Fig. 5-6 shows the thermal flux, normalized to an average of 1 in the core, through the primary shield which consists of concentric rings of boral, water, and carbon steel. The absolute value of the thermal and fast fluxes at the end of life at full power can be found by multiplying the scale by 1.5×10^{13}.

After shutdown the average value of the thermal flux in the core is initially about 1.3×10^{4}. This is a function of thepolonium-beryllium and photoneutron sources in the core and the shutdown multiplication constant of the core. Section 6.0 will provide complete data on shutdown conditions.

Instrument chamber tubes are to be located at essentially two type positions within the shield.

Position 1:

Two tubes are located within a cut in the second shield ring on a center 33 inches from the core centerline.

Position 2:

Three tubes (including the BF_3 tube) are to be located within shield tank water on a center 33 inches from the core centerline. The second shield ring does not extend to these counter positions.

Estimates of the average thermal neutron flux at these positions follow, based on knowledge of the average core fluxes and flux distribution through the shield.

Flux at 6.5 Megawatts

Position 1:

$\phi = 0.78 \times 10^{9}$ neutrons/cm^2-sec — beginning of life

$\phi = 1.06 \times 10^{9}$ — end of life

Position 2:

$\phi = 5.79 \times 10^{9}$ — beginning of life

$\phi = 7.94 \times 10^{9}$ — end of life

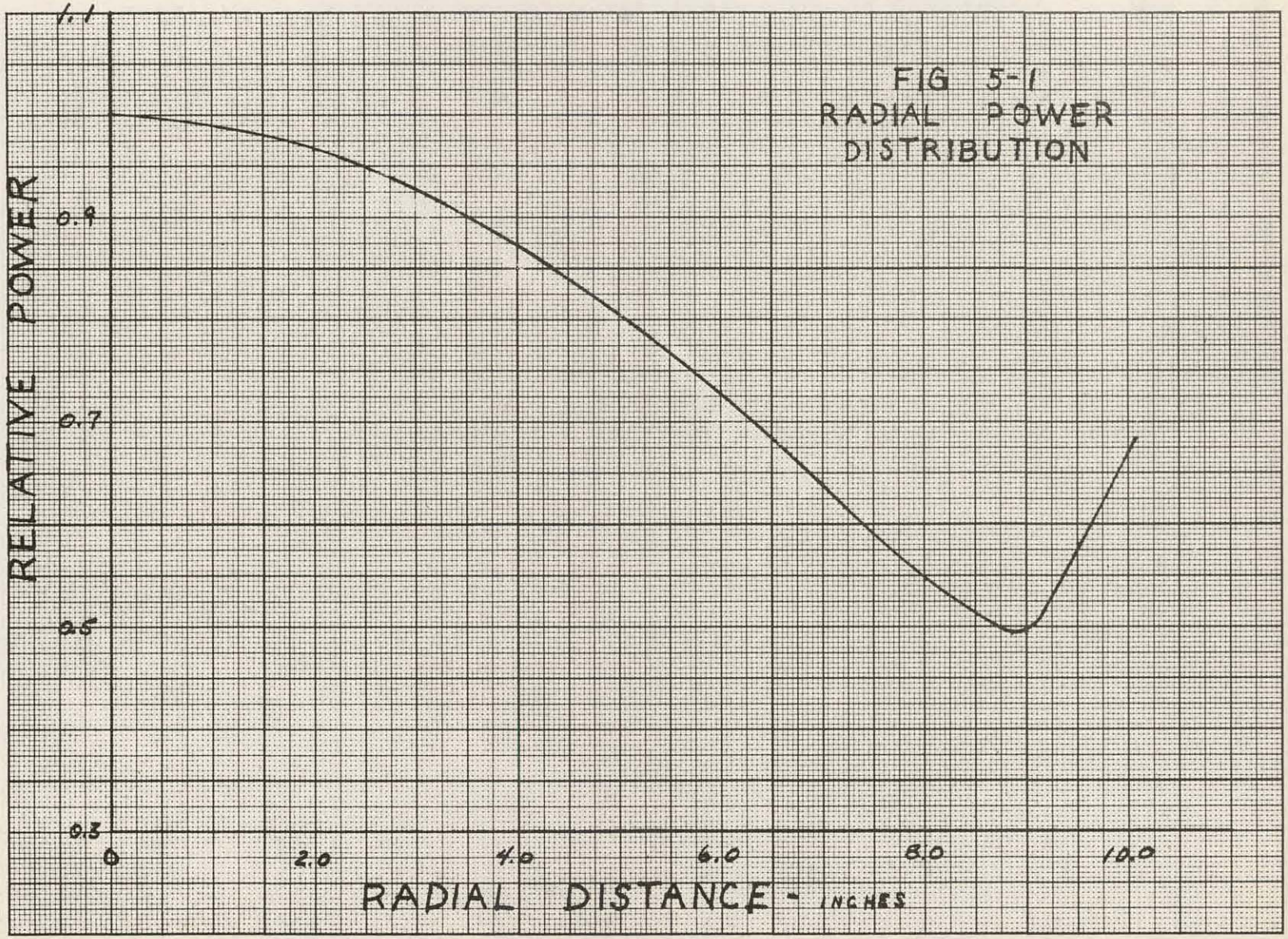
FIG 5-1
RADIAL POWER
DISTRIBUTION
RELATIVE POWER
1.1
0.9
0.7
0.5
0.3
0
2.0
4.0
6.0
8.0
10.0
RADIAL DISTANCE - INCHES

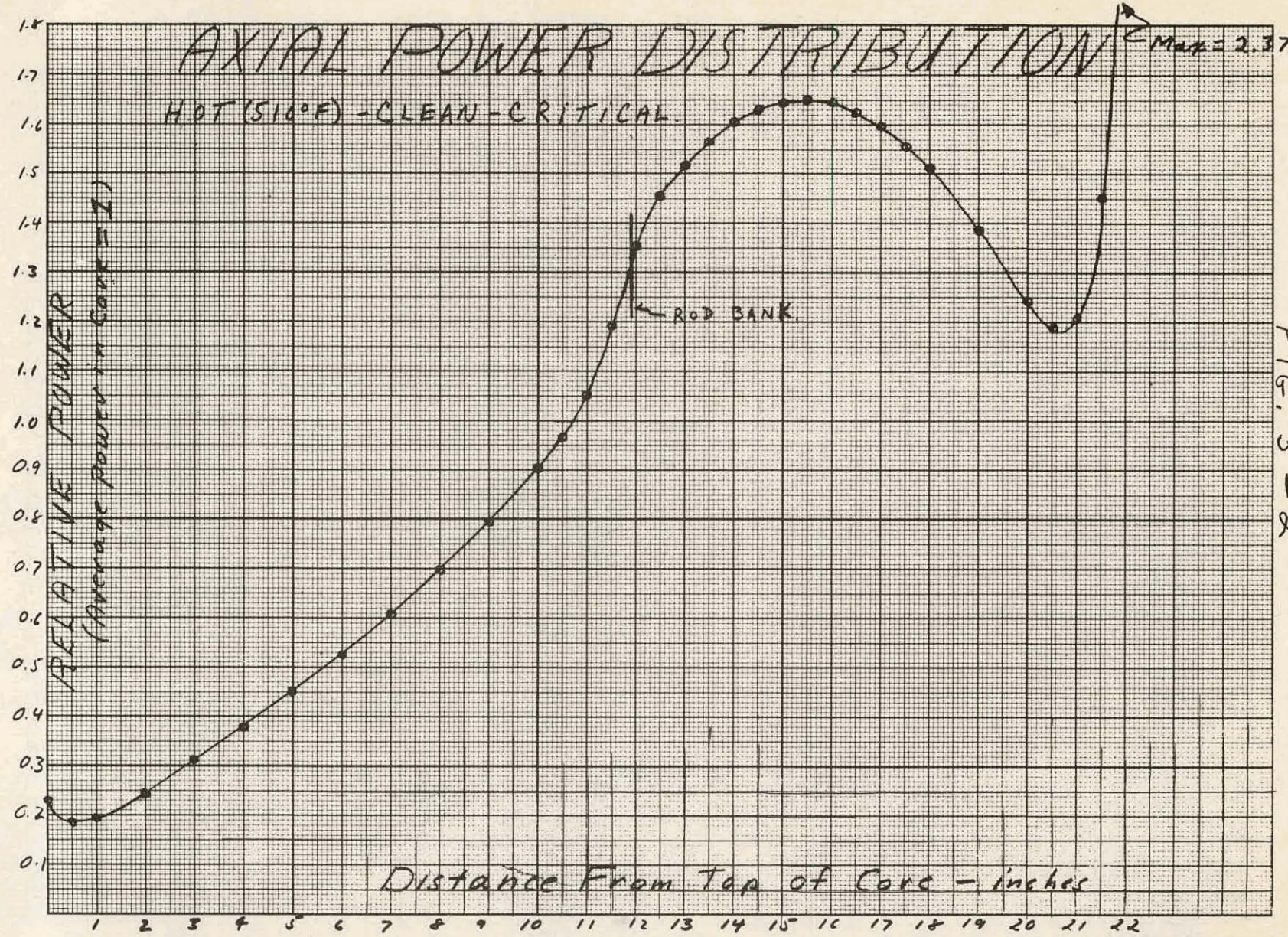
AXIAL POWER DISTRIBUTION
HOT (516°F) - CLEAN - CRITICAL
$F_{Max} = 2.371$
ROD BANK
RELATIVE POWER (Average power in core = 1)
Distance From Top of Core - inches
1.8
1.7
1.6
1.5
1.4
1.3
1.2
1.1
1.0
0.9
0.8
0.7
0.6
0.5
0.4
0.3
0.2
0.1
1 2 3 4 5 6 7 8 9 10 11 12 13 14 15 16 17 18 19 20 21 22

FIG. 5-2

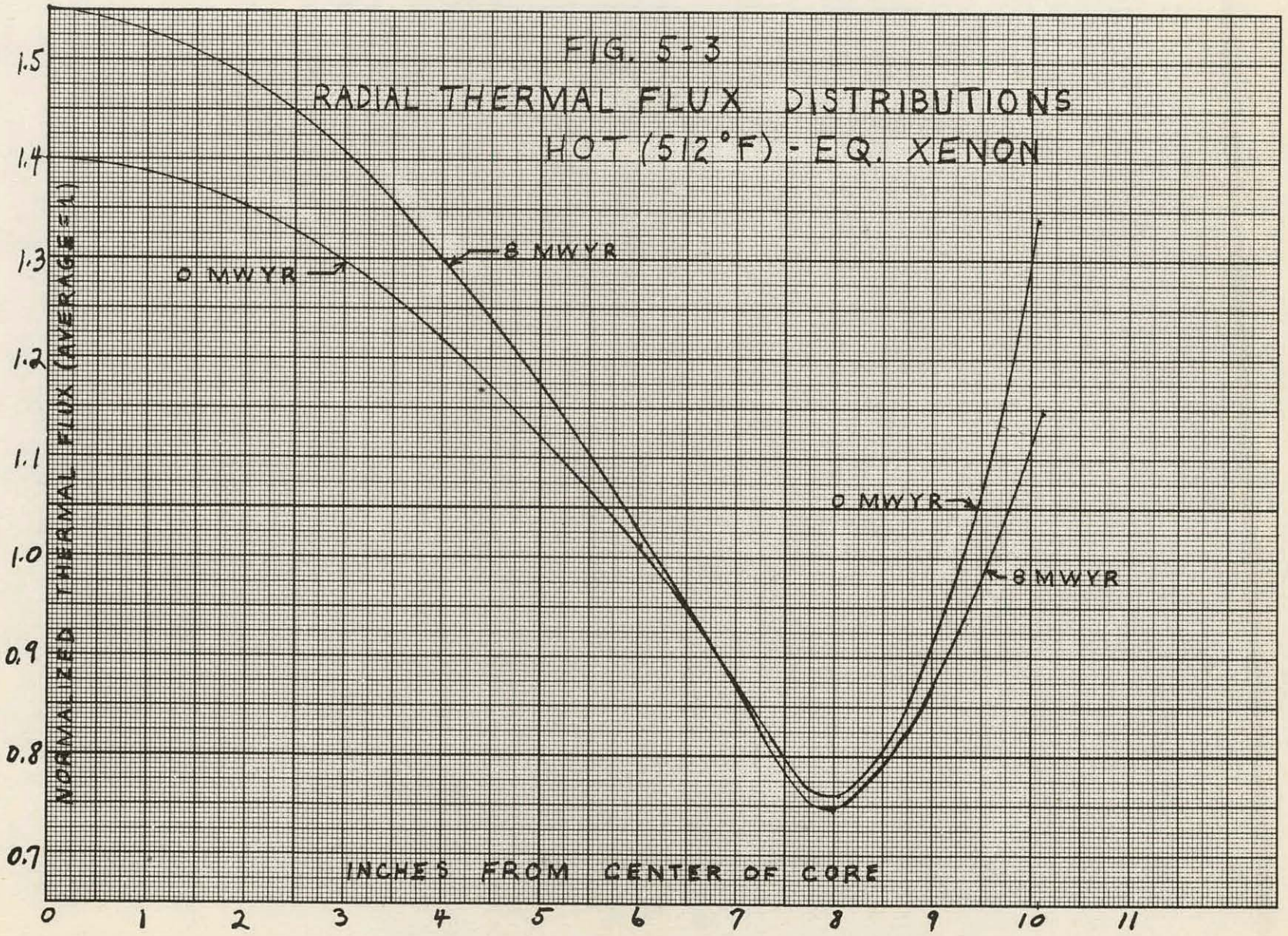
FIG. 5-3
RADIAL THERMAL FLUX DISTRIBUTIONS
HOT (512°F) - EQ. XENON
NORMALIZED THERMAL FLUX (AVERAGE = 1)
1.5
1.4
1.3
1.2
1.1
1.0
0.9
0.8
0.7
0 MWYR
8 MWYR
0 MWYR
8 MWYR
INCHES FROM CENTER OF CORE
0
1
2
3
4
5
6
7
8
9
10
11

FIG. 5-4

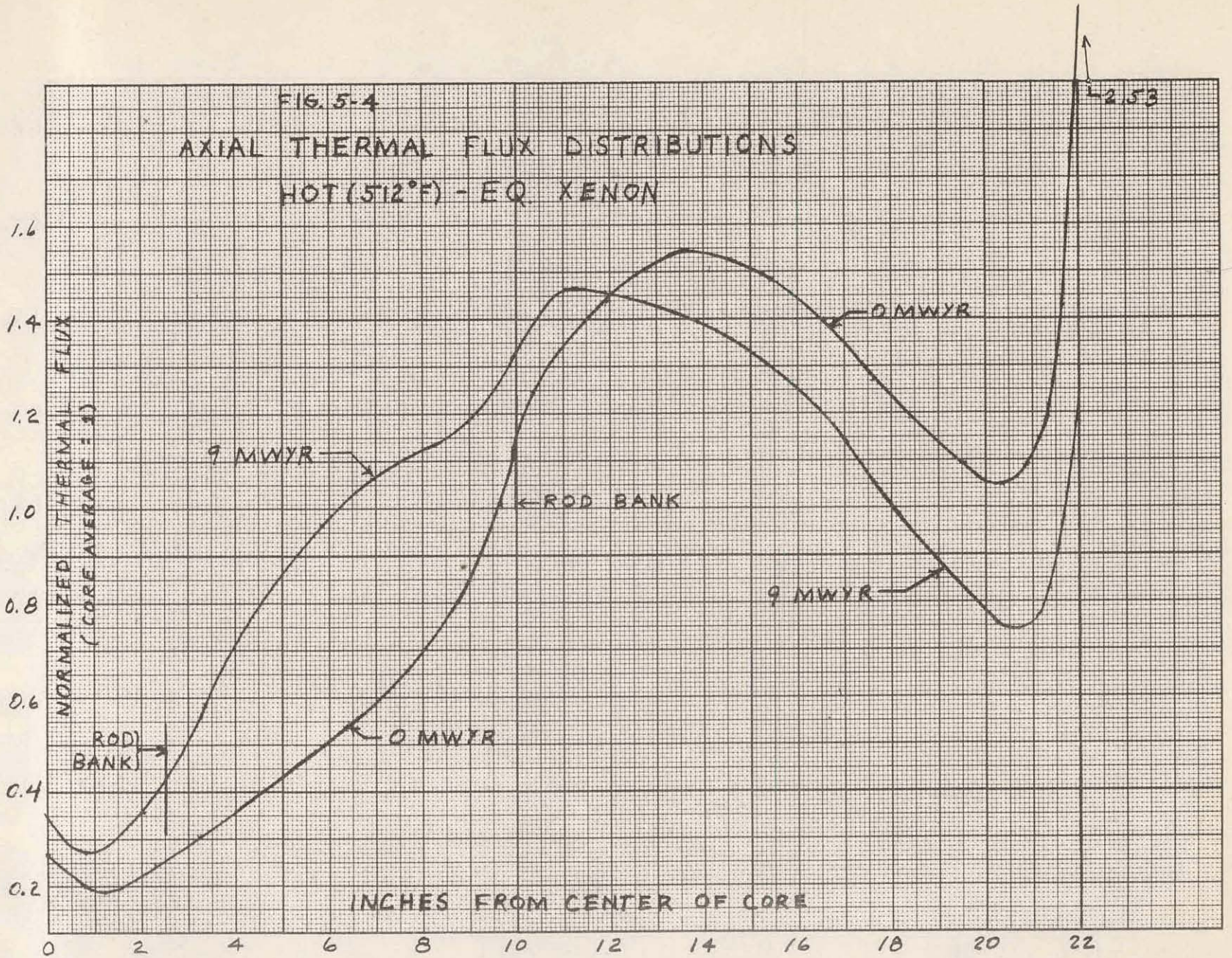
AXIAL THERMAL FLUX DISTRIBUTIONS
HOT (512°F) - EQ. XENON
NORMALIZED THERMAL FLUX (CORE AVERAGE = 1)
INCHES FROM CENTER OF CORE
1.6
1.4
1.2
1.0
0.8
0.6
0.4
0.2
0
2
4
6
8
10
12
14
16
18
20
22
9 MWYR
0 MWYR
ROD BANK
9 MWYR
0 MWYR
ROD BANK
L 2.58

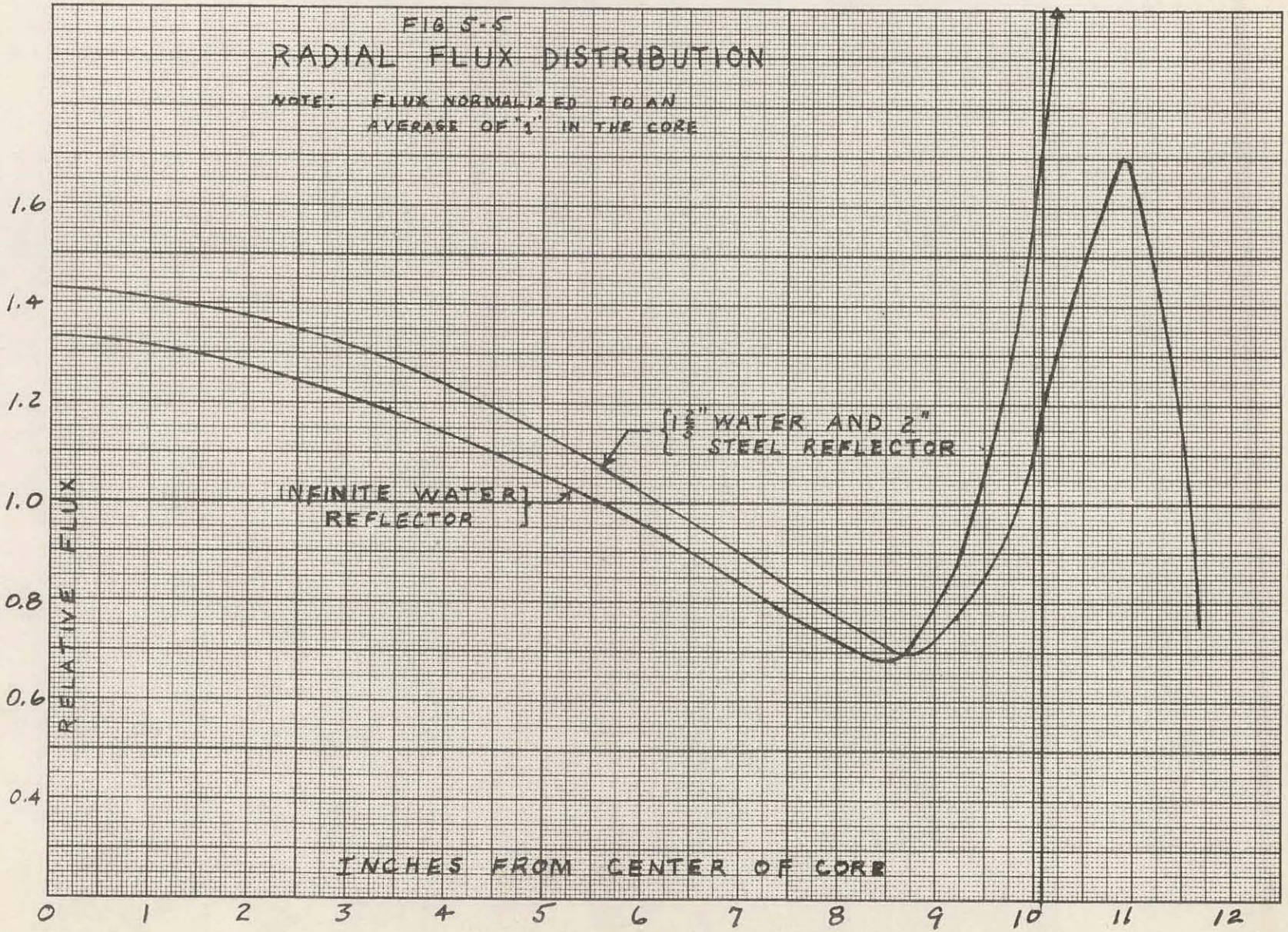
FIG 5-5
RADIAL FLUX DISTRIBUTION
NOTE: FLUX NORMALIZED TO AN AVERAGE OF "1" IN THE CORE
1.6
1.4
1.2
1.0
0.8
0.6
0.4
RELATIVE FLUX
1 1/3" WATER AND 2" STEEL REFLECTOR
INFINITE WATER REFLECTOR
INCHES FROM CENTER OF CORE
0
1
2
3
4
5
6
7
8
9
10
11
12

Shutdown Flux

Position 1:

ϕ = 0.96 beginning of life

Position 2:

ϕ = 7.2 beginning of life

These values may be reduced considerably by proper positioning of the tubes in the vertical dimension.

Gamma flux at both positions for 6.5 megawatt operation is approximately 260 r/hr.

5.4 Fast flux on pressure vessel

In an attempt to reduce weight, the inside diameter of the pressure vessel of the Skid Mounted Reactor was reduced to 25" in the early stages of the design. Bringing the pressure vessel in so near the core increased the incident fast flux to such an extent that it became mandatory to change the pressure vessel material from carbon to stainless steel. The properties of stainless steel, however, increased the thermal stresses from gamma heating to such an extent that several inches of thermal shielding would have been necessary to reduce thermal stress to the desired value. Addition of thermal shields increased the diameter and weight of the pressure vessel - thermal shield combination. Therefore it proved advantageous to increase the diameter of the pressure vessel to 38" where the incident fast flux is tolerable on carbon steel, thus resulting in the reference design.

5.4.1 Method of calculation

Two-group radial flux calculations gave the flux distributions shown in Fig. 5-6; the fast flux shown is distributed in energy between 0.4 ev and 10 Mev. The flux of interest, however, is that above 1 Mev since radiation damage to carbon steel is dependent upon the integrated flux above 1 Mev.

The method used to calculate the above -1 - Mev flux is detailed in WAPD-45 (25). The basic equation is:

$$\phi_H(E) = \frac{\nu R_f}{N_H}\left[\frac{f(E)}{\sigma_H(E)} \neq \frac{1}{E\,\sigma_H(E)} \int_E^\infty f(E')\,dE'\right]$$

ν = 2.46 neutrons per fission

R_f = fission rate, fissions/cm^3-sec.

N_H = nuclear density of hydrogen, nuclei/cm^3

$\sigma_H(E)$ = hydrogen scattering cross section, cm^2/nucleus

$f(E)$ = fraction of fission neutrons born with energy E per unit energy interval

$\int_{E}^{\infty} f(E')dE'$ = fraction of fission neutrons born above energy E

The calculation above will overestimate the fraction of the total fast flux which is above 1 Mev since inelastic scattering with the heavy elements in the core is ignored.

After the above 1- Mev flux has been calculated in the core, it is still necessary to arrive at a corresponding flux on the pressure vessel. The Valprod code used to calculate the distribution of the fluxes is inadequate to investigate rigorously the effect of the thermal shield-water combination because of the two-group limitation. To assume that the spectrum of the fast flux is the same on thepressure vessel as in the core would give an overestimate of the above 1- Mev flux because of the inelastic scattering in the steel thermal shields. Therefore an attempt has been made to estimate the effect of thermal shields and the inelastic scattering in the core on the above 1- Mev flux. It appears that a conservative estimate of these two effects would be:

1) Fast flux through a water reflector only has same spectrum as calculated core fast flux.
2) Through four inches of thermal shielding, the flux above 1 Mev is attenuated until it constitutes a fraction of the total fast flux equal to one-half its calculated fraction in the core.
3) Through two inches of thermal shielding, the flux above 1 Mev is attenuated until it constitutes a fraction of the total fast flux equal to three-fourths its calculated fraction in the core.

These estimates have been applied to the above 1- Mev fluxes of Table 5-1.

5.4.2 Comparison with APPR-1 and 1a

Table 5-1 contains calculated values of fast and above -1- Mev fluxes and "nvt" above 1 Mev for APPR-1, APPR-1a, and the Skid Mounted Reactor.

Table 5-1

Flux and "nvt" above 1 Mev Incident on Pressure Vessel

	$\phi_{f(>0.4\ ev)}$	$\phi_{f(>1\ Mev)}$	nvt
APPR-1 (20-yr. lifetime)	3.8×10^{11}	9.8×10^{10}	6.2×10^{19}
APPR-1a (20-yr. lifetime)	2.3×10^{12}	4.1×10^{11}	2.6×10^{20}
Skid Mounted (20-yr. lifetime) 25" Vessel	2.30×10^{13}	7.10×10^{12}	4.46×10^{21}
38" Vessel	2.06×10^{12}	4.80×10^{11}	3.12×10^{20}

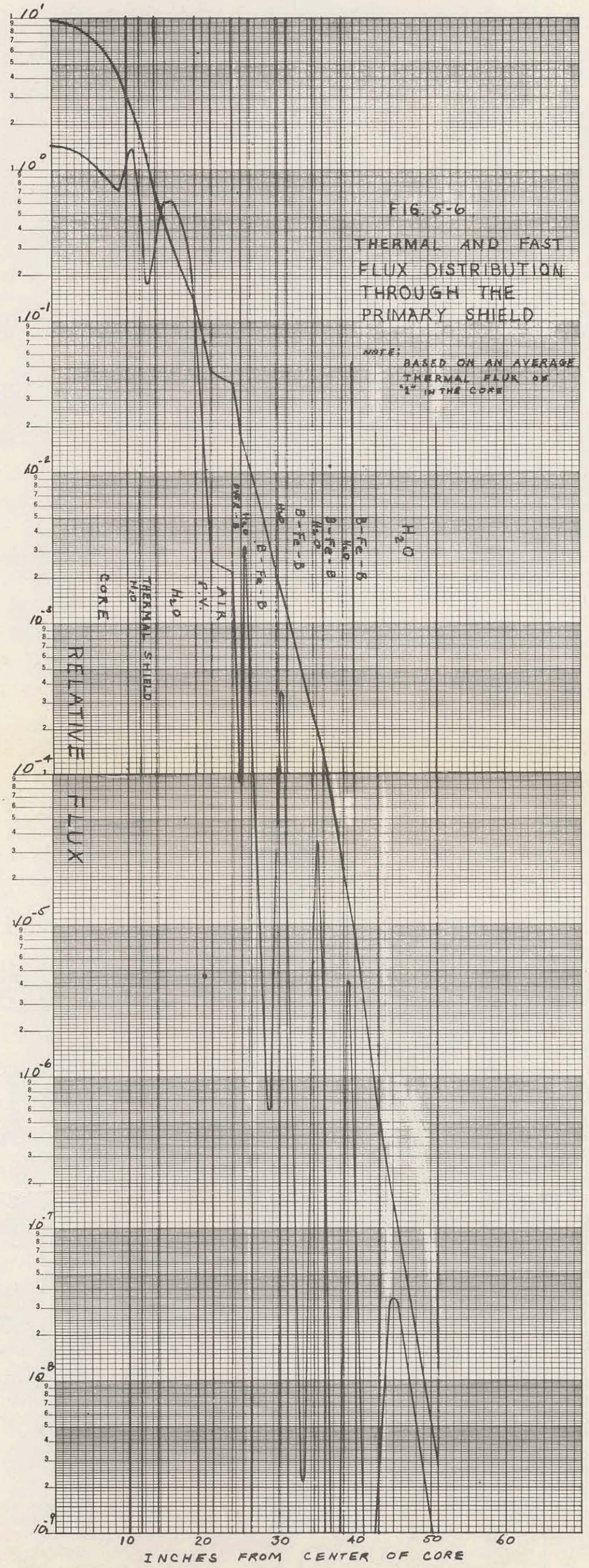
FIG. 5-6
THERMAL AND FAST FLUX DISTRIBUTION THROUGH THE PRIMARY SHIELD
NOTE: BASED ON AN AVERAGE THERMAL FLUX OF "1" IN THE CORE
RELATIVE FLUX
COKE
THERMAL SHIELD H2O
H2O
F.V.
AIR
B-Fe-B
B-Fe-B H2
B-Fe-B H2O
B-Fe-B H2O
H2O
10^1
10^0
10^-1
10^-2
10^-3
10^-4
10^-5
10^-6
10^-7
10^-8
10^-9
10
20
30
40
50
60
INCHES FROM CENTER OF CORE

5.5 Conclusions

Power peaking will not be a problem in the Skid Mounted Reactor. Radially, the presence of the thermal shield only an average of 1 2/3 inches from the core edge reduces the power peak at the edge of the core considerably from 1.47 $\frac{P_{max.}}{P_{av.}}$ with an all water reflector to 0.95 $\frac{P_{max.}}{P_{av.}}$.

In the axial direction the peaking will be lower than in the APPR-1 core because the rod bank controls less reactivity andis not inserted as deep. In the most adverse case (hot, clean, 0 MWYR), the APPR-1 five rod bank is inserted 15 inches while the Skid bank is inserted only 12 inches.

Thermal stress on the carbon steel pressure vessel has been reduced to tolerable values by the addition of a thermal shield and increased inner diameter of the vessel.

6.0 SOURCE STRENGTH DETERMINATION

To insure a sufficient count rate on the BF_3 chamber during reactor start-up, a neutron source must be incorporated within the core area. Determination of the strength of such a source follows.

6.1 Correlation of APPR-1 measurements with theory

6.1.1 APPR-1 measurements

Since the complete computation of required source strengths involves some rather complex theory, results of experimental measurements made on the APPR-1 will be incorporated wherever feasible. Source strength specification for the APPR-1 and experimental data are given below.

Sources

15 curie polonium - beryllium source (3.8×10^7 neutrons/sec. initial)

3" x 3" x 0.5" beryllium block as a photo-neutron source utilizing gamma rays from fission products

Measured Shutdown Count Rates, BF_3 Chamber

Date Measured	Temp.	Megawatt Years Operation	Time After Shutdown	Count Rate
April 11, 1957	68°F	0	0 days	7 counts per sec (17)
May 26, 1958	112°F	6.15	5.08	4 counts per sec (22)

6.1.2 Determination of average core flux/source strength

One of the most difficult quantities to compute in predicting count rate due to a given source is average core flux/source strength. This quantity will be established for the APPR-1 by using the count rate measured during the early days of reactor operation. See page 130 of AP Note 59 (17).

Measured count rate = 7 cps
Counter sensitivity = 4.5 cps/nv nv = thermal flux

$\phi_{eff} / \phi_{peak} = 0.30$ Figure I-21, APAE 17 (14)

$\phi_{peak} / \bar{\phi} = 3.6 \times 10^{-4}$ Figure I-21 APAE 17 (14)

$S = 3.8 \times 10^{7}$ neutrons/sec.

Shutdown $K_{eff} = 0.93$ initial excess reactivity - total rod worth

where

S = neutron source strength

$\bar{\phi}$ = average core flux due to source

ϕ_{peak} = value of flux peak in water gap preceding second shield ring. BF_3 chamber is located in 2nd shield ring.

ϕ_{eff} = effective counter flux. (An average around the counter tube with attenuation due to steel tube taken into account)

$$\phi/S = \frac{7}{(4.5)\ (.30)\ (3.6 \times 10^{-4})\ (3.8 \times 10^{7})}$$

$$\bar{\phi}/S = 3.79 \times 10^{-4}\ cm^{-2}$$

This value will be used for APPR-1 type cores for a sub-initial K_{eff} of .93 and with the same ratio of thermal to fast core flux. For different values of K_{eff} the curve of Figure 6-1 will be utilized. The curve is based on a classified Westinghouse Reactor but normalized to the preceeding value of $\bar{\phi}/S$. The assumption is made that $\bar{\phi}/S$ is directly proportional to the ratio of thermal to fast core flux since ϕ is taken as thermal flux. Hence, a corresponding correction should be employed for cores with a different thermal to fast flux ratio. For the skid mounted reactor this corrective ratio is 0.9. Figure 6-1 assumes this correction.

6.1.3 Correlation of photo-neutron source

The strength of the Po-Be source had fallen off more than a factor of ten when the count rate measurement of 4 cps was made on May 26, 1958.

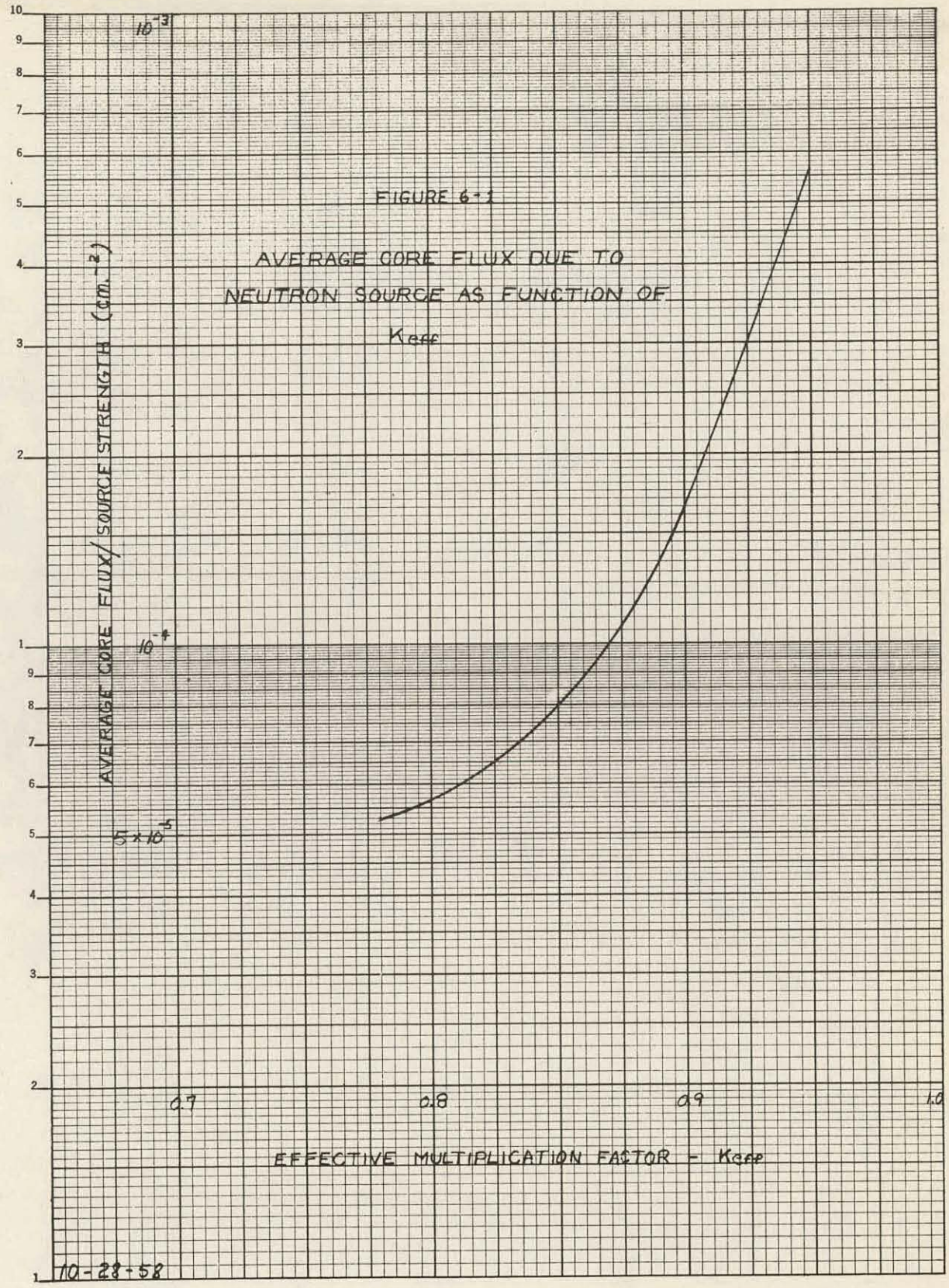
FIGURE 6-1
AVERAGE CORE FLUX DUE TO NEUTRON SOURCE AS FUNCTION OF Keff
AVERAGE CORE FLUX/SOURCE STRENGTH (cm.⁻²)
10⁻³
10⁻⁴
5 x 10⁻⁵
0.7
0.8
0.9
1.0
EFFECTIVE MULTIPLICATION FACTOR - Keff
10-28-58

(See Figure I-25 APAE 17) (14). Therefore, this measurement provided a good point of correlation for the beryllium block photo-neutron source. A prediction of this source strength and the resulting count rate was made. The factor necessary to force the predicted values of count rate into agreement with the measured 4 cps was retained as a correction factor to be used for count rate prediction on the Skid Mounted Reactor.

The calculational procedure was based upon that used for the APPR-1a as given APAE 17, (14) page 47. More recent data was used where appropriate and simplifications made where possible.

Photo-neutron source strength computation corresponding to the measured point follow.

The neutron source arrises from the following reation.

$$_4Be^9 + \gamma = 2\ _2He^4 + {}_0n^1 \text{ (threshold = 1.64 Mev)}$$

Source of the gamma ray are fission products. Hence, a gamma source strength of energy greater than 1.64 Mev must be established. Then the resulting gamma flux on the beryllium block attached to the side of the core is determined. The resulting (γ,n) reaction rate immediately establishes the strength of the neutron source.

Gamma source strengths were based on gamma spectrum data from NDA-27-39 (19). Establishment of the resulting gamma flux at the beryllium block was based on shielding methods given in TID 7004 (20) for a cylindrical source. Total gamma attenuation coefficients were also obtained from this reference. The microscopic beryllium (γ,n) cross section as a function of energy is given in Figure 6-2*.

Reference to the above sources of information reveals the following facts. Approximately 95 percent of the (γ,n) reaction is due to the 2.5 Mev gamma of La^{140}. For the other gammas of interest the attenuation coefficient differs little from that appropriate for the 2.5 Mev gamma. Therefore, gammas other than those of energy 2.5 Mev were weighted only with the Be cross section. Hence, only one shielding calculation is necessary. Further, gammas other than the 2.5 Mev of La^{140} can be considered as one gamma of energy 2 Mev with a yield equal to that of the total given in NDA-27-39 for Group V (1.8-2.3 Mev). Computations were based on yields given for 1000 hours and infinite operation at 10 megawatts (MW) and after one and ten days shut-down periods. The yield from La^{140} was taken as the total of Group VI (2.2-2.6 Mev).

* It will be noted that the gamma spectrum data and beryllium cross section used here are from different sources than that used in APAE 17. Those used here are felt to be more accurate.

Gamma Yield (S_γ)

	Energy Group Mev	Energy Per Gamma Mev	1 day shutdown $S_\gamma \sigma^{Be}$ photons-cm^2/sec	10 day shutdown photons-cm^2/sec
1000 hr operation	2.2-2.6	2.5	2.64×10^{-13}	1.80×10^{-13}
	1.8-2.2	2	5.94×10^{-14}	8.3×10^{-15}
		Total	3.23×10^{-13}	1.88×10^{-13}
	Error due to grouping		-11%	-1.1%
infinite operation	2.2-2.6	2.5	3.24×10^{-13}	2.04×10^{-13}
	1.8-2.2	2	7.30×10^{-14}	2.07×10^{-14}
		Total	3.97×10^{-13}	2.25×10^{-13}
	Error due to grouping		0.65%	3.7%

Gamma Flux

The beryllium block was considered a field point located midway on the side of a finite cylinder equivalent to the core. The quantity ϕ_γ/S_v at the beryllium block was computed from the shielding formula found in TID 7004(20).

ϕ_γ = gamma flux

S_v = gamma source strength per unit volume (gamma yield ÷ core volume; core volume = 1.395×10^5 cm.^{3})

One attenuation coefficient was used for a core consisting of 80% water, 19.6% iron, and 0.4% uranium. The total attenuation coefficient for an energy of 2.5 Mev was chosen. No build-up factor was used since scattering below the threshold energy of 1.64 Mev is effectively a removal.* (average attenuation coefficient = 0.0945 cm-1)

$\phi_\gamma/S_v = 4.14$ core radius = 28.19 cm

* Difference in results obtained with this one cylinder method is only 10% from that obtained by use of the three cylinder method suggested in APAE-17.

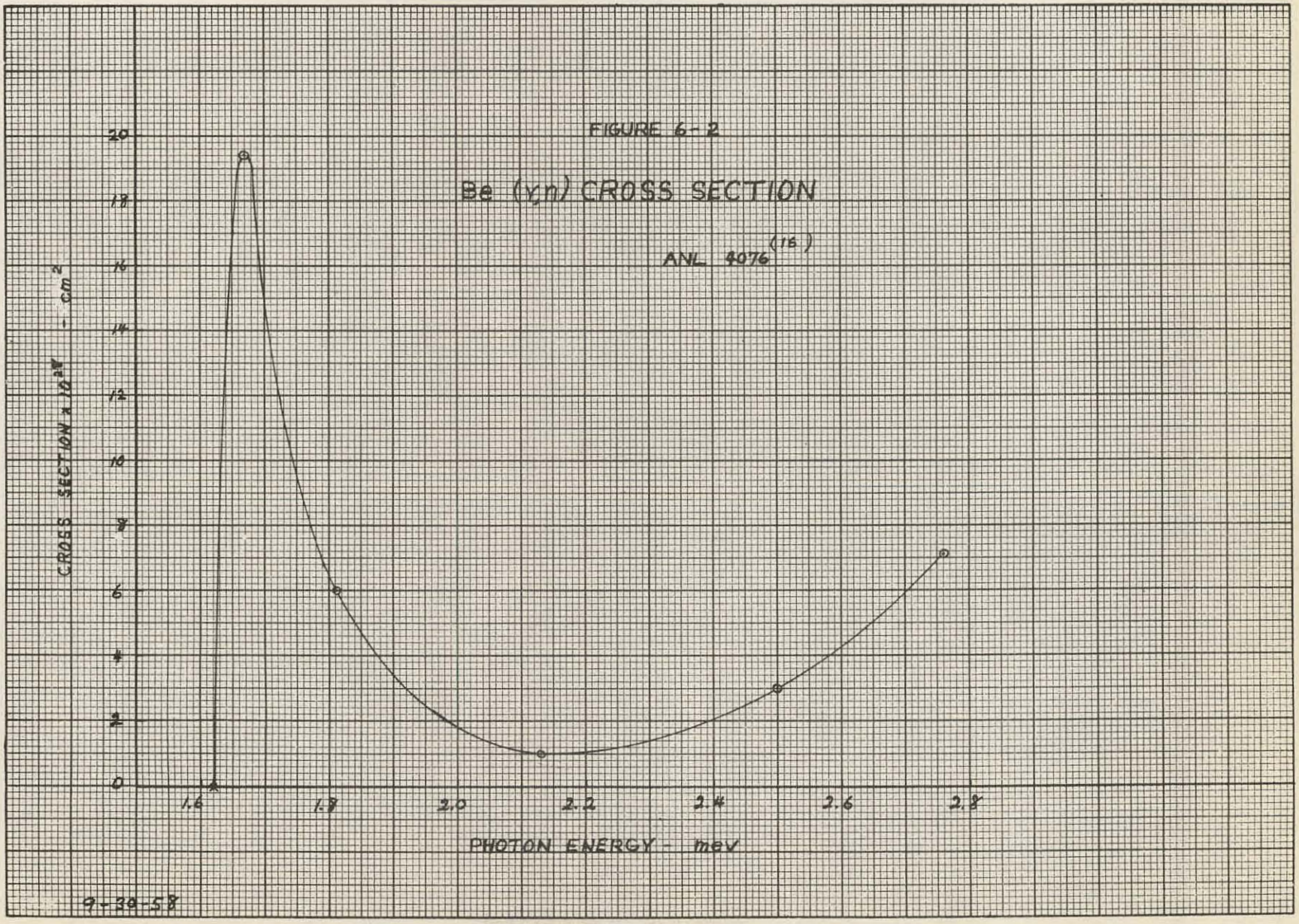
FIGURE 6-2
Be (γ,n) CROSS SECTION
ANL 4076 (16)
CROSS SECTION x 10^28 - cm^2
20
18
16
14
12
10
8
6
4
2
0
1.6
1.8
2.0
2.2
2.4
2.6
2.8
PHOTON ENERGY - mev
9-30-58

The expression for the resulting neutron source strength follows.

$$S = \phi_\gamma \sigma_{Be_N} Be_{\nu Be}$$

N^{Be} = number density

= $.1236 \times 10^{24}$ nuclei/cm.^{3}

ν^{Be} = volume beryllium

= 73.6 cm.^{3}

Source strengths for 1000 hour and infinite operation times after one and ten day shutdown periods were readily obtainable with the use of the corresponding gamma yields. To obtain the source strength for operating times corresponding to 6.15 megawatt years and 5.08 day shutdown (needed to correlate measured count rate), linear interpolation between the above points was employed** The result follows:

$$S = 7.4 \times 10^7 \text{ neutron/sec.}$$

Computation of the resulting count rate utilizes much of the same data used with the Po-Be source. However, the value $\bar{\phi}/S$ must be corrected for core burnout. For 6.15 megawatt years of operation,

$$\Delta K_{eff} = -0.023 \text{ estimated from rod bank measurements}$$

Reference to Figure 6-1 gives the following corresponding correction factor.

burnup correction = .557

Therefore, $\bar{\phi}/S = (.557)\ (3.79 \times 10^{-4})$

$= 2.11 \times 10^{-4}$ cm^{-2}

count rate $= S \times \frac{\bar{\phi}}{S} \times \frac{\phi}{\bar{\phi}}$ peak $\times \frac{\phi_{eff}}{\bar{\phi}_{peak}}$ x counter sensitivity ***

$= (7.4 \times 10^7)\ (2.11 \times 10^{-4})\ (2.09 \times 10^{-4})\ (.32) \times (4.5)$

$= 4.69$ cps

Measured value is 4 cps. Therefore, correction factor is

$$C = \frac{4}{4.69}$$

$$= .85$$

** Infinite operation was considered to be 10,000 hrs. Operation was assumed to be continuous at 10 Mw.

***The values $\phi_{peak}/\bar{\phi}$ and ϕ_{eff}/ϕ_{peak} used here differ from those employed in connection with the Po-Be source. The reason is due to the fact that boron was added to the shield water before the second count rate was measured. Flux distribution from which these values were obtained can be found in Fig. 1.2 and 1.3 of APAE 35 (15).

6.2 Neutron start-up source strength - skid mounted reactor

Count rates were computed for given neutron sources and were found to be sufficient. Hence, these sources are specified for the 6.5 Mw Skid Mounted Reactor. Initial source estimates were based on those used in the APPR-1 and the resulting count rates.

6.2.1 Polonium-beryllium source

Prediction of count rate due to a given polonium-beryllium source follows. The method employed follows directly from Section 6.1.

1. A 15 curie polonium-beryllium source was chosen. Corresponding neutron strength is

$$S = 3.8 \times 10^7 \text{ neutrons/sec.}$$ p. 41, APAE 17 (14)

2. Shutdown initial K_{eff} was estimated to be 0.93 from rod worth and excess reactivity values

$$\bar{\phi}/S = 3.41 \times 10^{-4} \text{ cm.}^{-2}$$ Figure 6-1

3. $\bar{\phi} = \bar{\phi}/S \times S$
$= (3.41 \times 10^{-4})(3.8 \times 10^7)$
$= 1.295 \times 10^4$ n/cm^2-sec shutdown core flux

4. $\phi_{eff}/\bar{\phi} = 5.55 \times 10^{-4}$ (Includes transmission factor of .88 through steel tube enclosing counter) Figure 6-3

5. $\phi_{eff} = \phi_{eff}/\bar{\phi} \times \bar{\phi}$

$(5.55 \times 10^{-4})(1.295 \times 10^4)$

7.2 neutrons/cm^2-sec effective shutdown BF_3 counter flux

6. counter sensitivity = 4.5 cps/nv typical value

7. count rate = ϕ_{eff} x (counter sensitivity)

$= (7.2)(4.5)$

$= 32$ cps

6.2.2 Photo-neutron source

Prediction of count rate due to a beryllium - fission product gamma photo-neutron source follows. The method employed follows directly from Section 6.1.

FIGURE 6-3

STARTUP RADIAL FLUX DISTRIBUTION TO BF_3 COUNTER TUBE

(thermal neutrons)

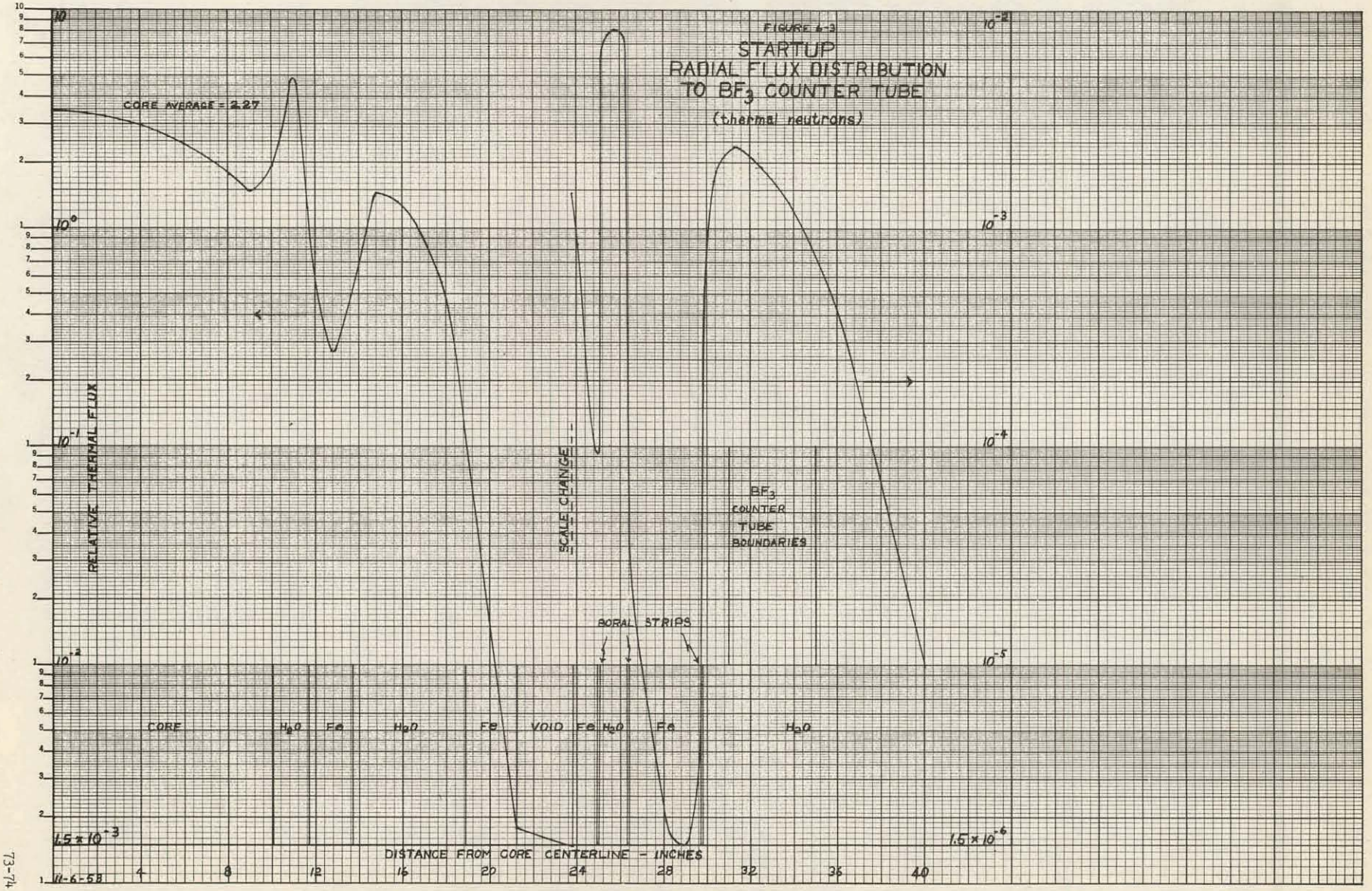

1. The source consists of a 0.5" x 3" x 12" beryllium block bombarded by fission product gammas.

2. Source strength calculations were based on 1000 hours of operation at 6.5 megawatts ten days after shut-down.

3. $S_\gamma \sigma^{Be} = 1.22 \times 10^{-13}$ photons-cm^2/sec — Section 6.1

4. $\phi_\gamma / S_V = 4.17$ — method of TID 7004 (20)

$S_V = S_\gamma$ / core volume

core volume = 1.15×10^5 cm.3

core radius = 25.6 cm.

assumed core composition = 80% H_2O; 19.6% Fe; 0.4% U

average attenuation coefficient = 0.0945 cm^{-1}

5. $S = \phi_\gamma \sigma^{Be} N^{Be} V^{Be}$ x correction factor

$= 1.03 \times 10^8$ neutrons/sec.

correction factor = .85

$N^{Be} = 0.1236 \times 10^{24}$

$V^{Be} = 220$ cm.3

This value assumes effective volume to be 0.75 actual volume.

6. $\bar{\phi}/S = 3.32 \times 10^{-4}$ cm.$^{-2}$ — Figure 6-1

Assumes $\Delta K_{eff} = 0.02$ based on 1.14 megawatt year operation for APPR-1, See Figure 3E Progress Report No. 6 (18).

7. $\phi_{eff}/\bar{\phi} = 5.55 \times 10^{-4}$ — Figure 6-3

Value includes transmission factor of 0.88 through steel tube enclosing counter.

8. Counter sensitivity = 4.5 cps/nv

9. Count rate = $S \times \frac{\bar{\phi}}{S} \times \frac{\phi_{eff}}{\bar{\phi}}$ x counter sensitivity

$= (1.03 \times 10^8)\ (3.32 \times 10^{-4})\ (5.55 \times 10^{-4})\ (4.5)$

= 85 counts per second

10. If the reactor remains shut-down for 81 days, the count will drop to approximately 2 cps. This value is based on the decay of the 2.2-2.6 Mev gamma group as given in NDA-27-39 (19).

11. Count rate at the end of core life was estimated as follows:

Infinite operation at 6.5 megawatts and ten day shut-down is assumed. The value of step 9 was corrected for this longer operation time and for the change in shut-down K_{eff}.

operation time correction = 1.13 reference (19)

correction due to K_{eff} = 0.29 Based on Figure 6-1 assuming $\Delta K_{eff} = 0.062$. See reference (18)

count rate = (85) (1.13) (.29)

= 28 cps

6.2.3 Conclusion

The following start-up neutron sources should be incorporated in the 6.5 Mw Skid Mounted Core.

15 curie Po-Be source

0.5" x 3" x 12" beryllium block

The resulting count rate at shut-down will be quite adequate for start-up for any reasonable operational program during the lifetime of the core. Sufficient margin is allowed in the event there is considerable delay in transporting the Po-Be source due to the unique geographical location of the reactor.

7.0 ANALYSIS OF SPENT FUEL PIT CRITICALITY

Calculations were performed to show that the reactivity of the spent fuel pit will at no time exceed 0.70.

The calculated method chosen was that of modified two group theory.

The expression for reactivity follows:

$$K = \frac{\eta f p}{(1 + B^2 \tau)(1 + B^2 L^2)} + \frac{\eta_r f_r (1 - p)}{(1 + B^2 \tau)}$$

K = total reactivity

η = neutrons per fuel absorption (thermal)

f = thermal utilization

η_r = neutrons per fuel absorption (resonance)

f_r = resonance utilization

B^2 = buckling

τ = age to thermal

L = thermal diffusion length

p = resonance escape probability

The fuel elements are to be stored within a 1% boron steel lattice 1/4" thick immersed in water.* To insure a conservative result the following assumptions were made:

1. Only fresh fuel elements are stored (no control rod elements).
2. Lattice is filled to capacity, including the space taken up by the hopper.
3. Self-shielding factor of one is used for the fuel element.
4. There is no thermal leakage. $\left(\frac{1}{1+B^2L^2} = 1\right)$

Thermal constants were computed for a homogenized core but utilized a self-shielding factor for the boron steel absorption. This self-shielding factor was computed by the P_3 Code for slab geometry. Fast constants were computed by the MUFT III Code, utilizing homogenized number densities. The final results follow:

Thermal contribution = .500
Fast contribution = .144

K = .644

* Boron steel containing one percent boron possesses good mechanical properties and is readily available. Hence, this boron concentration was chosen, and the necessary total boron content of the pit adjusted by controlling the lattice thickness. The resulting 1/4" value is quite compatible with mechanical considerations.

7.1 Calculation model

Detailed steps of the computation are given below:

Diameter of spent fuel pit: $2R = 32$ in.
$R = 40.6$ cm

Volume fractions:

fuel element	$f^f = .526$
1% boron steel lattice	$f^b = .117$
water gaps (exterior to fuel element)	$f^w = .357$
	1.000

Thermal Contribution

Absorption cross sections:

fuel element	$\Sigma^f = .3914$ cm^{-1}
U^{235}	$\Sigma^{25} = .302$
1% boron steel	$\Sigma^b = 3.58$
water	$\Sigma^w = .0221$

Self-shielding factor boron steel:

The P_3 approximation was used for slab geometry to determine a self-shielding factor for the boron steel absorption. The geometry incorporated is pictured below:

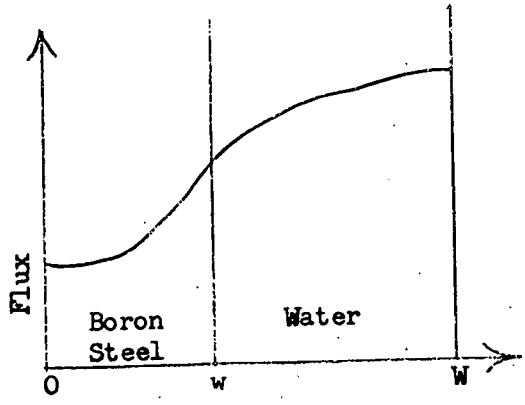

Distance from Steel Center

$w = .318$ cm (1/8")

$W-w = .320$ cm

W was taken where flux peak was thought to occur.

$\Sigma^b = 3.58\ cm^{-1}$

$\Sigma_s^b = 0.918\ cm^{-1}$ boron steel scattering cross section

$1-\mu_o = 0.988$ 1- average cosine of scattering angle, boron steel

$\Sigma^w = 0.0221\ cm^{-1}$

$\Sigma_s^w = 3.0\ cm^{-1}$ H_2O scattering cross section (based on measured diffusion length)

$1-\mu_o^w = .676$ 1- average cosine of scattering angle, H_2O

Self-shielding factor was taken to be the value at the water-steel interface divided by the average flux in the steel. This self-shielding factor was found to be:

$$S = .40$$

Thermal utilization follows:

$$f = \frac{f^f \Sigma^{25}}{f^f \Sigma^f + S f^b \Sigma^b + f^w \Sigma^w}$$

$$= \frac{(.526)(.302)}{(.526)(.391) + (.40)(.117)(3.58) + (.357)(.0221)}$$

$$= .418$$

$$\eta = 2.077$$

$$\eta f = .870$$

Fast Contribution

Homogenized number densities corresponding to the core and volume fractions listed earlier were used as input for the MUFT III Code. The resulting fast group constants appear below:

$$\gamma = 31.1 \qquad \eta_r f_r = \frac{\nu \Sigma_f}{\Sigma_a} \qquad p = .67$$

$$= 0.51$$

Axial buckling was taken to be that of the core. (Table 2-1)

$$B_z^2 = .00191$$

Geometric buckling is used in the radial direction.

$$B_r^2 = \left(\frac{jo}{R}\right)^2$$

$$= \left(\frac{2.405}{40.6}\right)^2$$

$$= .00352$$

Total buckling

$$B^2 = B_z^2 + B_r^2$$

$$= .00543$$

Fast leakage

$$\alpha_f = \frac{1}{1 + B^2 \tau}$$

$$= \frac{1}{1 + (.00543)(31.1)} = .856$$

Total Reactivity

The expression for total reactivity follows. Recall that the thermal non-leakage factor is taken as unity.

$$K = \frac{\eta f p}{1 + B^2 \tau} + \frac{\eta_n f_n (1-p)}{1 + B^2 \tau}$$

$$= (.870)(.67)(.856) + (.51)(.33)(.856)$$

$$= .500 + .144$$

$$= .644$$

7.2 Comparison with ZPE

This low value of reactivity is compatible with ZPE experiments. It will be noted on p. 50 of APAE-21 (21) that the value of B-10 mass per fuel element required for criticality is .775 gm per fuel element. The 1% boron steel lattice used in the Skid Mounted spent fuel pit results in a value of 9 gm per fuel element for lattice height equal to that of the active element.

7.3 Conclusion

To insure sub-criticality of the spent fuel pit, the stored fuel elements should be placed in individual cells of a lattice possessing the following characteristics:

1. Minimum height of lattice is equal that of the active fuel element height with element in stored position.

2. Lattice material consists of 1% boron steel in 1/4" plates.

3. Center-to-center dimension of an individual cell is 3.5"

4. For shielding and cooling purposes the entire pit is filled with water.

The reactivity of such a spent fuel pit loaded to maximum capacity (52 elements)* with fresh APPR-1 type elements will not exceed 0.70 and hence pose no criticality problem.

7.4 Relocation effect

To facilitate a more feasible operating program and to reduce shielding requirements, the spent fuel pit has been relocated outside the vapor container. Though the design capacity has been increased to 49 fuel elements (7 x 7 array), the radius of the equivalent cylinder is smaller than that designated in the foregoing criticality calculation. Therefore, the corresponding value of effective multiplication will be lower, and the conclusions concerning criticality given in Section 7.3 remain valid.

* Design capacity is 46 elements. Conceivably, however, six additional elements could inadvertently be fitted into the space allowed for the loading hopper.

8.0 Nomenclature

B	Fraction burnout
B^2 Cm^{-2}	Buckling
D_f Cm	Fast diffusion coefficient
D_{th} Cm	Thermal diffusion coefficient
g'	Thermal shielding factor
K_f	Fast multiplication factor
K_{th}	Thermal multiplication factor
K_{eff}	Effective multiplication factor of core
L Cm	Diffusion length
N^{25} atoms/cm^3	U-235 atom concentration
N^{B-10} atoms/cm^3	Boron-10 atom concentration
p	Resonance escape probability
P MW	Reactor power
S_r	Radial reflector savings
S_z	Axial reflector savings
t Sec	Time
V Cm^3	Core volume
α	Xenon non-uniform factor
α_f	Fast U-235 capture to fission ratio
α_{th}	Thermal U-235 capture to fission ratio
β	Fraction thermal fissions
γ_1	Iodine fraction fission yield
∇^2	Laplacian Operator
γ_2	Xenon fraction fission yield
λ_1 sec^{-1}	Iodine decay constant
λ_2 sec^{-1}	Xenon decay constant

$\nu \Sigma_{th}^{f}$	neuts/cm	Neutrons per fission times thermal macroscopic fission cross section
ρ		Percent reactivity $\frac{K_{eff}-1}{K_{eff}}$
σ_{th}^{a-B}	cm^2	Boron-10 thermal absorption cross section
σ_{f}^{a-B}	cm^2	Boron-10 fast absorption cross section
σ_{th}^{a}	cm^2	U-235 thermal absorption cross section
σ_{f}^{a}	cm^2	U-235 fast absorption cross section
σ_{th}^{f}	cm^2	U-235 thermal fission cross section
$\sigma_{f_a}^{f}$	cm^2	U-235 fast fission cross section
σ_{xe}	cm^2	Xenon thermal absorption cross section
Σ_{th}^{a}	cm^{-1}	Macroscopic thermal absorption cross section
Σ_{xe}^{a}	cm^{-1}	Macroscopic xenon absorption cross section
Σ^{p}	cm^{-1}	Rod bank equivalent poison cross section
Σ_{a}^{sub}	cm^{-1}	Cross section representing effect of substituting 5 control rod elements for 5 fixed elements
Σ^{s}		Macroscopic scattering cross section
Σ^{tr}		Macroscopic transport cross section
Σ^{r}		Macroscopic removal (slowing down) cross section
τ	cm^2	Fermi age
ϕ_{th}	neuts/cm^2-sec	Thermal flux
ϕ_{f}	neuts/cm^2-sec	Fast flux
$\bar{\phi}_{real}^{th}$	neuts/cm^2-sec	Real average thermal flux in core
$\bar{\phi}'_{region}$		Average region flux from Valprod or Windowshade
$\bar{\phi}_{core}$		Average core flux from Valprod or Windowshade

9.0 References

(1) G.J. Habetler "One Space Dimensional Multigroup for the IBM-650, Part I, Equations", KAPL - 1415, December, 1955.

(2) P.V. Oby, "Modified Two-Group Multiregion Calculation using the Valprod Code for the IBM-650", APAE Note 24 (Revised) Aug. 14, 1957.

(3) F.B. Fairbanks, "Two Group Multiregion Axial Windowshade Calculations on the IBM-650", APAE Memo 88, March 29, 1957.

(4) S.S. Rosen, "Supplement to MUFT III Code Multiregion Fourier Transform Calculation", AP Note 90, Dec. 6, 1957.

(5) B.J. Byrne, R.L. Caton, "Two Dimensional P_3 Calculation for APPR Type Fixed Fuel Elements", AP Note 96, February 14, 1958.

(6) B.J. Byrne, P.V. Oby, "Analysis of Extended Zero Power Experiments on the Army Package Power Reactor ZPE-2", APAE 27, May 7, 1958.

(7) T.G. Williamson, M.J. Leibson, B.J. Byrne, "Reactor Analysis APPR-1 Core II", APAE-32, July 15, 1958.

(8) P.V. Oby, "Scram I: Control Rod Worth Calculation on the IBM 650", APAE Memo 89, April 16, 1957.

(9) S.D. MacKay, H.W. Geisler, J.W. Noaks, "Extended Zero Power Experiments on the Army Package Power Reactor ZPE-2", APAE-21, Nov. 15, 1957.

(10) J.W. Noaks, W.R. Johnson "Army Package Power Reactor Zero Power Experiments ZPE-1", APAE 8, Feb. 8, 1957.

(11) S.D. MacKay, "Progress Report No. 6, Task Number VII Contract No. AT(30-3)-326", Aug. 21 to Sept. 20, 1958.

(12) T.G. Williamson, "APPR-1 Burnout Calculations", APAE Memo 126, April 10, 1958, and AP Note 117.

(13) S.D. MacKay, "Progress Report No. 5, Task Number VII, Contract No. AT(30-3)-326 July 21 to Aug. 20, 1958.

(14) "Phase III Report Army Package Power Reactor Field Unit No. 1 APPR-1a Design Analysis, Volume 1" APAE 17, May 15, 1957.

(15) S.S. Rosen, et al, "APPR-1 Research and Development Program Shielding Experiments and Analysis Task No. VI", APAE 35, Oct. 15, 1958.

(16) "Experimental Nuclear Physics Div. and Theoretical Nuclear Physics Div. Report for July, Aug. and Sept. 1947", Argonne National Lab. 47, ANL-4076.

(17) J. Meem, et al, APPR-1 "Operating Log, Feb. 28 to Apr. 23, 1957" AP Note 59.

(18) S.D. MacKay and D.C. Tubbs, Task No. VII, Program Report No. 6, Aug. 21, to Sept. 20, 1958.

(19) F.J. Clark "Decay of Fission Product Gammas", NDA-27-39, Dec. 30, 1954.

(20) Theodore Rockwell III, "Reactor Shielding Design Manual", TID-7004, March, 1956.

(21) J.W. Noaks, et al, Extended Zero Power Experiments on the Army Package Power Reactor ZPE-2, APAE 21, Nov. 15, 1957.

(22) S.D. MacKay, Task No. VII, Progress Report No. 4, June 21 to July 20.

(23) Tsu and Beecher "Thermodynamic Properties of Compressed Water".

(24) S.D. MacKay, "Progress Report No. 1, Task Number VII".

(25) F.C. Brooks and H.L. Glick, "The Fast Neutron Flux Spectrum of a Proton Moderated Thermal Reactor", WAPD-45, November, 1951.

B. SHIELDING DESIGN ANALYSIS

1.0 CONTRACT DESIGN REQUIREMENTS

Shielding design requirements for the 6.5 tMw permafrost reactor are:

1. Shielding must be adequate to permit access to the primary skid 2.5 hours after shutdown.

2. Shielding must be adequate to permit operating personnel working an 84-hour week to conform to government established radiation tolerance standards which allow an average integrated total body dose of 300 millirem per week (mr/wk). A maximum permissible integrated total body exposure of 3 rem may be received in a period of any short duration within a thirteen consecutive week period and annual exposure may not exceed 5 rem/year.

3. Shielding must be adequate to permit routine access around the secondary shielding and to permit removal of spent fuel elements from the spent fuel pit during reactor operation.

1.1 Design Dose Rates at Various Locations and Operating Conditions

Table 1-1 indicates the maximum permissible design dose rates at selected important locations for both shutdown and operating conditions and includes calculated dose rates at these locations. The site layout is shown in Dwg.

All shielding calculations were made for infinite operation at 6.5 Mw. During normal operation, personnel at the control console and turbine-generator skids should not receive more than the tolerance dose rate. (Dose rates at other skids will be smaller since they are farther from the vapor container.) As used here, tolerance refers to a dose rate of 1.19 mr/hr, while gives a dose of 100 mr in an 84-hour week. As is pointed out in succeeding sections, conservative calculational methods will insure that actual measured dose rates will be considerably lower than those calculated and will therefore allow a margin for performing short time maintenance operations in relatively high radiation areas.

The design dose rate from the reactor and primary shield has been set at 50 mr/hr at 2-1/2 hours after shutdown. With the primary shield as designed, the dose rate will be about 33 mr/hr after 2-1/2 hours shutdown.

Spent fuel pit shielding has been designed to give the maximum permissible design dose rate of 1 mr/hr 24 hours after shutdown.

The sides and ends of the secondary shielding structure are designed to give 30 mr/hr on the surface during operation except where this dose rate must be lowered for the benefit of manned stations in the secondary system.

The top and bottom of the secondary shield structure are designed to prevent excessive scattering of radiation into the area around the sides of the structure. Top and bottom shielding does not permit routine access on top or under the shield structure during operation.

Table 1-1

Radiation Dose Rate from 6.5 Mw Permafrost Reactor

	Design Specification mr/hr	Calculated mr/hr
1. Normal Operation		
1.1 Control Console Skid	1.19	0.87
1.2 Turbine Generator Skid	1.19	0.87
1.3 Feed Water and Heat Exchanger Skid	1.5	1.5
1.4 Surface of Secondary Shield	30	24.2
2. Equipment Maintenance after Reactor Shutdown		
2.1 Dose Rate on Surface of Primary Shield Tank - 2-1/2 hrs. after Shutdown	50	33
3. Dose Rate outside Spent Fuel Pit Shielding (24 hours after shutdown)	1	1

1.2 General Design Principles

During reactor operation, activation of the primary coolant results in all parts of the primary system becoming severe gamma sources. This radiation has a 7.4 sec. half life. After shutdown, this source decays rapidly and the activity drops to a level at which no shielding is required for this radiation, even to work near the primary system. Consequently, considerable shielding of the primary system is necessary only during reactor operation. This shielding is accomplished by the concrete which separates the vapor container from the manned stations of the installation.

The reactor requires a considerably greater amount of radiation attenuation during operation than the primary coolant. With the reactor shut down, the radiation level is greatly reduced, but considerable shielding is still needed to protect personnel working in the vapor container from accumulated fission product activity in the core. These two functions are accomplished by the primary shield surrounding the reactor vessel.

The shielding available in the primary shield is described in Table 1-2.

Since the Skid Mounted Reactor must be air transportable, the primary shielding design principle is that the shielding weight on the primary skid must be kept to an absolute minimum. This principle dictates that the pressure vessel be of the minimum possible diameter which will survive radiation damage and thermal stresses. All shield rings must also be of a minimum diameter to give a shield tank of minimum weight.

Because of the stringent restrictions on weight and outside diameter of the primary shield, no optimization between primary and secondary shielding has been attempted. The primary shield has been designed to meet the minimum requirement of access to the primary skid after shutdown.

Table 1-2

Description of Primary Shield - Radial

Description	Material	Outer Radius Inches	Thickness Inches
Core	-	10.08*	-
Reflector	Primary Water	11.76	1.68
Thermal Shield	Stainless Steel	13.76	2.00
Cooling Passage	Primary Water	18.88	5.12
Pressure Vessel Cladding	Stainless Steel	19.00	0.12
Pressure Vessel	Carbon Steel	21.38	2.38
Insulation	(Considered Void)	23.38	2.00
Insulation Retainer	Steel	23.50	0.12
Clearance	Void	24.05	0.55
Pressure Vessel Support Ring	Steel	25.05	1.00
P.V. Support Ring Cladding	Boral	25.175	0.125
Cooling Passage	Shield Water	26.425	1.25
Shield Ring Cladding	Boral	26.550	0.125
1st Shield Ring	Steel	29.800	3.25
Shield Ring Cladding	Boral	29.925	0.125
Cooling Passage	Shield Water	31.175	1.25
Shield Ring Cladding	Boral	31.300	0.125
2nd Shield Ring	Steel	34.550	3.25
Shield Ring Cladding	Boral	34.675	0.125
Cooling Passage	Shield Water	35.925	1.25
Shield Ring Cladding	Boral	36.050	0.125
3rd Shield Ring	Steel	39.300	3.25
Shield Ring Cladding	Boral	39.425	0.125
Cooling Passage	Shield Water	40.675	1.25
Shield Ring Cladding	Boral	40.800	0.125
4th Shield Ring	Steel	44.050	3.25
Shield Ring Cladding	Boral	44.175	0.125
Neutron Shield	Shield Water	51.000	6.825
Tank Wall Cladding	Boral	51.125	0.125
Tank Wall	Steel	51.500	0.375

* Equivalent radius based on actual core cross-section

2.0 PRIMARY SHIELD ANALYSIS

The basic purpose of the primary shield is to attenuate neutron and gamma radiation escaping from the core to acceptable dose rate levels. However, the primary shield itself becomes activated due to capture of neutrons escaping from the core and therefore becomes a source of gamma radiation. The problem then becomes that of achieving the required attenuation of core radiation with the minimum amount of shielding activation. Shield activation may be minimized by judicious choice and spatial arrangement of shielding materials.

The primary shield analysis was completed using the shielding codes developed at Alco. Dose rates from these shielding codes have been checked against experimental measurements in the APPR-1 and calculated dose rates have been found to be consistently higher than those measured (see Ref. 1). In addition, a hand calculation of the dose rate from the core after shutdown om the surface of the shield tank for the skid mounted configuration was made to check the machine output.

2.1 Configurations Considered

The basic configuration considered for the primary shielding is similar to that of APPR-1 in that it is made up of concentric annuli of water and steel. However, in the Skid Mounted shield the steel rings are clad on both sides with Boral to reduce activation by thermal neutron capture.

Since most of the dose after shutdown comes from the core, thermal shield and pressure vessel the dose is quite insensitive to the arrangement of the steel rings in the shield tank, that is, the calculated dose rate is a function only of the total steel thickness in the shield tank. Therefore, the arrangement of the shield rings in the tank was dictated by weight and mechanical rather than shielding considerations.

2.2 Reference Configuration

The reference configuration is shown in Dwg. No. R9-46-1039 and described in Table 1-1. There are four 3-1/4-inch steel rings sandwiched between 1/8-inch Boral sheets in the shield. The Boral-steel sandwiches are separated by 1-1/4 inches of water. The inner surface of the outer tank wall and the outer surface of the pressure vessel support ring are also clad with Boral.

2.3 Shutdown Dose Calculation

After shutdown significant contributions to the dose rate in the vapor container are made by:

1. Fission products and activated steel in core.
2. Activated steel in the primary shield.
3. Activated components around the primary shield.
4. Activated corrosion products in primary coolant.

Of the above four sources, only the first two lend themselves to fairly rigorous theoretical analysis. For the last two sources use must be made of data accumulated during APPR-1 operation.

2.3.1 Calculational Model

2.3.1.1 Core Source and Attenuation

The core was considered a volumetric source uniformly distributed in the form of a cylinder. The well known equation for calculation of the dose rate from such a source was taken from the "Reactor Shielding Design Manual"(2) and for a point opposite the core midpoint is:

Eq. 2.2 $$D = \frac{BS_v R_o^2}{2(a + z)} F(\theta, b_2) \times \frac{1}{K_D}$$

K_D = factor for converting from flux to dose

Other symbols defined in TID 7004 (2)

Fission product decay gammas are usually divided into seven energy groups. Data on the seven groups are available in "Decay of Fission Product Gammas"(3) and "Fission Product Decay Gamma Energy Spectrum"(4). Volumetric source strengths for the seven groups taken from Ref. 3 are listed in Table 2-1.

Activation gammas from stainless steel in the core were also considered. Activation gamma production calculations are outlined in Sections 2.3.1.2 and 2.3.3.

2.3.1.2 Activation Sources and Attenuation

The activated steel rings in the primary shield were treated as infinite slabs and a correction applied to account for the actual cylindrical geometry. The basic equation from TID 7004 (2) with the cylindrical correction is:

Eq. 2.1 $$D = \sqrt{\frac{r_s}{r_D}} \times \frac{BS_v}{2\mu_s} \left[E_2(b_1) - E_2(b_3)\right] \times \frac{1}{K_D}$$

r_s = radius of cylindrical source
r_D = radius of cylindrical surface through dose point
K_D = factor for converting from flux to dose

Other symbols as defined in TID 7004 (2)

Each steel slab is divided into thinner slabs and each thin slab is attenuated through all material between the slab and the dose point.

Since Boral is applied to steel surfaces exposed to water in the shield tank, thermal flux and hence thermal activation of the steel is reduced to a minimum. However, the Boral has a much smaller effect on the fast flux and fast activation. Resonance integrals of Pomerance and Macklin (5) were used to calculate activation of the shielding materials by the fast flux.

Data on gamma yields from activated elements were taken from the Activation Handbook (6). The compositions of carbon and stainless steel used in the calculation follow.

	Composition of 304 Stainless Steel (ρ = 7.9 gm/cm^3)
Carbon	0.08% by weight
Manganese	2.00
Silicon	1.00
Chromium	19.00
Nickel	9.50
Cobalt	0.05
Iron (by difference)	68.37

	Carbon Steel - C-1015 (ρ = 7.84 gm/cm^3)
Carbon	0.15% by weight
Manganese	0.53
Phosphorus	0.018
Sulphur	0.031
Silicon	0.17
Cobalt	0.01
Iron (by difference)	99.091

Stainless steel composition, except for cobalt content, was taken from Allegheny Ludlum Blue Sheet for Allegheny Metal 18-8 (7). Carbon steel composition, except for cobalt, was taken from Modern Steels and Their Properties (8). Cobalt content of both stainless and carbon steel was taken from Bopp and Sisman (9).

In the machine calculation, at 2.5 hrs. after shutdown, the decay gammas from stainless and carbon steel are lumped into one energy group having an average energy of 1.65 Mev. Materials are assumed to have been exposed long enough so that all activities are saturated.

TABLE 2-1

Fission Product Source Strengths after Shutdown

$$\left(S_v \ \frac{\text{Mev}}{\text{sec - cm}^3} \right)$$

Group	Energy Range (Mev)	Effective Energy	2.5 hrs. after shutdown		1 day after shutdown	
			∞ - Operation	1000-hr Operation	∞-Operation	1000-hr Operation
1	0.1 - 0.4	0.35	8.9×10^{10}	8.39×10^{10}	7.21×10^{10}	6.56×10^{10}
2	0.4 - 0.9	0.75	5.77×10^{11}	4.4×10^{11}	4.13×10^{11}	2.74×10^{11}
3	0.9 - 1.35	1.35	6.05×10^{10}	6.05×10^{10}	6.83×10^{9}	6.75×10^{9}
4	1.35 - 1.8	1.6	2.40×10^{11}	1.84×10^{11}	1.76×10^{11}	1.59×10^{11}
5	1.8 - 2.2	2.10	6.75×10^{10}	6.64×10^{10}	4.58×10^{9}	3.74×10^{9}
6	2.2 - 2.6	2.5	1.89×10^{10}	1.73×10^{10}	1.52×10^{10}	1.24×10^{10}
7	2.80	2.80	9.04×10^{8}	9.04×10^{8}	4.4×10^{6}	4.4×10^{6}

Core Volume = 1.15×10^{5} cm^3

Po = 6.5 Mw

For short times after shutdown (< 10 hrs) Mn^{56} is the chief source of radiation in carbon and stainless steels. For longer times after shutdown Fe^{59} and Co^{60} become the chief sources.

Activation analysis of the skid-mounted shielding is complicated by the fact that the steel surfaces exposed to water in the shield tank are covered with Boral to reduce activation due to thermal neutron capture. However, the Boral has a smaller effect on the fast flux and fast activation, which is ordinarily negligible when compared to thermal activation.

Little work has been done on fast flux activation of shielding materials in configurations such as the skid-mounted and APPR-1 shields. The approach used in the machine calculation is to use the resonance integrals of Pomerance and Macklin (5), and assume the fast flux to be proportional to 1/E. The use of the resonance integrals of Ref. 5 will give an overestimate of fast activation because they are based upon foil activation (no self-shielding) whereas the shield is made up of massive slabs of steel.

No experimental data are available on fast activation of large slabs of steel. Data are available on thermal activation (see Ref. 10); thermal activation sources from the machine were found to check closely with the data of Ref. 10.

2.3.1.3 Model Comparison with APPR-1 Measurements

Since the skid-mounted shielding is similar to that of APPR-1, it appears worthwhile to make use of APPR-1 experimental data to approximate the skid mounted dose rate. With this purpose in mind all the materials in the skid-mounted shielding were combined and the calculated skid mounted dose rate compared to the measured dose rate at a corresponding point in the APPR-1 shield. Since the exposed steel in the skid-mounted shield tank is Boral clad, the data from APPR-1 represents an upper limit for the skid mounted dose rate.

Total shielding between the skid mounted core and the outside of the shield tank is as follows:

6.79 inches water @ ρ = 0.8 gm/cm^3
12.44 inches water @ ρ = 0.98 gm/cm^3
18.775 inches steel

The closest corresponding point in the APPR-1 shield is between the seventh and eighth shield rings. This region has the following materials between the dose point and the core.

10.7 inches water @ ρ = 0.8 gm/cm^3
6.25 inches water @ ρ = 0.98 gm/cm^3
18.75 inches steel

The dose rate in this region of the APPR-1 at 2.5 hrs. after shutdown from Fig. 293 of APAE 35 (1) is about 130 mr/hr.

Comparison of the skid mounted dose rate to APPR-1 experimental measurements is valid at 2.5 hours after shutdown because the Mn^{56} activity is the chief source of radiation at this time and was saturated in APPR-1 before doses were measured.

2.3.2 Dose from Core

The dose rate from the core was calculated both by hand and with the IBM 650 machine code developed by Alco. The two calculations employ the basic equation of Section 2.3.1.1 with minor differences which will be detailed in the following sections.

2.3.2.1 Machine Calculation

Complete details of the Machine Calculation are contained in APAE 35 (1) and APAE Memo 142 (11).

In the machine calculation, at 2.5 hours after shutdown, the fission product decay gammas of Groups 3, 4, 5, 6, 7 of Table 2-1 are lumped into one group which is assumed to have an effective energy of 1.65 Mev and the 650 machine calculates attenuation through the shield and buildup for gammas of this energy. Groups 1 and 2 of Table 2-1 are also lumped into one group, but the dose rate from this group is negligible in comparison to Groups 3, 4, 5, 6 and 7 of Table 2-1.

The first part of the machine program calculates S_v (gammas/sec-cm^3) and μ_c(cm^{-1}) the linear absorption coefficient in the core. S_v is calculated from the following equation (see Ref. 1).

$$S_v = \sum_i V_i \left[\bar{\phi}_{th} F_i + \bar{\phi}_f G_i \right] \qquad (2\text{-}3)$$

S_v = source strength, gammas/sec-cm^3 (assumed to be at 1.65 Mev)
V_i = volume fraction of material i in the core
$\bar{\phi}_{th}$ = average full power thermal neutron flux in the core, neutrons/cm^2-sec
$\bar{\phi}_f$ = average full power fast neutron flux in the core, neutrons/cm^2-sec
F_i = gammas/cm^3-sec arising in material i per unit thermal neutron flux
G_i = gammas/cm^3-sec arising in material i per unit fast neutron flux

(See APAE 35 (1) for complete details.)

Files of F and G factors for core materials (U^{235} and stainless steel) are available for the machine calculation for various times after shutdown. Therefore, only the average fast and thermal neutron fluxes in the core and the material volume fractions are necessary as input to the machine calculations to calculate S_v.

The actual average thermal flux is 1.5×10^{13}. However, material in file on U^{235} is based upon the fission cross section of U^{235} at 0.025 ev corrected for a Maxwellian distribution as follows:

$$\sigma^{f}_{0.025\ ev} = 580 \text{ barns}$$

$$\sigma^{f}_{thermal} = 0.886 \times 580 = 514 \text{ barns}$$

However, according to Appendix III, APAE Memo 126 (12), temperature and heterogeneous effects in APPR-1 reduce this cross section to 327 barns or about 0.65 times the value used in the machine files. In order to keep the files general, the cross section was left as it was and the average thermal flux was multiplied by 0.65 giving the average thermal flux listed in the input which follows:

Material	Volume Fraction*
H_2O	0.795207
Stainless Steel	0.173590
$U^{235}O_2$	0.017259

$\bar{\phi}_{th} = 9.8 \times 10^{12}$ neutrons/cm^2-sec

$\bar{\phi}_{fast} = 9.1 \times 10^{13}$ neutrons/cm^2-sec

* Sum is not 100% because some materials such as $U^{238}O_2$, B^{10}, C which do not effect S_v have been omitted.

The core absorption coefficient, μ_c is calculated by the machine as follows:

$$\mu_c = \sum_i V_i \mu_i$$

V_i = volume fraction of material i in the core.

μ_i = absorption coefficient of material i in the core.

Files of absorption coefficients for materials of interest are available. After calculating S_v and μ_c the machine calculates dose rate by Eq. 2.2. Repeating Eq. 2.2

$$D = \frac{BS_v R_o^2}{2(a+z)} F(\Theta, b_2) \times \frac{1}{K_D}$$

Input to this part of the machine program is merely the dimensions of the core and shielding materials from Table 1-1.

The machine calculates geometric and material attenuation to get the unscattered dose and then calculates and applies the dose buildup factor B to get the total dose.

Buildups are calculated and used in the following manner:

1) All thicknesses of the same material are summed up and a buildup factor for each material is calculated by the equation (2)

$$B = A_1 e^{-\alpha_1 b} + (1 - A_1) e^{-\alpha_2 b}$$

Files of buildup parameters A_1, α_1, α_2 from Ref. 2 are available for materials of interest.

2) The buildup factors are then multiplied together and the product applied to the unscattered gamma dose.

3) Buildup due to self-absorption in the core is not used.

Results of the machine calculation of the dose rate from the core at a point on the core midplane on the surface of the shield are:

$\mu_c = 0.1154$ cm^{-1} $\qquad$ $\mu_c Z = 1.66$

$B = 161$

$S_v = 3.1 \times 10^{11}$ $\frac{\text{gammas}}{\text{sec-cm}^3}$ @ 1.65 Mev

$\phi = 1.03 \times 10^4$ $\frac{\text{gammas}}{\text{sec-cm}^2}$ @ 1.65 Mev

D = 28.6 mr/hr

2.3.2.2 Hand Calculation

In the hand calculation each group of gammas of Table 2-1 is treated separately using the appropriate gamma absorption coefficients and buildup factors. Groups 1, 2 and 3 give a dose rate insignificant compared to that of Groups 4, 5, 6 and 7; therefore only the dose rates of the last four groups were calculated. Eq. 2.2 is the basic equation used.

In the hand calculation the buildup factor is treated differently from the way it is treated in the machine calculation. In the hand calculation the total number of relaxation lengths in the shield plus the "$\mu_c Z$" (a measure of self absorption in the core) is used for attenuation. A dose buildup factor corresponding to the total number of shield relaxation lengths plus "$\mu_c Z$" is applied. Iron buildup was used since steel is by far the most important shielding constituent of the shield. (Except for Group 4, water buildup is nearly the same as iron buildup.)

Complete details of the hand calculation are contained in Table 2-2. In addition to the calculation of Table 2-2 which is for 2.5 hours after shutdown, dose rates were also calculated at 12 and 24 hours after shutdown at a point on the shield surface opposite the core center. A summary of results follows:

Time After Shutdown, Hr.	Dose Rate from Core, mr/hr
2.5	15.8
12	7.5
24	6.4

2.3.3 Dose from Activated Materials in the Shield

The dose rate from the activated materials in the shield was calculated with the IBM 650 code developed by Alco. Complete details of the machine calculation are contained in APAE 35 (1) and APAE Memo 142 (11). Equation 2.1 is the basic equation employed.

Repeating Eq. 2.1:

$$D = \sqrt{\frac{r_s}{r_D}} \times \frac{BS_v}{2\mu_s} \left[E_2(b_1) - E_2(b_3) \right] \times \frac{1}{K_D}$$

(See Section 2.3.1.2 and TID 7004 (2) for definition of symbols.)

Briefly, S_v and B are calculated as in the core calculation described in Section 2.3.2.1. Files are available which contain data on neutron cross sections, gamma yields, gamma absorption coefficients and buildup parameters for different shielding materials including carbon and stainless steel. Files are also made up so that S_v may be calculated for various times after shutdown.

At times shorter than 12 hours after shutdown, gammas from activated shield materials are put into two energy groups. All gammas below 1 Mev are considered to have an average energy of 0.75 Mev; all gammas above 1 Mev are considered to have an average energy of 1.65 Mev.

TABLE 2-2

Hand Calculation of Dose Rate from Core

R_o = 25.6 cm t_{Fe} = 48.2 cm (Assumes contribution of 0.92 cm due to Boral)
h = 55.9 cm t_{H_2O} = 44.4 cm (Assumes density of 0.8 gm/cm^3 for reflector H_2O)

Infinite operation at 6.5×10^6 watts a = 96.09 cm
2 1/2 hours after shutdown core composition: 79.5% H_2O ; 20.5% Fe

Gamma Group	Group Energy Yield (Mev/sec-watt)	Energy Per Photon (Mev)	Volumetric Source (S_v) (photons/cm^3-sec.)	Linear Absorption Coefficient Fe (cm^{-1})	Linear Absorption Coefficient H_2O (cm^{-1})
IV	2.76×10^9	1.6	1.5×10^{11}	0.356	0.055
V	7.8×10^8	2.1	3.23×10^{10}	0.310	0.048
VI	2.21×10^8	2.5	7.67×10^9	0.293	0.0438
VII	1.04×10^7	2.8	3.23×10^8	0.284	0.041

Gamma Group	b_1	μ_c (cm^{-1})	m	$(\frac{1}{m})\mu_c z$	b_2	$B_{Fe}(b_2)$	Θ	$F(b_2, \Theta)$
IV	19.6	0.108	1.68	1.31	21.8	40	13.5°	6.0×10^{-11}
V	17.07	0.0941	1.58	1.26	19.06	24	13.4°	1.05×10^{-9}
VI	16.07	0.0879	1.53	1.24	17.97	20	13.4°	3.1×10^{-9}
VII	15.51	0.0843	1.49	1.23	17.34	17.5	13.3°	5.8×10^{-9}

Gamma Group	ϕ (photons/cm^2-sec)	K_D (photon hours/roentgen-cm^2-sec)	Dose Rate = ϕ/K_D r/hr
IV	1.01×10^3	3.7×10^5	2.74×10^{-3}
V	2.28×10^3	3.0×10^5	7.58×10^{-3}
VI	1.33×10^3	2.6×10^5	5.1×10^{-3}
VII	9.11×10^1	2.4×10^5	0.38×10^{-3}

Total = 15.8 milliroentgen/hour

At 12 hours and longer after shutdown, gammas above 1 Mev are considered to have an average energy of 1.25 Mev. This change is made because after 12 hours shutdown Co^{60} and Fe^{59} become more important than Mn^{56} as gamma sources since saturation of all activities is assumed.

Input to the machine calculation is merely the fast and thermal fluxes throughout the shield and the thickness of materials in the shield.

Table 2-3 contains fluxes used in the machine calculation. Fluxes in Table 2-3 were taken from Valprod Calculation No. 2624 results of which are plotted in Fig. 5-6 of Section 5 of Core Design Analysis. Thermal fluxes for points inside the pressure vessel have been multiplied by 0.8 to correct for temperature effects on thermal cross sections of water and stainless steel. (See Section 2.3.2.1.)

Boral in the shield has been treated as water as a source and shield after shutdown. Neither water nor Boral would contribute appreciably to dose rate after shutdown.

Results of the machine calculation of dose rate due to shield activation after shutdown are as follows:

Group	Average Energy	Dose Rate 2.5 hrs after shutdown	Dose Rate 24 hrs after shutdown
1	1.65 Mev	31.4 mr/hr	10.3 mr/hr
2	0.75 Mev	11.8 mr/hr	Negligible
	Total	43.2 mr/hr	10.3 mr/hr

2.3.4 Dose Rate from Sources outside Shield Tank

In addition to the radiation from the shield tank there are two other sources of radiation in the vapor container after shutdown. These are:

1) Activated corrosion products distributed throughout the primary system
2) Activated components in the vapor container

These two sources do not lend themselves to rigorous theoretical analysis, but health physics surveys made in APPR-1 give an indication of the relative importance of the two sources and the general dose rate level to be expected in the vapor container from the two sources.

TABLE 2-3

Fluxes Used in the Machine Calculation of Dose Rate from Activated Materials.

Point	Location	ϕ_{th}	ϕ_f
1	Core-Reflector I.F.(Interface)	1.23×10^{13}	4.84×10^{13}
2	Reflector Midpoint	1.59×10^{13}	3.74×10^{13}
3	Reflector-Thermal Shield I.F.	6.96×10^{12}	3.04×10^{13}
4	Thermal Shield Midpoint	2.05×10^{12}	2.0×10^{13}
5	" " -Coolant I.F.	3.39×10^{12}	1.14×10^{13}
6	Coolant Passage -1	9.88×10^{12}	5.99×10^{12}
7	Coolant Passage -2	7.60×10^{12}	3.32×10^{12}
8	Coolant-Pressure Vessel I.F.	1.91×10^{12}	2.16×10^{12}
9	Pressure Vessel -1	4.13×10^{11}	1.62×10^{12}
10	Pressure Vessel -2	1.21×10^{11}	1.16×10^{12}
11	Pressure Vessel-Void I.F.	3.04×10^{10}	7.48×10^{11}
12	Void-Support Ring I.F.	3.37×10^{10}	6.21×10^{11}
13	Support Ring Midpoint	1.10×10^{10}	4.69×10^{11}
14	Support Ring-Boral I.F.	1.48×10^{9}	3.28×10^{11}
15	Water Annulus Midpoint	5.15×10^{10}	2.18×10^{11}
16	Boral-1st. Shield Ring I.F.	2.48×10^{8}	1.70×10^{11}
17	1st. Shield Ring Midpoint	1.57×10^{7}	8.90×10^{10}
18	1st. Shield Ring-Boral I.F.	2.83×10^{7}	3.82×10^{10}
19	Water Annulus Midpoint	5.46×10^{9}	2.57×10^{10}
20	Boral-2nd Shield Ring I.F.	2.03×10^{7}	2.00×10^{10}
21	2nd. Shield Ring Midpoint	9.42×10^{5}	1.05×10^{10}
22	2nd. Shield Ring-Boral I.F.	4.50×10^{6}	4.50×10^{9}
23	Water Annulus Midpoint	5.52×10^{8}	2.99×10^{9}

TABLE 2-3 (Continued)

Point	Location	ϕ_{th}	ϕ_{f}
24	Boral-3rd. Shield Ring I.F.	1.80×10^{6}	2.34×10^{9}
25	3rd. Shield Ring Midpoint	7.60×10^{4}	1.19×10^{9}
26	3rd. Shield Ring-Boral I.F.	2.56×10^{5}	4.56×10^{8}
27	Water Annulus Midpoint	8.12×10^{9}	3.56×10^{8}
28	Boral-4th. Shield Ring I.F.	1.53×10^{5}	2.74×10^{8}
29	4th. Shield Ring Midpoint	5.40×10^{3}	1.35×10^{8}
30	4th. Shield Ring-Boral I.F.	2.39×10^{4}	4.62×10^{7}
31	Water Annulus Midpoint	2.47×10^{6}	1.09×10^{7}
32	Boral - Tank Wall I.F.	5.49×10^{4}	2.57×10^{6}
33	Tank Wall Midpoint	1.25×10^{4}	2.38×10^{6}
34	Outside of Tank Wall	1.05×10^{4}	2.20×10^{6}

Experimental data from APPR-1 are applicable to the Skid Mounted Reactor because:

1) Activation of corrosion products in the two plants is comparable.
2) Neutron fluxes escaping from the shield tanks of the two plants are comparable.

Surveys made in APPR-1 lead to the following conclusions which have been applied to the Skid Mounted Reactor:

1) Dose rate from vapor container component activation is small compared to dose rate from distributed activated corrosion products.
2) A general radiation field exists in the vapor container from these two sources which gives a dose rate of about 30 mr/hr at 2.5 hours after shutdown and about 6 mr/hr at 24 hours after shutdown.

2.3.5 Total Dose Rate after Shutdown

Results from the machine calculation indicate a dose rate on the shield surface of 72 mr/hr (43 mr/hr from shield activation and 29 mr/hr from fission product gammas) for infinite operation at 6.5 Mw and 2.5 hours shutdown time. However, APAE 35 (1) shows that the machine calculation gives dose rates consistently higher than those measured in APPR-1. For instance, from Table 2.13 and Fig. 2.3 of APAE 35 (1) between the seventh and eighth shield rings of APPR-1 where total shielding is approximately equal to that in the Skid Mounted Reactor the machine calculated dose rate is about six times the measured dose rate. Therefore, it seems to be a conservative estimate to say that personnel standing at the primary skid 2.5 hours after shutdown would be subjected to 33 mr/hr from the primary shield rather than the 72 mr/hr calculated by the machine program.

Adding to the dose rate from the shield tank that from activated corrosion products and vapor container components gives a total dose rate of 63 mr/hr at 2.5 hrs. after shutdown for infinite operation at 6.5 Mw.

2.3.6 Conclusions

The important measure of the effectiveness of a shield is the dose accumulated by personnel outside the shield.

Fig. 2.1 is a plot of dose rate outside the shield tank, vs time after shutdown for infinite operation at 6.5 Mw and is based on the following data:

Source	Time After Shutdown 2.5 hrs.	12 hrs.	24 hrs.
Core	15.6 mr/hr	7.5	6.4 mr/hr
Shield	16.9	7.8	3.9
Activated Corrosion Products	30	15	6 mr/hr
Total	62.5 mr/hr	30.3	16.3

Core dose rates were calculated by hand (see Table 2-2 of Section 2.3.2.2). Shield dose rates were calculated by the machine; the dose rate at 2.5 hours after shutdown was reduced to give a total dose rate of 33 mr/hr at shield tank surface (see Section 2.3.5) including the 15.6 mr/hr from the core hand calculation. Shield dose rates at 12 and 24 hours after shutdown were reduced by the same factor. Dose rates from activated corrosion products were estimated from health physics surveys in APPR-1.

From Fig. 2-1 it can be seen that the dose accumulated by personnel working at the shield tank for 4 hours from 4 to 8 hours after shutdown would be about 140 mr.

2.4 Operating Dose Rate Calculation

Operating dose rate from the reactor and the shield tank must be calculated in order to determine thickness of secondary shielding necessary to reduce the operating dose rate to allowable levels.

During operation significant sources of gamma radiation which escape from the shield tank are:

1. Prompt fission gammas.
2. Fission product decay gammas.
3. Radiative capture gammas in U^{235} and in the shield.
4. Decay gammas from activated materials in the shield tank.

2.4.1 Calculational Model

2.4.1.1 Core Source and Attenuation

The calculational model used in the operating dose rate calculation was, in general, the same as that used in the shutdown dose rate calculation. Magnitude of the source strengths and energy spectrum, of course, are much different.

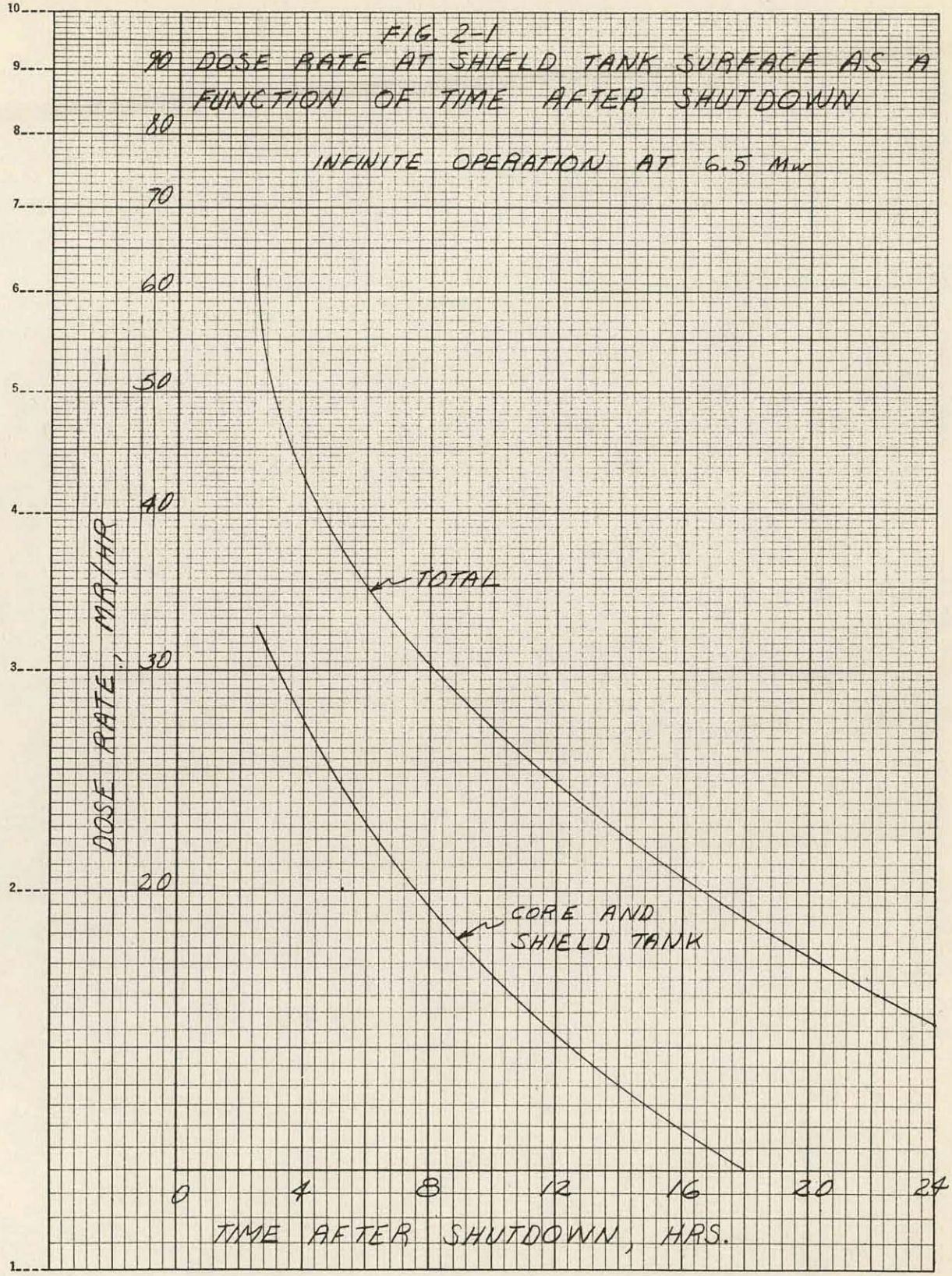
FIG. 2-1
DOSE RATE AT SHIELD TANK SURFACE AS A FUNCTION OF TIME AFTER SHUTDOWN
INFINITE OPERATION AT 6.5 Mw
DOSE RATE, MR/HR
90
80
70
60
50
40
30
20
TOTAL
CORE AND SHIELD TANK
0
4
8
12
16
20
24
TIME AFTER SHUTDOWN, HRS.

The machine program was used in the operating dose rate calculation. Files for the fission gamma yield are based upon the Motz spectrum for fission gammas as follows (see p. 47, Ref. 14):

$$N(E)\,dE = 18.5\,e^{-1.24E}dE \qquad \text{gammas/fission-Mev}$$
$$(E \text{ in Mev})$$

The above expression assumes a total of 12 Mev of gamma energy per fission event. Total gamma energy released from the fission event and its decay products is 11 Mev. One Mev is assumed to be released in radiative capture in U^{235} per fission and the radiative capture gammas are assumed to have the same spectrum as the fission gammas.

In addition to gammas from U^{235}, capture and activation gammas from stainless steel and capture gammas from water were considered. Data for the files for capture gamma production and energy spectra were taken from Table 3.6 of TID 7004 (2). Data for the files for activation gamma production were taken from Ref. 6.

In preparing the files, data on resonance capture integrals from Ref. 5 were used where available. For materials whose resonance capture integrals were not available a 1/v variation of absorption cross section was assumed. Thermal absorption cross sections for all the machine calculations were taken from BNL 325 (15). Thermal activation cross sections were taken from Ref. 6.

Capture and activation gamma sources in the core during operation were calculated basically in the same manner as outlined in the shutdown calculation (see Sections 2.3.1.2 and 2.3.3).

During operation gammas produced range in energy up to 7 Mev. All gammas are put into five energy groups as follows:

Group	Energy Range, Mev	Average Energy, Mev
1	>7	7.0
2	5-7	6.0
3	3-5	4.0
4	1-3	2.0
5	0-1	0.75

2.4.1.2 Capture Sources in Shield and Attenuation

During operation, capture sources in the shield and their attenuation are calculated in much the same manner as activation sources after shutdown (see Sections 2.3.1.2 and 2.3.3.) All activities are assumed to be saturated and operating at equilibrium values. Sources of data for capture and activation gammas are listed in Section 2.4.1.1. Activation and capture gammas produced during operation are put into the five energy groups listed in Section 2.4.1.1.

TABLE 2-4

Results of Machine Calculation of Operating Dose Rate from Core

Group	Energy Range, Mev	Average Energy Mev	S_v Gammas per sec per cm^3	μ_c	$\mu_c z$	B(b)	ϕ Gammas per cm^2 per sec	Dose Rate, R/hr
1	>7	7.0	3.52×10^{11}	0.0661	1.46	11.5	1.68×10^{6}	14.0
2	5-7	6.0	3.95×10^{11}	0.0675	1.47	14.2	1.79×10^{6}	13.4
3	3-5	4.0	8.51×10^{11}	0.0749	1.52	26.2	2.08×10^{6}	11.4
4	1-3	2.0	1.11×10^{13}	0.0994	1.61	118	2.86×10^{6}	9.1
5	0-1	0.75	2.88×10^{13}	0.1712	----	----	---------	Negligible
							Total	47.9 R/hr

2.4.2 Model Comparison with APPR-1

As has been shown in Section 2.3.1.3, the primary shielding in APPR-1 out to the water annulus between the last two shield rings is approximately equal to the total primary shielding of the Skid Mounted Reactor. At this point in the APPR-1 shield the total measured dose rate during full power operation is 86.4 R/hr and the machine calculation gave 315 R/hr at the same point (see Table 2.12 of Ref. 1).

Again the measured dose rate of 86.4 R/hr in APPR-1 would be expected to be an upper limit for the Skid Mounted Reactor. However, the machine calculated operating dose rate of 161 R/hr has been used in this report.

2.4.3 Dose from Core

Input to the core dose rate calculation during operation is the same as that for the shutdown calculation; the machine merely uses an operating file rather than a shutdown file. The input consists of core dimensions (height and radius), volume fractions in the core, kinds of materials and their thickness in the shield, and fast and thermal average fluxes in the core. Material types and thickness were taken from Table 1-1; volume fractions and fluxes are listed in Section 2.3.2.1.

Table 2-4 contains the output of the core operating dose rate calculation. Total calculated dose rate from the core is 47.9 R/hr.

2.4.4 Dose from Capture and Activation Sources in the Shield

Input to the operating dose rate calculation for capture sources in the shield is the same as that for the shutdown activation calculation and consists of thicknesses and types of materials in the shield and fluxes throughout the shield. Fluxes used are listed in Table 2-3; types and dimensions of materials were taken from Table 1-1.

Table 2-5 contains the output of the operating dose rate calculation. Total calculated dose rate from the shield is 112.7 R/hr.

TABLE 2-5

Results of Machine Calculation of Operating Dose Rate from Capture and Activation Sources in the Shield.

Group	Energy Range, Mev	Average Energy, Mev	Gammas/cm^2-sec	Dose Rate, R/hr
1	7	7.0	8.58×10^6	71.8
2	5-7	6.0	3.63×10^6	27.1
3	3-5	4.0	2.18×10^6	12.0
4	1-3	2.0	5.77×10^5	1.8
5	0-1	-.75	1.77×10^4	Negligible
			Total	112.7

2.4.5 Total Dose on Surface of Shield Tank

The total dose rate on the surface of the shield tank is the sum of the core dose rate from Section 2.4.3 and the shield dose rate from Section 2.4.4. This total is 161 R/hr.

It has been shown in APAE 35 (1) that the machine calculation gives dose rates consistently higher than those measured. It has also been shown in Section 2.4.2 that the dose rate measured in APPR-1 outside a shield thickness corresponding approximately to total thickness of the skid mounted reactor is 86.4 R/hr and the machine calculated dose rate at the same point is 315 R/hr. Nevertheless, the 161 R/hr calculated outside the skid mounted shield has been used in following sections of this report.

2.5 Control Rod Drive Shielding

Control rod drive shielding after shutdown has been a difficult problem in both APPR-1 and APPR-1a. In these designs, to replace rod drives, personnel must approach quite close to the core.

Dose rates in APPR-1 control rod drive pit range from 940 mr/hr at 20 minutes after shutdown to 480 mr/hr at 2 1/2 hours after shutdown. (See Table 7, Ref. 13). The geometry of the shield tank and control rod drive pit make it difficult to apply shielding effectively although this has been done in both designs.

The control rod drives of the skid mounted reactor and their relation to the core, pressure vessel, and shield tank may be seen in Dwg. Nos. R9-46-1039 and R9-47-1013. In the skid mounted configuration personnel do not have to approach any closer to the core than the outside of the shield tank. Therefore, shielding may be provided in the shield tank to protect personnel changing rod drives.

In addition to the fixed elements in the core there are five control rod fuel elements which are below the core after shutdown. To determine how far down the shield rings must extend to protect the control rod drive it was stipulated that the amount of shielding intersecting a ray from the bottom of any control rod fuel element to the control rod drives must be the same as is intersected by a ray from the core surface out horizontally to the shield tank surface.

In order to calculate the amount of shielding material intersected by a ray from the bottom of the fuel elements to the control rod drives it was necessary to determine equivalences of steel and water. (Boral was neglected).

The equivalence of shield water and steel taken from Table 6.11 of Ref. 2 for 2 Mev gammas is: 1.7" steel = 11.6" water.

Water in the pressure vessel was assumed to have a density of 0.8 gm/cm^3 and therefore its equivalence with steel is:

1" steel = 8.53" Primary Water

The problem then becomes that of scaling off a drawing the thickness of materials intersecting a ray from the bottom of the control rod fuel elements to the area occupied by personnel changing control rod drives and extending the shield rings down until enough shielding material in intersected.

Dose rate from core and shield tank expected in this area would be less than the 33 mr/hr expected at the surface of the shield tank opposite the core.

2.6 Nozzle Shielding

Drawing No. R9-46-1039 shows the relation of the reactor outlet nozzle to the core and the shield rings. It can be seen that insulation around the nozzle and pipe in the shield tank affords a streaming path through the primary shield for radiation from the core and from the control rod elements below the core.

The approach to this problem was essentially the same as that used for the control rod drive shielding. That is, the nozzle and shield rings were drawn full size and rays drawn from the core and control rod fuel elements through the insulation to the outside of the primary shield tank.

The following equivalences of materials were used (see Table 6.11, Ref. 2):

1" Lead = 11.6" water = 1.7" iron

Where less than the full amount of shielding material was intersected, insulation will be taken off and replaced with lead until the desired amount of shielding is intersected.

2.7 Radiation Heating in the Shield Tank

During operation a significant amount of heat is deposited in the shield tank by radiation escaping from the core, pressure vessel and thermal shield. In order to size the cooling coil needed to remove the heat, the rate of heat deposition is calculated in the following section. A basic assumption is that all radiation incident on the pressure vessel support ring is absorbed in the shield tank.

2.7.1 Neutron Heating

All neutron heating is due to the absorption of the kinetic energy of fast neutrons.

From Table 2-3, the fast neutron flux incident on the pressure vessel support ring is 7.47×10^{11} n/cm^2-sec. This is the fast flux averaged over the 22" height of the core. The corresponding area on the support ring is:

$$\pi \times 48" \times 22" = 3.32 \times 10^3 \text{ in}^2$$

$$= 2.14 \times 10^4 \text{ cm}^2$$

Assuming an average of 1 Mev per fast neutron the total amount of neutron energy incident on the support ring over the 22" height of the core is:

$$2.14 \times 10^4 \text{ cm}^2 \times 7.47 \times 10^{11} \text{ n/cm}^2\text{-sec} \times 1 \text{ Mev/n} = 1.6 \times 10^{16} \text{ Mev/sec}$$

Fluxes above and below the core are smaller than core fluxes and fall off rapidly (see Fig. 2-2.) However, neutron energy incident on a 10" high section of the support ring below the level of the core was calculated as follows:

$\bar{\phi}_F$ = average core fast flux

$$\bar{\phi}_F = 9.36 \times 10^{13}$$

From Fig. 2.2 the ratio of the fast flux at the bottom of the core to the core fast flux is:

$$\frac{\phi_F}{\bar{\phi}_F} = \frac{6.18 \times 10^{13}}{9.36 \times 10^{13}} = 0.66$$

The ratio of the fast flux 10" below the core to the core fast flux is:

$$\frac{\phi}{\bar{\phi}_F} = \frac{3.84 \times 10^{12}}{9.36 \times 10^{13}} = 0.041$$

Taking a linear average from the bottom of the core to 10" below the core:

$$\frac{\bar{\phi}}{\bar{\phi}_F} = \frac{0.66 + 0.041}{2} = 0.35$$

$$\bar{\phi} = 0.35 \times \bar{\phi}_F$$

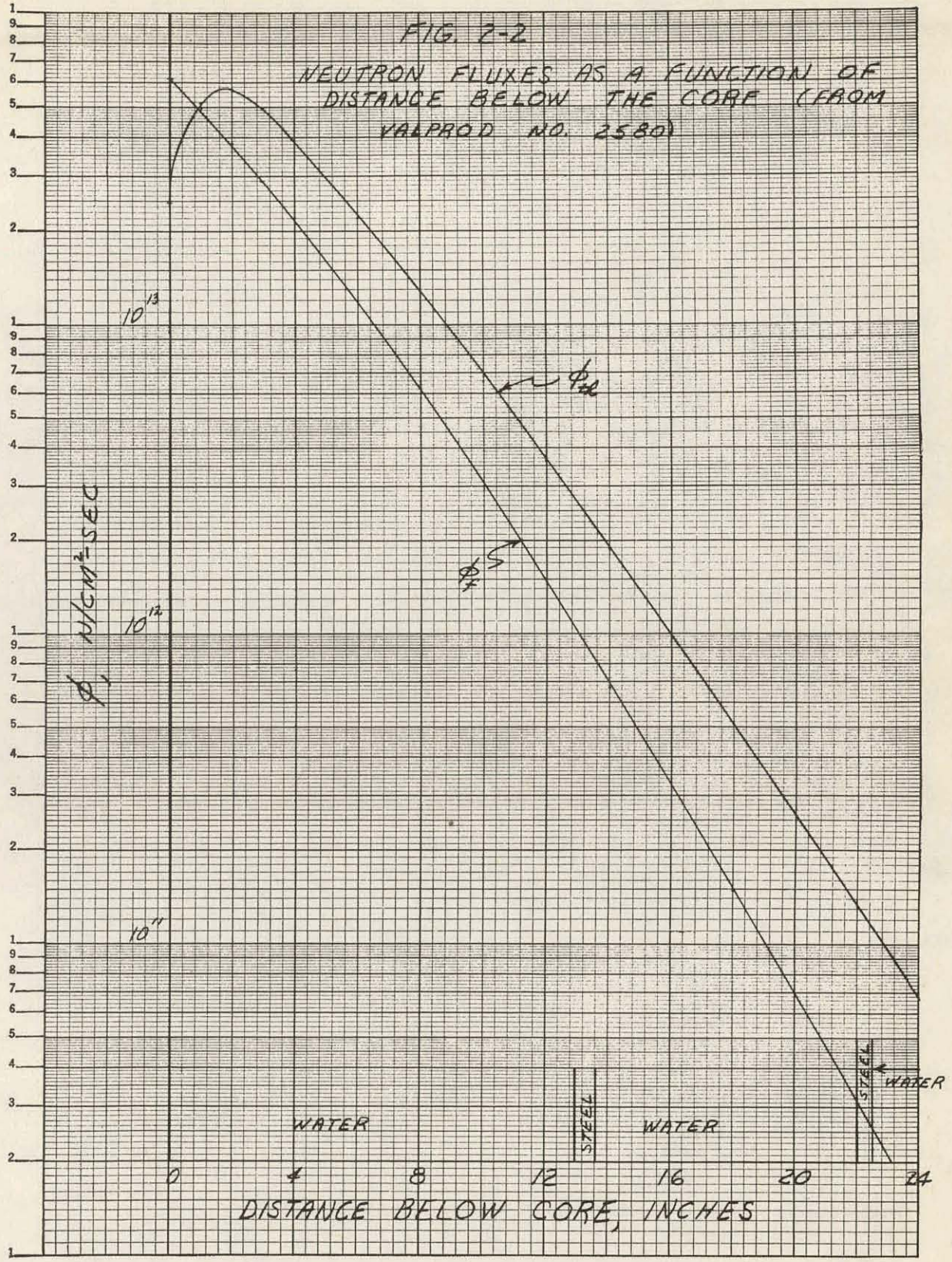
FIG. 2-2
NEUTRON FLUXES AS A FUNCTION OF DISTANCE BELOW THE CORE (FROM VALPROD NO. 2580)
10^{13}
10^{12}
10^{11}
ϕ_{th}
ϕ_f
ϕ, N/CM²-SEC
WATER
STEEL
WATER
STEEL
WATER
0
4
8
12
16
20
24
DISTANCE BELOW CORE, INCHES

Or an average fast flux over the 10" section of the support ring would be:

$$\phi = 0.35 \times 7.47 \times 10^{11} \text{ n/cm}^2\text{-sec} = 2.62 \times 10^{11} \text{ n/cm}^2\text{-sec}$$

The area upon which this flux is incident is:

$$\pi \times 48" \times 10" = 1.51 \times 10^3 \text{ cm}^2$$

$$= 9.74 \times 10^3 \text{ cm}^2$$

Total neutron energy incident on a 10" section of the support ring below the level of the core is:

$$9.74 \times 10^3 \text{cm}^2 \times 2.62 \times 10^{11} \text{ n/cm}^2 \text{ sec} \times 1 \text{ Mev/n}$$

$$= 2.55 \times 10^{15} \text{ Mev/sec}$$

The fast flux below this 10" band below the core may be neglected. Since the flux above the core is much smaller than the flux below the core, the heat deposition above the core may also be neglected (see Fig. 7, Ref. 13).

Total heating due to neutrons is then:

$$1.6 \times 10^{16} \text{ Mev/sec} + 2.55 \times 10^{15} \text{ Mev/sec} = 1.86 \times 10^{16} \text{ Mev/sec}$$

2.7.2 Heating from Core and Pressure Vessel Gammas

A machine calculation was made to determine the gamma flux incident on a section of the support ring corresponding to the core height. The results which include core gammas and capture gammas, follow:

E(Mev)	ϕ_γ, γ/sec-cm^2	ϕ_E, Mev/sec-cm^2
7	2.10×10^{11}	1.48×10^{12}
6	1.17×10^{11}	7.02×10^{11}
4	1.52×10^{11}	6.10×10^{11}
2	8.06×10^{11}	1.61×10^{12}
0.75	3.82×10^{11}	2.86×10^{11}
	Total	4.69×10^{12} Mev/sec-cm^2

$$4.69 \times 10^{12} \text{ Mev/sec-cm}^2 \times 2.14 \times 10^4 \text{cm}^2 = 1.00 \times 10^{17} \text{ Mev/sec}$$

From Fig. 80, Ref. 29, the total gamma flux below the core falls off similarly to the fast neutron flux. Therefore, the heating rate due to core gammas in the 10" section below the core is:

$$\frac{2.55 \times 10^{15}}{1.60 \times 10^{16}} \times 1.00 \times 10^{17} \text{ Mev/sec} = 1.59 \times 10^{16} \text{ Mev/sec}$$

Total gamma heating is:

$$1.60 \times 10^{16} \text{ Mev/sec} + 1.00 \times 10^{17} \text{ Mev/sec} = 1.16 \times 10^{17} \text{ Mev/sec}$$

2.7.3 Heating from Captures in the Shield Tank

Neutrons incident on the inner surface of the pressure vessel support ring are captured in the steel, boron and water in the shield tank resulting in the production of capture gammas except in the case of boron. The reaction in boron is as follows:

$$0n^1 + 5B^{10} \rightarrow 3Li^7 + 2He^4 + 2.8 \text{ Mev}$$

Thus, while boron serves as a gamma suppressor, appreciable amounts of heat are released in the shield tank in the form of kinetic energy of the boron reaction products. The heat release will in fact be greater than had the neutrons been absorbed in water.

The total amount of gamma radiation released per neutron capture is equal to the binding energy of the additional neutron. In the case of carbon steel, this has been taken to be 8 Mev; for water (hydrogen) it has been taken to be 2.2 Mev. It has been assumed that all capture gammas are absorbed in the tank.

The equation used to calculate heat production in the different materials in the shield tank is:

$$H = \sum_i \left[\Sigma^a_{th} \bar{\phi}_{th} + \Sigma^a_F \bar{\phi}_F \right] V_i E_i$$

$\left[\Sigma^a_{th} \bar{\phi}_{th} + \Sigma^a_F \bar{\phi}_F \right]$ = absorptions per cm^3 of ith material

V_i = volume of ith material

E_i = energy released per capture in ith material

Table 2-6 contains details of the calculation. To account for gamma production above and below the core, the radial fluxes which are averaged over the height of the active core were used over an area extending over the height of the core plus 10 inches below the core. Heat production rates were calculated for the first five regions of the shield. Since the fluxes fall off exponentially, it is not necessary to calculate captures further out in the shield. Fast and thermal cross sections are the same as those used in the Valprod calculation, results of which are plotted in Fig. 5-6 of Core Design Analysis.

Table 2-6: Calculation of Heat Produced by Captures in the Shield Tank

Region*	Σ^a_{th}, cm^{-1}	Σ^a_F, cm^{-1}	$\bar{\phi}_{th}$, n/cm^2-sec	$\bar{\phi}_F$, n/cm^2-sec	$\left[\Sigma^a_{th}\bar{\phi}_{th} + \Sigma^a_F\bar{\phi}_F\right]$ Captures/cm^3-sec
1	0.16864	0.008	1.69×10^{10}	4.69×10^{11}	6.6×10^{9}
2	16.715	0.59	5.2×10^{9}	2.6×10^{11}	2.4×10^{11}
3	0.115	0.001	2.6×10^{10}	2.18×10^{11}	3.21×10^{9}
4	16.715	0.59	5.5×10^{9}	5.2×10^{10}	1.23×10^{11}
5	0.16864	0.008	1.3×10^{8}	8.9×10^{10}	7.15×10^{8}

Region*	V, cm^3	E, Mev/Capture	$V \times E \times \left[\Sigma^a_{th}\bar{\phi}_{th} + \Sigma^a_F\bar{\phi}_F\right]$ Mev/Sec
1	5.6×10^{4}	8	2.59×10^{15}
2	1.033×10^{4}	2.8	6.95×10^{15}
3	1.26×10^{5}	2.2	8.97×10^{14}
4	1.28×10^{4}	2.8	4.42×10^{15}
5	3.52×10^{5}	8	7.61×10^{14}
			$H = 1.56 \times 10^{16}$ Mev/sec

*Region - 1 - Pressure Vessel Support Ring
2 - Pressure Vessel Support Ring Boral Cladding
3 - 1st Water Annulus
4 - Boral Cladding on 1st. Shield Ring
5 - 1st. Shield Ring

2.7.4 Conclusions

Total radiation heating rates in the shield tank as calculated in the preceding sections are:

Neutrons	0.19×10^{17} Mev/sec
Gammas from Core, Thermal Shield and Pressure Vessel	1.16×10^{17} Mev/sec
Captures in the Shield Tank	0.16×10^{17} Mev/sec
Total	1.51×10^{17} Mev/sec

$$1.51 \times 10^{17} \text{ Mev/sec} \times 5.472 \times 10^{-13} \frac{\text{Btu-sec}}{\text{Mev-hr}} = 8.25 \times 10^{4} \text{ Btu/hr}$$

Over 75% of the total heating rate is based upon the machine shielding calculation. Because the machine calculation has been shown to yield higher dose rates and heating rates than those measured, the heating coil for the shield tank has been sized to remove 72,000 Btu/hr of gamma and neutron heat.

2.8 Gamma Flux on the Instruments

A machine calculation was performed to determine the operating dose rate on the nuclear instruments in the shield tank. Neutron fluxes used in this calculation were the same as those listed in Table 2-3 of Section 2.3.3. These are end of life neutron fluxes and therefore give the highest gamma dose rate to be expected on the instruments. Thermal neutron fluxes are markedly different for the two instrument positions shown in Dwg. No. R9-46-1039 as a result of the different amounts of water behind the instruments. This difference will have little effect upon the gamma flux and the gamma dose rate has been assumed to be the same for all instruments.

Shutdown gamma dose rates on the instruments in the skid mounted shield tank have been estimated from experimental data taken in APPR-1. Table 2-7 contains a comparison of gamma dose rates measured in APPR-1 and calculated for the Skid Mounted Reactor.

Table 2-7: Gamma Dose Rates on the Instruments In APPR-1 and the Skid Mounted Reactor

	Operating	
	Calculated	Measured
APPR-1	5×10^{5} R/hr	2.5×10^{5} R/hr
Skid Mounted	3×10^{5} R/hr	-----
	24 Hrs. After Shutdown	
	Estimated*	Measured
APPR-1	------	10^{3} R/hr
Skid Mounted	5×10^{2} R/hr	

*Estimated from APPR-1 Measurements

3.0 SECONDARY SHIELDING ANALYSIS

The primary shield was designed on the basis of minimum weight and access to the primary skid 8.0 hours after shutdown. Therefore, a high level of radiation would be expected around the primary skid during operation.

The allowable continuous radiation received by any personnel is based on the amount that may be received in one year. This allowable radiation is 5 R/yr. In any one week, this is equivalent to a radiation level of 96.2 mr/week. Since base personnel are scheduled to be on duty 84 hours a week, the hourly permissable dose rate in operating areas can be approximately 1 mr/hr.

At the site, the radiation emanates from the core itself, the primary shield (shield tank) and the N-16 activity in the primary water. In order to decrease the level of the operating radiation to base personnel, the primary system is located within the secondary shield, in this case, snow.

This section will deal with the thickness of secondary shielding required to decrease the operating radiation to 1 mr/hr. The operating radiation consists of the contribution from the N-16 activity of the primary water and from the activation of the primary shield.

3.1 N-16 Activity in Primary Water

In all reactors where water is used as a primary coolant, there is activation of the water. This is due to the capture of a neutron by O-16 as shown in the following reaction which has a threshold of approximately 10 Mev.

$$ {}_{8}O^{16} + {}_{0}n^{1} \longrightarrow {}_{7}N^{16} + {}_{1}p^{1} $$

The extent of the activation is a sensitive function of the influx time and the total cycle time.

A simplified method was employed to calculate the N-16 activity. This method was used since it was shown to give comparable results to a more precise and lengthy method (1).

3.1.1 Calculation of N-16 Activity

In this reactor, the water will be activated in both the core and the reflector. The activity was calculated using the following equations:

core

$$A_c(0) = \Sigma_a \bar{\phi}_c \left(\frac{1-e^{-\lambda t_c}}{1-e^{-\lambda t_T}} \right) \tag{3-1}$$

reflector

$$A_R(0) = \Sigma_a \bar{\phi}_R \left(\frac{1-e^{-t_R}}{1-e^{-t_T}} \right) \tag{3-2}$$

Total

$$A_T(0) = A_c(0) + A_R(0) \tag{3-3}$$

where

$A_c(0)$ = activity due to activation in core, dis/sec-cm^3

$A_R(0)$ = activity due to activation in reflector, dis/sec-cm^3

$\bar{\phi}_c$ = average activation flux in core, neutrons/cm^2-sec

$\bar{\phi}_R$ = average activation flux in reflector, neutrons/cm^2-sec

Σ_a = activation cross section of O-16, cm^{-1} = 4.274×10^{-4}

λ = disintegration constant of N-16, sec^{-1} = 0.0943

T_t = time for one complete cycle, sec = 11.819

t_c = time water spends in core, sec = 0.586

t_R = time water spends in reflector, sec = 3.737

The activation flux is that part of the fast flux above 10 Mev which consists of the uncollided and collided flux. The uncollided flux is described by equation 3-4 (17)

$$\phi_u(E) = \frac{\nu R_F \quad f(E)}{\Sigma_o(E) + \Sigma_H(E) + \Sigma_{Fe}(E)} \tag{3-4}$$

where

$\phi_u(E)$ = uncollided activation flux, neutrons/cm^2-sec-Mev

ν = neutrons/fission = 2.46

R_f = (P) (CF)/V, Fissions/cm^3-sec = 1.83 x 10^{12}

P = Power output, watts = 5.5 x 10^6

(CF) = Conversion factor, Fission/Watt-sec = 3.24 x 10^{10}

V = Volume of Core, cm^3 = 1.151 x 10^5

f(E) = Watt's fission spectrum, neutrons/fission neutron

$\Sigma_o(E)$ = macroscopic cross section of oxygen, cm^{-1}

$\Sigma_H(E)$ = macroscopic cross section of hydrogen, cm^{-1}

$\Sigma_{Fe}(E)$ = macroscopic cross section of iron, cm^{-1}

Watt's fission spectrum is defined by equation 3-5.

$$f(E) = 0.484\, e^{-E} \operatorname{Sinh} \sqrt{2E} \qquad (3\text{-}5)$$

where

E = neutron energy, Mev

Table 3-1 gives the calculation and numbers that were used to obtain the uncollided flux.

The collided flux above 10 Mev is defined by equation 3-6 (17).

$$\phi_c(E) = \frac{\nu R_f}{E \Sigma_H(E)} \left[(1-p) \int_E^{\infty} f(E')\, dE' + p e^{-E/T} \left\{ \left(\frac{E}{T}\right)^2 + \left(\frac{E}{T}\right) + 1 \right\} \right] \qquad (3\text{-}6)$$

In this case the second term is negligible.

where

$$p = \frac{\int_E^\infty \frac{\Sigma_o(E') \, \Sigma_{Fe}(E')}{\Sigma_H(E') + \Sigma_o(E') + \Sigma_{Fe}(E')} f(E') \, dE'}{\int_E^\infty f(E') \, dE'}$$

E = energy, Mev

T = nuclear temperature of the residual nucleus, Mev

Table 3-1

Calculation of Uncollided Flux

E(Mev)	f(E)	$\sigma_H(E)$ (barns)	$\sigma_o(E)$ (barns)	$\sigma_{Fe}(E)$ (barns)	Σ_t^* (cm^{-1})	$\phi_u(E)$ n/cm^2-sec-Mev
10	9.616×10^{-4}	0.94	1.25	2.95	0.1092	3.962×10^{10}
11	4.401×10^{-4}	0.87	1.33	2.82	0.1061	1.866×10^{10}
12	1.994×10^{-4}	0.79	1.41	2.68	0.1025	8.756×10^{9}
13	8.962×10^{-5}	0.74	1.50	2.58	0.1009	3.997×10^{9}
14	3.997×10^{-5}	0.69	1.54	2.52	0.0988	1.821×10^{9}
15	1.771×10^{-5}	0.65	1.57	2.45	0.0968	8.242×10^{8}
16	7.795×10^{-6}	0.61	1.59	2.39	0.0947	3.706×10^{8}
17	3.413×10^{-6}	0.57	1.61	2.34	0.0927	1.656×10^{8}

$$^*\Sigma_t = N_H \sigma_H(E) + N_O \sigma_O(E) + N_{Fe} \sigma_{Fe}(E)$$

$N_H = 4.1381 \times 10^{22}$ atoms/cm^3

$N_O = 2.1635 \times 10^{22}$ atoms/cm^3

$N_{Fe} = 1.4653 \times 10^{22}$ atoms/cm^3

Table 3-2 outlines the calculation of the collided flux above 10 Mev. The total energy dependent flux is the sum of the uncollided and collided flux and is given in Table 3-3.

Table 3-2

Calculation of Collided Flux

E(Mev)	$\Sigma_H(E)$	$\Sigma_O(E)+\Sigma_{Fe}(E)$	$\Sigma_t(E)$	$\int_E f(E')dE'$	p	ϕ_c n/cm^2-sec-Mev
10	0.03893	0.07027	0.1092	1.305×10^{-3}	0.767	3.626×10^{9}
11	0.0360	0.07010	0.1061	5.477×10^{-4}	0.891	6.76×10^{8}
12	0.03272	0.06978	0.1025	2.464×10^{-4}	0.843	4.14×10^{8}
13	0.03064	0.07026	0.1009	1.077×10^{-4}	0.811	2.308×10^{8}
14	0.02856	0.07024	0.0988	4.72×10^{-5}	0.763	1.261×10^{8}
15	0.02692	0.06987	0.09679	1.84×10^{-5}	0.649	7.215×10^{8}
16	0.02524	0.06942	0.09466	5.28×10^{-6}	0.584	2.451×10^{7}
17	0.02359	0.06912	0.09271	2.3×10^{-6}	0.513	1.261×10^{7}

Table 3-3

Total Energy Dependent Flux

E(Mev)	ϕ (E) n/cm^2-sec-Mev
10	4.327×10^{10}
11	1.935×10^{10}
12	9.204×10^{9}
13	4.229×10^{9}
14	1.947×10^{9}
15	8.957×10^{8}
16	3.952×10^{8}
17	1.783×10^{8}

The total flux above 10 Mev is defined by equation 3-7.

$$\phi_{act}(n/cm^2\text{-sec}) = \int_{10}^{\infty} (E)\, dE \qquad (3\text{-}7)$$

where

$$\phi(E) = 1.11 \times 10^{14}\ e^{-0.7833E}$$

Therefore $\phi_{act} = 5.565 \times 10^{10}$ neutrons/cm^2-sec

In order to obtain the average flux over 6.5 Mev in the core and reflector, the following assumption is made: the neutron flux above 10 Mev has the same radial distribution as the fast group flux. Therefore, the average fluxes above 10 Mev in the core and reflectors are 3.509×10^{10} and 1.0×10^{10} neutrons/cm^2-sec respectively.

3.1.2 Results

From equations 3-1, 3-2, and 3-3 the activation of the primary water by the O^{16} $(n,p)N^{16}$ reaction is as follows:

Activation in disintegrations/sec-cm^3

Core

$$A_C(0) = 1.432 \times 10^6$$

Reflector

$$A_R(0) = 2.225 \times 10^6$$

Total

$$A_T(0) = 3.657 \times 10^6$$

3.1.3 Comparison with APPR-1

A rough comparison can be obtained from the measured N-16 activity and known cycle times in the APPR-1. The experimentally obtained activity is 1.63×10^6 dis/sec-cm^3. Therefore,

$$A_{APPR-1}(0) = 1.63 \times 10^6 = \Sigma_{a1}\,\phi_1\,\left(\frac{1-e^{-\lambda t_{c1}}}{1-e^{-\lambda t_{t1}}}\right) = 0.0614\,\Sigma_{a1}\,\phi_1$$

$$A_{SKID}(0) = A_2 = \Sigma_{a2}\,\phi_2\,\left(\frac{1-e^{-\lambda t_{c2}}}{1-e^{-\lambda t_{t2}}}\right) = 0.0801\,\Sigma_{a2}\,\phi_2$$

but $$\frac{\Sigma_{a2}}{\Sigma_{a1}} = \frac{\rho_2}{\rho_1} = \frac{48.9\ \#/ft^3}{51.77\ \#/ft^3} = 0.9426$$

and assuming

$$\frac{(\phi_{fast})\ APPR\text{-}1}{\phi_1} = \frac{(\phi_{fast})SKID}{\phi_2},$$

$$\frac{\phi_2}{\phi_1} = \frac{0.981 \times 10^{14}}{1.0095 \times 10^{14}} = 0.972$$

and $$\frac{\Sigma_{a2}\,\phi_2}{\Sigma_{a1}\,\phi_1} = 0.918$$

$$\therefore\ \frac{A_2}{1.63 \times 10^6} = \frac{0.0801\,\Sigma_{a2}\,\phi_2}{0.0614\,\Sigma_{a1}\,\phi_1} = 1.198$$

From the scaling of the measured activity in the APPR-1, the activity in the skid mount would be 1.952×10^6 dis/sec-cm^3 or approximately 47% lower than the previously calculated value of 3.657×10^6 dis/sec-cm^3 which is the number that will be used on the secondary shielding calculations.

3.2 Attenuation of N-16 Gammas Through Secondary Shielding

In section 3.1, the N-16 activity in the primary coolant was calculated at the reactor outlet. This section describes the calculation of the attenuation of the N-16 gammas through the secondary shield.

3.2.1 Calculation Model

The method used to calculate the gamma dose rate from the primary coolant is described fully in RAS-I (17) and AP NOTE 63 (18) as developed by the Electric Boat Division of General Dynamics Corp.

RAS-I takes the source due to the N-16 activity and attenuates it through shields within the vapor container and the secondary shield. To obtain the source geometry, the primary coolant piping and steam generator is divided into sections about one foot in length. The foot long sources are then approximated by a point source at the center of the actual source having a strength of C_s (gamma/sec). The point sources are then located in a three dimensional co-ordinate system. Essentially, the same setup is used to determine the shadow shields within the vapor container (including piping and steam generator). The input to the computer consists of the properties of the sources, piping, steam generator and other components in the vapor container. The points at which the dose rates are to be calculated are also included in the input. The shadow shield, source point and dose point descriptions are given in Tables 3-4, 3-5 and 3-6 respectively. The location of all dose planes is given in Figs. 3-1a and 3-1b and the dose points in the planes are given in Figs. 3-2a to 3-2e.

The computer calculates the inverse square attenuation and the self-absorption of the source to the selected dose point. After this, the machine checks to see if the gamma ray passes through a shadow shield. If it does, the computer attenuates the source through the shadow shield. For secondary shielding the machine uses two shields of specified thickness. Then it uses Peebles data (19) to compute slant attenuation and buildup in the shield. The dose rate at the selected dose point from all sources is summed up by the machine which then prints the dose rate as the output.

3.2.2 Calculated Dose Outside of Secondary Shield

During the shielding task conducted on the APPR-1 (1), measurements were performed determining the dose rate of various positions on the outside of the secondary shield. In all cases, the dose rate calculated by RAS-I was between a factor of 1½ and 3 greater than the measured rate. According to Ref. (17) (pg. 93 and 94) the machine calculation has been checked against the STR Mark I shield test and the calculated dose rates were consistently higher than the measured doses. Therefore, the RAS-I calculation can be used to determine the dose rates on the outside surface of the secondary shielding.

The dose rates were calculated at 31 positions in the secondary shielding around the vapor container. The results from the RAS-I calculation are given in Table 3-7. The dose points were selected so that isodose lines could be determined as a function of depth and distance from

TABLE 3-4

Shadow Shield Description

Type	ID_A	R (ft)	X_1 (ft)	Y_1 (ft)	Z_1 (ft)	$\overline{OA}$	X_2 (ft)	Y_2 (ft)	Z_2 (ft)
Reactor	01	3.67	20.0	35.0	29.2	.00	20.0	35.0	35.1
Pump	02	0.58	26.3	32.4	32.0	.00	26.3	32.4	34.8
Reactor Tank (Top)	03	5.00	20.0	35.0	40.2	.02	20.0	35.0	51.2
Reactor Tank (side)	04	4.29	20.0	35.0	27.6	.04	20.0	35.0	35.1
Large upper boiler section	05	2.29	34.6	33.3	30.3	.09	39.2	33.3	30.3
Boiler end	06	1.58	29.3	33.3	29.5	.10	30.6	33.3	29.5
Small upper boiler section	07	1.88	31.6	33.3	29.9	.13	34.6	33.3	29.9
Lower pressurizer	08	1.25	30.2	37.9	29.3	.13	30.2	37.9	31.5
Boiler tube	09	1.19	31.1	33.3	29.5	.28	39.1	33.3	39.5
Upper pressurizer	10	1.25	30.2	37.9	31.5	.29	30.2	37.9	34.4
Schedule 0 Pipe	11	0.43	24.3	34.2	29.9	.45	28.9	34.2	29.9
	12	0.43	28.9	32.4	29.0	.45	27.1	32.4	29.0
	13	0.43	27.0	32.4	29.1	.45	26.3	32.4	29.8
	14	0.43	26.3	32.4	29.9	.45	26.3	32.4	31.0
	15	0.43	26.3	31.5	11.5	.45	22.5	31.5	11.5

TABLE 3-5

Source Point Description

Type	ID_A	ID_B	X_s(ft)	Y_s(ft)	Z_s(ft)	C_s
Boiler End	06	001	29.3	33.3	29.5	245.39
Boiler Tube	09	001	31.6	33.3	29.5	50.55
	09	002	32.6	33.3	29.5	50.55
	09	003	33.6	33.3	29.5	50.55
	09	004	34.6	33.3	29.5	50.55
	09	005	35.6	33.3	29.5	50.55
	09	006	36.6	33.3	29.5	50.55
	09	007	37.6	33.3	29.5	50.55
	09	008	38.6	33.3	29.5	50.55
Schedule 0 Pipe	11	001	24.8	34.2	29.9	21.96
	11	002	25.8	34.2	29.9	19.08
	11	003	26.6	34.2	29.9	18.95
	11	004	27.5	34.2	29.9	18.82
	11	005	28.4	34.2	29.9	21.36
	12	001	28.5	32.4	29.0	13.55
	12	002	27.6	32.4	29.0	16.14
	13	001	26.7	32.4	29.4	17.42
	14	001	26.3	32.4	30.4	18.19
	15	001	25.8	31.5	31.5	15.75
	15	002	24.8	31.5	31.5	14.33
	15	003	23.9	31.5	31.5	14.23
	15	004	23.0	31.5	31.5	15.41

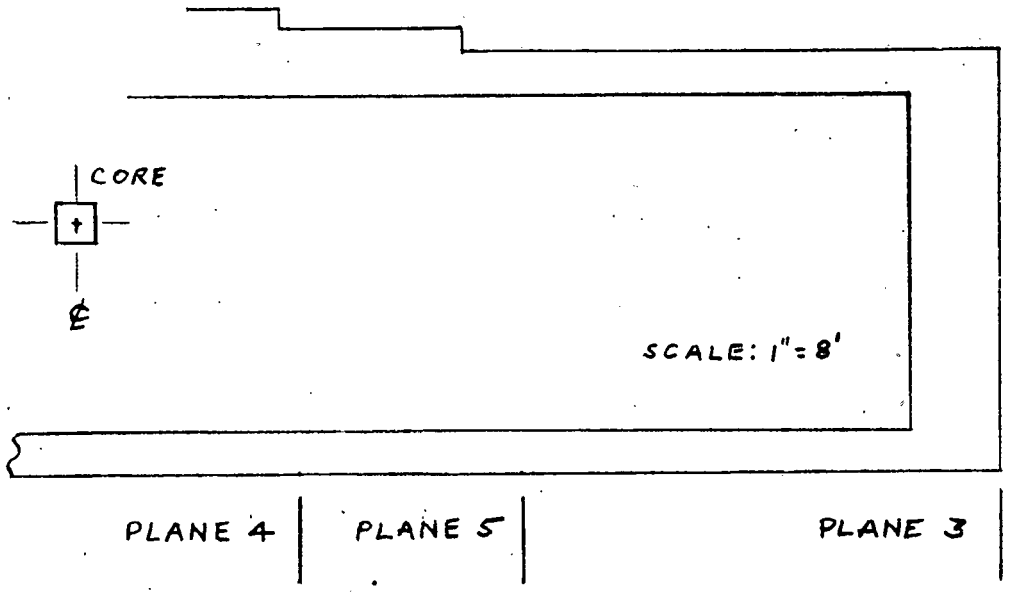

FIG. 3-1a. ELEVATION VIEW - DOSE PLANE LOCATION

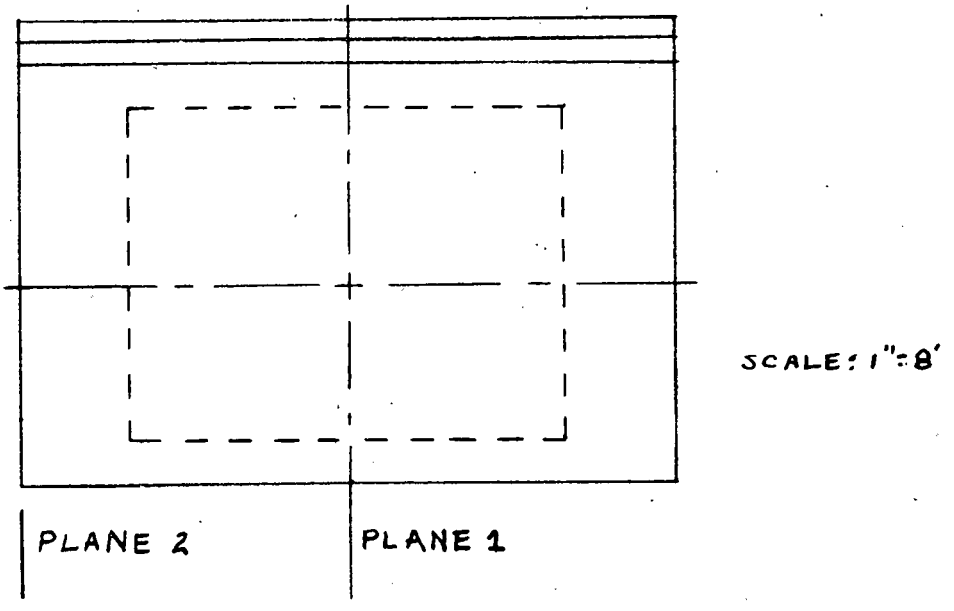

FIG. 3-1b SIDE VIEW - DOSE PLANE LOCATION

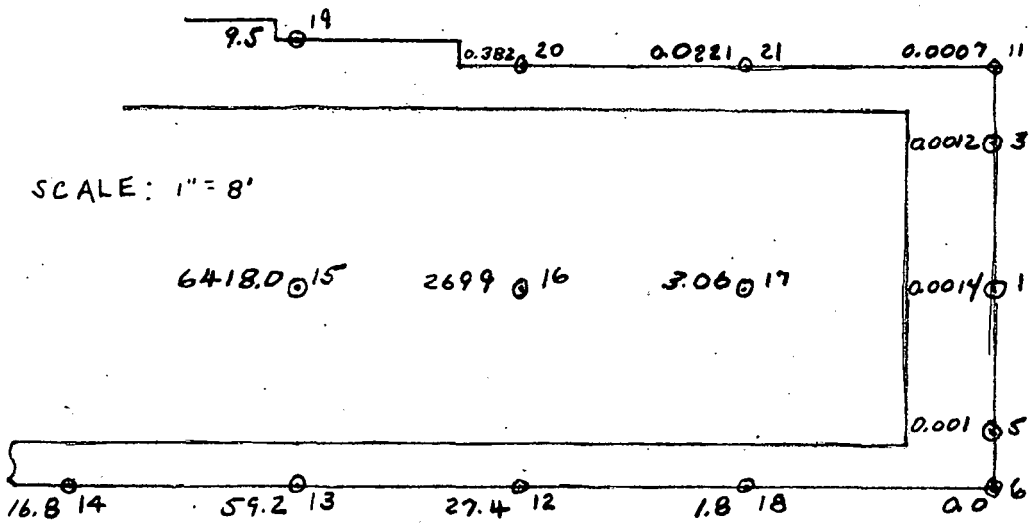

FIG. 3-2a. ELEVATION VIEW - DOSE POINT LOCATION ON PLANE 1
DOSE RATES - mR/hR

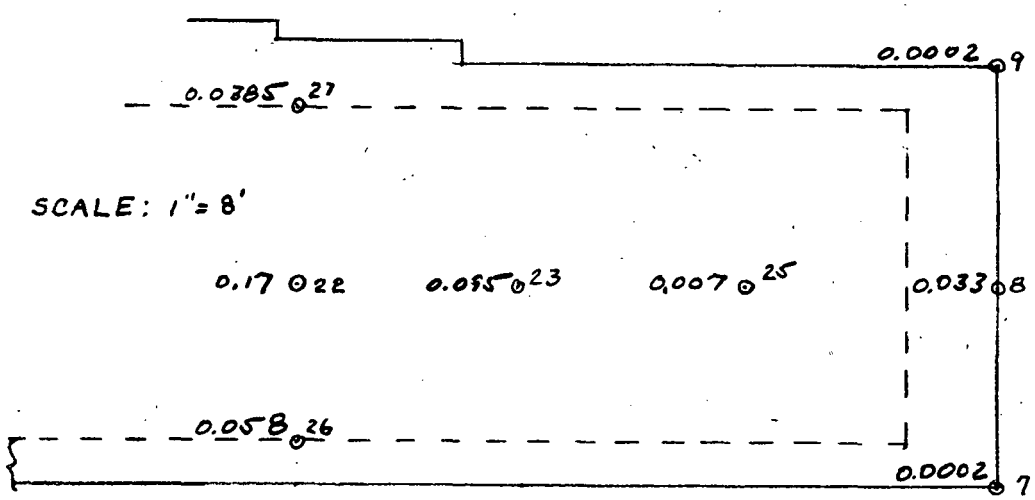

FIG. 3-2b. ELEVATION VIEW - DOSE POINT LOCATION ON PLANE 2.
DOSE RATES - mR/hR

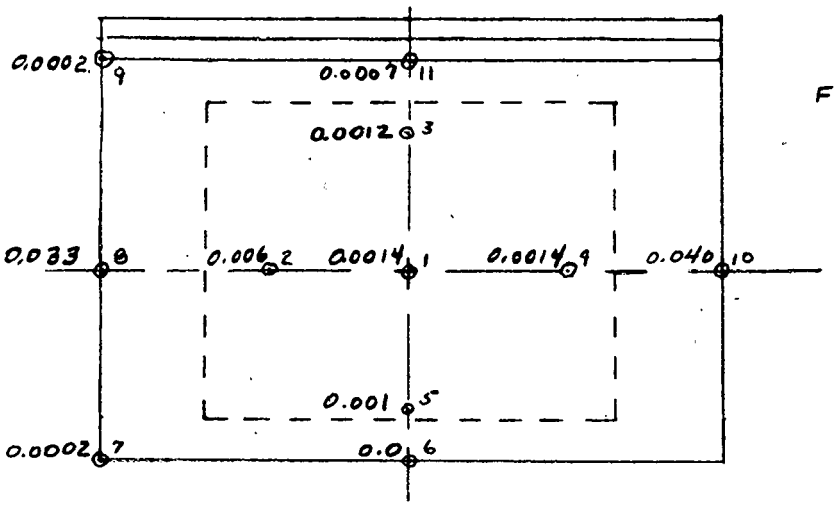

FIG. 3-2c. SIDE VIEW - DOSE POINT LOCATION ON PLANE 3 DOSE RATES - mR/hR

SCALE: 1" = 8'

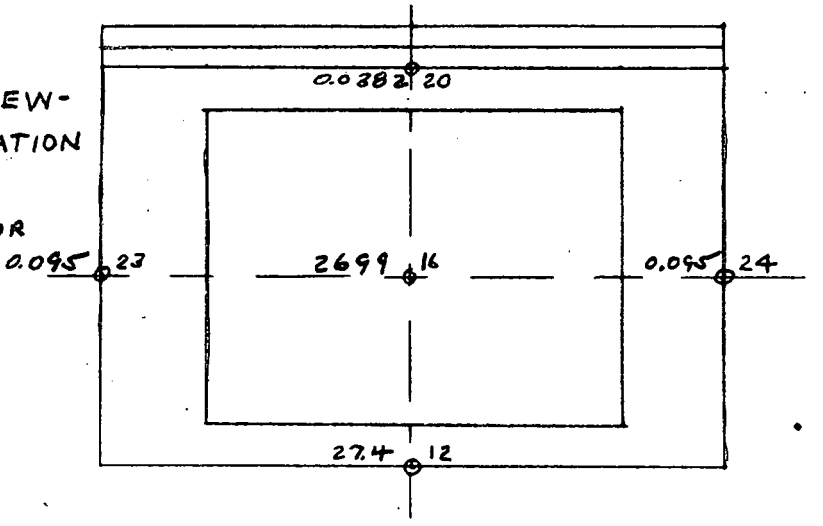

FIG. 3-2d. SIDE VIEW - DOSE POINT LOCATION ON PLANE 5 DOSE RATES - mR/hR

SCALE: 1" = 8'

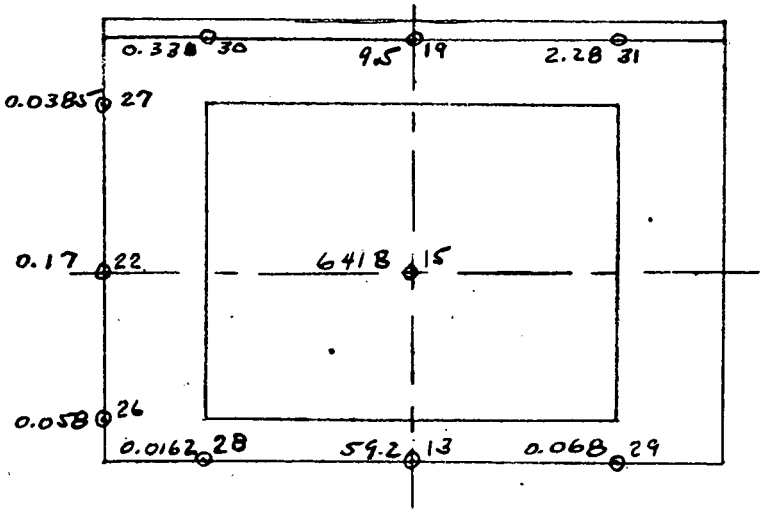

FIG. 3-2e. SIDE VIEW - DOSE POINT LOCATION ON PLANE 4 DOSE RATES - mR/hR

TABLE 3-6

Dose Point Description

Plane	Dose Point Identification	b_1	X_D	Y_D	Z_D	C_{b1}	C_{b2}
1	012	2	40.0	35.0	18.8	02.318*	20.500
1	013	2	30.0	35.0	18.8	02.318*	20.500
1	014	2	20.0	35.0	18.8	02.318*	20.500
1	015	0	30.0	35.0	27.7	10.000*	02.318*
1	016	0	40.0	35.0	27.7	10.000*	02.318*
1	017	0	49.3	35.0	27.7	10.000*	02.318*
1	018	2	49.3	35.0	18.8	02.318*	20.500
1	019	5	30.0	35.0	38.8	20.500	01.600
1	020	2	40.0	35.0	37.8	02.318*	20.500
1	021	2	49.3	35.0	37.8	02.318*	20.500
1	028	5	30.0	44.5	18.8	20.500	01.600
1	029	5	30.0	25.5	18.8	20.500	01.600
1	030	5	30.0	44.5	38.8	20.500	01.600
1	031	5	30.0	25.5	38.8	20.500	01.600
2	001	5	61.4	35.0	27.7	20.500	01.600
2	002	5	61.4	41.5	27.7	20.500	01.600
2	003	5	61.4	35.0	34.3	20.500	01.600
2	004	5	61.4	28.5	27.7	20.500	01.600
2	005	5	61.4	35.0	21.2	20.500	01.600
2	007	5	61.4	49.5	18.8	20.500	01.600
2	008	5	61.4	49.5	27.7	20.500	01.600
2	009	5	61.4	49.5	37.8	20.500	01.600
2	010	5	61.4	20.5	27.7	20.500	01.600
2	011	5	61.4	35.0	37.8	20.500	01.600
3	006	5	61.4	35.0	18.8	20.500	01.600
3	022	5	30.0	49.5	27.7	20.500	01.600
3	023	5	40.0	49.5	27.7	20.500	01.600
3	024	5	40.0	49.5	27.7	20.500	01.600
3	025	5	49.3	49.5	27.7	20.500	01.600
3	026	5	30.0	49.5	20.7	20.500	01.600
3	027	5	30.0	49.5	35.7	20.500	01.600

* C_{b1} and C_{b2} have been multiplied by 10^{-2} to fit input.

Therefore calculated dose rates must be multiplied by 10^2.

the vapor container. From the results given in Table 3-7, the various dose rates in the different planes are given in Fig. 3-2a to Fig. 3-2e.

Table 3-7

Dose Rates from RAS-I Program (Secondary Shield)

Dose Point	Dose (mr/hr)	Dose Point	Dose (mr/hr)
1	0.0014	18	1.8000
2	0.0060	19	9.5000
3	0.0012	20	0.3820
4	0.0014	21	0.0220
5	0.0010	22	0.1700
6	0.0000	23	0.0950
7	0.0002	24	0.0950
8	0.0330	25	0.0070
9	0.0002	26	0.0580
10	0.0400	27	0.0385
11	0.0007	28	0.0162
12	27.4000	29	0.0680
13	59.2000	30	0.3380
14	16.8000	31	2.2800
15	6417.5800		
16	2699.0500		
17	3.0600		

FIG. 3-3

ATTENUATION BY CONCRETE FOR 6-Mev GAMMAS VS. CONCRETE THICKNESS

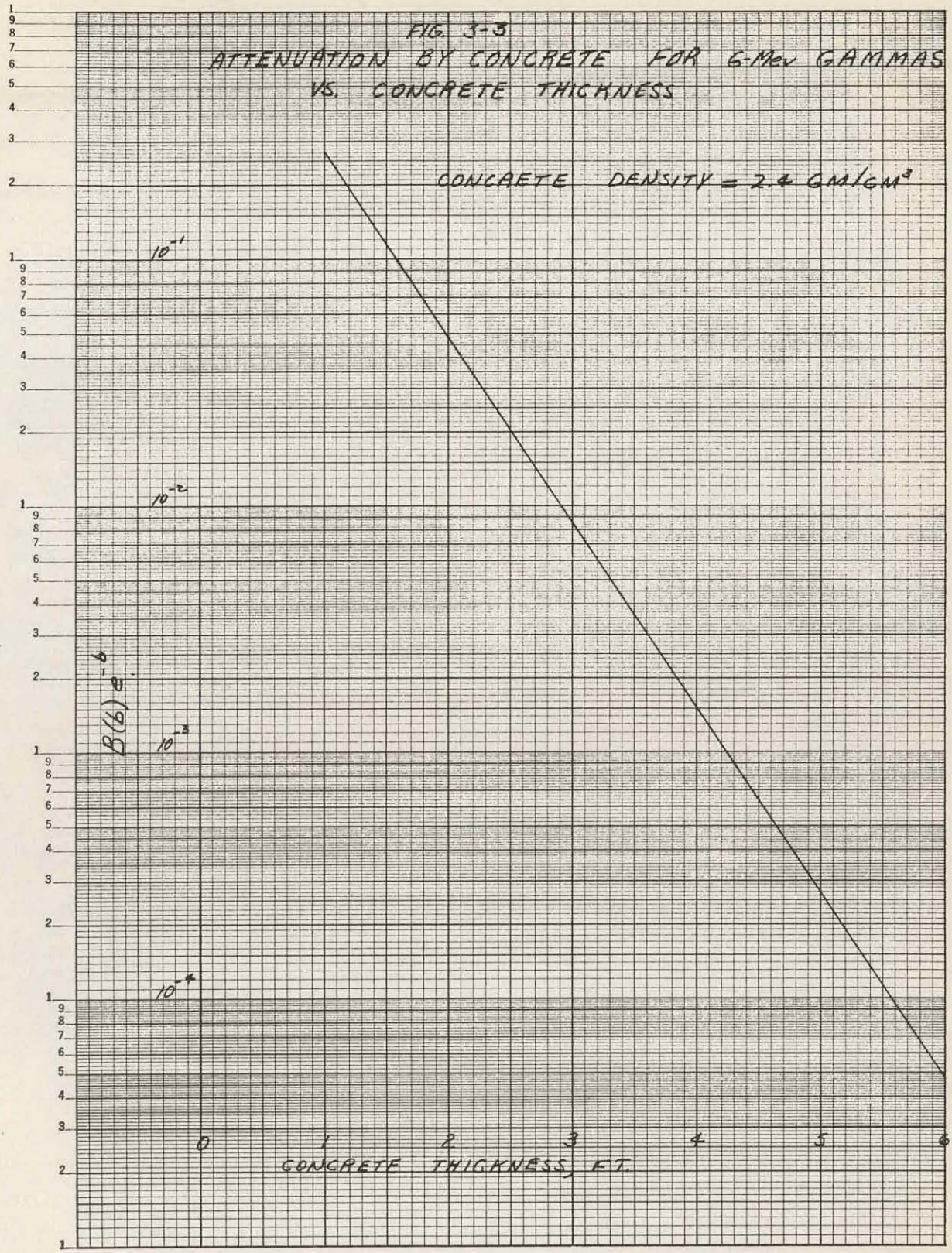

3.3 Attenuation of Radiation from Shield Tank

3.3.1 Calculation Model

With the primary shielding designed for access after shutdown, the dose rate from the reactor and the shield tank through the secondary shield will be much greater than the dose rate from the primary coolant.

The following equation was used to calculate the reactor and shield tank dose rate through the secondary shielding:

$$D_2 = \left(\frac{r_1}{r_2}\right)^2 \quad D_1 \quad e^{-b} \, B(b) \qquad (3\text{-}8)$$

where D_2 = dose rate at a distance r_2 from the core center

D_1 = dose rate on the surface of the shield tank oposite the core midplane

D_1 = 161 R/hr (from section 2.4)

r_1 = radius of shield tank

r_1 = 4.25 ft.

r_2 = distance from core center to point at which dose rate is to be calculated

t = thickness of concrete in secondary shield

$b = \mu t$

μ = linear absorption coefficient of concrete for 6 Mev gammas, cm^{-1}

$B(b)$ = dose buildup factor (for concrete)

$B(b) = A_1 e^{-\alpha_1 \mu t} + A_2 e^{-\alpha_2 \mu t}$

Figure 3-3 is a plot of $B(b)e^{-b}$ for concrete for 6 Mev gammas. Parameters used in calculations for the plot follow:

$\alpha_1 = -0.058$ $\quad \mu = 0.0641 \ cm^{-1}$ for 6 Mev gammas

$\alpha_2 = 0.083$

$A_1 = 3.08$ $\quad$ Concrete density = 2.4 gm/cm^3

$A_2 = 2.08$

The assumption that the entire dose rate on the surface of the shield tank is due to 6-Mev gammas is undoubtedly somewhat conservative.

Knowing the design dose rate at some point outside the secondary shield, the necessary shield thickness can be calculated using Eq. 3-8 and Fig. 3-3. A sample calculation follows.

The area to be protected is the turbine generator skid where r_2 is approximately 71 ft. Here the design dose rate is 1.19 mev/hr. From Eq. 3-8:

$$1.19 \text{ mev/hr} = \left(\frac{4.25}{71}\right)^2 \times 1.61 \times 10^5 \text{ mev/hr} \quad e^{-b} B(b)$$

$$B(b)e^{-b} = \frac{1.19}{1.61 \times 10^5} \left(\frac{71}{4.25}\right) = 2.06 \times 10^{-3}$$

From Fig. 3-3 the concrete thickness corresponding to $B(b)e^{-b}$ calculated above is 3.82 ft. Therefore it may be concluded that 4 ft. of concrete at the entrance end of the secondary shield will reduce the dose rate at the turbine generator skid to design levels. Since the other manned stations of the secondary system are approximately the same distance from the reactor they will have approximately the same dose rate levels.

Dose rate at the turbine generator skid through four feet of concrete is:

$$\frac{1.52 \times 10^{-3}}{2.06 \times 10^{-3}} \times 1.19 \text{ mev/hr} = 0.87 \text{ Mev/hr}$$

It has been shown that 4 ft. of concrete is adequate for protection of the secondary system. However, the dose rate on the surface of the secondary shielding must be checked to determine that the dose rate there is sufficient to allow access during operation.

At the entrance end of the secondary shield:

$r_2 = 41$ ft.

$$D_2 = \left(\frac{4.25}{41}\right)^2 \times 1.61 \times 10^5 \text{ mev/hr} \times 1.52 \times 10^{-3}$$

$D_2 = 2.63$ mev/hr

On the side of the secondary shield at the point nearest to the core:

$r_2 = 13.5$ ft.

$$D_2 = \left(\frac{4.25}{13.5}\right)^2 \times 1.61 \times 10^5 \text{ mev/hr} \times 1.52 \times 10^{-3}$$

$D_2 = 24.2$ mev/hr

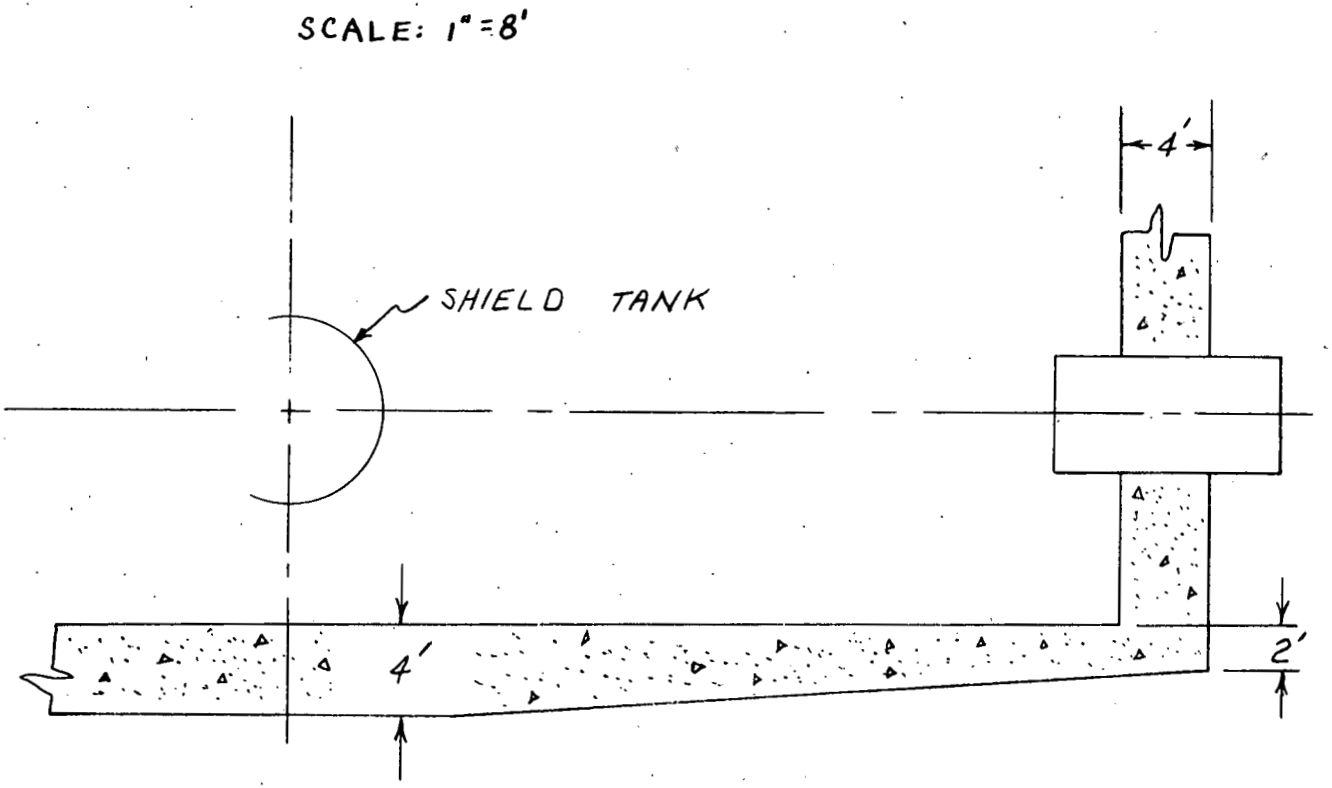

FIG. 3-4 — HORIZONTAL SECTION SHOWING NECESSARY CONCRETE THICKNESS

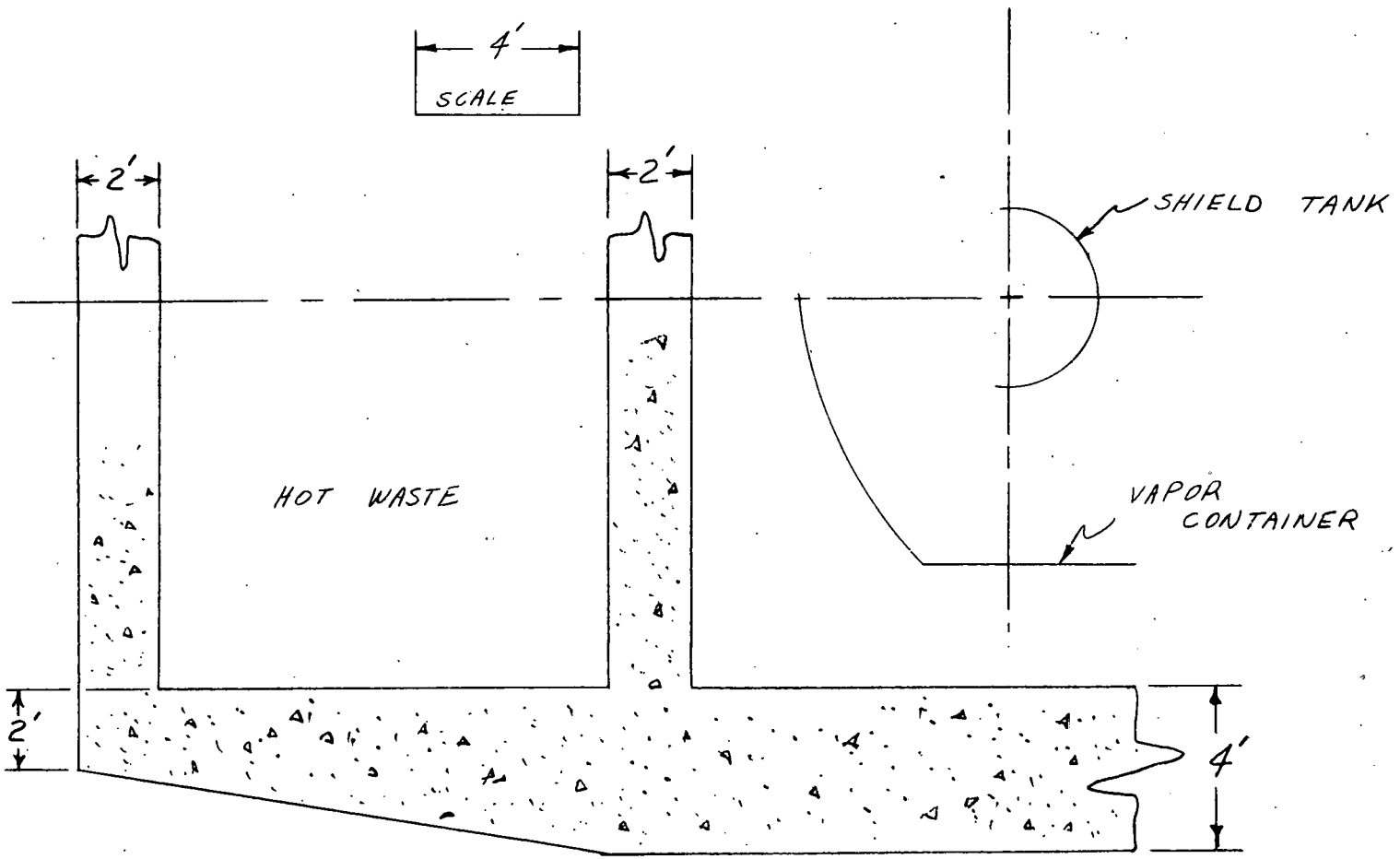

FIG. 3-5 — HORIZONTAL SECTION BELOW CORE SHOWING NECESSARY CONCRETE SHIELDING BEHIND REACTOR

3.4 Secondary Shield Thickness Required

Comparing the dose rates calculated from the shield tank in Section 3.3.1 to those calculated from primary coolant activation in Section 3.2 it can be seen that the primary coolant dose rate is much smaller. Therefore, the necessary concrete thickness may be determined from shield tank dose rate only.

In Section 3.3.1 it has been shown that 4 ft. of concrete is adequate on the sides and on the entrance end of the secondary shield. In addition, on the sides of the shield as the dose point moves from the reactor to the entrance end of the shield, rays from the reactor intersect more shielding due to slant penetration and shield thickness may therefore be reduced. Fig. 3-4 shows the necessary shielding for the sides and entrance end of the secondary shield. Fig. 3-5 shows the necessary concrete in the secondary shield back of the reactor.

3.5 Conclusions

The preceding sections have defined a secondary shield which is adequate to permit access to the side and ends of the secondary shield during operation. Thicknesses are shown in Fig. 3-4 and 3-5. It should be noted that some of these thicknesses are different from those shown in Dwg. No. AEL 413 which shows preliminary estimates of secondary shielding.

Dose rates on the sides and ends of the secondary shield will range downward from 30 mev/hr.

Several means exist for reducing the thickness of secondary shielding. Some of these are:

1. Some concrete can be removed from the top of the secondary shield and replaced with a much smaller amount of lead on top of the lower shield tank.

2. The dose rates calculated in the preceding sections are for points straight out from the shield tank. Therefore these dose rates would be encountered about ten feet above ground level. If it can be assumed that the fairly low dose rate of 30 Mev/hr need extend only as high as about six feet above ground level, some concrete may be removed from the sides of the shield due to slant penetration from the shield tank.

3. If the design dose rate on the sides of the shield may be increased, some concrete may be removed from the sides of the shield. In addition, since the shielding under the vapor container is designed primarily to keep scattering to the sides to tolerable levels, shielding under the vapor container could be reduced. Raising the design dose rate to 200 mev/hr, for instance, would permit removal of about one foot of concrete from the sides and bottom of the shield. This dose rate would limit access to the shield.

4.0 SPENT FUEL SHIELDING

Provision must be made for removing the spent core and storing it until it is shipped off the installation. The spent fuel shielding must do the following:

1) Protect personnel from the complete core whether in the pressure vessel or in the spent fuel pit.

2) Protect personnel from the single element being transferred from the pressure vessel to the spent fuel pit.

4.1 Water Tank Above Core

The water tank above the core performs the function of shielding personnel transferring spent fuel elements from the pressure vessel to the spent fuel pit and also provides a medium for removing decay heat from the spent core in the pressure vessel. The actual height of water above the core is determined from shielding considerations.

To arrive at a necessary water depth above the core, it was first assumed that the allowable dose rate at the surface of the water would be received during the transfer of individual fuel elements since the fuel elements must be raised above seven feet above the core during transfer. Then the dose rate from the complete core was checked through the column of water.

4.1.1 Calculation Model

Because of the fairly large distance between the surface of the water tank above the core and the top of the core itself, the conventional methods for calculating dose rates above cylinder ends fail to give accurate answers. Therefore, the core was treated as a point source.

In calculating the dose rate from the individual fuel elements the same difficulty was encountered. However, since the fuel element height is much greater than its width, the fuel element was divided into eight smaller sections (approximately cubes) and dose rates calculated for each section. A correction factor was then applied to account for self-absorption in the small sections.

Calculations were made on the basis of 6.5 MW operation for infinite time; time after shutdown was 1 day.

4.1.2 Dose Rate During Element Transfer

The individual fuel element was divided into eight sections, each section having the dimensions 2.750 x 2.863 inches. The total dose rate from the eight sections one foot above the surface of the water directly above the element was calculated using the following equations:

$$D = \sum_{j\,0}^{7} \sum_{i-1}^{7} \frac{Sv_i \, Ve^{-b_{i\,j}} \, B_i}{4\pi r^2 \, K_{D_i}}$$

S_{v_i} = specific activity of ith energy group Mev/sec-cm^3

V = Volume of a section, 3.66×10^2 cm^3

r = 244 cm (7 ft of water plus 1 ft)

K_{D_i} = factor for converting energy flux of ith energy group to dose rate

$$b_{ij} = \mu_{i_{H_2O}} \times t_{H_2O} + \mu_{\text{fuel element}} \times j \times 2.75 \text{ inches} \times 2.54 \frac{\text{cm}}{\text{inch}}$$

From the definition of b_{ij} it can be seen that the dose rate from each section is attenuated through all the sections above it. Geometric attenuation, however, was kept constant (for ease of calculation) by using the minimum r for the eight sections.

Table 4-1 contains details of the calculation of the single element calculation.

Dose rates for the eight sections and total dose rate follow:

Section		Dose Rate (mr/hr)
1	(top 2.75 inches of fuel element)	30.06
2		16.97
3		9.26
4		4.70
5		2.47
6		1.30
7		0.68
8	(bottom 2.75 inches of fuel element)	0.37
		65.81

Table 4-1

Calculation of Dose Rate from Single Fuel Element

t_{H_2O} = 7 ft. = 214 cm

$V_{Section}$ = 3.66×10^2 cm^3

R = 8 ft. = 244 cm

$\mu_{\text{fuel element}} = \mu_{\text{core}} = \mu_c$

Section 1

Group	S_v, $\frac{\text{Mev}}{\text{sec-cm}^3}$	μ_{H_2O}	b_{H_2O}	e^{-b}	B_{H_2O} (b)
4	1.755×10^{11}	0.055	11.78	7.7×10^{-6}	19
5	4.583×10^{9}	0.049	10.48	2.8×10^{-5}	11.8
6	1.528×10^{10}	0.044	9.41	8.05×10^{-5}	9.2

Group	K_D	$\frac{VS_v}{4\pi R^2 K_D}$	D, mr/hr
4	6.05×10^5	1.417×10^2	20.8
5	6.5×10^5	3.452×10^0	1.13
6	6.8×10^5	1.099×10^1	8.13
			30.06

Section 2

Group	μ_c	b_2	$b_3 = b_2 \mu_{bH_2O}$	$B_{H_2O}(b_3)$	e^{-b_3}	D, $\frac{mr}{hr}$
4	0.108	0.754	12.534	22	3.6×10^{-6}	11.25
5	0.0941	0.658	11.138	13	1.45×10^{-5}	0.65
6	0.0879	0.620	10.03	10.5	4.4×10^{-5}	5.07
						16.97

$b_2 = \mu_c \times 2.75'' \times 2.54 \frac{cm}{in}$

Table 4-1 (continued)

Section 3

Group	b_2	$b_3 = b_2 \neq b_{H_2O}$	$B_{H_2O}(b_3)$	e^{-b_3}	D, mr/hr
4	1.508	13.288	23	1.8×10^{-6}	5.86
5	1.316	11.80	14	7.5×10^{-6}	0.37
6	1.240	10.65	11.5	2.4×10^{-5}	3.03
					9.26

$b_2 = 2 \times b_2$ of Section 2

Section 4

Group	b_2	b_3	$B_{H_2O}(b_3)$	e^{-b_3}	D, mr/hr
4	2.262	14.04	24.6	8×10^{-7}	2.79
5	1.974	12.45	14.5	3.9×10^{-6}	0.20
6	1.860	11.27	12.0	1.3×10^{-5}	1.71
					4.70

Section 5

Group	b_2	b_3	$B_{H_2O}(b_3)$	e^{-b_3}	D, mr/hr
4	3.016	14.8	26.5	3.8×10^{-7}	1.43
5	2.632	13.11	16	2×10^{-6}	0.11
6	2.480	11.89	12.4	6.8×10^{-6}	0.93
					2.47

Section 6

Group	b_2	b_3	$B_{H_2O}(b_3)$	e^{-b_3}	D, mr/hr
4	3.770	15.55	28.5	1.75×10^{-7}	0.71
5	3.290	13.77	16.7	1.01×10^{-6}	0.06
6	3.100	12.51	13	3.75×10^{-6}	0.53
					1.30

Table 4-1 (continued)

Section 7

Group	b_2	b_3	$B_{H_2O}(b_3)$	e^{-b_3}	D, mr/hr
4	4.524	16.30	30.5	8.2×10^{-8}	0.35
5	3.948	14.43	17.5	5.3×10^{-7}	0.03
6	3.720	13.13	13.7	2×10^{-6}	0.30
					0.68

Section 8

Group	b_2	b_3	$B_{H_2O}(b_3)$	e^{-b_3}	D, mr/hr
4	5.278	17.06	33	4×10^{-8}	0.19
5	4.606	15.09	18.4	2.8×10^{-7}	0.02
6	4.340	13.75	14.5	1.02×10^{-6}	0.16
					0.37

The preceding calculation does not take into account the effect of self-absorption in the sections of the fuel elements. Equation 4-1 was taken from Ref. 21 to account for self absorption:

$$S.A. = \frac{3}{4(\mu_c a)^2}\left[\mu_c a + e^{-2\mu_c a} - \frac{1}{2\mu_c a}(1-e^{-2\mu_c a})\right] \quad (4\text{-}1)$$

a = half height of section, 1.375 inches

μ_c = total linear absorption coefficient of core, cm^{-1}

The minimum self-absorption factor will be calculated when is a minimum; that is, for Group 6 which has the highest energy gamma. The self-absorption factor calculated for this group was 0.83. If this factor is applied to the dose rate calculated without self-absorption, the result is 54.6 mr/hr one foot above the surface of the water in the tank above the core when the top of a single fuel element is 7 feet below the surface.

4.1.3 Dose After Shutdown (Full Core)

The dose rate from the complete core on the surface of the water above the core was calculated using the following equation:

$$D = \sum_{i=1}^{7} \frac{S_{v_i} V e^{-b_i}}{4\pi r^2 K_{D_i}} B_i$$

V = core volume, 1.15×10^5 cm^3

$b_i = \mu_i \times 519$ cm (17 ft of water above core)

r = 519 cm

(See Section 4.1.2 for definition of symbols)

No self-absorption correction was made. The calculated dose rate was 1.76×10^{-3} mr/hr.

Table 4-2 contains details of the calculation for the whole core.

Table 4-2

Dose Rate above Complete Core

t_{H_2O} = 17 ft = 519 cm r

$r^2 = 2.69 \times 10^5$

Group	S_v, $\frac{Mev}{sec\text{-}cm^3}$	H_2O	b_{H_2O}	e^{-b}	B_{H_2O}	D,mr/hr
4	1.755×10^{11}	0.055	28.5	4.2×10^{-13}	60	1.547×10^{-4}
5	4.583×10^{9}	0.048	25.4	9.1×10^{-12}	33	4.65×10^{-5}
6	1.528×10^{10}	0.044	22.8	1.3×10^{-10}	24	1.534×10^{-3}
						1.735×10^{-3}

The dose rate on the walkway above the vapor container from the complete core was calculated in a manner similar to that above. It was found that the equivalent of 11 feet of water was needed between the core and the walkway to reduce the dose rate on the walkway floor to 11.6 mr/hr. It was also found that rays from the core could go through the tank on a slant and intercept less than this minimum of eleven feet. Where this was possible concrete and lead was placed in and around the tank to attenuate core gammas to the allowable level. Lead, water and steel equivalences were taken from Table 6.11 of Ref. 3.

4.2 Water Level in Spent Fuel Pit

At end of life, the spent fuel elements are transferred to a storage area where the elements are cooled down before being shipped for reprocessing. While the elements are in the spent fuel pit, shielding must be provided so that personnel working above the pit do not receive excessive radiation. The shield-

ing is in the form of water placed above the spent core.

4.2.1 Calculation Model

In order to determine the shielding required for the spent fuel pit, the following assumptions were made.

1. Infinite operation at 10 MW
2. 24 hours of shutdown
3. Equivalent sphere to determine self-absorption in core
4. Point source for attenuation of gamma-rays
5. Personnel are always directly above spent core
6. Radioactive sources can be divided into three energy groups

The self-absorption in the core was calculated using a spherical source. On the basis of equivalent volumes (1.15×10^5 cm^3), the radius of the equivalent sphere is 30.17 cm. From Eq. 4-1, the self-absorption factor of the core was calculated for all three energy groups (20).

The numbers used in the calculations and results are given on Table 4-3.

The fission product gammas sources are also given in Table 4-3 for the three energy groups. The sources were obtained from NDA-27-39 (4) for infinite operation and 24 hours of shutdown.

The required amount of shield water above the spent core was based on the attenuation of gamma rays from a point source using equation 4-2 for all three energy groups.

Table 4-3

Calculation of Spent Fuel Pit Shielding

	Energy Group		
	IV	V	VI
E(Mev)	1.6	2.1	2.5
μ_{core}(cm-1)	0.108	0.0941	0.0879
$(\mu r)_{core}$	3.258	2.839	2.652

Table 4-3 (Con't)

	Energy Group		
	IV	V	VI
$F(\mu r)_{core}$	0.219	0.247	0.263
$\mu_{H_2O}(cm^{-1})$	0.055	0.048	0.0438
S(Mev/sec-watt)	3.1×10^{9}	8.1×10^{7}	2.7×10^{8}
S_o(Mev/sec)	2.015×10^{16}	5.265×10^{14}	1.755×10^{15}
$C_e\left(\frac{\gamma/cm^2\text{-sec}}{mr/hr}\right)$	365	315	265
$(b_1)_1$	18.44	16.43	14.75
$(b_1)_2$	21.79	19.42	17.43
$(b_1)_3$	20.12	17.92	16.09
B_1	41.0	21.8	15.9
B_2	53.0	26.8	19.1
B_3	47.0	24.2	17.6
$e^{-(b_1)_1}$	9.808×10^{-9}	7.318×10^{-8}	3.927×10^{-7}
$e^{-(b_1)_2}$	3.441×10^{-10}	3.68×10^{-9}	2.693×10^{-8}
$e^{-(b_1)_3}$	1.828×10^{-9}	1.65×10^{-8}	1.028×10^{-7}
D_1(mr/hr)	3.441	0.466	7.701
D_2(mr/hr)	0.112	0.021	0.454
D_3(mr/hr)	0.618	0.098	1.875

a_1 = 11 feet a_2 = 13 feet a_3 = 12 feet

$(D_1)_T$ = 11.608 mr/hr $(D_2)_T$ = 0.587 mr/hr $(D_3)_T$ = 2.591 mr/hr

$$D(E) = \frac{B(E)\ F(E)\ S_o(E)\ e^{-b_1(E)}}{4\pi a^2} \qquad (4\text{-}2)$$

where

$D(E)$ = dose at desired point, mr/hr

$F(E)$ = self-absorption factor

$B(E)$ = dose buildup factor

$S_o(E)$ = source strength of point source, gammas/sec

a = distance from point source to dose point

$b_1(E) = \mu_{H_2O}(E)\ t_{H_2O}$

$\mu_{H_2O}(E)$ = linear absorption coefficient of water, cm^{-1}

t_{H_2O} = thickness of water shield

The calculation of the dose rate at the top of the spent fuel pit for 11, 12, and 13 feet of shield water for all energy groups is given in Table 4-3.

4.2.2 Dose Rate on Top of Spent Fuel Pit

The dose rate was calculated for 11, 12, and 13 feet of shield water. For 11 feet of shield water, the dose rate was 11.608 mr/hr on top the spent fuel pit. With 12 and 13 feet of shield water, the dose rates are 2.591 and 0.587 mr/hr respectively. The results of the calculation are given in Fig. 4-1. For a dose rate no higher than 5 mr/hr on the top of the spent fuel pit 24 hours after shutdown, approximately 11.5 ft. of shield water is required above the center of the core.

4.3 Radial Shielding For Spent Fuel Pit

The spent fuel pit in the permofrost installation is located so that it is accessible during operation. Because of its location, Dwg. AEL-413, concrete is used as the main shielding material in the radial direction. The spent fuel elements are arranged in a lattice that is 3 feet by 3 feet located 3 feet from the concrete wall.

The radial shielding consists of three parts as follows:

1. 3 feet of water
2. 3 feet of concrete
3. 3 inches of lead

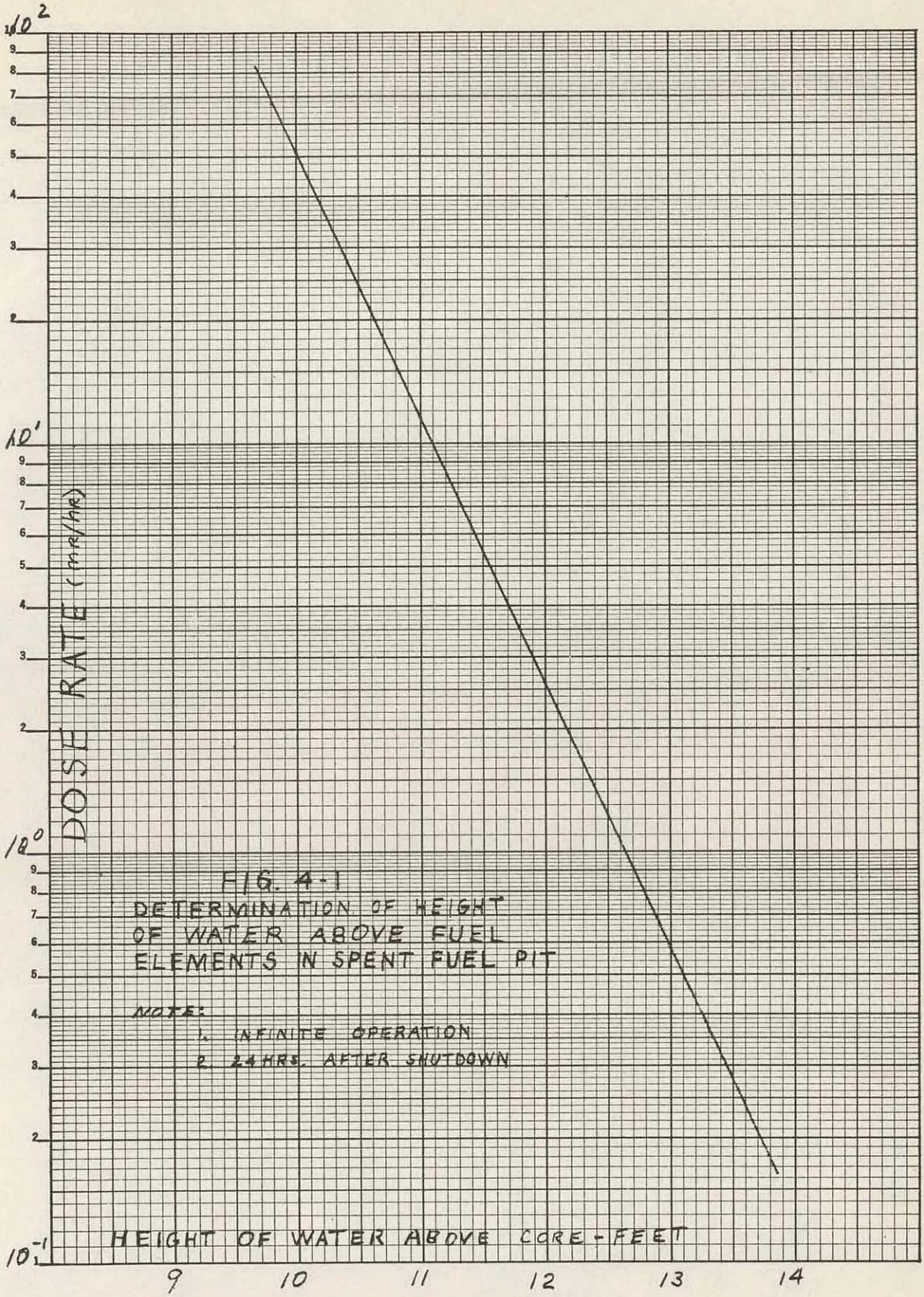

FIG. 4-1
DETERMINATION OF HEIGHT OF WATER ABOVE FUEL ELEMENTS IN SPENT FUEL PIT

NOTE:
1. INFINITE OPERATION
2. 24 HRS. AFTER SHUTDOWN

The three inches of lead is placed against the inside surface of the concrete wall In the configuration as given above, the dose rate on the outside surface of the concrete wall will be about 1 mr/hr. This condition exists 24 hours after shutdown which is the approximate time that the elements are placed in the spent fuel pit.

4.4 Shielding for Shipping Cask

It was decided to use the spent fuel shipping cask that was designed for the APPR-1. The design analysis was presented in AP Memo 63 (21). The following assumptions were used in the calculation:

1. Fuel element activity 1.5 times the average activity
2. Six spent fuel elements per shipping cask
3. Reactor operation time was taken as infinite
4. Four shutdown times: 10, 20, 30, and 90 days

The dose rates on the surface of the shipping cask and one meter from surface is given in Table 4-4 for different lead thicknesses and the four cooling times.

From the calculated results, 9.5 inches of lead is needed so that the dose rate one meter from the surface is less than 10 mr/hr with a cooling time of 90 days. The dose rate on the surface of the spent fuel shipping cask will be under 40 mr/hr for the conditions stated in the previous section.

Table 4-4

Radial Dose Rates - Spent Fuel Cask

Lead Thickness Inches	Dose Rate in mr/hr at Surface after Shutdown				Dose rate in mr/hr one meter from Surface after Shutdown			
	10 days	20 days	30 days	90 days	10 days	20 days	30 days	90 days
9.5	-	-	-	59.3	-	-	-	9.46
10.0	429	323	226	26.6	90	67	46	5.15
10.5	207	156	109	12.1	48	36	25	2.81
11.0	105	80	56	-	27	20	14	-
11.5	54	42	29	-	15	11	8	-
12.0	29.7	23.1	16.4	-	8.3	6.3	4.4	-

4.5 Conclusions

From the foregoing sections it may be concluded that adequate shielding has been designed for the spent core and that core removal operations may be carried out within the allowable dose rate limits of Section 1.0.

5.0 HEAT RELEASE DISTRIBUTION

The reactor vessel as originally designed in APAE-33 (22) was based on a two inch thick vessel wall located 6.15 cm. from the edge of the core. In this design, there was to be no thermal shields between the core and the reactor vessel as can be seen in Drawing AEL-335 of APAE-33 (22). This was proposed because of the necessity of compactness. However, detailed calculations on this proposed design showed that the vessel was overstressed due to gamma heating. In order to decrease the stress to within the allowable stress, work was performed on various configurations. Table 5.1 gives the list of configurations that were investigated.

The gamma heating was calculated for all seven cases at a power output of 6.5 MW. Case 7 is the configuration that was finally selected.

5.1 Reactor Vessel Wall at Midplane

5.1.1. Calculation Model

The calculation of the gamma heating in the reactor vessel was based on a cylindrical core with the thermal shields and the reactor vessel as cylindrical shells. The calculation was performed at the midplane of the core and is divided into core and secondary gammas. The complete calculation was performed by an IBM 650 program (11). The code is divided into 4 parts. The first routine calculates the source strength, S_c, and the macroscopic cross section of source material, μ_c. The attenuation of core gammas is then computed by a second routine utilizing μ_c and S_c and material and geometrical specification set up by a third routine. The results of these operations is the volumetric heat release, H (BTU/in^3 - sec), in the reactor vessel. The calculation of the gamma attentuation is based on equation 5-1.

TABLE 5-1

Reactor Vessel Configurations

Case #	Reactor Vessel			Thermal Shield		
	Inside Dia.	Thickness	Material	Inside Dia.	Thickness	Material
1	25"	2"	304SS		None	
2	25"	1-3/4"	304SS		None	
3	28.5"	2"	304SS	23.5"	2"	304-SS
4	30.5"	2"	304SS	23.5"	3"	304-SS

TABLE 5-1 (Cont'd)

Reactor Vessel Configurations

Case #	Reactor Vessel			Thermal Shield		
	Inside Dia.	Thickness	Material	Inside Dia.	Thickness	Material
5	30.5"	2"	304SS	23.5"	3"	Borated 304-SS
6	37.75"	1/8" Clad/ 2-3/8" Vessel	304SS SA-212	33"	1"	304-SS
7	37.75"	1/8" Clad/ 2-3/8" Vessel	304-SS SA-212	23.5"	2"	304-SS

$$H(E) = \frac{C\ B\ S\ R^2}{\underset{2(a+Z)}{e\ a\ c\ o}} F\left[\theta, b_2\right] \qquad (5\text{-}1)$$

where B_a = Energy absorption build-up factor

S_c = Source strength of core, (cm^{-3} - sec^{-1})

R_o = Radius of volume source, cm

a = distance from source to heat release point, cm

Z = effective self-attenuation distance, cm

$$F\left[\theta, b_2\right] = \int_0^{\infty} e^{-b_2 \sec\theta'}\, d\theta'$$

$\theta = \mathrm{Tan}^{-1} \left(\frac{h/2}{a+Z}\right)$, degrees

h = height of volume source, cm

$b_2 = b_1 + \mu_c Z$

$b_1 = \sum_i \mu_i t_i$

μ_c = Macroscopic cross section of core, cm^{-1}

μ_i = Macroscopic cross section of i^{th} shield, cm^{-1}

t_i = Thickness of $_i$th shield

$$C_e = H(E)/\phi_\gamma(E) = (2.488 \times 10^{-15} \frac{BTU\text{-}cm^3}{Mev\text{-}in^3}) \mu_a(E) E$$

$\phi_\gamma(E)$ = Gamma flux, photons/cm^2-sec

$\mu_a(E)$ = Energy absorption cross section for vessel, cm^{-1}

E = Energy of gamma, Mev

The second contribution to the volumetric heat release in the reactor vessel is due to capture and decay gammas emanating from various components of the shield. This calculation is also computed by the IBM 650 (11) and is based on equation 5-2.

$$H(E) = \frac{C_e B_a S_V}{2\mu_s} \left[E_2(b_1) - E_2(b_3)\right] \qquad (5\text{-}2)$$

where S_V = source strength of volume source, (cm^{-3}-sec^{-1})

μ_s = macroscopic cross section of source material, cm^{-1}

$$E_2(b) = b \int_b^\infty \frac{e^{-t}}{t^2} dt$$

$b_3 = b_i \mu_s h$

h = thickness of source slab, cm

5.1.2 Application to APPR-1

The volumetric heat release was calculated for the thermal shield and the reactor vessel of the APPR-1 by ASTRA (23). From experimental temperature measurements on the APPR-1 reactor vessel, a volumetric heat release was calculated. To compare with the above quantities, the heat release rate was calculated using the IBM 650 codes. The values of the volumetric heat releases on the inside surface of the reactor vessel and thermal shield is given in Table 5-2.

TABLE 5-2

Voluemtric Heat Release in APPR-1 Thermal Shield and Reactor Vessel

	Reactor Vessel	Thermal Shield
ASTRA	43,300 BTU/FT^3-Hr	249,000 BTU/Ft^3-Hr
Alco (IBM 650)	37,000 BTU/FT^3-Hr	162,000 BTU/Ft^3-Hr
Experimental Temperature measurements	20,000 BTU/FT^3-Hr	None

From the above table, the IBM 650 calculation gives results closer to the experimentally inferred number than does the ASTRA computation. The results from the machine calculation are within a factor of two to the volumetric heat release based on experimental temperature measurements. The heat release distribution through the reactor vessel is given in Fig. 5-1, for all calculation models. This figure shows that the machine calculation gives a reliable answer.

5.1.3 Calculated Distribution (Core Gamma)

The gammas emanating from the core is divided into 5 energy groups as given in Table 5-3.

TABLE 5-3

Energy Groups of Gammas

Group	Energy (Mev)
1	Greater than 7
2	5-7
3	3-5
4	1-3
5	less than 1

The gamma heating in the reactor vessel was calculated for all cases. The contribution from each energy group from the core is given in Table 5-4, for the final configuration, case 7.

5.1.4 Calculated Distribution (secondary gammas)

For each calculation of the distribution due to core gammas, the distribution due to secondary gammas was computed. The results that were obtained for case 7 is given in Table 5-5 based on the same energy grouping.

5.1.5 Calculated Distribution (Total Gammas)

The total volumetric heat release is the summation of the heat release due to core and secondary gammas. The results for the final configuration, case 7, are given in Fig. 5-2 and in Table 5-6.

At the interface between the clad and the reactor vessel, the total volumetric heat release, H, is 0.01781 BTU/in^3-sec or 1.108×10^5 BTU/FT^3-hr. The distribution can be described by the following equation:

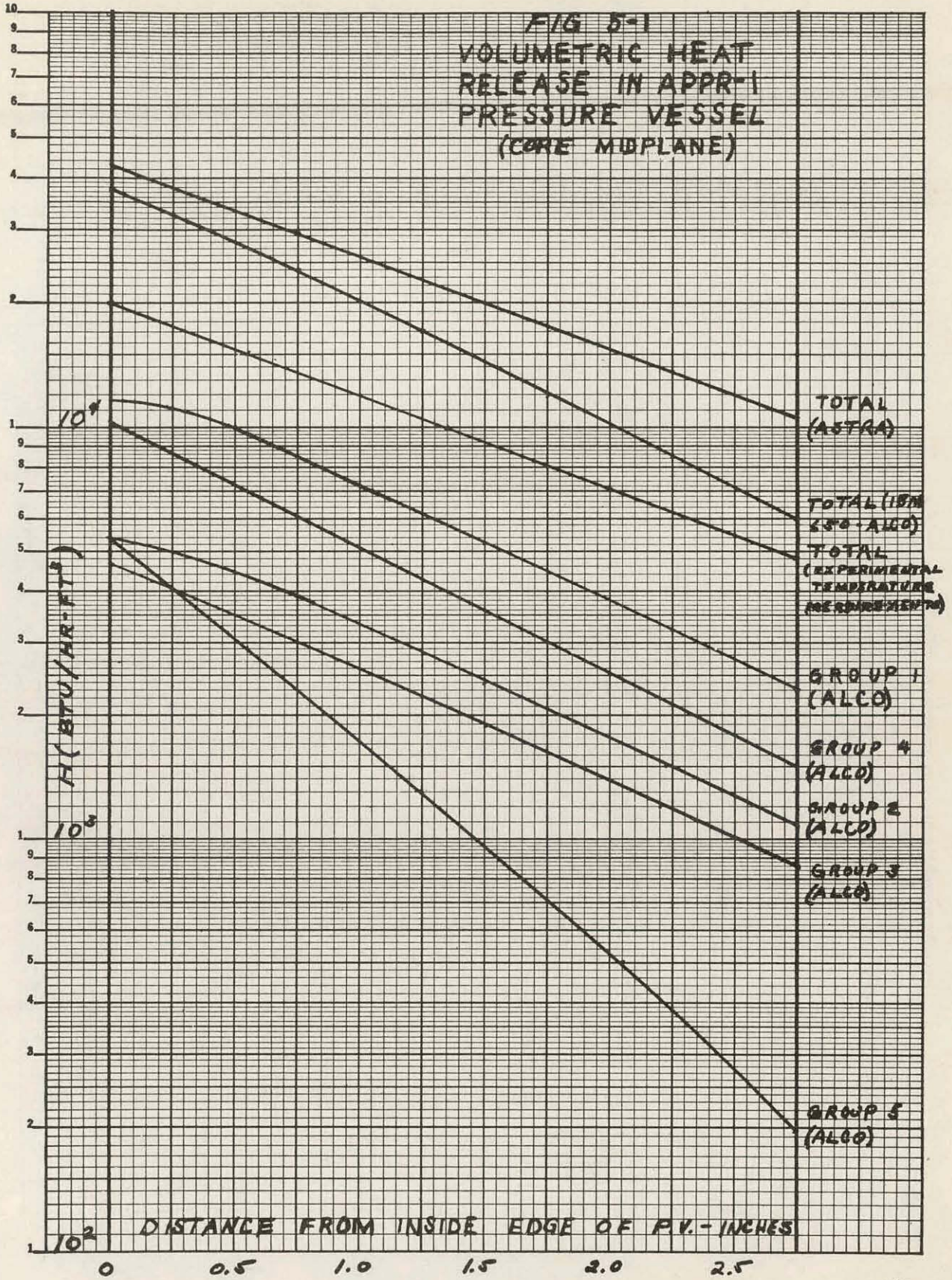
FIG 5-1
VOLUMETRIC HEAT RELEASE IN APPR-1 PRESSURE VESSEL (CORE MIDPLANE)
TOTAL (ASTRA)
TOTAL (ISM 650 - ALCO)
TOTAL (EXPERIMENTAL TEMPERATURE MEASUREMENTS)
GROUP 1 (ALCO)
GROUP 4 (ALCO)
GROUP 2 (ALCO)
GROUP 3 (ALCO)
GROUP 5 (ALCO)
H (BTU/HR-FT³)
DISTANCE FROM INSIDE EDGE OF P.V. - INCHES
10⁴
10³
10²
0
0.5
1.0
1.5
2.0
2.5

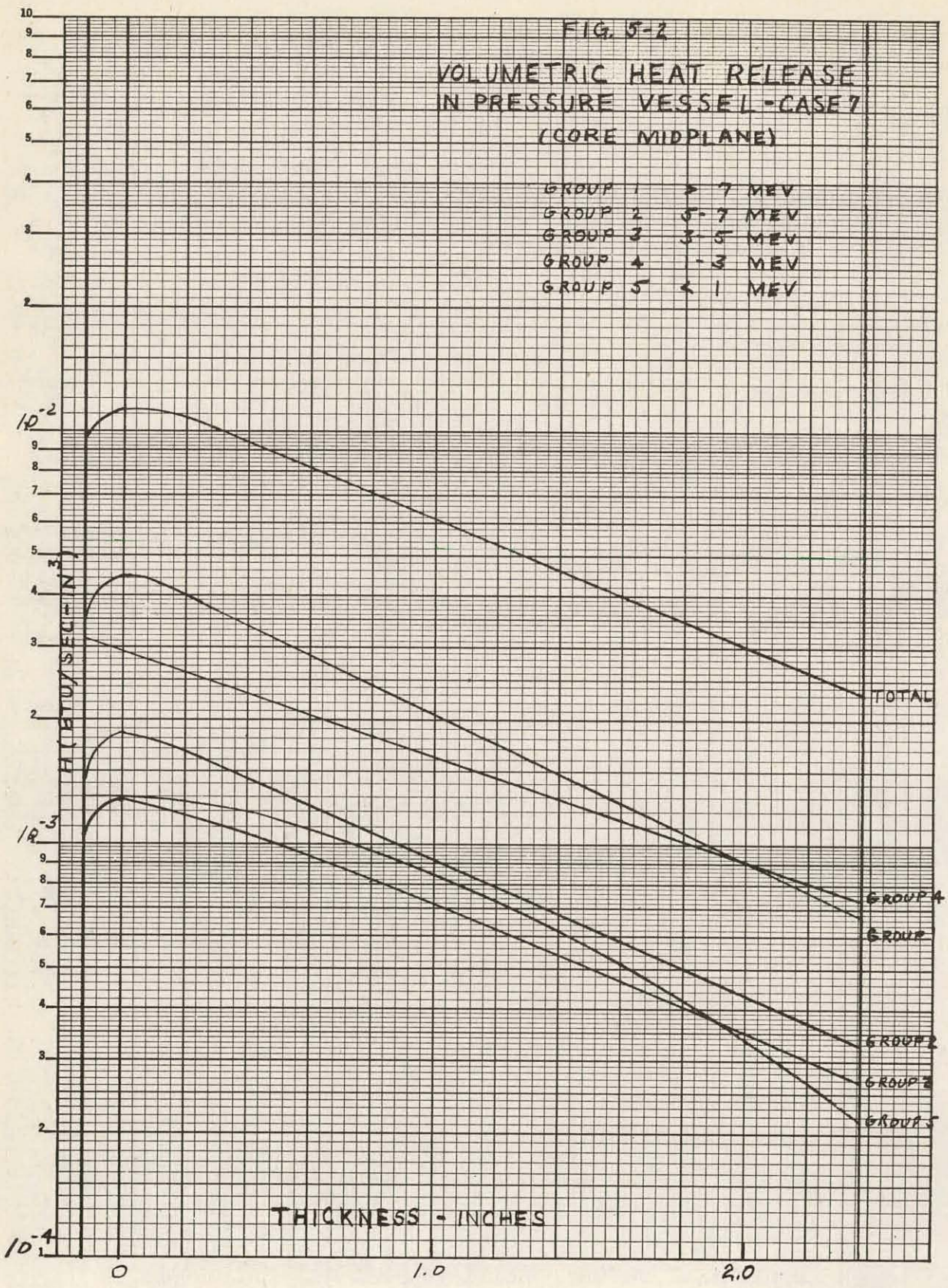
FIG. 5-2
VOLUMETRIC HEAT RELEASE
IN PRESSURE VESSEL - CASE 7
(CORE MIDPLANE)
GROUP 1 > 7 MEV
GROUP 2 5 - 7 MEV
GROUP 3 3 - 5 MEV
GROUP 4 1 - 3 MEV
GROUP 5 < 1 MEV
H (BTU/SEC-IN³)
TOTAL
GROUP 4
GROUP
GROUP 2
GROUP 3
GROUP 5
THICKNESS - INCHES
0
1.0
2.0

TABLE 5-4

Volumetric Heat Release in Pressure Vessel at Core Midplane due to Core
$H(BTU/IN^3\text{-sec})$

Energy (Mev)	Inside Surface of Clad	Interface Between Clad & Vessel	7/16" from Interface	14/16" from Interface	1-5/16" from Interface	1-12/16" from Interface	Outside Surface of Vessel
>7	4.20×10^{-4}	3.82×10^{-4}	3.01×10^{-4}	2.28×10^{-4}	1.81×10^{-4}	1.42×10^{-4}	1.09×10^{-4}
5-7	4.08×10^{-4}	3.80×10^{-4}	2.97×10^{-4}	2.33×10^{-4}	1.82×10^{-4}	1.44×10^{-4}	1.12×10^{-4}
3-5	5.07×10^{-4}	4.71×10^{-4}	3.79×10^{-4}	3.02×10^{-4}	2.43×10^{-4}	1.89×10^{-4}	1.47×10^{-4}
1-3	2.297×10^{-3}	2.121×10^{-3}	1.849×10^{-3}	1.533×10^{-3}	1.248×10^{-3}	9.70×10^{-4}	7.42×10^{-4}
<1	1.249×10^{-3}	1.089×10^{-3}	1.158×10^{-3}	9.26×10^{-4}	6.48×10^{-4}	4.21×10^{-4}	2.65×10^{-4}
Total	4.881×10^{-3}	4.443×10^{-3}	3.984×10^{-3}	3.222×10^{-3}	2.502×10^{-3}	1.866×10^{-3}	1.375×10^{-3}

TABLE 5-5

Volumetric Heat Release in Pressure Vessel at Core Midplane Due to Secondary Gammas
H (BTU/IN^3-sec)

Energy (Mev)	Inside Surface of Clad	Interface Between Clad & Vessel	7/16" from Interface	14/16" from Interface	1-5/16" from Interface	1-12/16" from Interface	Outside Surface of Vessel
7	2.691×10^{-3}	4.187×10^{-3}	2.983×10^{-3}	2.068×10^{-3}	1.431×10^{-3}	9.89×10^{-4}	6.72×10^{-4}
5-7	1.042×10^{-3}	1.525×10^{-3}	1.113×10^{-3}	7.80×10^{-4}	5.44×10^{-4}	3.79×10^{-4}	2.59×10^{-4}
3-5	5.62×10^{-4}	8.31×10^{-4}	6.60×10^{-4}	4.72×10^{-4}	3.33×10^{-4}	2.33×10^{-4}	1.60×10^{-4}
1-3	5.34×10^{-4}	4.98×10^{-4}	3.33×10^{-4}	2.32×10^{-4}	1.63×10^{-4}	1.14×10^{-4}	7.9×10^{-5}
1	5.8×10^{-5}	9.4×10^{-5}	5.6×10^{-5}	3.6×10^{-5}	2.1×10^{-5}	1.2×10^{-5}	0.7×10^{-5}
Total	4.887×10^{-3}	7.135×10^{-3}	5.145×10^{-3}	3.588×10^{-3}	2.492×10^{-3}	1.727×10^{-3}	1.177×10^{-3}

TABLE 5-6

Volumetric Heat Release in Pressure Vessel at Cone Midplane Due to Total Gammas
H (BTU/IN^3-sec)

Energy (Mev)	Inside Surface of Clad	Interface Between Clad & Vessel	7/16" from Interface	14/16" from Interface	1-5/16" from Interface	1-12/16" from Interface	Outside Surface of Vessel
7	3.111×15^{-3}	4.569×10^{-3}	3.284×10^{-3}	2.296×10^{-3}	1.612×10^{-3}	1.130×10^{-3}	7.81×10^{-4}
5-7	1.450×10^{-3}	1.904×10^{-3}	1.410×10^{-3}	1.013×10^{-3}	7.26×10^{-4}	5.23×10^{-4}	3.71×10^{-4}
3-5	1.069×10^{-3}	1.303×10^{-3}	1.039×10^{-3}	7.74×10^{-4}	5.76×10^{-4}	4.22×10^{-4}	3.07×10^{-4}
1-3	2.831×10^{-3}	2.619×10^{-3}	2.181×10^{-3}	1.765×10^{-3}	1.410×10^{-3}	1.084×10^{-3}	8.21×10^{-4}
1	1.307×10^{-3}	1.182×10^{-3}	1.214×10^{-3}	9.61×10^{-4}	6.70×10^{-4}	4.34×10^{-4}	2.72×10^{-4}
Total	9.770×10^{-3}	1.157×10^{-2}	9.128×10^{-3}	6.809×10^{-3}	4.994×10^{-3}	3.593×10^{-3}	2.552×10^{-3}

$$H = 0.0125e^{-0.67395\,x}\ BTU/in^3\text{-sec} \qquad (5\text{-}3)$$

The volumetric heat release distribution for the other cases are given in Table 5-7.

TABLE 5-7

Volumetric Heat Release Distributions for All Configurations

Case #	Equation	Average Heat Release
1	$H = 0.08697e^{-0.762\,x}$ BTU/in^3-sec	$H = 0.0447$ BTU/in^3-sec
2	$H = 0.08697e^{-0.762\,x}$ BTU/in^3-sec	$H = 0.0482$ BTU/in^3-sec
3	$H = 0.0200e^{-0.6611x}$ BTU/in^3-sec	$H = 0.0111$ BTU/in^3-sec
4	$H = 0.0120e^{-0.6453x}$ BTU/in^3-sec	$H = 0.0068$ BTU/in^3-sec
5	$H = 0.0098e^{-0.5736x}$ BTU/in^3-sec	$H = 0.0058$ BTU/in^3-sec
6	$H = 0.0222e^{-0.6868x}$ BTU/in^3-sec	$H = 0.0114$ BTU/in^3-sec
7	$H = 0.0120e^{-0.674x}$ BTU/in^3-sec	$H = 0.0063$ BTU/in^3-sec

The thermal stress in the reactor vessel due to gamma heating was calculated on the basis of the above operations.

5.2 Axial Heat Distribution in Reactor Vessel Wall

A calculation was made to establish the heat release distribution at various axially positions in the vessel. The heat release distribution was calculated in the outlet nozzle and the flange above the core to facilitate the thermal stress calculations in these members.

5.2.1 Outlet Nozzle

The outlet nozzle is located about 6 inches below the bottom of the core. The average thickness of the nozzle is 10 inches.

The machine calculations of core gamma attenuation is set up to determine the heat distribution at the midplane of the core and therefore can not be used axially (11). A simplified model was used to calculate the volumetric heat release as a function of axial position as given in equation 5-4.

$$H_a = H_m e^{-\sum_i \mu_i t_i (1-\sec\psi)} \qquad (5\text{-}4)$$

where H_a = Volumetric heat release at any axial position, BTU/in^3-sec

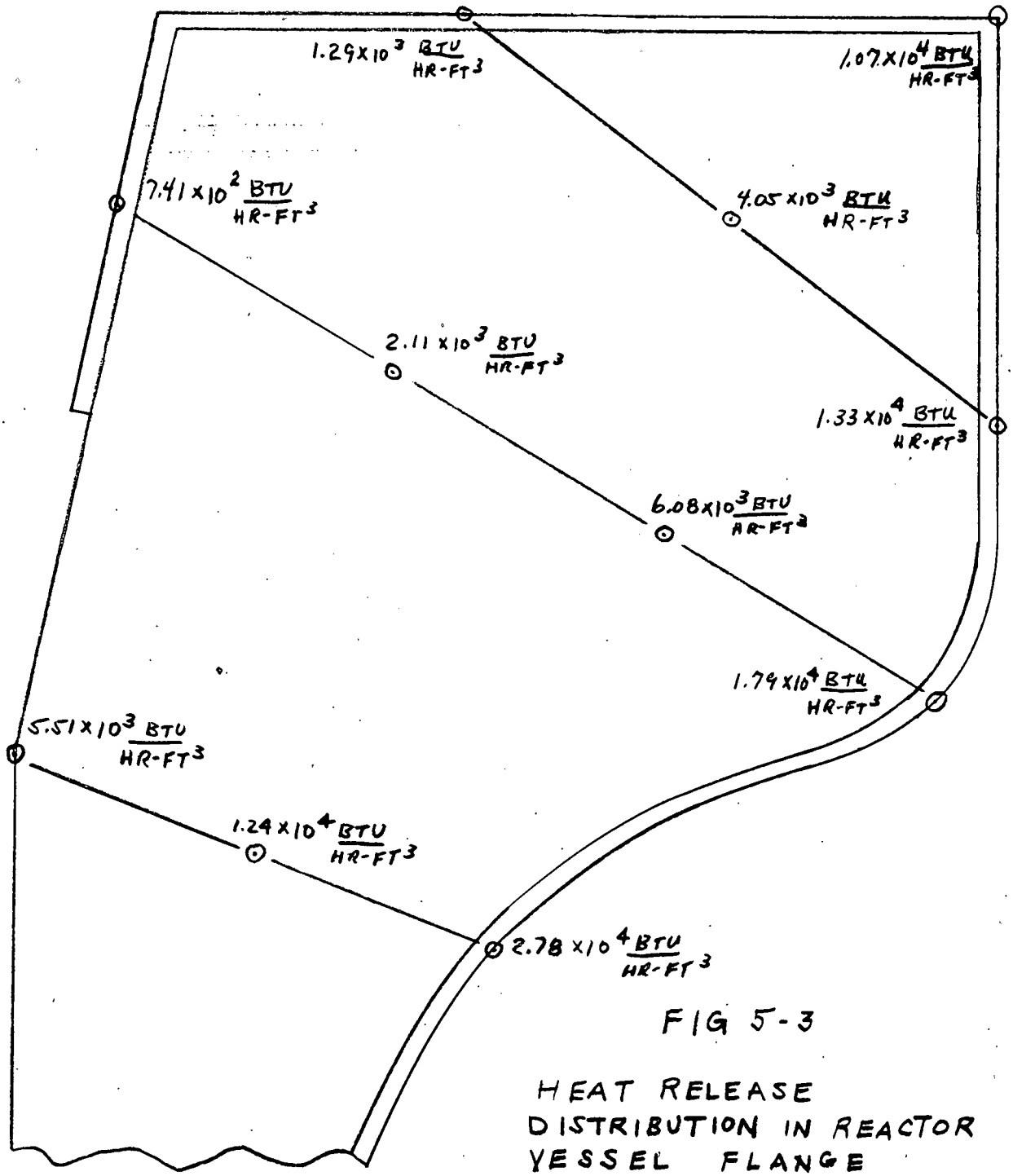

FIG 5-3

HEAT RELEASE DISTRIBUTION IN REACTOR VESSEL FLANGE

H_m = Volumetric heat release Core midplane, BTU/in^3-sec

μ_i = macroscopic cross-section of i^{th} shield, cm^{-1}

t_i = thickness of i^{th} shield, cm

$\psi = \text{Tan}^{-1} \left(\frac{h'}{a + R_o} \right)$, degrees

R_o = Radius of cylinder source, cm

a = Distance from source to heat release point, cm

h' = Axial distance above midplane of core, cm

The heating at the inside surface of the nozzle calculated from equation 5-4 is 11,700 BTU/hr-Ft^3. At the midplace of the core, the heat release at the inside surface of the vessel due to secondary gamma is equal to that due to core gammas. As a conservative approach, it can be assumed that the secondary contribution is equal to the contribution from the core on the inside surface of the nozzle. Therefore, the volumetric heat release distribution at the nozzle is 23,400 BTU/hr-ft^3.

5.2.2 Flange on Top of Reactor Vessel

The heat release distribution was calculated on the inside surface of the flange and at various interior points. The contribution of core gamma was based on the attenuation of the core gamma flux on the inside surface of the thermal shield through the shield, reflector and reactor vessel flange. Equations 5-5a and 5-5b were used to calculate the attenuation of the flux

(Thru steel) $$\phi_2 = \phi_1 B_a e^{-\mu t} \qquad (5\text{-}5a)$$

(Thru water) $$\phi_2 = \phi_1 \qquad (5\text{-}5b)$$

where B_a = Energy absorption build-up factor

μ = macroscopic cross section of steel, cm^{-1}

t = thickness of steel, cm

These equations assume that the only attenuation is due to steel. Water was considered transparent to gamma rays. As another conservative assumption, the contribution due to secondary gammas was set equal to heat release distribution due to core gammas. The total heat release distribution is shown in Fig. 5-3.

6.0 DEMINERALIZER SHIELDING

Due to corrosion and activation of the structural material in the primary system, the primary coolant becomes activated. This activity is due to both soluble and insoluble nuclides in the coolant. In order to remove these nuclides, a resin filled demineralizer is placed in the primary coolant blowdown line. Therefore, the demineralizer acts as a filter for insoluble nuclides and as a chemical exchange medium for soluble nuclides. In this manner, the activated nuclide concentration in the primary coolant is kept down.

The activation of the primary coolant is due to several nuclear reactions. With stainless steel as the structural material, the following reactions will take place in the material.

1. Cr^{50} (n,γ) Cr^{51}
2. Ni^{64} (n,γ) Ni^{65}
3. Fe^{54} (n,p) Mn^{54}
4. Mn^{55} (n,γ) Mn^{56}
5. Fe^{56} (n,p) Mn^{56}
6. Ni^{58} (n,p) Co^{58}
7. Co^{59} (n,γ) Co^{60}
8. Fe^{58} (n,γ) Fe^{59}

Since the demineralizer removes all the activated nuclides from the blowdown line, the demineralizer in turn becomes a radioactive source. This necessitates the shielding of the demineralizer by a lead cask.

6.1 Corrosion Product Concentration in Demineralizer

The concentration of active nuclides in the demineralizer was calculated from equations 6-1, 6-2, 6-3, and 6-4.

$$n_D = X + Y + Z \tag{6-1}$$

$$X = \frac{C_o S_o N_a F_n F_s \sigma \phi_e}{V_I A} \left[\frac{1 - e^{-\lambda t}}{\lambda(\lambda + Q/V_w)} + \frac{e^{-\lambda t_{-e}} - (Q/V_w)t}{\lambda(\lambda - Q/V_w)} + \cdot \frac{e^{-(\lambda + Q/V_w)t_{-e}} - \lambda t}{(\lambda + Q/V_w)(Q/V_w)} + \frac{e^{-\lambda t_{-e}} - (\lambda + Q/V_w)t}{\lambda (Q/V_w)} \right] \tag{6-2}$$

$$Y = \frac{Q\, C_o S_a N_a F_n F_s \sigma\, \phi_a}{V_I A\, \lambda V_w} \left[\frac{1-e^{-\lambda t}}{\lambda(\lambda + Q/V_w)} + \frac{e^{-\lambda t} - e^{-(\lambda + Q/V_w)t}}{(Q/V_w)^2} - \frac{te^{-\lambda t}}{(Q/V_w)} + \frac{e^{-(\lambda + Q/V_w)t}\, e^{-\lambda t}}{(\lambda + Q/V_w)\,(Q/V_w)} \right] \quad (6\text{-}3)$$

$$Z = \frac{Q f_n f_s N_a \sigma S_a \phi_a}{4A\, V_I(\lambda + Q/V_w)} \ell\rho \left[\frac{1-e^{-\lambda t}}{\lambda V_w} + \frac{e^{-(\lambda + Q/V_w)t} - e^{-\lambda t}}{Q} \right] \quad (6\text{-}4)$$

where n_D = concentration of active nuclides in demineralizer, atom/cm^3

C_o = release rate, gm/cm^2 -sec = 0.965×10^{-11}

S_o = total primary system corrosion area, cm^2 = 2.5398×10^6.

$(S_o)_N$ = for normal Co stainless steel, cm^2 = 1.0728×10^6

$(S_o)_L$ = for low Co stainless steel, cm^2 = 1.468×10^6

S_a = primary system corrosion area exposed to flux, cm^2 = 1.524×10^6

$(S_a)_N$ = for normal Co stainless steel, cm^2 = 5.65×10^4

$(S_a)_L$ = for low Co stainless steel, cm^2 = 1.468×10^6

N_a = Avogadro's number, atoms/mole = 6.023×10^{23}

σ_i = thermal activation cross section of target nuclide, cm^2/atom

A_i = Atomic weight of target nuclide, gm/mole

Q = flow rate through demineralizer, cm^3/sec = 63.6

λ_i = disintegration constant of active nuclide, sec^{-1}

V_w = volume of primary water, cm^3 = 1.9944×10^6

ρ_i = density of target nuclide, gm/cm^3

ℓ = recoil distance, cm = 10^{-5}

t = time of operation, sec = 3.156×10^7

TABLE 6-1

Properties of the Nuclides

Reaction	f_s	f_n	σ(barn)	λ(sec^{-1})	ρ(gm/cm^3)	A(gram/mole)
Cr^{50}-Cr^{51}	0.19	0.043	7.4	3.03×10^{-7}	7.1	52.01
Ni^{64}-Ni^{65}	0.095	0.012	1.066	7.433×10^{-5}	8.9	58.71
Fe^{54}-Mn^{54}	0.6847	0.058	0.011	2.57×10^{-8}	7.6	55.85
Mn^{55}-Mn^{56}	0.015	1.00	9.1	7.433×10^{-5}	7.2	54.94
Fe^{56}-Mn^{56}	0.6847	0.917	0.0166	7.433×10^{-5}	7.8	55.85
Ni^{58}-Co^{58}	0.095	0.678	0.0664	1.117×10^{-7}	8.9	58.71
Co^{59}-Co^{60} (normal)	0.004	1.0	24.3	4.17×10^{-9}	8.9	58.94
(Low Co steel)	0.0004	1.0	24.3	4.17×10^{-9}	8.9	58.94
Fe^{58}-Fe^{59}	0.6847	0.003	0.6	1.74×10^{-7}	7.8	55.85

ϕ_e = thermal neutron flux; effective; weighted by core geometry and fraction of cycle time spent in each region-core, and reflectors, neutron/cm^2-sec = 6.078×10^{12}.

ϕ_a = thermal neutron flux; averaged over core geometry - not dependent upon primary cycle time, neutrons/cm^2-sec = 1.722×10^{13}.

f_s = fractional abundance of chemical element in system-material weight fraction.

f_n = fraction abundance of target nuclide in chemical element-weight fraction.

V_I = effective volume of resin bed in demineralizer, cm^3 = 5.66×10^4.

The derivation of the above equations is given in APAE-17 (24). Comparison of the analytic calculation with experimental measurements is given in ref. (1). The release rate, Co, was obtained from fitting APPR-1 data. The differences and the difficulties in performing these analytical calculations are also given in ref. (1).

The properties of the various nuclides are given in Table 6-1.

The concentration of active nuclides in the demineralizer after one (1) year of full power operation at 10 MW is given in Table 6-2.

TABLE 6-2

Concentration of Active Nuclides in Demineralizer

Nuclide	Concentration, n_D (atom/cm^3)
Cr^{51}	5.292×10^{14}
Ni^{65}	5.091×10^{8}
Mn^{54}	7.192×10^{12}
Mn^{56}	5.548×10^{10}
Fe^{59}	2.678×10^{12}
Co^{60}	3.116×10^{14}
Co^{58}	1.735×10^{13}

6.2 Volumetric Source Strength of Demineralizer

The next step in determining the shielding required for the demineralizer is the calculation of the volumetric source strength. The source strength is based on the buildup of active nuclides in the demineralizer.

Equation 6-5 was used to calculate the source strengths.

$$S_v = \lambda n_D \left(\frac{\gamma}{d}\right) E \qquad (6\text{-}5)$$

where S_V = source strength of volume source, Mev/cm^3 -sec

n_D = concentration of active nuclides in demineralizer, atom/cm^3

λ = disintegration constant, sec^{-1}

E = gamma energy, Mev

$\left(\frac{\gamma}{d}\right)$ = number of gammas of energy, E, released per disintegration

The constants to equation 6-5 and the source strength of the volume source, S_V, due to each of the activated nuclides are given in Table 6-3.

TABLE 6-3

Calculation of Volumetric Source Strength

Nuclide	λ(sec^{-1})	$\left(\frac{\gamma}{d}\right)$	E(mev)	S_V (mev/cm^3-sec)
Cr^{51}	3.03×10^{-7}	0.1	0.32	5.131×10^{6}
Ni^{65}	7.433×10^{-5}	0.4	0.37	5.601×10^{2}
		0.25	1.49	1.410×10^{4}
		0.18	1.12	7.630×10^{3}
Mn^{54}	2.57×10^{-8}	1.0	0.84	1.553×10^{5}
Mn^{56}	7.433×10^{-5}	1.0	0.84	3.464×10^{6}
		0.3	1.81	2.239×10^{6}
		0.2	2.13	1.757×10^{6}
Co^{58}	1.117×10^{-7}	1.0	0.81	1.570×10^{6}
Fe^{59}	1.74×10^{-7}	0.5	1.3	3.029×10^{5}
		0.5	1.1	2.563×10^{5}
Co^{60}	4.17×10^{-9}	1.0	1.33	1.728×10^{6}
		1.0	1.17	1.520×10^{6}

FIG 6-1
DEMINERALIZER SHIPPING CASK
SCALE = $\frac{1}{8}$ SIZE

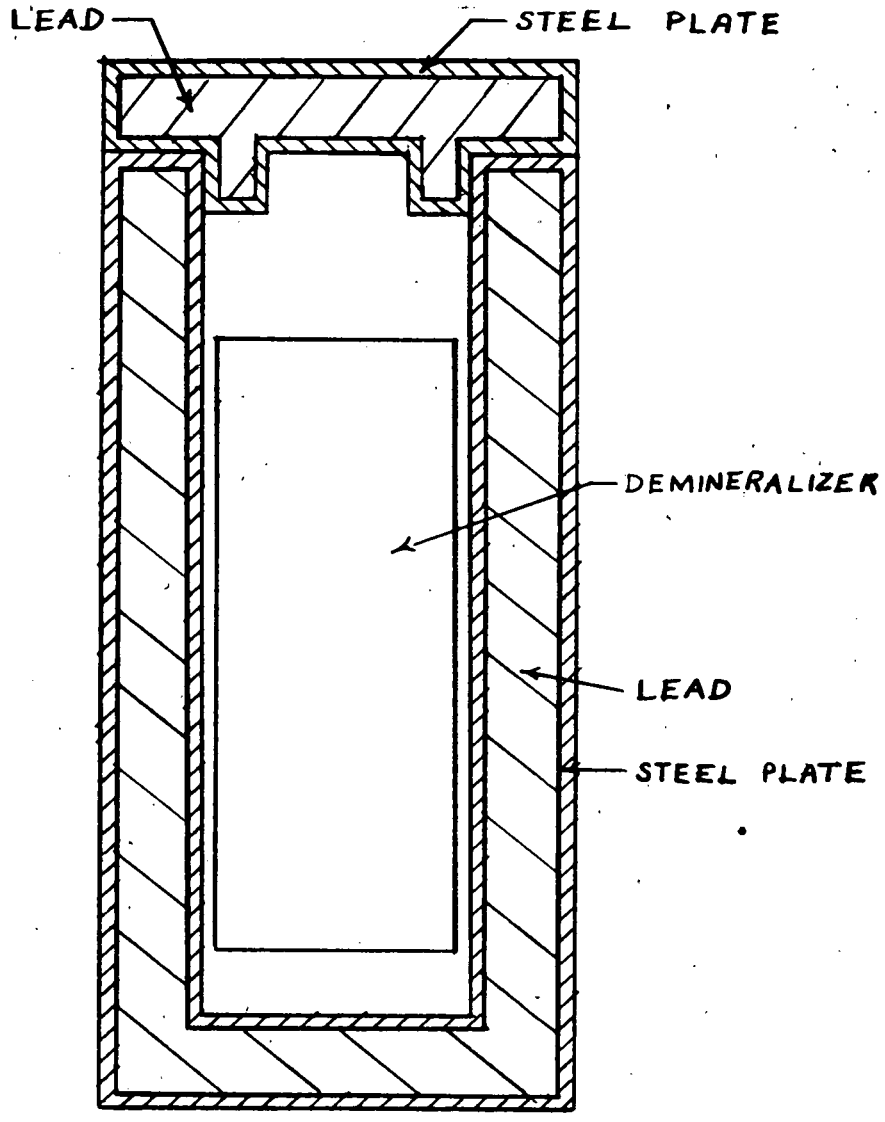

The different gammas emitted from the active nuclide were consolidated into five groups to facilitate the calculation of the dose rate due to the active nuclides in the demineralizer. The energy groups that were used and the volumetric source strength for each group is given in Table 6-4.

TABLE 6-4

Energy Grouping and Source Strength

Group Number	Group Energy (mev)	S_v(mev/cm^3-sec)
1	2.13	1.757×10^6
2	1.81	2.239×10^6
3	1.2-1.5	2.045×10^6
4	1.0-1.2	1.784×10^6
5	<1.0	1.032×10^7

6.3 Demineralizer Shielding

Since the activity in the demineralizer builds up during reactor operation, it is desirable to operate it in a lead shield cask so that the dose rate on the surface of the lead cask be no more than 70 mr/hr. The following sections will discuss the selection of the size of the lead cask.

6.3.1 Radial Shielding Demineralizer

The IBM 650 shielding program (11) was modified in order to calculate the dose on the outside surface of the lead shield cask. This program calculates the dose rate at any desired point due to a cylindrical source with intervening shield materials. Fig. 6-1 shows the geometry of the demineralizer and lead cask. The equation that the machine solves is given on page 360 of Rockwell (3) where $\Theta_1 = \Theta_2 = \Theta$.

The calculation was performed using the energy groups and volumetric source strengths given in Table 6-4. In order to determine the effect of lead thickness on dose rate, four different cases were calculated. They were two, three, four, and five inches of lead. The dose rates on the outside surface of the cask due to the different energy groups are given in Table 6-5 for each size of the lead cask.

The results are also shown on Fig. 6-2. For a maximum dose rate of 70 mr/hr on the surface of the lead cask, 3.87 inches of lead is required for the cask. This value is very conservative as the buildup factor is defined as follows:

$$B_T = \prod_i B_i \qquad (6\text{-}6)$$

where B_i Buildup factor of i^{th} material

TABLE 6-5

Dose Rate on Surface of Loaded Demineralizer Shipping Cask

Energy Group	Thickness of Lead in Cask			
	2" of Lead	3" of Lead	4" of Lead	5" of Lead
1	278.5 mr/hr	88.2 mr/hr	23.52 mr/hr	6.67 mr/hr
2	302.1 "	88.1 "	21.48 "	5.59 "
3	157.2 "	32.4 "	6.48 "	1.28 "
4	89.6 "	15.5 "	2.53 "	0.42 "
5	128.0 "	11.3 "	1.19 "	0.09 "
Total	955.4 mr/hr	235.5 mr/hr	55.20 mr/hr	14.05 mr/hr

The buildup factor can be calculated in a different manner as follows:

$$B_T = A_i\, e^{-\alpha_1 b_1} + (1-A_1)\, e^{-\alpha_2 b_1} \qquad (6\text{-}7)$$

where $b_1 = \sum_i \mu_i t_i$ for all shield materials. The buildup factors are smaller and therefore do not give as conservative an answer as the machine calculation. The results from the hand calculations are given in Fig. 6-2. From this curve a lead thickness of 3.41 inches will limit the dose rate on the outside surface of the lead cask to 70 mr/hr. It is recommended that the results from the hand calculation be used as the radial thickness of the lead cask.

6.3.2 Vertical Shielding of Demineralizer

From studies performed during the shielding program of Task VI (1), it is known that less lead shielding is needed for the top and bottom of the lead cask. The following equations were used to determine the maximum dose rates with a three inch lead cask.

Upper Limit

$$D = \frac{BSV}{2\mu_s C_e}\left[E_2\ (b_1) - \frac{E_2\ (b_1 \operatorname{Sec}\theta_1)}{\operatorname{Sec}\theta_1}\right] \qquad (6\text{-}8)$$

Lower Limit

$$D = \frac{BSV}{2\mu_s C_e}\left[E_2\ (b_1) - \frac{E_2\ (b_1 \operatorname{Sec}\theta_3)}{\operatorname{Sec}\theta_3}\right] \qquad (6\text{-}9)$$

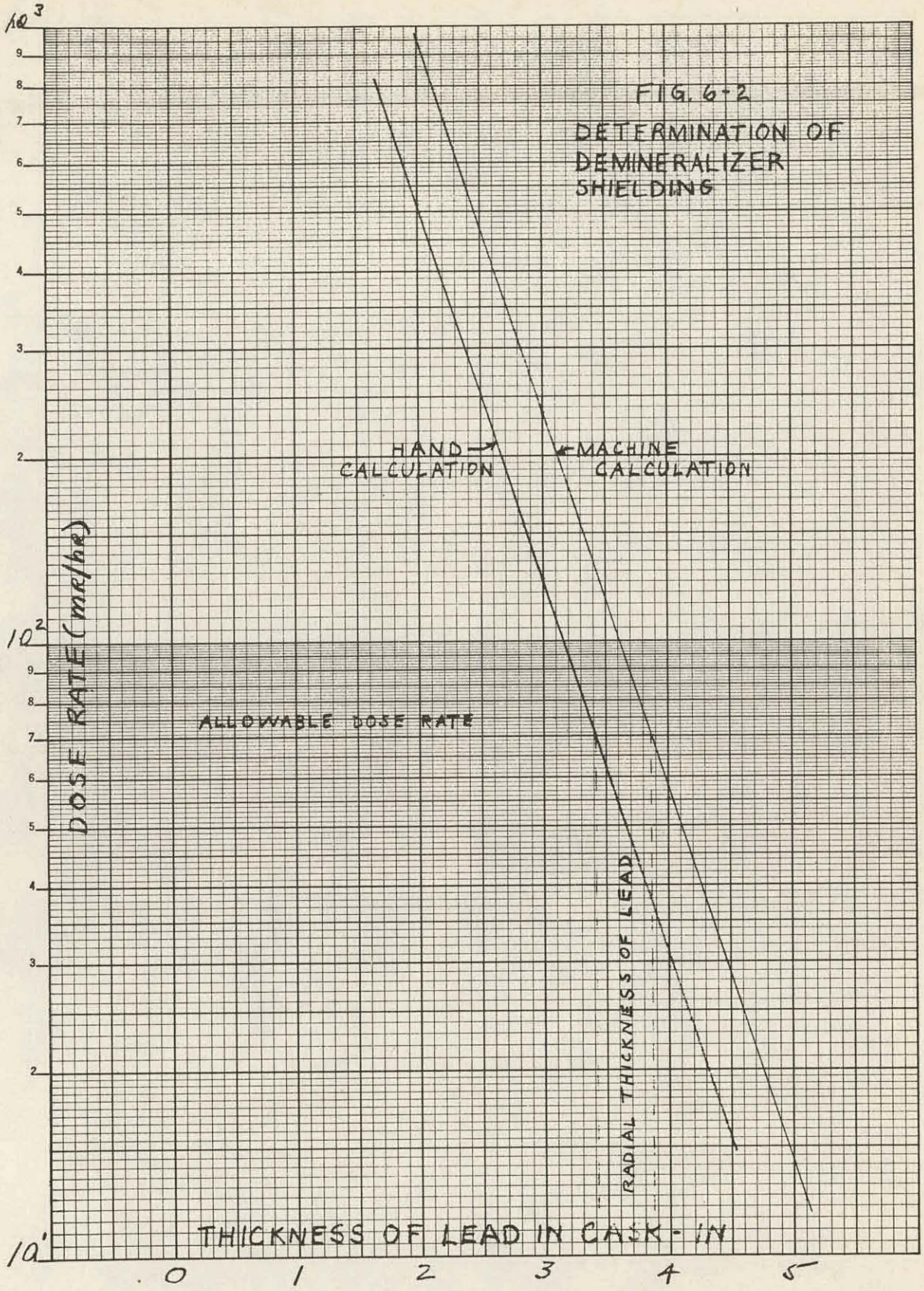
FIG. 6-2
DETERMINATION OF
DEMINERALIZER
SHIELDING
HAND CALCULATION
MACHINE CALCULATION
ALLOWABLE DOSE RATE
DOSE RATE (mr/hr)
RADIAL THICKNESS OF LEAD
THICKNESS OF LEAD IN CASK - IN
10³
10²
10¹
0
1
2
3
4
5

where

$$E_2(b) = b\int_b^{\infty} \frac{e^{-t}}{t^2}\, dt$$

$$\theta_1 = \text{Tan}^{-1}\left(\frac{R_o}{a'}\right), \text{ degrees}$$

$$\theta_3 = \text{Tan}^{-1}\left(\frac{R_o}{a'\ h'}\right), \text{ degrees}$$

$$h' = 3/\mu_s, \text{ cm.}$$

a' = distance from top or bottom of cylindrical source to dose point, cm.

From the above calculation about 2.94 inches of lead would be required for the top and bottom parts of the lead cask. This is shown in Fig. 6-1.

6.3.3 Dose Rate After Removal

After removal of the demineralizer from the system, the dose rate on the surface of the cask will decrease rapidly for the first forty hours. The decay of the dose rate will then decrease very slowly compared to the initial decrease. Within the first forty hours, all of the short lived activity will decay away giving an initial fast decrease in the dose. Thereafter, the dose rate decreased slowly due to the decay of the long-lived nuclides. Experimental and analytical work on this subject is given in APAE-35 (1). The dose rate after a cooling period of about two days would be within 40 mr/hr on the surface of the lead cask shielding.

6.3.4 Results

The shipping cask consists of two 5/8" thick concentric steel cylinders with 3.41" of lead between them. This is consistent with the APPR-1 design. Since there is little difference between this cask and the cask designed for the 1500 KW plant, it may be advisable to use the same cask.

For the above cask, the dose rate one meter from the source is 15% of the dose rate on the surface of the shipping cask. With a dose rate of 58 mr/hr on the cask surface, the dose rate one meter from the source would be 8.7 mr/hr. This radioactive source would meet I.C.C. shipping regulations.

7.0 WASTE TANK SHIELDING

The waste tank will be used to store radioactive waste. This waste may include the primary coolant and two months plant waste. The shielding of the waste tank is based on normal usage and not on abnormal nuclear incidents. This menas that the radioactive source in the waste tank will be due to activated corrosion products in the primary coolant and active material in the plant waste. The high energy gamma rays (energy groups 1 and 2) are from the disintegration of the short-lived nuclides present in the primary water. These nuclides have half-lives of approximately 2.6 hours (25). Therefore, the activity due to these nuclides will diminish rapidly and disappear within a day or two after the primary water is drained into the waste tank. The shielding required will be such that the allowable dose on the shield surface shall not exceed 1 mr/hr.

7.1 Primary Coolant Activation

The activity of the primary coolant is due to the activation and corrosion of structural materials in the primary system. The nuclear reactions giving rise to this activation are the same as described in Section 6.0.

The concentration of the various activated corrosion products in the primary coolant was calculated by equation 7-1, 7-2, 7-3, and 7-4. The derivation of the following equations is presented in APAE-17 (24).

$$n_w = U + V + W \qquad (7\text{-}1)$$

$$U = \frac{C_o S_o N_a \sigma f_s f_n \phi_e}{AQ} \left[\frac{1-e^{-(\lambda + Q/V_w)t}}{(\lambda + Q/V_w)} + \frac{e^{-(\lambda + Q/V_w)t} - e^{-(Q/V_w)t}}{\lambda} \right] \qquad (7\text{-}2)$$

$$V = \frac{C_o S_a N_a f_n f_s \sigma \phi_a}{A \lambda V_w} \left[\frac{1-e^{-(\lambda + Q/V_w)t}}{\lambda + Q/V_w} + \frac{e^{-(\lambda + Q/V_w)t} - e^{-\lambda t}}{Q/V_w} \right] \qquad (7\text{-}3)$$

$$W = \frac{f_h f_s N_a \rho S \sigma \ell \phi_a}{4AV_w (\lambda + Q/V_w)} \left[1 - e^{-(\lambda + Q/V_w)t} \right] \qquad (7\text{-}4)$$

where n_w = concentration of active nuclides in primary coolant, atom/cm^3
and the other symbols are defined in Section 6.1.

The preceding equations were solved for a power output of 6.5MW for one year at full power operation. The results of this calculation is given in Table 7-1.

TABLE 7-1

Corrosion Product Concentrations in Primary Coolant

Nuclide	Concentration(atom/cm^3)	Total Atoms
Cr^{51}	1.428×10^{11}	2.999×10^{17}
Ni^{65}	3.368×10^{7}	7.073×10^{13}
Mn^{54}	4.462×10^{8}	9.370×10^{14}
Mn^{56}	3.670×10^{9}	7.707×10^{15}
Co^{58}	1.898×10^{9}	3.986×10^{15}
Fe^{59}	4.222×10^{8}	8.866×10^{14}
Co^{60}	1.684×10^{10}	3.536×10^{16}

The gamma rays from all the nuclides were divided into five energy groups. The total source strength of the volume source due to the primary coolant is given in Table 7-2.

TABLE 7-2

Total Source Strength Due to the Primary Coolant

Group Number	Total Source Strength (mev/sec)
1	2.440×10^{11}
2	3.111×10^{11}
3	2.254×10^{9}
4	1.317×10^{9}
5	4.852×10^{11}

7.2 Plant Waste Activity (26)

In two months of operation, the accumulation of normal waste would amount to about 300 gallons or 1.136×10^{6} cm^3. The average activity of the waste would be approximately 0.2 c/cm^3 or 2.272×10^{5} c. The total source

strength due to this activity is 9.245×10^9 Mev/sec. The following was assumed in order to calculate the total source of the normal plant waste.

1. Average energy of radioactive nuclides — 1.1 Mev

2. One photon per disintegration of radioactive nuclide.

This radioactive source, since the average energy is 1.1 Mev, was included in Energy Group 4 along with the contribution from the primary coolant.

7.3 Volumetric Source Strength in Waste Tank

The source strength of the volume source in the waste tank is equal to the total source strength calculated in sections 7-1 and 7-2 divided by the volume of the waste tank. The volume of the waste tank assuming that it is filled to capacity is 1.939×10^7 cm^3. A list of the volumetric source strength for each energy group is given in Table 7-3.

TABLE 7-3

Volumetric Source Strength in Waste Tank

Group Number	Total Source (Mev/sec)	Volumetric Source (Mev/cm^3-sec)
1	2.440×10^{11}	1.258×10^4
2	3.111×10^{11}	1.604×10^4
3	2.254×10^9	1.162×10^2
4	1.056×10^{10}	5.446×10^2
5	4.852×10^{11}	2.502×10^4

7.4 Waste Tank Shielding

The shielding of the waste tank was based on the use of any of the following material:

1. Concrete, ρ = 2.4 gm/cc.
2. Water, ρ = 1.0 gm/cc.
3. Steel, ρ = 7.9 gm/cc

The method used to calculate the dose rate on the surface of the different shields is identical to the method used in Section 6. The IBM Shielding code (11) was used to perform all the numerical calculations. The dose rates on

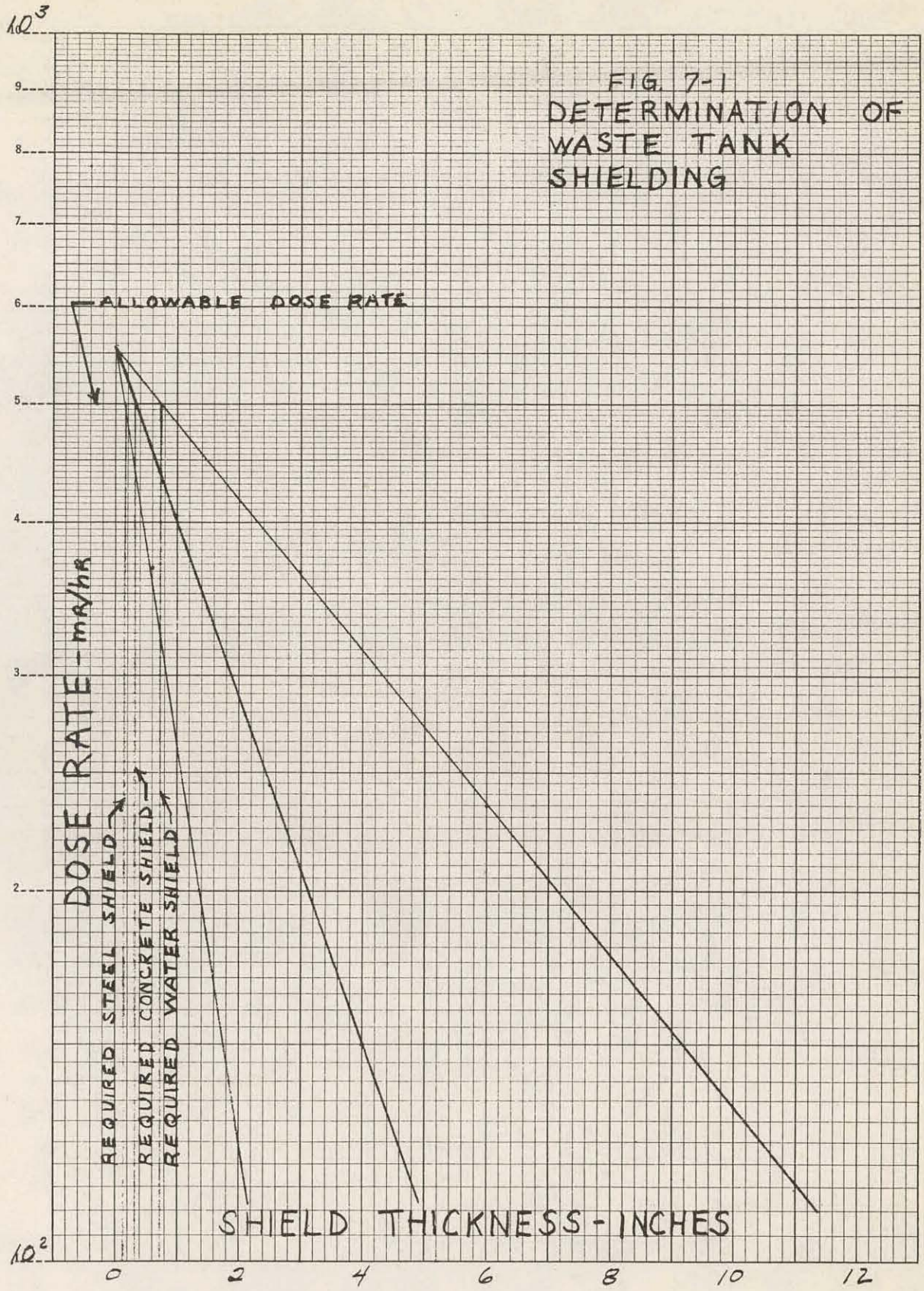
FIG. 7-1
DETERMINATION OF WASTE TANK SHIELDING
10^3
9
8
7
6
5
4
3
2
10^2
ALLOWABLE DOSE RATE
DOSE RATE - mR/hr
REQUIRED STEEL SHIELD
REQUIRED CONCRETE SHIELD
REQUIRED WATER SHIELD
SHIELD THICKNESS - INCHES
0
2
4
6
8
10
12

on the shield surface as a function of shield material and thickness is given in Fig. 7-1. The required shield thickness for each shield material is given in Table 7-4 for an allowable dose rate of 500 mr/hr on the shield surface.

TABLE 7-4

Shield Thickness for Waste Tank

Material	Thickness-in.
Concrete (ρ = 2.4 gm/cc)	0.34
Water (ρ = 1.0 gm/cc)	0.75
Steel (ρ = 7.9 gm/cc)	0.18

Table 7-4 gives the required integral shielding of the primary water and is dumped into the waste tank. If under normal conditions, only plant waste is stored in the hot waste tank, no integral shielding will be necessary other than the standard wall thickness of the tank. The dose rate was measured on the surface of the hot waste tank of the APPR-1. With only normal plant waste in the tank, the measured dose rate on the surface of the tank was 20 mr/hr. This is well below the design dose rate of 500 mr/hr.

To reduce the dose rate to a value less than 1 mr/hr, approximately 2 feet of concrete would be needed. The maximum dose rate would then be about 0.5 mr/hr.

8.0 ACTIVATION OF COMPONENTS

During the course of reactor operation, the various components within the pressure vessel and the components of the primary shield are activated by the neutron flux. The relocation of components of the primary system is dependent upon the activation of the above equipment.

8.1 Pressure Vessel and Primary Shield Component

The dose rates five feet from each component after one year full power operation for various shutdown times are given in Table 8-1.

To be able to handle the components, the dose rate due to the activity of each part should not exceed 75 mr/hr five feet from the source. The following table is intended to serve as a guide in the determination of the decision as to the feasibility of relocating various components. These rates can be used as a basis for planning but actual dose rates must be measured when actual relocation operations are undertaken. The results given in Table 8-2 are for 1 year of full power operation.

TABLE 8-1

DOSE RATES * FROM ACTIVATED COMPONENTS

Component	Shutdown Times			
	1 day	10 days	30 days	1 year
Thermal Shield	4.04×10^{7}	3.53×10^{7}	2.89×10^{7}	1.05×10^{7}
Pressure Vessel	8.32×10^{5}	7.28×10^{5}	5.95×10^{5}	2.17×10^{5}
Pressure Vessel Cover	1.3×10^{3}	1.14×10^{3}	9.3×10^{2}	3.38×10^{2}
Pressure Vessel Support Ring	1.06×10^{5}	9.23×10^{4}	7.54×10^{4}	2.75×10^{4}
1st Steel Ring	2.02×10^{4}	1.77×10^{4}	1.44×10^{4}	5.27×10^{3}
2nd Steel Ring	2.41×10^{3}	2.10×10^{3}	1.72×10^{3}	6.25×10^{2}
3rd Steel Ring	2.72×10^{2}	2.38×10^{2}	1.94×10^{2}	7.09×10^{1}
4th Steel Ring	3.06×10^{1}	2.67×10^{1}	2.18×10^{1}	7.93×10^{0}
Shield Tank	4.42×10^{-1}	3.86×10^{-1}	3.15×10^{-1}	1.15×10^{-1}

* All dose rates are in units of Mr/hr.

TABLE 8-2

FEASIBILITY OF RELOCATION OF COMPONENTS

Component	Shutdown Times 1 day	10 days	30 days	1 year
Control Rod Basket	N	N	N	N
Rod Drive Shaft	N	N	N	N
Thermal Shield	N	N	N	N
Pressure Vessel	N	N	N	N
Pressure Vessel Cover	N	N	N	N
Pressure Vessel Support Ring	N	N	N	N
1st Shield Ring	N	N	N	N
2nd Shield Ring	N	N	N	N
3rd Shield Ring	N	N	N	R *
4th Shield Ring	R	R	R	R
Shield Tank	R	R	R	R

Symbols Used: N - Can not be relocated (dose 75 mr/hr)

R - Can be relocated (dose 75 mr/hr)

* Indicates dose rate within a factor of 2 of 75 mr/hr

REFERENCES

II SHIELDING ANALYSIS

1. S.S. Rosen, et al, "APPR-1 Research and Development Program, Shielding Experiments and Analysis, Task No. VI," APAE No. 35, October 15, 1958

2. "Reactor Shielding Design Manual", TID 7004, March 1956.

3. F.H. Clark, "Decay of Fission Product Gammas", NDA 27-39, December 30, 1954.

4. J. Moteff, "Fission Product Decay Gamma Energy Spectrum", APEX 134, 1953.

5. R.L. Marklin and H. S. Pomerance, "Proceedings of the International Conference on Peaceful Uses of Atomic Energy in Geneva, August 1955, Vol. 5, page 96.

6. "Revised Activation Handbook for Aircraft Designers", ANP Document No. NARF-57-50T, FZK-9-124, September 1957, Convair, Fort Worth, Texas.

7. "Allegheny Ludlum Blue Sheet, Allegheny Metal 18-8", Allegheny Ludlum Steel Corporation, Pittsburgh 22, Pennsylvania

8. "Modern Steels and Their Properties, "Bethlehem Steel Company, Bethlehem, Pa., 1955.

9. C.D. Bopp and D. Sisman, Nucleonics 14, No.1, page 46, 1956.

10. C.D. Bopp, "Gamma Radiation Induced in Engineering Materials," ORNL 1371, 1953.

11. P.V. Oby, et al, "Primary Shielding Calculation on the IBM 650 (Roc Codes)," APAE Memo 142, October 15, 1958.

12. T. G. Williamson, "APPR-1 Burnout Calculations," APAE Memo 126, April 10,1958

13. E.M. Reiback and H.L. Hoover, "Phase III Report, Army Package Power Reactor Field Unit No. 1, APPR-1a, Primary Shield Design Analysis," APAE No. 17, Vol. 1, Supp. 2, July 16, 1958.

14. Herbert Goldstein, "The Attenuation of Gamma Rays and Neutrons in Reactor Shields, "Supt. of Documents,U. S. Government Printing Office, Washington 25, D.C., May 1, 1957.

15. D.J. Hughes and J. A. Harvey, "Neutron Cross Sections," BNL-325, July 1, 1955.

16. F. C. Brooks and H.L. Glick, WAPD-45

17. Czapek, E., et al, "Gamma Shield Design for Primary Coolant Sources Using the IBM Type 650 Computer", RAS-1, Report No. 74 September 1956.

18. Rosen, S.S., "Supplement to RAS-I", AP Note 63, June 26, 1957

19. Peebles, "Gamma Ray Transmission Through Finite Slabs", R-240, Rand Corporation, December 1, 1952.

20. Moteff, J., "Miscellaneous Data for Shielding Calculations", APEX-176, December 1, 1954.

21. DeYoung, R.C., "Container for Irradiated APPR-1 Fuel Elements", AP Memo 63, October 31, 1956.

22. Tully, J.P., et al "2000 K.W. Skid Mounted APPR Power Plant", APAE NO. 33, May 1, 1958.

23. Kroeger, H.R., I.M. Neou, and J.L. Meem, "The Effect of Gamma Heating on the APPR-1 Pressure Vessel", 415E2.1, ASTRA, July 1956.

24. "Phase 3 Report APPR Field Unit No.1, APPR-1A Vol. 1", APAE No. 17 Vol. 1, May 15, 1957.

25. Small, W.J. and J.L. Zegger, "Short Lived Circulating Activity in the APPR", AP Memo 109, August 28, 1957.

26. Clark, R. J., "Private Communication to M.J. Leibson", October 1958.

C. TRANSIENT ANALYSIS

1.0 PRIMARY SYSTEM KINETICS

1.1 General kinetic model

1.1.1 Description

The general kinetic model used is that developed in APAE 38 (1) for the APPR-1. The validity of this model in representing plant transients introduced by control rod and load perturbations was demonstrated by comparison with plant data. The validity of this model in representing the 1000 ekw Packaged Nuclear Power Plant is assumed because of its basic similarity to the APPR-1.

1.1.2 Nomenclature

Symbols

A	Heat Transfer Surface Area, $ft.^2$
C	Specific heat, Btu/lb-^oF
F	Coolant Flow Rate, Fraction of Rated Value
h	Average core film coefficient, Btu/hr-Ft^2 - ^oF
k	Potential power contribution from precursors Btu/sec
ℓ	Mean neutron lifetime, birth to absorption, sec^{-1}
L	Load factor of steam generator power output
p	Primary system pressure, psia
P	Power output of core, Btu/sec
R	Rate of primary system flow, lb/sec
S	Slope of pressurizer characteristic, $\Delta p / \Delta V_{tot}$ psi/ft^3
t	Time, sec
T	Temperature, ^oF
V	Volume, ft^3
W	Weight, lb
α	Fraction of power generated in fuel plates and cladding
β	Delayed neutron fraction of a group
γ	Volume coefficient of primary coolant expansion, $^oF^{-1}$
δ	Excess reactivity of core
$\mathcal{J}$	Excess reactivity coefficient, $^oF^{-1}$ or $psia^{-1}$
Θ	Temperature difference at design load, ^oF
λ	Decay constant of a delayed neutron group, sec^{-1}
τ	Time lag, sec

Subscripts:

C	Mean core coolant condition
D	Design power output condition, steady state
E	Exchanger tubing
F	Mean fuel plate condition
G	Mean steam generator condition, primary (tube) side
i	i^{th} delayed neutron group
L	Liquid in steam generator
neg	Negative increase in primary coolant volume
p	Primary pressure
pos	Positive increase in primary coolant volume
r	Control rod insertion
S	Mean steam conditions in generator corresp. to saturation
tot	Total for primary system

1-8	Thermo. properties:	Condition of location in schematic diagram
1-5	Nuclear Parameters:	Particular i^{th} delayed neutron group

1.1.3 Differential equations

The following set of differential equations describing primary loop component behavior is derived in APAE 38 (1). They are repeated here for ready reference.

Core thermal kinetics:

$$\frac{d}{dt} T_F(t) = \frac{\alpha}{W_F C_F} P(t) - \frac{\alpha_D^P}{W_F C_F \Theta_{FC}} T_F(t) + \frac{\alpha P_D}{W_F C_F \Theta_{FC}} T_c(t)$$

where

$$T_F(0) = \frac{\Theta_{FC}}{P_D} P(0)$$

$$\frac{d}{dt} T_c(t) = \frac{1-\alpha}{W_c C_c} P(t) + \frac{\alpha \Theta_{1,2}}{\tau_c \Theta_{FC}} T_F(t) - \left[\frac{\alpha \Theta_{1,2}}{\tau_c \Theta_{FC}} + \frac{2}{\tau_c}\right] T_c(t) + \frac{2}{\tau_c} T_1(t)$$

where

$$T_c(0) = 0$$

Core nuclear kinetics:

$$\frac{d}{dt} P(t) = \frac{\delta_r + \gamma_T T_c(t) + \gamma_p p(t)}{\ell} P(t) - \frac{\Sigma \beta_i P(t) + \sum_{i=1}^{5} \lambda_i K_i(t)}{\ell}$$

$$\frac{d}{dt} K_i(t) = \frac{\beta_i}{\ell} P(t) - \lambda_i K_i(t)$$

where

$$K_i(0) = \frac{\beta_i}{\lambda_i \ell} P(0)$$

Kinetics of plenum chambers and piping:

$$\frac{d}{dt} T_1(t \neq \tau_{5,6}) = \frac{2}{\tau_{6,1}} T_G(t) - \frac{1}{\tau_{6,1}} T_4(t) - \frac{1}{\tau_{6,1}} T_1(t \neq \tau_{5,6})$$

where

$$T_1(\tau_{5,6}) = T_1(0) = -\frac{P(0)}{2RC_c}$$

$$\frac{d}{dt} T_4(t \neq \tau_{3,4}) = \frac{2}{\tau_{2,3}} T_c(t) - \frac{1}{\tau_{2,3}} T_1(t) - \frac{1}{\tau_{2,3}} T_4(t \neq \tau_{3,4})$$

where

$$T_4(\tau_{3,4}) = T_4(0) = \frac{P(0)}{2RC_c}$$

Kinetics of steam generator:

The basic kinetic model developed in APAE 38(1) is used in the study since superheated steam generation is not involved.

$$\frac{d}{dt} T_G(t) = \frac{2}{\tau_G} T_4(t) - \left[\frac{2}{\tau_G} + \frac{2\Theta_{1,2}}{\tau_G \Theta_{Gs}}\right] T_G(t) + \frac{\Theta_{1,2}}{\tau_G \Theta_{Gs}} T_s(t)$$

where

$$T_G(0) = T_c(0) = 0$$

$$\frac{d}{dt} T_s(t) = \frac{P_D}{(W_L C_L + W_E C_E)\Theta_{Gs}} T_G(t) - \frac{P_D}{(W_L C_L + W_E C_E)\Theta_{Gs}} T_s(t)$$

$$- \frac{P_D}{W_L C_L + W_E C_E} L(t)$$

where $T_s(0) = -_{Gs}$

Pressurizer kinetics:

$$V_{tot}(t) = \gamma V_c T_c(t) + \gamma V_{2,4} T_4(t) + \gamma V_{5,1} T_1(t) + \gamma V_G T_G(t)$$
$$+ \text{Constant}$$

where

$$V_{tot}(t) = 0$$

$$p(t) = S_{pos} \Delta V_{tot}(t) \quad ; \Delta V_{tot}(t) \geq 0$$

$$p(t) = S_{neg} \Delta V_{tot}(t) \quad ; \Delta V_{tot}(t) \leq 0$$

1.2 Scaled kinetic model

1.2.1 Plant constants

C_c	1.196	$W_{6,1}$	604.8
C_E	0.130	α	0.94
C_F	0.121	β_1	0.91×10^{-3}

Plant constants continued:

C_L	1.162	β_2	2.96×10^{-3}
ℓ	2.5×10^{-5}	β_3	1.31×10^{-3}
P_D	6166	β_4	1.68×10^{-3}
R	269.6 (2505 GPM)	β_5	0.26×10^{-3}
S_{pos}	186	γ	1.126×10^{-3}
S_{neg}	111	γ_p	$\neq 3.1 \times 10^{-6}$
V_c	3.222	γ_T	$- 3.4 \times 10^{-4}$
V_G	8.45	Θ_{FC}	25.49
$V_{2,3}$	6.031	Θ_{Gs}	49.0
$V_{3,4}$	23.87	$\Theta_{1,2}$	19.1
$V_{5,6}$	12.05	λ_1	1.58
$V_{6,1}$	12.35	λ_2	0.328
V_L	89.0	λ_3	0.126
W_c	157.8	λ_4	0.035
W_E	1547	λ_5	0.0128
W_F	429.7	τ_c	0.5857
W_G	413.2	τ_G	1.533
W_L	4613	$\tau_{2,3}$	1.095
$W_{2,3}$	295.3	$\tau_{3,4}$	4.336
$W_{3,4}$	1169	$\tau_{5,6}$	2.188
$W_{5,6}$	589.8	$\tau_{6,1}$	2.243

1.2.2 Time and amplitude scaling factors

A time scaling factor of unity (computer and real time scales equal) was used because of the speed of the transients involved and the ease of scaling.

An amplitude scaling factor of unity (one volt per physical unit) was used for ease of interpreting computer results and for ease of scaling. Proper voltage levels were then obtained by the use of multiples or fraction of the variables.

1.2.3 Potentiometer settings

A listing of servo-set potentiometer settings is given in Table 1-1. Each setting is stated in terms of both plant symbols and specific numerical value.

1.2.4 Analog circuit diagram

The circuit diagram for wiring the electronic analog computer is shown in Fig. 1-1. Feedback connections have been included to demonstrate the many interactions involved.

1.3 Analog computer model response

The transient response of the kinetic model was determined for a series of load perturbations. Fig. 1-2 illustrates reponse to instantaneous load reductions and Fig. 1-3 to instantaneous load increases. A listing of run numbers and the corresponding conditions applied is given in Table 1-2.

Only plant load perturbations were considered since primary pressure variations due to control rod perturbations would be of less magnitude than those due to the worst load changes considered.

1.4 Selection of pressurizer size

A pressurizer vessel containing 12.1 cubic feet of vapor and 5.9 cubic feet of liquid was selected as being more than adequate for any primary system volume changes that would be encountered in the operation of the power plant.

Analog computer analysis of the plant model indicates that the maximum primary pressure variations are $\pm$ 132 and -120 psi when the anticipated value of temperature coefficient is used. These pressure swings correspond to instantaneous load drop and rise respectively between 100% and 0% of rating.

An extrapolated value of -3.4×10^{-4} is anticipated for the temperature coefficient of reactivity. Although expectations of this high a coefficient are well justified, it is conceivable that a value as low as -3.0×10^{-4} might exist, though this is a highly conservative extrapolation. Under

such circumstances the maximum primary pressure variations are + 156 and -130 psi corresponding to the extreme load perturbations mentioned.

The computer model is very conservative in determining positive primary pressure surges since adiabatic vapor compression is assumed in the pressurizer. Heat transfer by vapor condensation on vessel walls and liquid free surface is neglected. A comparison of adiabatic model and actual plant response to similar perturbations showed the pressure surges to be in the ratio of about 2 to 1 respectively for the APPR-1. See APAE 38 (1) for further details.

Primary pressure surges of the model are also conservative since secondary system heat losses and auxiliary uses of steam are not included. The minimum load on the steam generator is actually in the order of 1/2% of rating.

The primary system is designed to structurally withstand under code regulations an internal pressure of 2000 psia, providing for a 250 psi pressure surge from the normal operating pressure of 1750 psia before opening of the safety valve. The pressurizer design is therefore seen to be more than adequate in meeting demands from extreme plant perturbations and uncertainties in specifications of plant constants.

It is found that a pressurizer containing 7.2 cubic feet of vapor would result in a maximum pressure change of 250 psi for a load decrease. The pressure decrease would be 210 psi for a load change from 0 to 100%. This would be the minimum size pressurizer consistant with the design.

Table 1-1

Servo-set Potentiometer Settings

Pot No.	Setting	Value	Pot No.	Setting	Value
0			9	$\alpha P_D/10\, W_F C_F \theta_{FC}$	0.4373
1	Recorder Channels		10	$200\theta_{FC}/P_D$	0.8266
2			11	$400\,(1-\alpha)W_c C_c$	0.1272
3			12	$2\alpha\theta_{1,2}/10\tau_c\theta_{FC}$	0.2405
4			13	$2/10\tau_c$	0.3415
5			14	$\alpha\theta_{1,2}/10\tau_c\theta_{FC}+.2\tau_c$	0.4618
6			15	$\mathcal{S}_T/100\ell$	0.1360
7	$\alpha P_D/20 W_F C_F \theta_{FC}$	0.2187	16	$35\gamma V_c$	0.1270
8	$20\alpha/W_F C_F$	0.3616	17	$3.5\gamma V_{2,4}$	0.1178

18	$35\gamma V_C$	0.3329
19	$35\gamma V_{5,1}$	0.9614
20	$S_{neg}/210$	0.5286
21	$S_{pos}/2100$	0.0884
22	$3\ \gamma_p/5\ell$	0.0744
23	$2/10\ \tau_{2,3}$	0.1826
24	$1/10\ \tau_{2,3}$	0.0913
25	$1/10\ \tau_{2,3}$	0.0913
26	$200/RC_c$	0.6202
27	$12/10\ \tau^2_{3,4}$	0.06383
28	$12/10\ \tau^2_{3,4}$	0.06383
29	$240/C_cW_{3,4}$	0.1717
30	$6/10\ \tau_{3,4}$	0.1384
31	$6/10\ \tau_{3,4}$	0.1384
32	$2/10\tau_G$	0.1305
33	$2\ \theta_{1,2}/\theta_{Gs}\ \tau_G$	0.5087
34	$\frac{2}{10\tau_G}\ /\theta_{1,2}-\frac{}{10\theta_{Gs}\tau_G}$	0.1559
35	$1000/(W_LC_L + W_EC_E)$	0.1856
36	$P_D/W_LC_L + W_EC_E)^2\theta_{Gs}$	0.0117
37	$P_D/W_LC_L/ W_EC_E)\ \theta_{Gs}$	0.0234
38	$84\theta_{Gs}/P_D$	0.6675
39	$2/10\ \tau_{6,1}$	0.0892
40	$1/\tau_{6,1}$	0.4458
41	$1/\tau_{6,1}$	0.4458
42	$200/RC_c$	0.6202
43	$12/10\tau^2_{5,6}$	0.2507
44	$12/10\tau^2_{5,6}$	0.2507
45	$240/C_cW_{5,6}$	0.3402
46	$6/10\ \tau_{5,6}$	.2743
47	$6/10\ \tau_{5.6}$	.2743
48	$\Sigma\beta_i/500\ell$	0.5696
49	$\lambda_1\beta_1/100\ell$	0.5751
50	$\lambda_1/10$	0.1580
51	$\lambda_2\beta_2/100\ell$	0.3884
52	λ_2	0.3280
53	$\lambda_3\beta_3/10\ell$	0.6602
54	λ_3	0.1260
55	$\lambda_4\beta_4/10\ell$	0.2352
56	λ_4	0.0350
57	$\lambda_5\beta_5/10\ell$	0.0133
58	λ_5	0.0128
59	$2\beta_1/100\ell$	0.7280
60	$84\beta_2/10^4\ell$	0.9946
61	$84\beta_3/10^4\ell$	0.4402
62	$84\beta_4/10^4\ell$	0.5649
63	$2\beta_5/100\ell$	0.2080
64	1/2	0.5000
65	200/840	0.2381
66	—	—
67	--	—

Table 1-2

Analog Computer Model Runs

Run Number	Conditions Applied
1	F.L. to 0% inst.
2	F.L. to 0% inst., no $\mathcal{S}_p$
3	F.L. to 0% inst., $\mathcal{S}_t = -3.0 \times 10^{-4}$
4	F.L. to 10% inst.
5	F.L. to 25% inst.
6	0% to F.L. inst.
7	0% to F.L. inst., no $\mathcal{S}_p$
8	0% to F.L. inst., $\mathcal{S}_t = -3.0 \times 10^{-4}$
9	5% to F.L. inst.
10	10% to F.L. inst.
11	25% to F.L. inst.

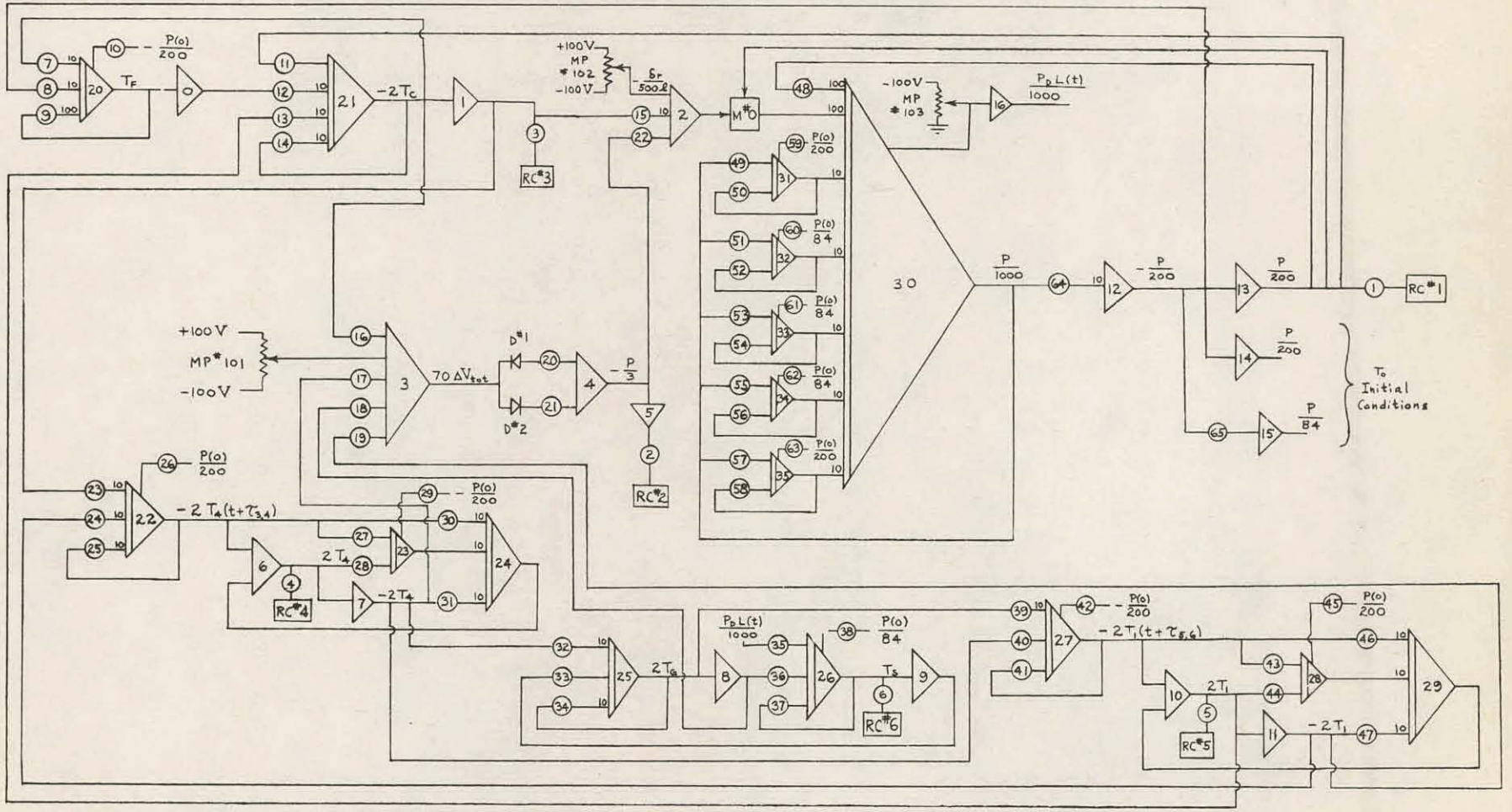

FIG. 1.1 - ELECTRONIC ANALOG COMPUTER CIRCUIT DIAGRAM

FOR PLANT KINETIC MODEL

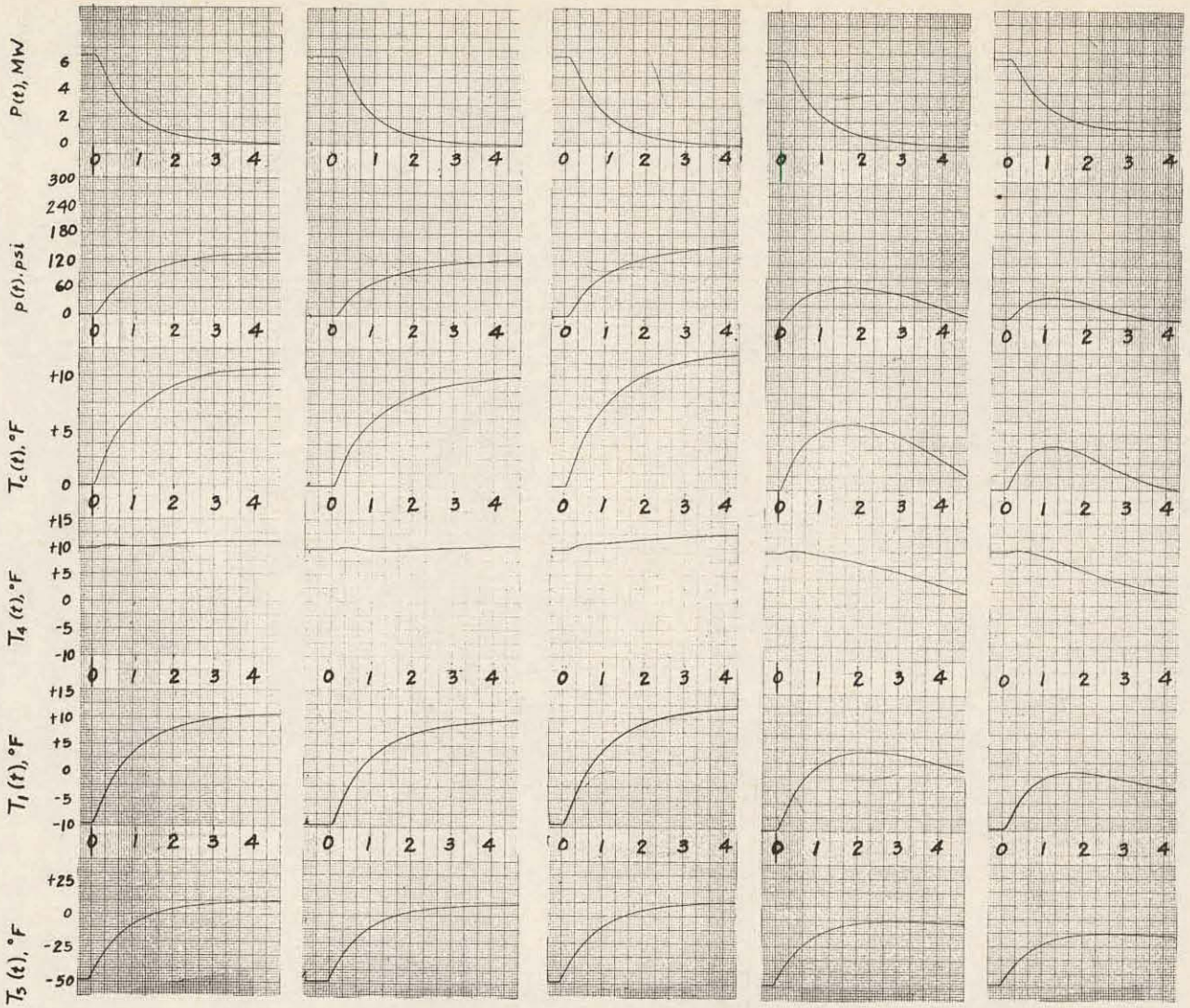

FIG. 1-2 PLANT RESPONSE TO INSTANTANEOUS LOAD REDUCTIONS

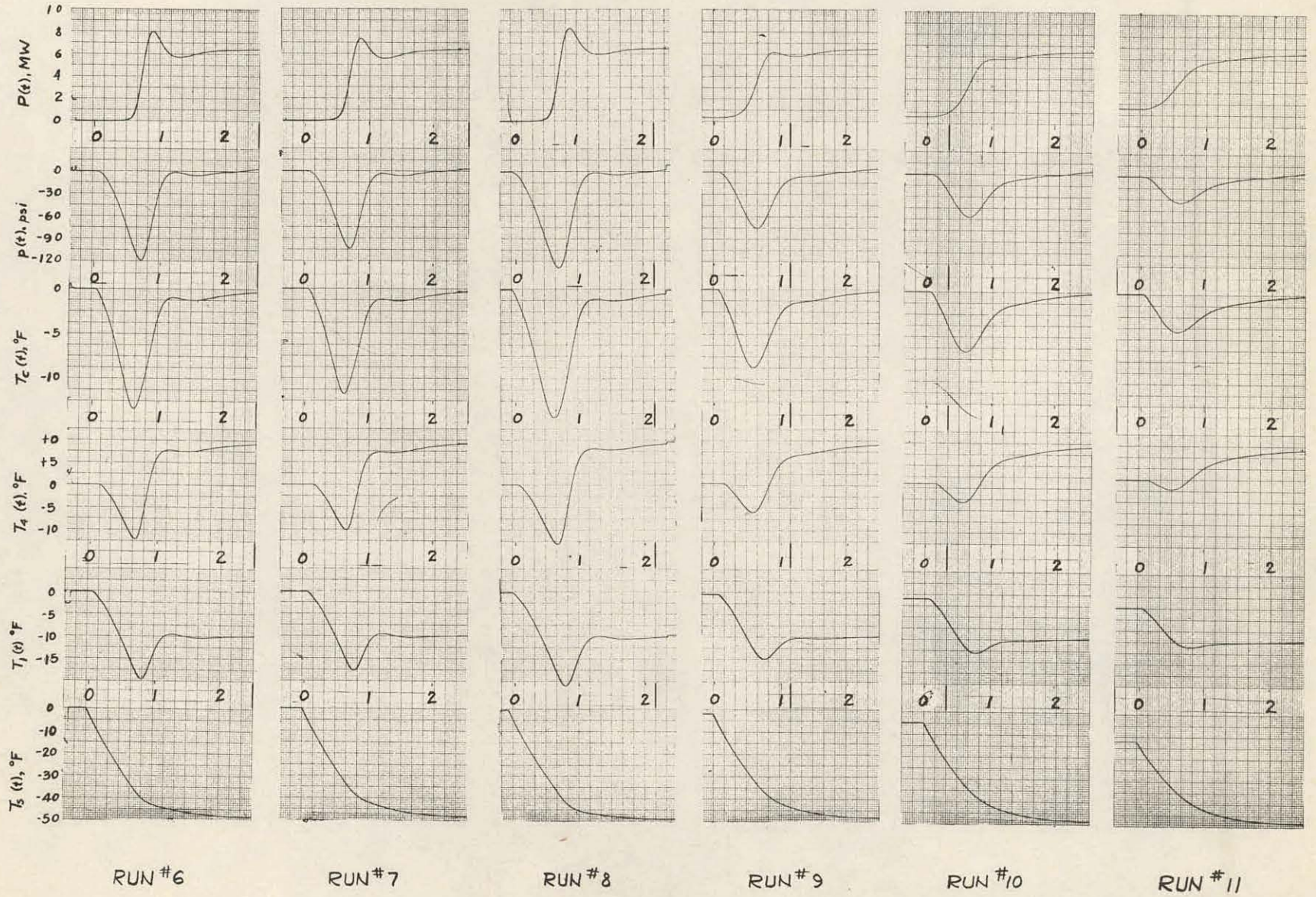

FIG. 1-3 PLANT RESPONSE TO INSTANTANEOUS LOAD INCREASES

2.0 REACTOR BEHAVIOR FOLLOWING PUMP FAILURE

2.1 General kinetic model

2.1.1 Description

In this study the response of the reactor following a failure of the primary coolant pump was invetigated. The nature of this failure was assumed to be one in which the impeller of the pump becomes frozen thus impeding coolant flow. This is a conservative assumption.

Coolant flow due to natural convection is neglected in the computer equations due to the physical location of the steam generator. Murray(2) has shown that when the steam generator is located below the reactor vessel coolant flow due to natural convection will be negligible.

After pump failure the diminishing rate of coolant flow results in increased temperatures both in the fuel and in the coolant within the core. If the reactor continues to operate at rated power this temperature rise will cause boiling within the reactor vessel. It is thus necessary to incorporate a reactor scram system activated when the coolant decreases to pre-set value of maximum flow rate. This study is intended to indicate whether boiling temperatures will occur before the reactor is scrammed.

2.1.2 Pump coastdown characteristics

In calculating the rate of pump coastdown after an accident the kinetic energy possessed by the moving coolant is equated to the friction of the loop. The normalized flow rate "G (t)" is integrated over the range of flow yielding: (3)

$$G(t)^{0.8} = \frac{a}{t+a}$$

where: $$a = \frac{\sum_{i=1}^{i} \frac{L_i}{A_i} \; F(t=0)}{0.8 \; g \; H(t=0)}$$

L_i = length of pipe section "i" (ft)

A_i = cross sectional area of pipe (ft^2)

$F(t=0)$ = design coolant flow rate (ft/sec)

$H(t=0)$ = head drop around coolant loop (ft)

g = acceleration due to gravity

In the system under consideration, it was assumed that the impeller of the coolant pump had become frozen and thus was further impeding coolant flow. A value of 22 ft was used as the negative head. This was obtained from data of a pump similar to that envisioned in this design.

The value of "a" thus becomes:

$$a = \frac{59.69 \times 5.58}{0.8 \times 32.2 \times 46.0} = 0.281$$

2.1.3 Differential equations

Utilizing the notation of section 1.1.2 the general kinetic equations are:[1]

$$\frac{dP(t)}{dt} = \left(\frac{0.01 \quad \delta_r + \gamma_t \; T_c(t) + \sum_{i=1}^{5} \beta_i}{\ell} \right) P(t)$$

where:

$$\frac{dk_i}{dt}(t) = \frac{\beta_i P(t)}{\ell} - \lambda_i k_i(t)$$

The pressure coefficient of reactivity commonly included in the above expression is neglected because there will be insufficient circulation of coolant external to the pressure vessel within the time being considered.

Performing a heat balance on the fuel and coolant within the core yields:

$$\frac{d\,T_F(t)}{dt} = \frac{\alpha P(t)}{W_F C_F} - \frac{Ah}{W_F C_F} \left(T_F(t) - T_c(t) \right)$$

and

$$\frac{dTc}{dt}(t) = \frac{(1-\alpha) \quad P(t)}{W_c \; C_c} + \frac{hA}{W_c C_c} \left(T_F(t) - T_c(t) \right)$$

$$-\frac{2 \; R}{W_c} \left(T_c(t) - T_{inlet} \right)$$

where:

$$T_F(t=0) = \Theta_{F,C}$$

$$T_F(t=0) = 0$$

The meaning of symbols used is indicated in section 1.2.2

The flow rate, F (t), is given in section 2.1.2 by:

$$G(t)=\frac{F(t)}{F(t=0)} = \left(\frac{a}{a+t}\right)^{1.25}$$

where: F (t= 0) = rated coolant flow

t = time after pump failure accident

The constant "a" is dependent upon the physical configuration of the primary loop.

The average film coefficient in the core is a function of the flow mass rate to the 0.8 power.

then: $$\frac{h\ (t)}{h\ (0)} = \left(\frac{F\ (t)}{F\ (0)}\right)^{0.8} = \left(\frac{a}{t+a}\right)$$

$$h\ (0) = \frac{P_D}{A\alpha\Theta_{FC}}$$

The previous equations for the fuel and coolant temperatures becomes:

$$\frac{dT_F(t)}{dt} = \frac{\alpha}{W_F\ C_F}\ P\ (t) - \frac{A}{W_F C_F}\ h\ (0)\ \left(\frac{a}{a+t}\right)\ (T_F\ (t)-T_c(t)\ )$$

$$\frac{dT_c(t)}{dt} = \frac{(1-\alpha)}{W_c C_c}\ P\ (t) + \frac{A\ h(0)}{W_c C_c}\ \left(\frac{a}{a+t}\right)\ (T_F(t) - T_c(t))-$$

$$\left[\frac{2R}{W_c}\ \left(\frac{a}{a+t}\right)^{1.25}\ T_c(t)\right]$$

2.2 Constants for differential equations

2.2.1 Time and amplitude scaling factors

A scaling factor was chosen in order that ten computer seconds would equal one second in real time. This was dictated by the rapid sequence of events following a pump failure accident and the need to get detailed behavior during this time.

An amplitude scaling factor of one volt equals one physical unit was chosen for this section of the analysis. The magnitude of the quantities generated were scaled proportionally in order that their magnitudes would not exceed $\pm$ 100 volts.

2.2.2. Potentiometer setting

Table 2-1 lists the physical quantities in each potentiometer setting as well as their absolute magnitude in this problem.

TABLE 2 - 1 POTENTIOMETER SETTINGS

Potentiometer	Quantity	Magnitude	Potentiometer	Quantity	Magnitude
1	1/2	0.5000	16	λ_3 /10	0.0126
2	$84\beta_2/10{,}000\ell$	0.9946	17	$\lambda_4\beta_4$ /100ℓ	0.0235
3	20/84	0.2381	18	λ_4/10	0.0035
4	$2\beta_1/100\ell$	0.7280	19	$\lambda_5\beta_5$ /100ℓ	0.0013
5	$84\beta_3$ /10,000ℓ	0.4402	20	λ_5 /10	0.0013
6	$84\beta_4/10{,}000\ell$	0.5649	21	$100\Theta_{F,c}$ P_D	0.4134
7	168 ϑ_T /10,000ℓ	0.2285	22	A h_o/10 $W_F C_F$	0.3830
8	$2\beta_5$ /100ℓ	0.2080	23	$10\alpha/W_F C_F$	0.1584
9	T_{in}/200	0.0428	24	A h_o/10 $W_c C_c$	0.1218
10	$\sum_i \beta_i$ /50ℓ	0.5696	25	R_D/10 W_c	0.1711
11	$\lambda_1\beta_1$ /100ℓ	0.5751	26	50 $(1-\alpha)W_c W_c$	0.0132
12	λ_1 /10	0.1580	27	a/10	0.0281
13	$\lambda_2\beta_2$ /100ℓ	0.3884	28	1 /100	0.0100
14	λ_2 /10	0.0328	29	a/10	0.0281
15	$\lambda_3\beta_3$ /100ℓ	0.0660			

2.2.3 Analog circuit diagram

Fig. 2-1 shows in symbolic form the analog circuitry used in this study. The notation is that utilized and explained in APAE-38 (3).

2.3 Results of analog pump failure simulation

Solution of the coupled differential equations during the pump failure condition yields values of the average fuel surface temperature and the average coolant temperature. These solutions are shown in Fig. 2-2.

The statistical hot channel for this system has been designed at 617°F. This is the saturation temperature at design pressure. The hot channel factor has been calculated assuming the simultaneous occurence of all hot flux factors at the same point. This is definitely a conservative assumption. More realistically the hottest channel would probably be near 607°F. Experimental data (4) indicate that nucleate boiling does not begin until the fuel surface temperature exceeds saturation temperature by as much as 30°F. By conservatively assigning a one second delay between the low flow scram signal and reactor shutdown one can estimate the rise in temperature within the hottest channel. Fig. 2-2 indicates a temperature rise of 31° F for the average fuel surface temperature during the second following the reactor scram signal assuming forced convection. The behavior of the hottest channel will follow this trend. Thus only limited nucleate boiling probably will occur within the hottest channel during a pump failure.

The analog results indicate a permissible 3.9 second delay between low flow scram and reactor shutdown. The average fuel surface temperature will not reach saturation before reactor shutdown.

2.4 Conclusions

Results of analog simulation of a pump failure accident in which the pump impeller becomes frozen indicate that only limited nucleate boiling will probably occur before reactor shutdown. The average fuel surface temperature during this accident will not reach saturation before reactor shutdown and therefore no general boiling will occur.

3.0 REFERENCES

1. Brondel, J.O., and J. R. Tomonto, "Plant Transient Analysis of the APPR-1 by Analog Methods," APAE-38.

2. Murray, R.L., "Notes on Decay Heating after Power Failure," APAE Memo 144.

3. Coneybear, J.F., "Pump Failure and the APPR-1," Astra Report 415-E-4.1.

4. Jens, W.H., "Analysis of Heat Transfer, Burnout, Pressure Drop, and Density Data for High-Pressure Water," ANL-4627.

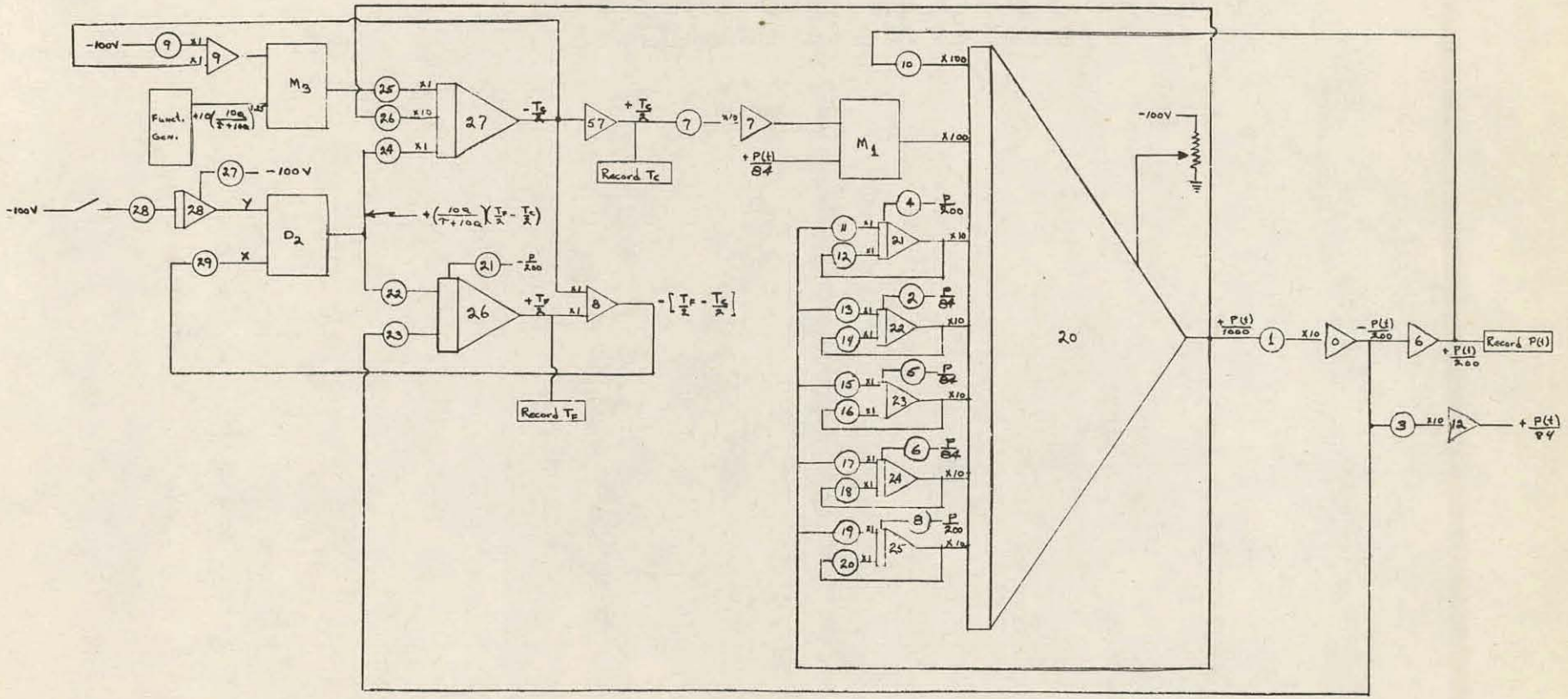

Figure 2-1 Analog Circuit Diagram

2-1

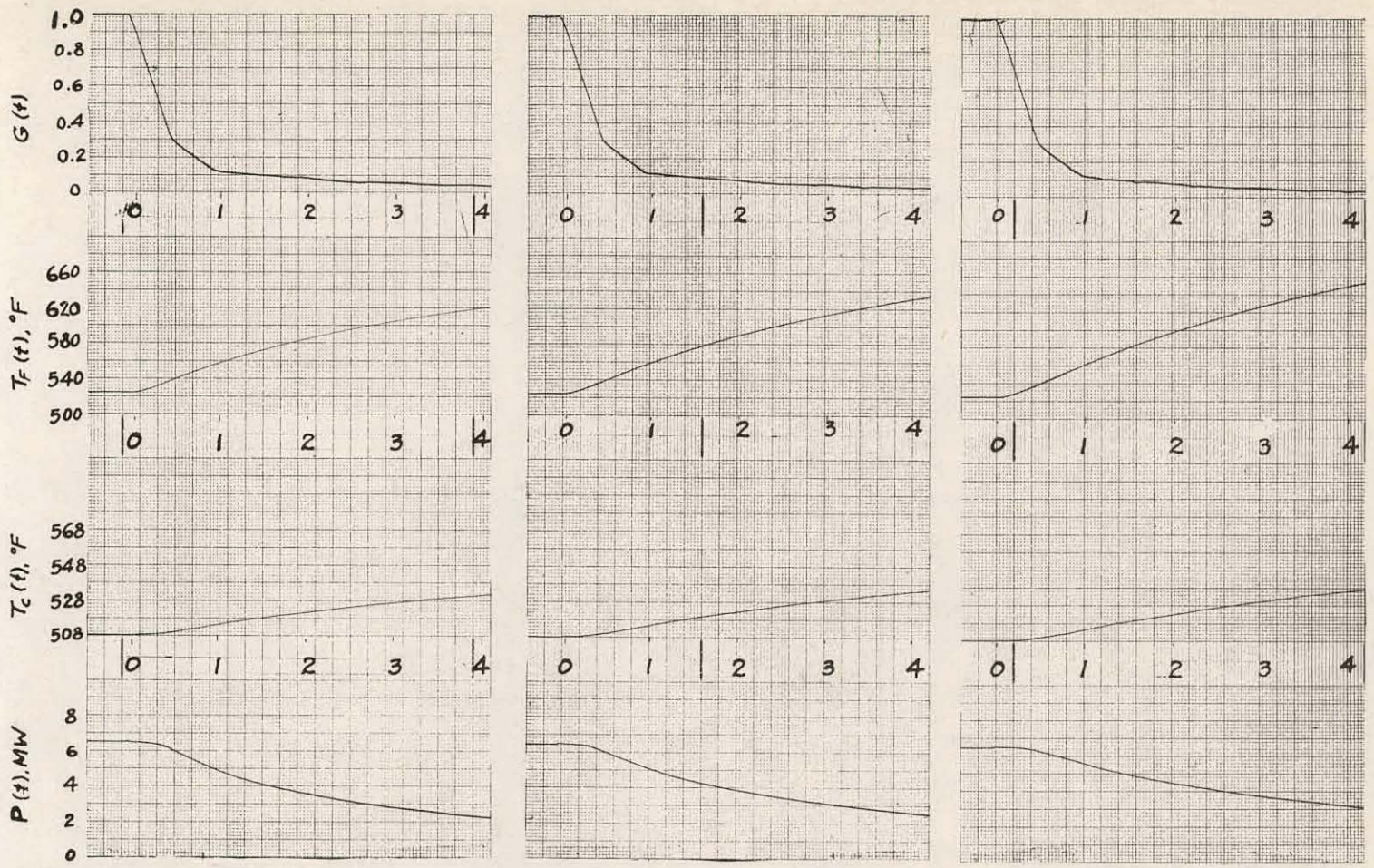

RUN #1
DESIGN PARAMETERS

RUN #2
$\gamma_T = -2.55 \times 10^{-4}$

RUN #3
$\gamma_T = -1.7 \times 10^{-4}$

ELAPSED TIME IN SECONDS

FIG. 2-2 ANALOG RESULTS FOR PUMP FAILURE CONDITION

D. CORE THERMAL AND HYDRAULIC DESIGN ANALYSIS

1.0 THERMAL DESIGN CRITERIA

The contract sets forth certain General Objectives and Project Guidelines that affect the thermal design of the Skid Mounted APPR. The most important of these are:

a. System reliability with minimum downtime for refueling.

b. Utilization of proven technology.

c. Availability for procurement by January 1, 1959.

On the basis of these project guidelines the Skid Mounted APPR has been designed thermally so that the maximum surface temperature in the hot channel does not exceed the saturation temperature. The thermal design criteria employed on the APPR-1 and APPR-1A has been reviewed prior to start of the thermal analysis of the Skid Mounted APPR.

The following criteria have been established for thermal design of APPR pressurized-water reactors:

1.1 Heat transfer coefficient

The heat transfer coefficient is to be calculated by use of the Dittus-Boelter equation with a constant coefficient of 0.021:

$$h = 0.021 \frac{K}{D} \left(\frac{\rho V D}{\mu}\right)^{0.8} \left(P_r\right)^{0.4}$$

where:

h = heat transfer coefficient, Btu/ft^{2}hr$^\circ$F

k = thermal conductivity, Btu/ft hr$^\circ$F

D = equivalent diameter of channel, ft

ρ = density of coolant, lb/ft^3

V = velocity of coolant, ft/hr

μ = viscosity of coolant, lb/ft-hr

Pr = Prandtl number of coolant

The coefficient 0.021 was established subsequent to a survey of the literature on experimental heat transfer data, and is felt to be conservative, but not extremely so. Papers reviewed are referenced at the end of this section.

1.2 Power distribution utilization

A calculated axial power distribution is to be used for the analysis. Values from a calculated radial power distribution are combined with a side plate flux peaking factor and other existing peaking factors to establish individual nuclear radial factors for the various elements or groups of similar elements. Methods for the establishment of these factors are outlined by B. Byrne in paper entitled, "Thermal Design Basis for APPR Type Elements". In addition a nuclear uncertainty factor of 1.05 is applied to both the bulk coolant temperature rise and the film temperature gradient to account for uncertainties in the calculation of power distributions. In the heat transfer analysis the assumption is made that 95% of the heat released in the core is released in the active fuel elements. The basis for this assumption is explained in 1.6.3 of this section.

1.3 Hot channel factors

Manufacturing, orifice sizing, and inlet box effect hot channel factors are derived in 1.6.1 of this section for APPR-1 elements and are listed below. Elements with other dimensions should be treated similarly.

Average factors are those which apply to the bulk coolant temperature rise, and local factors, those which apply to the film temperature gradient.

TABLE 1.1 HOT CHANNEL FACTORS

Item	Factor	
	Average	Local
Plate spacing deviation	1.0706	1.1623
Uranium content deviation*	1.0050	1.0250
Length deviation	1.0357	1.0357
Clad thickness deviation	1.0064	1.0128
Orifice sizing	1.0417	1.0332
Inlet box effect:		
Fuel element	1.0309	1.0247
Control rod	1.0638	1.0507
Combined factor (Product of individual factors):		
Fuel element	1.2044	1.3230
Control rod	1.2428	1.3566

*This factor includes uranium content of the whole element along with homogeneity within the element.

1.4 Lattice requirements

Since it is not possible to tailor lattice flow as is done with the internal flow, the entire lattice flow must be based on the maximum fuel element requirement. Calculations (see 1.6.2 of this section) indicate that the larger tolerances on lattice channel dimensions constitute an additional hot channel factor of 1.033. It is therefore felt that the lattice flow should be established on the basis of an average lattice velocity 5% greater than the highest stationary fuel element velocity.

1.5 Instrumentation tolerances

Instrumentation tolerances for pressurized water reactors have been estimated by R. E. May, and indicated by G. Knighton in memos of 5/14/58 and 6/4/58 to be as follows:

system pressure	± 2.25%
core power	± 3.5%
inlet temperature	± 4°F

The above values are conservative and it is feasible to improve same with more accurate, and more costly instrumentation.

1.6 Calculations

1.6.1 Hot channel factors

The hot channel factors, as listed in Table 1.1 were calculated on the basis of the following maximum deviations:

TABLE 1.2

Item	Nominal	Max. Deviation
Internal plate spacing	.133"	(± .006 avg. (± .0133 local
Uranium Content		(± 0.5% average (± 2.5% local
Length	21.75"	± 0.75"
Clad thickness	.005"	(± .0005 avg. (± .001 local
Relative Channel Flow as Governed by Orifice Diameter	1.00	± 4% avg. and local

Table 1.2 (Cont'd.)

Item	Max. Deviation
Effect of inlet box on flow distribution:	
Fuel element	3%
Control rod	6%

Symbols and Nomenclature

a - Max. negative average deviation of plate spacing, in.

A - Channel flow area, in^2.

b - Max. positive local deviation of plate spacing, in.

c_p - Specific heat of water, Btu/lb.-°F.

C - Flow coefficient

d - Nominal plate spacing, in.

D - Hydraulic diameter of channel, in.

f - Channel friction factor

F - Hot channel factor

h - Water film heat transfer coefficient, $Btu/in.^2-°F.-sec.$

k - Thermal conductivity, $Btu-in./in.^2-°F.-sec.$

L - Channel length, in.

p - Perimeter of channel, in.

ΔP - Pressure drop across channel, in. of water

q - Heat flow rate, $Btu/in.^2-°F.-sec.$

Q - Volumetric heat generation rate in meat, $Btu/in.^3-sec.$

t - Thickness of meat or clad in fuel element, in.

T - Temperature, °F.

TR - Bulk temperature rise of channel flow, °F.

μ - Water viscosity, lb./in.-sec.

V - Water velocity in channel, in./sec.

Symbols and Nomenclature

w - Width of channel, in.

W - Relative weight of uranium per plate

X - Distance to point inside meat, measured from hot channel side perpendicular to plate, in.

ϕ - Thermal neutron flux

ρ - Water density, lb/in.^{3}

- Subscripts

a - Average conditions along length of channel

avg. - Average conditions across width of fuel plate meat

c - Clad

C - Contraction flow on entering channel

E - Expansion flow on leaving channel

f - Water film

h - Hot channel conditions

l - Local conditions along length of channel

m - Meat of fuel element

n - Nominal conditions

o - Outside channel (adjacent to hot channel)

p - Peak meat temperature

Δ T - Temperature gradient across water film

TR - Bulk temperature rise of channel flow

w - Water

1.6.1.1 Plate spacing deviation factors

(A) Average Hot Channel Factor

A flow passage may be restricted by plate bowing or sagging in the center, or by deviations in the plate edge spacing, the latter case being the most severe, thermally.

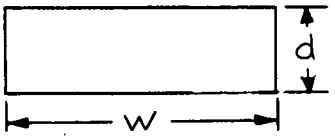

Nominal Channel

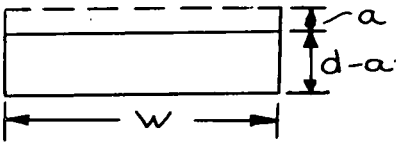

Average Hot Condition

The reduction in flow area = aw

$$A_n = dw$$

$$A_{ha} = dw - aw = (d-a)w$$

$$D_n = \frac{4A_n}{P_n} = \frac{4dw}{2(d+w)} = \frac{2dw}{d+w}$$

$$D_{ha} = \frac{4A_{ha}}{P_{ha}} = \frac{2(d-a)w}{(w+d-a)}$$

As the pressure drop ΔP across each channel of the same element is essentially equal and as contraction and expansion coefficients for the channels are negligible, velocity variation is only a function of the average hydraulic diameter deviation

$$\Delta p = \frac{V^2}{12(2g)}\left[C_c + f\frac{L}{D} + C_E\right]$$

where C_c and C_E are essentially zero

$$\frac{V_n^2}{V_{ha}^2} = \frac{D_n}{D_{ha}} = \frac{d}{(d+w)} \times \frac{(w+d-a)}{(d-a)}$$

$$\frac{V_n}{V_{ha}} = \sqrt{\frac{d(w+d-a)}{(d+w)(d-a)}}$$

$$F_{TR} = \frac{(TR)_{ha}}{(TR)_n} = \frac{A_n}{A_{ha}} \times \frac{V_n}{V_{ha}}$$

$$F_{TR} = \left(\frac{d}{d-a}\right)^{3/2}\left(\frac{d+w-a}{d+w}\right)^{1/2}$$

Substituting the numerical values applicable for APPR elements:

d = .133"

a = .006" (min. average deviation)

w = 2.733"

F_{TR} = 1.0706

(b) Local Hot Channel Factor

In defining the worst possible channel, thermally, the conservative approach is taken of considering that the average deviation could be the negative observed limit, while a local deviation could simultaneously be at the positive observed limit in the same channel.

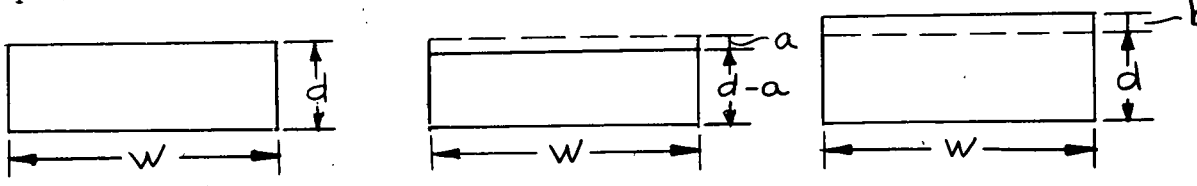

Nominal Channel | Average Hot Condition | Local Hot Condition

$$A_n = dw$$

$$A_{hl} = (d+b)\,w$$

$$\frac{D_{hl}}{D_n} = \frac{A_{hl}}{A_n} = \frac{d+b}{d}$$

The local deviation is assumed to be sufficiently gradual to permit complete diffusion.

$$\frac{V_n}{V_{hl}} = \frac{V_n}{V_{ha}} \times \frac{V_{ha}}{V_{hl}} = \frac{d+b}{(d-a)^{3/2}}\sqrt{\frac{d(d+w-a)}{(d+w)}}$$

The film coefficient is reduced not only by the drop in coolant velocity but also by the increase in hydraulic diameter:

$$h = .021 \frac{K}{D} \left(\frac{\rho V D}{\mu}\right)^{0.8} \left(\frac{C_p \mu}{K}\right)^{0.4}$$

$$F_{\Delta T} = \frac{\Delta T_{hl}}{\Delta T_n} = \frac{h_n}{h_{hl}}$$

$$= \left(\frac{V_n}{V_{hl}}\right)^{0.8} \left(\frac{D_{hl}}{D_n}\right)^{0.2}$$

$$= \frac{(d+b)^{0.8}}{(d-a)^{1.2}} \left[\frac{d(d+W-a)}{(d+W)}\right]^{0.4} \left(\frac{d+b}{d}\right)^{0.2}$$

$$F_{\Delta T} = d^{0.2} \frac{(d+b)}{(d-a)^{1.2}} \left(\frac{d+W-a}{d+W}\right)^{0.4}$$

Substituting values for APPR elements:

$b = .0133"$

$F_{\Delta T} = 1.1623$

1.6.1.2 Uranium content deviation

(a) Average Hot Channel Factor

Both fuel elements forming the hot channel are assumed to contain the maximum allowable uranium content per plate.

$$F_{TR} = \frac{TR_{ha}}{TR_n} = \frac{W_{ha}}{W_n}$$

The maximum allowable positive deviation of uranium content per plate is 0.5%.

$$F_{TR} = \frac{W_n (1+0.005)}{W_n} = 1.005$$

(b) Local Hot Channel Factor

$$F_{\Delta T} = \frac{\Delta T_h}{\Delta T_n} = \frac{W_{hl}}{W_n}$$

In addition to the 0.5% uranium content deviation per plate, there is a maximum allowable non-homogeneity within a plate of 2%. Assuming, conservatively, that the maximum positive deviation per plate and the maximum positive non-homogeneity deviation occur simultaneously, the maximum local uranium content deviation is 2.5%. $F_{\Delta T} = \frac{W_n (1 + .025)}{W_n} = 1.0250$

1.6.1.3 Active core length deviation

For a given volume of meat per plate, a negative deviation in active length increases the amount of meat per unit length and therefore per unit heat transfer area. This affects both the bulk coolant temperature rise and the film gradient. Based on the conservative approach that decreased length increased only meat thickness and not active width:

$$F_{TR} = F_{\Delta T} = \frac{L_n}{L_{min}}$$

for APPR fuel elements:

L_n = 21.75"

$L_{min.}$ = 21"

$$F_{TR} = F_{\Delta T} = \frac{21.75}{21} = 1.0357$$

It may be noticed that since the nominal meat width is also the minimum meat width, a corresponding calculation is not necessary for active width deviation.

1.6.1.4 Clad thickness deviation factors

- Derivation of General Equations

If the two clad thicknesses of a fuel plate are unequal, a greater portion of the total heat generated in the meat will pass out through the thinner clad because of lower thermal resistance. A hot channel is, therefore, defined as being composed of two fuel plates whose inner and outer clad thicknesses are at the minimum and maximum observed values respectively. Both the average and local hot channel factors are then equal to the proportional increase in the heat transmitted through the inner sides.

A cross section of the hot channel fuel plate is shown in the diagram below. The water temperatures are conservatively assumed equal.

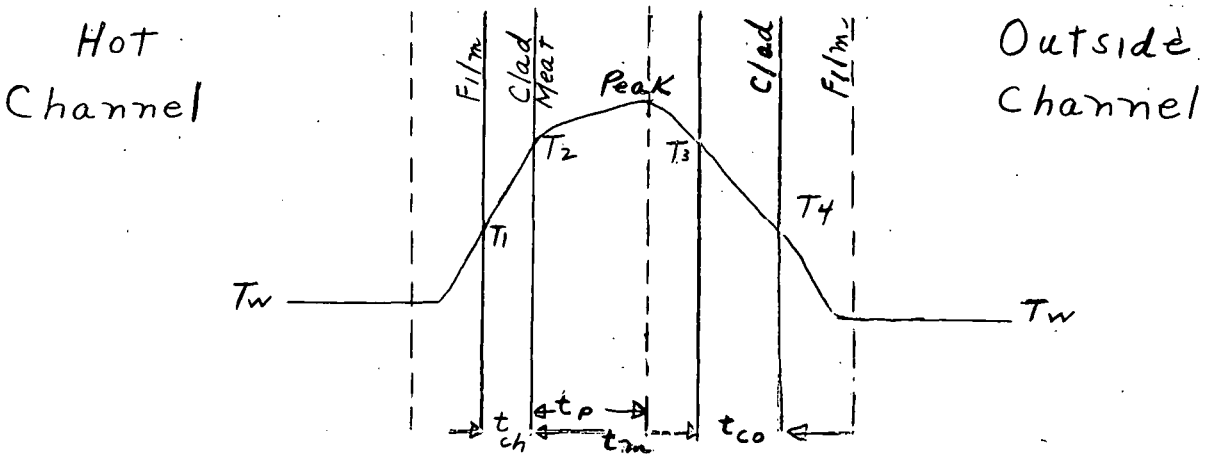

The determination of hot channel factors is derived in the following steps.

a) Determine the general differential equation for the temperature distribution through the meat as a volume heat source.

b) Determine the general solution for step (a). Substituting boundary conditions, solve for the general constants of integration.

c) Determine the location of the temperature peak by setting slope of temperature curve equal to zero. Portion the heat flow through two clads accordingly, in terms of meat boundary conditions.

d) Determine the temperature gradient through each clad and water film combination, using the results of step (c). The meat boundary conditions are then defined in terms of physical dimensions and properties.

e) Substitute the meat boundary conditions as determined by step (d) into the expressions for proportioning of heat flow as determined in step (c). The hot channel factor is then simply the ratio of the hot channel side flow to the average or nominal flow.

a) The general differential equation for temperature distribution through a volume heat source is determined as follows:

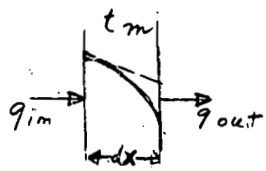

$$q_{in} = -K_m \left(\frac{dt_m}{dx}\right)_x$$

$$q_{out} = -K_m \left(\frac{dt_m}{dx}\right)_{x+dx}$$

$$q_{out} - q_{in} = Q\,dx$$

$$\left(\frac{dt_m}{dx}\right)_{x+dx} = \left(\frac{dt_m}{dx}\right)_x + \left(\frac{d^2t_m}{dx}\right)dx$$

By proper substitution and simplification:

$$q_{out} - q_{in} = -K_m \left(\frac{dt_m}{dx}\right)_{x+dx} + K_m \left(\frac{dt_m}{dx}\right)_x$$

$$Q\,dx = -K_m \left[\left(\frac{dt_m}{dx}\right)_x + \left(\frac{d^2t_m}{dx^2}\right)dx\right] + K_m \left(\frac{dt_m}{dx}\right)_x$$

$$Q\,dx = -K_m \left(\frac{d^2t_m}{dx^2}\right)dx$$

$$\frac{d^2t_m}{dx^2} = -\frac{Q}{K_m}$$

b) The differential equation is solved by the reduction of order method:

Let $\frac{dt_m}{dx} = y$; Then $\frac{dy}{dx} = -\frac{Q}{K_m}$

$$\int dy = -\frac{Q}{K_m}\int dx$$

$$\frac{dt_m}{dx} = -\frac{Q}{K_m}x + C_1$$

$$\int dt_m = -\frac{Q}{K_m}\int x\,dx + C_1\int dx$$

$$t_m = -\frac{Q}{2K_m}x^2 + C_1 x + C_2$$

Boundary conditions

$x = o;\ T_m = T_2$

$x = t_m;\ T_m = T_3$

By substitution of boundary conditions into the general solution:

$T_2 = c_2$

$T_3 = -\frac{Q}{2K_m}t_m^2 + c_1 t_m + T_2$

$c_1 = \frac{T_3 - T_2}{t_m} + \frac{Qt_m}{2K_m}$

Substituting these results to obtain the specific solution:

$$T_m = \frac{-Q}{2K_m}x^2 + \left[\frac{T_3 - T_2}{t_m} + \frac{Qt_m}{2K_m}\right]x + T_2$$

c) To find the point of temperature peaking, and therefore the point of direction change in heat transfer, determine t_p where $\frac{dT_m}{dx} = 0$:

$$\frac{dT_m}{dx} = -\frac{Q}{K_m} t_p + \left[\frac{T_3 - T_2}{t_m} + \frac{Qt_m}{2K_m}\right] = 0$$

$$t_p = \frac{t_m}{2} + \frac{K_m}{Qt_m}\left(T_3 - T_2\right)$$

It is seen from this expression for t_p that the peak temperature normally occurs in the center of the meat, but that a correction is necessary with unequal sink temperatures. This is, of course, as expected.

As heat generation per unit volume is uniform, the fraction of the total heat flow that is leaving the fuel plate on the hot channel side is equal to tp/tm. Therefore:

$$q_h = Q\, t_p$$

$$= \frac{Qt_m}{2} + \frac{K_m}{t_m}\left(T_3 - T_2\right)$$

$$q_o = Q\left(t_m - t_p\right)$$

$$= \frac{Qt_m}{2} - \frac{K_m}{t_m}\left(T_3 - T_2\right)$$

d) Since an expression is available for the heat flow rate through the clad and water film on either side, the corresponding temperature gradients can be determined:

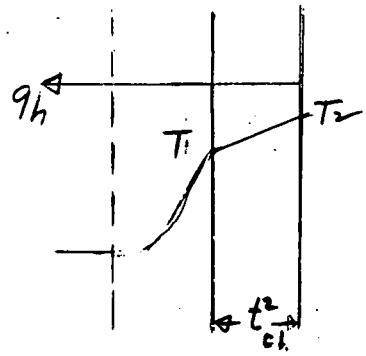

$$T_2 - T_w = q_h\left(\frac{1}{h_{ch}} + \frac{1}{h_f}\right)$$

$$= q_h\left(\frac{t_{ch}}{K_c} + \frac{1}{h_f}\right)$$

Similarly for the other plate side:

$$T_3 - T_w = q_o\left(\frac{t_c}{K_c} + \frac{1}{h_f}\right)$$

By subtraction and substitution for q_o :

$$T_3 - T_2 = q_n \left[\frac{t_{co}}{k_c} + \frac{1}{h_f}\right] - q_h \left[\frac{t_{ch}}{k_c} + \frac{1}{h_f}\right]$$

$$T_3 - T_2 = \left[Qt_m - q_h\right] \left[\frac{t_{co}}{k_c} + \frac{1}{h_f}\right] - q_h \left[\frac{t_{ch}}{k_c} + \frac{1}{h_f}\right]$$

$$T_3 - T_2 = Qt_m \left[\frac{t_{co}}{k_c} + \frac{1}{h_f}\right] - q_h \left[\frac{t_{ch}}{k_c} + \frac{2}{h_f} + \frac{t_{co}}{k_c}\right]$$

For convenience in handling, this latter expression will be written as:

$$T_3 - T_2 = Qt_m \alpha - q_h \beta \; ; \alpha = \frac{t_{co}}{K_c} + \frac{1}{h_f}$$

$$\beta = \frac{t_{co}}{K_c} + \frac{t_{ch}}{K_c} + \frac{2}{h_f}$$

e) The final expression for qh can now be determined by substituting this final relationship in paragraph (d) for $T_3 - T_2$ into the equation for qh in paragraph (c):

$$q_h = \frac{Qt_m}{2} + \frac{K_m}{t_m} (T_3 - T_2)$$

$$= \frac{Qt_m}{2} + \frac{K_m}{t_m} (Qt_m \alpha - q_h \beta)$$

$$= \frac{\frac{Qt_m}{2} + QK_m \alpha}{\frac{K_m}{t_m} \beta + 1}$$

The hot channel factor is now determined by dividing the maximum by the nominal heat flux.

$$F = \frac{q_h}{q_n} = \frac{\frac{Qt_m}{2} + QK_m \alpha}{\frac{\frac{K_m}{t_m} \beta + 1}{\frac{Qt_m}{2}}}$$

$$F = \frac{\cancel{2}t_m + 2\cancel{0}k_m \alpha}{\cancel{2}} \times \frac{t_m}{K_m \beta + t_m} \times \frac{\cancel{2}}{\cancel{2}t_m}$$

$$F = \frac{t_m + 2K_m \alpha}{t_m + K_m \beta} \; ; \quad \alpha = \frac{t_{co}}{K_c} + \frac{1}{h_f}$$

$$\beta = \frac{t_{co}}{K_c} + \frac{t_{ch}}{K_c} + \frac{2}{h_f}$$

It is seen that when the two clad thicknesses t_{co} and t_{ch} are equal, then

$\beta = 2$, and F = 1 as expected.

(a) Average Hot Channel Factor

The following numerical values are applicable for APPR elements:

t_m = .0200 in. (nominal)

t_{ch} = .0045 in. (minimum average)

t_{co} = .0055 in. (maximum average)

k_m = .000205 Btu/in ^oF sec (at 600^oF)

k_c = .000274 Btu/in ^oF sec (at 600^oF)

h_f* = .00459 Btu/in^2 ^oF sec

By computation:

α = 237.94 in^2 - ^oF - sec/Btu

β = 472.23 in^2 - ^oF - sec/Btu

Substituting into the expression for hot channel factors developed in section (a):

$$F_{TR} = \frac{TR_h}{TR_n} \quad \frac{qh}{qn} \quad \frac{t_m + 2\,Km\,\alpha}{t_m + k_m \beta}$$

F_{TR} = 1.0064

* To be precisely correct, h_f would have to be re-evaluated for each new core and for each element within the core. However, as even a large change in h_f has an insignificant effect on required flow, an average value is used.

(b) Local Hot Channel Factor

The following numerical values are applicable for the local factor:

t_{ch} = .0040 in. (minimum local)

t_{co} = .0060 in. (maximum local)

By computation:

α = 239.76 in^2 - ^oF - sec/Btu

β = 472.23 in^2 - ^oF - sec/Btu

Substituting into the expression for hot channel factors:

$$F_{\Delta T} = \frac{\Delta T_h}{\Delta T_n} = \frac{q_h}{q_n} = \frac{t_m + 2K_m \alpha}{t_m + K_m \beta}$$

F = 1.0128

1.6.1.5 Orifice sizing factors

The orifice diameter required to yield a given flow rate for a particular fuel element will be determined by a flow test rig. Some flow deviation allowance must be made for instrument error and experimental accuracy. As the calculated value of the proper orifice diameter is expressed to the nearest 1/64" for machining purposes, an additional deviation allowance must be introduced. Experience with the APPR-1 demonstrates that a combined maximum deviation of $\pm$ 4% is sufficient for both stationary element and control rod flow.

The hot channel factors associated with a 4% reduction in flow from an undersized orifice are determined in a manner similar to that used for the factors associated with plate spacing deviation with the exception that no change in the channel flow area is considered.

(A) Average Hot Channel Factor

$$F_{TR} = \frac{TR_h}{TR_n} = \frac{V_n}{V_h}$$

$$F_{TR} = \frac{V_n}{V_n(1-.04)} = 1.0417$$

(b) Local Hot Channel Factor

$$F_{\Delta T} = \frac{\Delta T_h}{\Delta T_n} = \left(\frac{h_n}{h_h} = \frac{V_n}{V_h}\right)^{0.8}$$

$$F_{\Delta T} = \left[\frac{V_n}{V_n(1-.04)}\right]^{0.8} = 1.0332$$

1.6.1.6 Inlet box effect on flow distribution

An allowance is made for uneven flow distribution on leaving the fuel element inlet boxes. For stationary elements, the outer channel flow was assumed to be 3% below average. For control rods the outer channel flow was assumed to be 6% below average. Further investigation of this subject is intended.

(a) Average Hot Channel Factor

$$F_{TR} = \frac{TR_h}{TR_n} = \frac{V_n}{V_h}$$

$$(F_{TR})_{F.E.} = \frac{V_n}{V_n(1-.03)} = 1.0309$$

$$(F_{TR})_{C.R.} = \frac{V_n}{V_n(1-.06)} = 1.0638$$

(b) Local Hot Channel Factor

$$F_{\Delta T} = \frac{\Delta T_h}{\Delta T_n} = \frac{h_n}{h_h} = \left(\frac{V_n}{V_h}\right)^{0.8}$$

$$\left(F_{\Delta T}\right)_{F.E.} = \left[\frac{V_n}{V_n(1-.03)}\right] = 1.0247$$

$$\left(F_{\Delta T}\right)_{C.R} = \left[\frac{V_n}{V_n(1-.06)}\right]^{0.8} = 1.0507$$

1.6.2 Lattice requirement determination

The manufacturing tolerances for the lattice passages are, by necessity, broader than those for the internal passages.

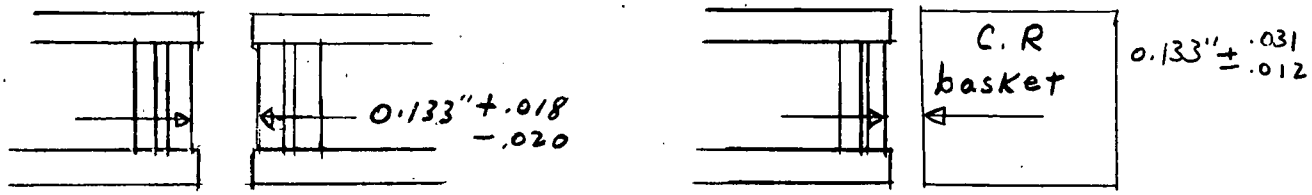

Since the larger lattice tolerances are a result of misalignment of entire elements rather than warping of individual plates, it is not possible for the average and local deviations to be in opposite directions. As the pressure drops across the various lattice channels are essentially equal, velocity variation is a function only of average hydraulic diameter deviation.

$$\frac{V_n^2}{V_h^2} = \frac{D_n}{D_h}$$

Since the effect on required flow of increased bulk coolant temperature rise hot channel factors is insignificant in comparison with the effect of increased film gradient hot channel factors, only the latter will be derived here.

$$h = .021 \frac{K}{D} \left(\frac{\rho V D}{\mu}\right)^{0.8} \left(\frac{C_p \mu}{K}\right)^{0.4}$$

$$F_{\Delta T} = \frac{\Delta T_h}{\Delta T_m} \qquad \frac{h_m}{h_h} = \left(\frac{V_m}{V_h}\right)^{0.8} \times \left(\frac{D_h}{D_m}\right)^{0.2}$$

$$= \left(\frac{D_m}{D_h}\right)^{0.4} \times \left(\frac{D_h}{D_m}\right)^{0.2}$$

$$F_{\Delta T} = \left(\frac{D_m}{D_h}\right)^{0.2}$$

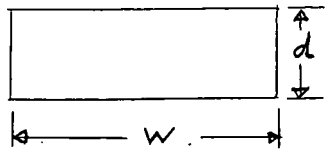

Nominal Channel

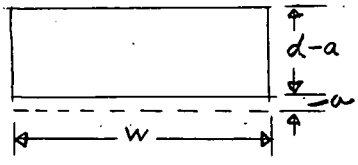

Hot Channel

$$A_n = dw$$

$$A_h = (d-a)w \; ; \quad F_{\Delta T} = \left[\left(\frac{d}{d-a}\right)\left(\frac{d+w-a}{d+w}\right)\right]$$

$$D_n = 4A_n/P_n = \frac{2dw}{(d+w)}$$

$$D_h = 4A_h/P_h = \frac{2(d-a)w}{d+w-a}$$

Between two fuel elements:

F = 1.033

Between fuel element and control rod basket

F = 1.019

It is therefore considered conservative to base the lattice flow on an average velocity 5% greater than the largest internal fuel element velocity.

1.6.3 Heat release distribution

The direct fission energy has the following distribution (Proceedings of the Symposium on the Physics of Fission Held at Chalk River, Ontario, May 14-18, 1956. Session C, CRP-642-A (July 1956).

Source	CRP-642A
Energy	1956
K of Fission Fragments	167.1 ± 2 Mev
KE of Fast Neutrons	5 ± 0.5 Mev
Prompt Gamma Rays	7→12 Mev
Fission Product Gamma Rays	7.5 Mev) ± 2 Mev
Beta Decay Energy	5.5 Mev)
Totals	192.1 + 9.5 − 4.5 Mev

It may be expected that most of the energy of the fast neutrons (5 Mev fissions) is released in the water moderator. Also a large fraction of the prompt gamma rays will be released in the fuel element side plates, end boxes, thermal shield, etc. In addition, there is a net energy gain in the n, γ reactions in materials other than the fuel plates. Calculation for the MTR (An Estimate of the Heat Generation and Distribution in the MTR, R. A. Gremesey, (IDO-16443) indicate that only 90% of the heat generated is released in the fuel elements. Until detail heat generation and distribution are available for a particular design, a heat generation rate of 0.95 times the maximum expected shall be used as a basis for thermal design.

2.0 THERMAL ANALYSIS

The thermal analysis of the core is the determination of the core flow requirements, based upon the thermal design criteria previously discussed.

2.1 General equations and results

The required core flow is determined by use of the following equations:

$$(1)\quad (T_{S\,max})_Z = T_{in} + (\Delta T)_Z + (\Delta\theta)_Z$$

$$(2)\quad (\Delta T)_Z = F_{avg} \cdot F_n F_{R\Delta T} \left[\frac{b\varphi}{wc_p} \int_0^{Z/L} \frac{\bar{P}}{\bar{\bar{P}}}\, d\left(\frac{Z}{L}\right) \right]$$

$$(3)\quad (\Delta\theta)_Z = F_{loc}\, F_n\, F_{R\Delta\theta} \left[\frac{\varphi}{h} \left(\frac{\bar{P}}{\bar{\bar{P}}} \right)_Z \right]$$

where:

$(T_S)_{max_Z}$	=	maximum surface temperature of fuel plate at Z	°F
T_{IN}	=	inlet temperature of coolant fluid	°F
(ΔT)	=	temperature rise of bulk coolant fluid from inlet to Z	°F
$(\Delta\theta)_Z$	=	temperature gradient across film at Z	°F

F_{avg} = bulk coolant temperature rise hot channel factor

F_{loc} = film temperature gradient hot channel factor

F_n = nuclear uncertainty factor

$F_{R\Delta T}$, $F_{R\Delta\theta}$ } individual nuclear factors for the various elements, which represent the ratio of the heat flux of the hottest plate in the element to the average core flux, and the ratio of the heat flux of the hottest spot on the hottest plate to the average core flux, respectively.

b = heat transfer area per flow channel, ft^2

φ = average core heat flux, $Btu/ft^2\text{-}hr$

w = flow per channel, lb/hr

C_p = specific heat of the bulk coolant fluid evaluated at the mean coolant temperature Btu/# °F.

h = film heat transfer coefficient, Btu/ft^2-hr-°F.

L = active length of fuel element, ft.

Z = distance along the active meat length of element, measured from inlet, ft.

$\frac{\bar{P}}{\bar{\bar{P}}}$ Ordinate of the axial power distribution normalized to an average of unity.

(4) b = 2 (active meat width)x(active meat length) of one fuel plate.

(5) $\varphi = \frac{P \times 3413{,}000}{A} \times (.95) \times (F_{inst})$

where:

P = total core heat output, MW

A = total heat transfer area, ft^2

F_{inst} = factor for instrument tolerance

(6) $h = .021 \frac{K}{D_e} \left(\frac{\rho V D_e}{\mu}\right)^{0.8} \left(\frac{C_p \mu}{K}\right)^{0.4}$

where:

k = thermal conductivity of coolant, Btu/ft hr°F

D_e = equivalent diameter of one flow channel, i.e., one water gap, ft.

ρ = density of bulk coolant, #/ft^3

V = coolant velocity through plates, ft/hr

μ = viscosity of bulk coolant, #/ft-hr

C_p = specific heat of bulk coolant fluid, Btu/#-°F

(7) $D_e = \frac{4 \text{ (flow area)}}{\text{wetted perimeter}}$

Evaluating the above equations for various values of "Z", the maximum surface temperature for each element or group of similar elements for a range of

assumed flow rates may be determined. The results are then plotted for each element as "$Ts_{max.}$ vs. G.P.M." (See Fig. 2.2).

Knowing the saturation temperature corresponding to system pressure and the instrumentation tolerances on pressure and inlet temperature, a maximum allowable surface temperature can be determined. The required flow for each element can then be determined by use of the previously mentioned plots. Lattice flow is calculated on the basis outlined in Item 1.4, Thermal Design Criteria.

The required flow thus calculated constitutes minimum core flow only. It is conservative in that the analysis assumes all worst possible factors and tolerances to occur simultaneously.

Since the calculated required flow was determined on the basis of a fully tailored core, i.e. equal maximum surface temperatures in all elements, it would be necessary to install, within the reactor vessel, a suitable orifice plate, designed to achieve the required velocity distribution. The proper size of the orifice holes for said plate would have to be determined experimentally on a flow rig, using simulated components prior to the completion of core and vessel fabrication.

It should be noted that since it is not possible to orifice control rod elements externally, and since the elements must be interchangeable, the flow for each control rod must be equal to the flow required by the hottest one, in this case the center element.

By the previously described method of analysis, the following results were arrived at as the tailored flow requirements for the Skid-mounted core:

Inlet Temperature	500 F
Outlet Temperature	519.5 F
Max. plate surface temperature	610 F
Minimum flow requirement of core	2445 gpm

The corresponding required velocity schedule for orificing the core is given in Table 2.1 as V/V avg. where V avg is the average core velocity.

As may be noticed from the velocity schedule, the variation of stationary fuel element flow requirements is very small. In fact the additional flow required in order to establish the flow through each stationary element equal to that through element 34, the hottest stationary element, is only 60 gpm. Since the advantage of tailoring is so minute for this core, it has been decided to use uniform flow.

Table 2.1

Velocity Schedule

Element No.	V/V avg core
44	1.0491
34	1.0140
33	0.9984
23	0.8978
22	1.0105
Lattice	1.0650

that is to allow equal flow for all stationary elements. It may be noticed, however that some orificing is still necessary to compensate for plenum chamber effects and for the difference between pressure drop through a control rod and that through a stationary element. On the above basis, the following design

conditions were established:

Flow per fixed element	58.5 gpm
Flow per control rod element	56 gpm
Lattice flow	353 gpm
Total core flow	2505 gpm
Inlet temperature	500°F
Outlet temperature	519.1°F
Maximum surface temperature	610°F

2.2 Calculations

2.2.1 General constants and dimensions

Full Thermal Power	6.5 MW
System Pressure	1750 psia
Inlet temperature	500 F

Stationary fuel element nominal dimensions

Meat thickness	0.020 in.
Meat width	2.500 in.
Meat height	22 in.
Channel width	2.733 in.
Channel depth	0.133 in.
No. of plates per element	18
No. of plates per core, 18 x 32 elements	576

Control rod fuel element nominal dimensions

Meat thickness	0.020 in.
Meat width	2.281 in.

Meat height	21 in.
Channel width	2.513 in.
Channel depth	0.133 in.
No. of plates per element	16
No. of plates per core, 16 x 5 elements	80

2.2.2 Heat transfer area

Heat transfer area per plate:

b 2 (meat length) (meat width)

$$b_{F.E.} \frac{2\ (22)\ (2.5)}{144} = 0.7639\ ft^2$$

$$bC.R.\ 2\ \frac{(21)\ (2.281)}{144} = 0.6653\ ft^2$$

for a control rod insertion of 9.25"

$$b_{C.R.}\ (9.25) = 0.2930\ ft^2$$

Total heat transfer area

$$A \quad 576\ b_{F.E.} + 80 b_{C.R.(9.25)} = 463.45\ ft^2$$

2.2.3 Average heat flux

Assuming that 95% of the total core power is generated in the fuel plates, and applying the instrumentation tolerance on power:

$$\varphi = \frac{P \times 0.95 \times F_{inst} \times 3413{,}000}{A}$$

$$\varphi = \frac{6.5 \times 0.95 \times 1.035 \times 3413{,}000}{463.45}$$

$$\varphi = 47{,}066.6\ Btu/ft^2 - hr$$

2.2.4 Bulk coolant temperature rise

$$(\Delta T)_z = F_{avg}\ F_n\ F_{R\Delta T} \left[\frac{b\varphi}{wC_p} \int_0^{z/L} \frac{\bar{P}}{\bar{\bar{P}}}\ d\left(\frac{z}{L}\right) \right]$$

where:

$(F_{avg})_{F.E.} = 1.2044$; $(F_{avg})_{C.R.} = 1.2428$

$F_n = 1.05$

$b_{F.E.} = 0.7639\ ft^2$; $b_{C.R.} = 0.6653\ ft^2$

$q = 47{,}066.6\ Btu/ft^2\ hr$

$C_p = 1.179\ \frac{Btu}{lb\text{-}^oF}$ @ 510 F

$$(\Delta T)_{Z_{F.E.}} = 3.80488 \times 10^4\ \frac{F_{R\Delta T}}{W} \int_0^{Z/L} \frac{\bar{P}}{\bar{\bar{P}}}\, d\left(\frac{Z}{L}\right)$$

$$(\Delta T)_{Z_{C.R.}} = 3.41942 \times 10^4\ \frac{F_{R\Delta T}}{W} \int_0^{Z/L} \frac{\bar{P}}{\bar{\bar{P}}}\, d\left(\frac{Z}{L}\right)$$

The integral represents the area under the curve of the axial normalized power distribution plotted versus Z/L.

The radial factors, $F_{R\Delta T}$ and $F_{R\Delta\theta}$, have been calculated by the nuclear group and are as follows (element numbers refer to Fig. 2.1):

Element No.	FR Δ T	FR Δ θ
44	1.238	1.490
24	1.113	1.325
34	1.211	1.472
33	1.208	1.454
23	1.146	1.319
22, 14, 13	1.143	1.483

FIGURE 2.1

CORE FUEL ELEMENT ARRANGEMENT AND NUMBERING SYSTEM FOR

SKID-MOUNTED REACTOR

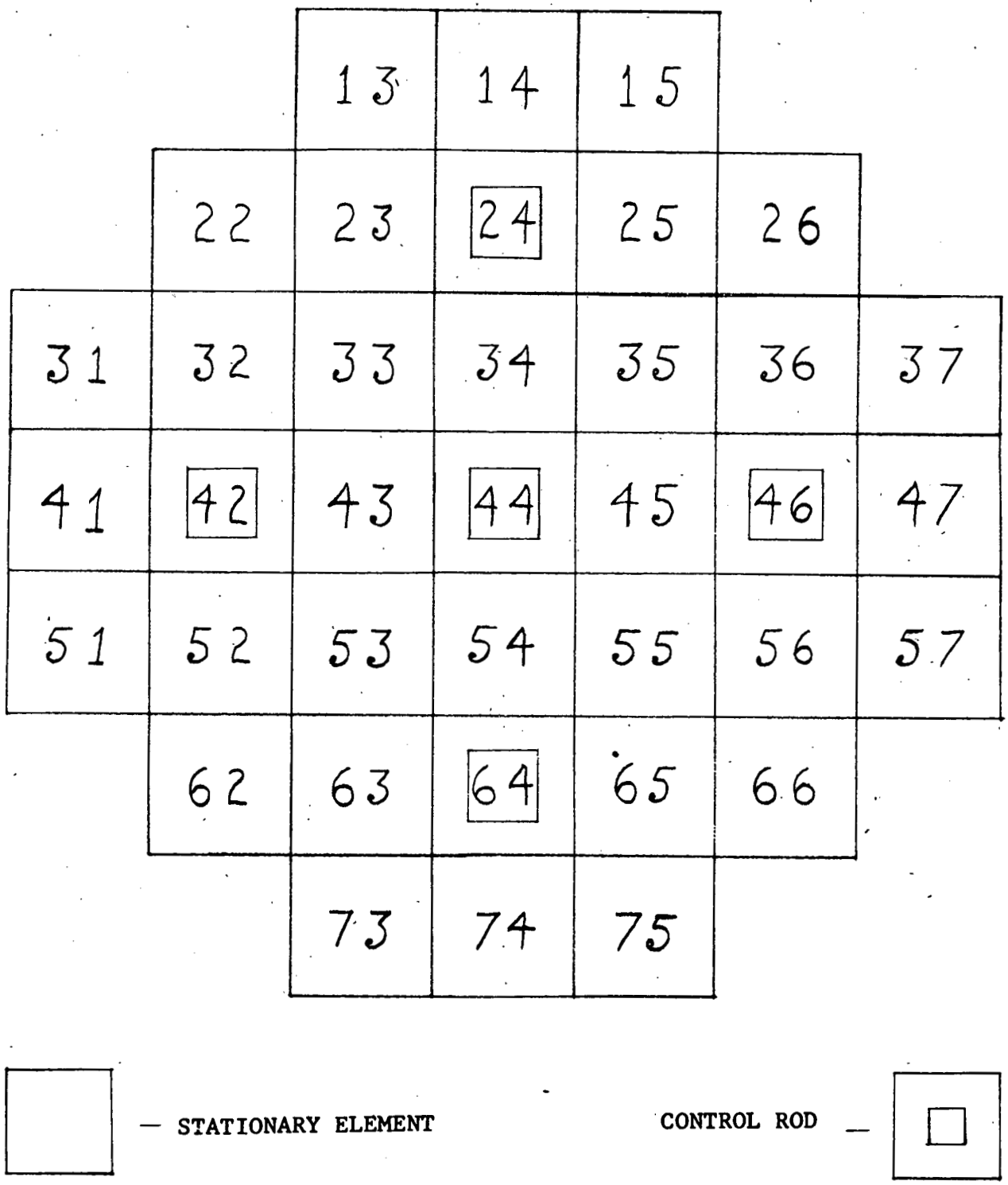

2.2.5 Heat transfer coefficient

$$h = .021 \frac{K}{D} \left(\frac{\rho V D}{\mu}\right)^{0.8} \left(\frac{C_p \mu}{K}\right)^{0.4}$$

where:

$D_{FE} = 0.02144$ ft

$D_{CR} = 0.02105$ ft

at 510 F

$k = 0.3496$ Btu/ft-hr-°F

$\rho = 48.52$ lb/ft^3

$\mu = 0.253$ lb/hr ft

$Pr = \frac{C_p \mu}{} \; 0.853$

$h_{F.E.} = 0.99567 \; V^{0.8}$

$h_{C.R.} \; 0.99670 \; V^{0.8}$

2.2.6 Water film temperature gradient

$$(\Delta\theta)_z = F_{loc} F_n F_{R\Delta\theta} \left[\frac{\psi}{h} \left(\frac{\bar{P}}{\bar{\bar{P}}}\right)_z\right]$$

where

$(F_{loc})_{F.E.} = 1.3230$; $F_{loc})_{C.R.} = 1.3566$

$F_n = 1.05$

$\psi = 47.066.6$ Btu/ft^2 - hr

$$(\Delta\theta)_{z_{F.E.}} = 6.56669 \times 10^4 \frac{F_{R\Delta\theta}}{V^{0.8}} \left(\frac{\bar{P}}{\bar{\bar{P}}}\right)_z$$

$$(\Delta\theta)_{z_{C.R.}} = 6.12651 \times 10^4 \frac{F_{R\Delta\theta}}{V^{0.8}} \left(\frac{\bar{P}}{\bar{\bar{P}}}\right)_z$$

2.2.7 Maximum surface temperatures

The above equations for $(\Delta T)_Z$ and $(\Delta \Theta)_Z$ were evaluated for 1/2" increments along the length of the core for various elements and flow rates. It was thus established that the hot spot always occurs axially, for the range of flows considered, at a position approximately 7.5" from the inlet to the active core. The values of $(T_s)_{max}$, as evaluated at this position for the various elements and a flow range from 30 - 100 gpm, are plotted in Figure 2.2.

2.2.8 Flow requirements

By applying to the saturation temperature at 1750 psi tolerances for instrumentation on system pressure and inlet temperature, a maximum allowable surface temperature of 610F was determined. The required flow for the various elements, corresponding to this temperature are listed in Table 2.2. The corresponding lattice flow is calculated as follows:

Lattice flow =

$$\text{Max. F.E. flow} \times \frac{\text{lattice area}}{\text{F.E. area}} \times 1.05$$

$$\text{Lattice flow} = 58.5 \text{ gpm} \times \frac{0.2465 \text{ ft}^2}{0.0429 \text{ ft}^2} \times 1.05$$

$$= 352.9 \text{ gpm}$$

Table 2.2

Total Required Flow

	Flow per Element GPM		No. of Similar Elements		
44	56.0	x	5	=	280.0
34	58.5	x	4	=	234.0

FIG. 2-2

Skid-Mounted APPR

Max. Wall Temperature vs. Element Flow 7/28/58

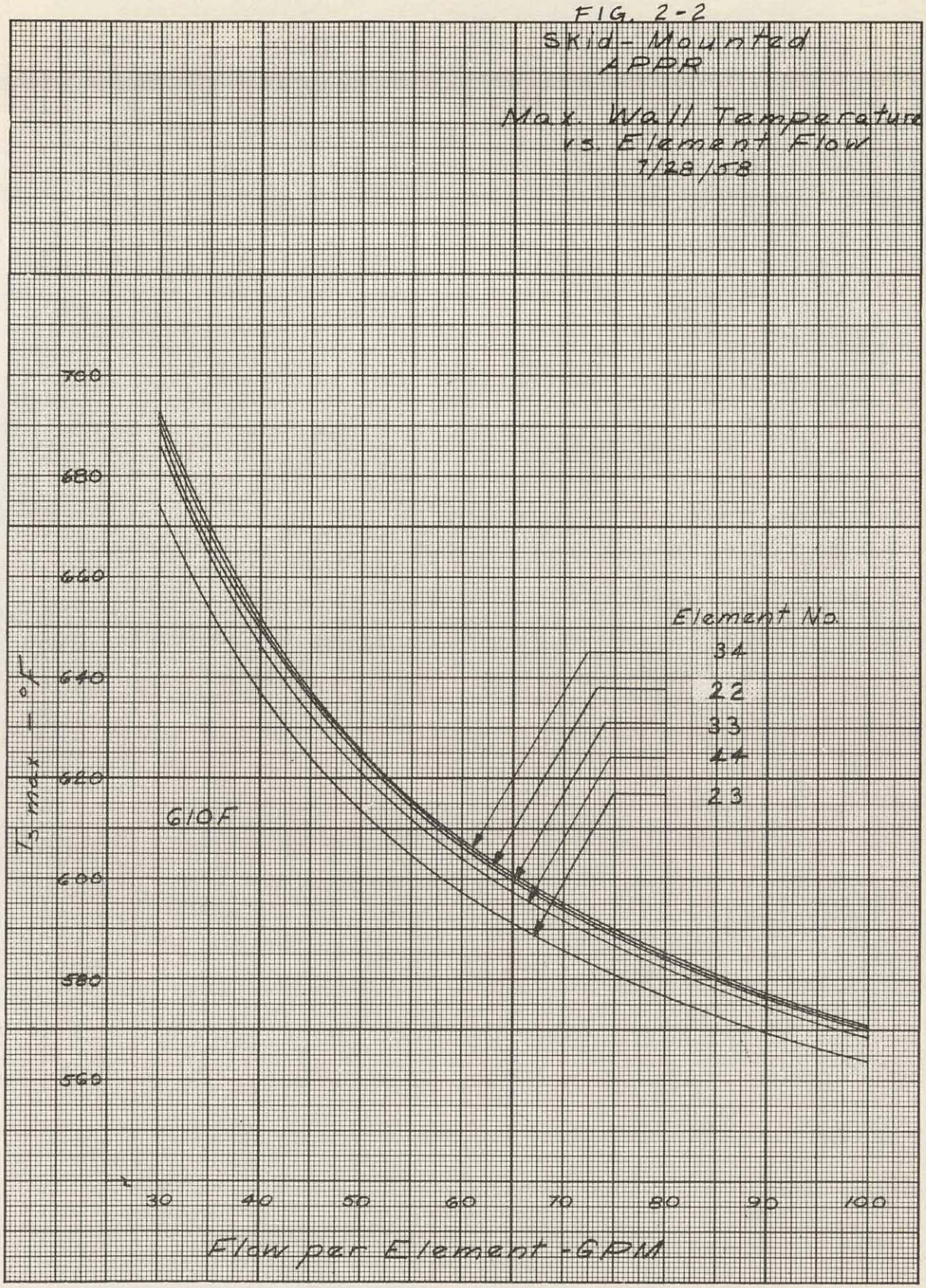

33	57.6	x	4	=	230.4
23	51.8	x	8	=	414.4
22	58.3	x	16	=	932.80
		Total Internal Flow			2091.6
		Lattice flow			352.9
		Total Required Core Flow			2444.5

The summation of the various element flows and the lattice flow composes the minimum required core flow.

For uniform flow the total flow requirement is composed of the following:

Control Rods

56.0 gpm/element x 5 control rods = 280 gpm

Stationary elements

58.5 gpm/element x 32 elements = 1872 gpm

Lattice

352.9 gpm or 353 gpm

Total core flow 2505 gpm

For uniform flow through the stationary elements the minimum core flow requirements is therefore 2505 gpm.

2.3 Conclusions

The thermal analysis has determined the required flow for the core to be 2445 gpm for the case of tailored flow, and 2505 gpm for a uniform flow core. Since tailoring the flow in the core would result in a savings of only 60 gpm, tailoring is of little advantage for this particular core and it therefore has been decided to use uniform flow. This will still necessitate a small amount of orificing to compensate for plenum effects and for the larger pressure drop which occurs through the control rod elements.

3.0 RATIO OF OPERATING TO BURNOUT HEAT FLUX

This section consists of the calculation of the maximum ratio of operating to burnout heat flux. This ratio is of interest in-so-far as it affects the core operation during an accident.

3.1 Operating heat flux

The maximum operating heat flux in the hottest control rod is determined by:

$$\left(\varphi_{OP}\right)_{CR\,max} = \varphi_{avg} \times \left(F_{R\Delta\theta}\right)_{CR\,max} \times \left(\frac{\bar{P}}{\bar{\bar{P}}}\right)_{max}$$

where

φ_{OP} max = maximum control rod operating heat flux, Btu/ft^2-hr

φ avg = average core heat flux, Btu/ft^2-hr

$\left(F_{R\Delta\theta}\right)_{CR}$ max = maximum radial control rod power distribution factor

$\left(\frac{\bar{P}}{\bar{\bar{P}}}\right)$ = maximum ordinate of the normalized axial power distribution.

For the skid-mounted core:

φ_{avg} = 47.067 Btu/ft-hr

$\left(F_{R\Delta\theta}\right)_{CR.max}$ = 1.490

$\left(\bar{P}/\bar{\bar{P}}\right)$ = 1.646

$\left(\varphi_{OP}\right)_{CR\,max}$ = (47,067) (1.490) (1.646)

= 115,434 Btu/ft^2 hr

Correspondingly, the maximum operating heat flux in the hottest stationary channel is:

$$\left(\varphi_{OP}\right)_{FE\,max} = \varphi_{AVG} \times \left(F_{R\Delta\theta}\right)_{FE\,max} \times \left(\bar{P}/\bar{\bar{P}}\right)_{max}$$

(47,067) (1.483) (1.646)

114,891 Btu/ft^2 - hr

3.2 Burnout heat flux

The burnout heat flux is calculated, using the Jens and Lottes equation (Ref. ANL-4627), as follows:

$$\left(\frac{\varphi}{10^6}\right)_{B.O.} = C\left(\frac{G}{10^6}\right)^m \left(t_{sat} - t_b\right)^{0.22}$$

where:

$(\varphi)_{BO}$ = burnout flux, Btu/ft^2 - hr

G = mass flow, lb/hr - ft^2

t_{SAT} = saturated temperature corresponding to flow conditions, °F

t_b = water temperature at the position of burnout, °F.

C, m = constants, function of total pressure (p. 52, ANL-4627)

For the hottest control rod:

G = 548,956 lb/hr ft^2

t_{sat} = 617.09F @ 1750 psi

t_b = 517.05F

C = 0.48 @ 1750 psia

m = 0.442 @ 1750 psia

$$\left(\frac{\varphi_{BO}}{10^6}\right)_{CR} = (0.48)(0.548956)^{0.442}(100.04)^{0.22}$$

$(\varphi_{BO})_{CR}$ = 1,014,545 Btu/ft^2 -hr

For the hottest stationary element:

$G = 529{,}453$ lb/hr - ft^2

$t_{sat} = 617.09$ F

$t_b = 516.56$ F

$C = 0.48$

$m = 0.442$

$$\left(\frac{\varphi_{BO}}{10^6}\right)_{FE} = (0.48)\,(0.529453)^{0.442}\,(100.53)^{0.22}$$

$$(\varphi_{BO})_{FE} = 998{,}412 \text{ Btu/ft}^2 - \text{hr}$$

3.3 Flux ratios

The ratio of operating to burnout heat flux, for the hottest control rod is:

$$\left(\frac{\varphi_{op}}{\varphi_{BO}}\right)_{CR} = \frac{115{,}434}{1{,}014{,}545} = 0.1138$$

The corresponding ratio for the hottest stationary elements, those in the outer ring, is:

$$\left(\frac{\varphi_{op}}{\varphi_{BO}}\right)_{FE} = \frac{114{,}891}{998{,}412} = 0.1151$$

3.4 Application of hot channel factors

The hot channel factors which are concerned with uranium content and meat thickness, and therefore affect the maximum possible operating flux, are the uranium content deviation factor and the meat length deviation factor. Locally these factors are 1.0250 and 1.0357, respectively. If these factors are applied to the flux ratios, the results are:

$$\left(\frac{\varphi_{op}}{\varphi_{BO}}\right)_{CR} = 0.1138 \times 1.0250 \times 1.0357 = 0.1208$$

$$\left(\frac{\varphi_{op}}{\varphi_{BO}}\right)_{FE} = 0.1151 \times 1.0250 \times 1.0357 = 0.1222$$

4.0 INTERNAL PLATE TEMPERATURES

The maximum internal plate temperature is calculated and is of interest for determination of the thermal stresses in the elements.

4.1 Method of calculation

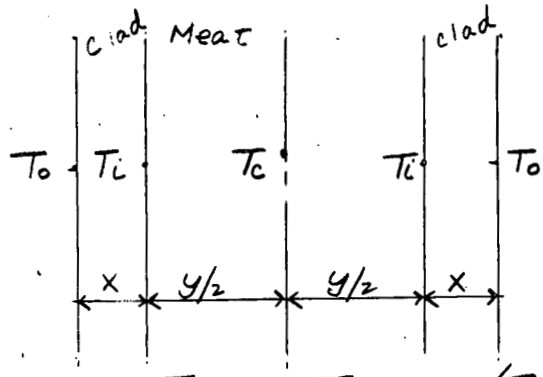

Considering the heat generation rate within the meat to be uniform:

$$T_{c\,max} = T_{o\,max} + (T_i - T_o)_{max} + (T_c - T_i)_{max}$$

$$(T_i - T_o)_{max} = \frac{\varphi_{max}(x)}{K_c}$$

and

$$(T_c - T_i)_{max} = \frac{\varphi_{max}(y/2)}{2K_m} = \frac{\varphi_{max}(y)}{4K_m}$$

where

$T_{c\,max}$ = maximum internal temperature, °F

$T_{o\,max}$ = maximum surface temperature, °F

$(T_i - T_o)_{max}$ = maximum temperature difference across the clad, °F

$(T_c - T_i)_{max}$ = maximum temperature difference between the center of the meat and the meat - clad interface, °F

φ_{max} = maximum core heat flux, Btu/ft^2 hr

x = thickness of the clad, ft

y = thickness of the meat, ft

K_c = thermal conductivity of the clad, Btu/ft-hr °F

K_m = thermal conductivity of the meat, Btu/ft-hr °F

The maximum core heat flux can be determined as follows:

$$\varphi_{max} = \varphi_{avg} \times (FR\Theta)_{max} \times (\bar{P}/\bar{\bar{P}})_{max}$$

4.2 Numerical calculation

For the Skid-Mounted APPR Core:

φ_{avg} = 47,067 Btu/ft^2 hr

$(FR\Theta)_{max}$ = 1.490

$(\bar{P}/\bar{\bar{P}})_{max}$ = 1.646

φ_{max} = (47,067) x (1.490) x (1.646)

φ_{max} = 115,434 Btu/ft^2 hr

X = 0.005 inches

y = 0.020 inches

K_c = 11.1 Btu/ft hr °F @ 612 F

K_m = 9.64 Btu/ft hr °F @ 612 F

$(T_o)_{max}$ = 617.09°F

Therefore:

$$(T_i - T_o)_{max} = \frac{(115434)\ (.005)}{(11.1)\ (12)} = 4.33^\circ F$$

$$(T_c - T_i)_{max} = \frac{(115434)\ (.020)}{4(9.64)\ (12)} = 5.00^\circ F$$

$T_{c\ max}$ = 617.09 4.33 5.00 = 626.42°F

4.3 Application of hot channel factors

If the hot channel factors concerned with uranium content and meat thickness (See Article 3.4) are applied to these values the results are as follows:

$(T_i - T_g)'_{max}$ = 4.33°F x 1.025 x 1.0357 = 4.60°F

$(T_c - T_i)'_{max}$ = 5.00°F x 1.0250 x 1.0357 = 5.30°F

$T_c'_{max}$ = 617.09 4.60 5.30 626.99°F

4.4 Comparison with APPR-1

Since the primary system pressure of the APPR-1 is 1200 psia in comparison with the system pressure of the Skid-Mounted core (1750 psia) the surface temperatures, and therefore the absolute values of the maximum internal temperatures, are not comparable. However, the magnitude of the thermal stresses is mainly dependent upon the temperature differences across the clad and across the meat, rather than the absolute temperatures.

Calculations completed for the APPR-1 (See Ref.9) showed the temperature difference across the clad, and the temperature difference from the clad-meat interface to the center of the meat each to be 9.9°F. Corresponding values for the Skid-Mounted APPR Core have been shown to be 4.6°F and 5.0° F respectively. It may be noticed that the corresponding values for the Skid-Mounted Core are smaller than those of the APPR-1 by a factor of approximately two. The calculation for the APPR-1 had been based upon equal thermal conductivities in the clad and in the meat. For the Skid-Mounted Core calculations the more conservative approach was taken, that of considering the thermal conductivity of the meat to be somewhat smaller than that of the clad.

5.0 THERMAL STRESS IN THE ELEMENTS

Thermal stresses are caused by temperature differences between points in the fuel element. The stresses are proportional to the temperature differences and the temperature differences are approximately proportional to heat flux, decreasing somewhat with increasing coolant velocity.

5.1 Use of experimental data

A program was begun in 1954 to test a stainless steel fuel element, of the type used in the APPR-1, in the STR mock-up. The element was to be tested for mechanical stability under combined hydraulic, thermal, and irradiation conditions present in the STR. Additional tests have been performed with a different element in the MTR.

The table below compares the irradiation conditions in the MTR with those in the APPR-1 (Ref. 11):

Table 5.1

	Units	MTR APPR Type I	MTR APPR Type II	APPR-1
Average heat flux	Btu/ft^2 hr	449,000	461,000	55,900
Specific power	Kw/Kg	9,000	9,000	550
Fuel Concentration in Matrix	gm/cm^3	1,240	1,817	1.31
Fuel loading	gm/cm^2	0.0315	0.0324	0.066
Fuel loading per plate	gm	10.36	10.67	23.65
Maximum Temperature of fuel	°F	-	-	566

A similar comparison is made with the STR in Ref. 11. However, as this information is classified, it is not reported here.

5.2 Experimental test conditions and results

A six-plate element was tested in the STR at a cooling water temperature and pressure of 500°F and 2050 psia, respectively. It was removed from the reactor after 157 full power hours of satisfactory operation, examined, and found to be in excellent condition. It was then returned to the reactor an additional 100 hours, the total burnup of U_{235} estimated to be 3%. Further information, which is classified, may be found in references 10 and 11.

Two series of tests were undertaken in the MTR. The first was performed with an 18 plate element, and the second with small capsulated fuel plate specimens.

The small specimens were of two types. Their basic characteristics are listed below:

	Type I	Type II
Design Life (MW-Yr)	15	30
Clad-core-clad thickness (mils)	5-10-5	6.5-7.-6.5
Core composition (weight%)	17.93 UO_2 0.19 B_4C 81.88 stainless	25.81 UO_2 0.35 B_4C 73.84 stainless
Clad Material	304L stainless steel	

The full size plates were of three types. Their basic characteristics are as follows:

		Type I	Type II	Type III
Design life (MW-Yr)		15	22.5	30
Plates of each type		6	6	6
Plate Clad-core-clad thickness		9-12-9	10-10-10	11-8-11
Core mixture composition	UO_2	18.75	22.18	26.89
	B_4C	0.21	0.27	0.39
	Stainless	81.04	77.55	72.75
Distance between plates			117 mils	

The plates were inserted in the core for an estimated burn-up of 25-42%. The velocity in the MTR core is approximately 30 fps. The specimens were removed from the core and examined. No gross damage occurred and there was no evidence of defects.

5.3 Comparison with Skid-mounted core conditions

It may be noticed that the average heat flux in the MTR was greater than that of the APPR-1 by a factor of 8.25. Since the average heat flux in the Skid-Mounted Core is only 47,067 Btu/ft^2-hr, that of the MTR is greater by a factor of 9.79. It is therefore evident that the Skid-Mounted Core has an even larger safety factor than the APPR-1 (which has been operating satisfactorily for 1-1/2 years).

In AP Memo 43, the temperature distributions and thermal stresses were calculated for a total power of 10 MW and a peak to average power of 4, corresponding to a maximum heat flux of 224,000 Btu/ft^2-hr. The maximum stress calculated was a tensile stress in the side plate near the outermost fuel plate. This value numerically was 28,300 psi. This calculation was based on extremely conservative assumptions and is an indication of the upper limit of possible stresses, rather than an actual expected value.

Since the maximum heat flux in the Skid-Mounted Core is 115,000 Btu/ft^2-hr, the corresponding upper stress limit is:

$$\frac{115}{224} \times 28{,}300 \text{ psi} = 14{,}530 \text{ psi}$$

5.4 Conclusions

On the basis of the comparison with experimental test data presented, the comparison with thermal stress calculations presented, and the fact that the APPR-1 is operating satisfactorily with thermal stresses approximately twice the value of those expected in the Skid-Mounted Core, it has been concluded that the thermal stresses in this core will be considerably below the allowable value. It is therefore considered not necessary to undertake a detailed analysis of thermal stresses in the fuel plates.

6.0 THERMAL STRESS IN REACTOR VESSEL

In addition to hydraulic stresses in the vessel, thermal stresses occur, caused by a temperature gradient across the vessel wall. This temperature gradient is caused by the heat generation of gammas absorbed or experiencing collisions in the vessel.

6.1 Method of calculations

If the heat generation rate in the wall is plotted versus distance through the wall on semi-log paper, it may be seen that it closely approximates a straight line. The heat generation rate through the wall may therefore be represented by an exponential of the form:

$$g_x = g e^{-ux}$$

where

g_o = heat generation rate at the inner surface of the vessel wall

X = distance through the wall, measured from the inner surface

u = slope of the curve on semi-log paper

g_x = heat generation rate at x distance from the inner surface

6.1.1 Temperature difference equation

If the equation of the heat generation rate is substituted in the general heat transfer equation:

$$-K\frac{d^2t}{dx^2} = g_x,$$

integration results in the following equation:

$$-Kt = \frac{g e^{-ux}}{u^2} + Cx + D$$

Utilizing the boundary conditions:

$X = 0, \quad T = T_L$

and $x = w, \frac{q}{A} = 0$ (since the vessel wall is insulated at its outer surface),

the constants may be evaluated:

$$C = \frac{q_o}{u} e^{-uw}$$

$$D = -KT_i - \frac{q_o}{u^2}$$

The final equation for the difference between the temperature at some distance x through the wall (T), and the temperature at the inner surface of the wall (T_i) is given by:

$$(T - T_i) = \frac{q_o}{Ku^2}\left(1 - e^{-ux} - xue^{-uw}\right)$$

where:

K: thermal conductivity of the vessel wall

w: thickness of the vessel wall

At x = w the equation reduces to:

$$(T_o - T_i) = \frac{q_o}{Ku^2}\left[1 - e^{-uw}(1 + uw)\right]$$

6.1.2 Thermal stress equation

If T_i is considered as a base temperature or an initial uniform temperature, then the increase above T_i, $(T - T_i)$ may be represented by t and:

$$t = \frac{q_o}{Ku^2}\left(1 - e^{-ux} - uxe^{-uw}\right)$$

Assuming the temperature distribution to be symmetrical with respect to the axis of the cylinder and constant along this axis, at a cross section distant

from the ends of the cylinder the tangential stress at some radius (r) may be represented by (Ref. 21):

$$\sigma_t = \frac{E}{1-\mu}\left[\frac{1}{r^2}\int_a^r \alpha t\,dr + \frac{r^2+a^2}{r^2(b^2-a^2)}\int_a^b \alpha t\,r\,dr - \alpha t\right]$$

where:

σ_t = tangential stress at radius (r)

E = Young's modulus

μ = Poisson's ratio

a = inner radius of the vessel

b = outer radius of the vessel

α = coefficient of linear expansion

t = increase in temperature above the uniform initial temperature

Since $x = r - a$,

the increase in temperature above T_i may also be represented by:

$$t = \frac{q_0}{K u^2}\left(1 - e^{-u(r-a)} - (r-a)\,u\,e^{-uw}\right)$$

or

$$t = \frac{q_0}{K u^2}\left[(1 + a u e^{-uw}) - e^{ua}\cdot e^{-ur} - (ue^{-uw})r\right]$$

Substituting the above expression for (t) in the equation for determining the tangential stress (σ_t), and integrating results in the following expression for σ_t:

$$\sigma_t = \left[\frac{E}{1-\mu}\right]\left[\frac{\alpha q_0}{K u^2}\right]\left[\frac{(1 + a u e^{-uw})\left(1 - \frac{a^2}{r^2}\right) + e^{-u(r-a)}(ur+1)}{2}\right]$$

$$-\frac{(ua+1)}{u^2 r^2} - \frac{u e^{-uw}}{3}\left(r - \frac{a^3}{r^2}\right) + \left\{\frac{r^2+a^2}{r^2(b^2-a^2)}\right\}\left\{\left(\frac{1+au e^{-uw}}{2}\right)\times\right.$$
$$(b^2-a^2) + \frac{e^{-uw}}{u^2}(ub+1) - \frac{ua+1}{u^2} - \frac{ue^{-uw}}{3}(b^3-a^3)\Big\}$$
$$\left. -1 + e^{-u(r-a)} + (r-a)\,u e^{-uw}\right]$$

Since the thermal stress in the vessel goes from a compressive stress at the inner surface to a tensile stress at the outer surface, the maximum stress must be at one of these surfaces. Evaluating the above equations at r = a and r = b yields:

$$\sigma_{t(r=a)} = \left[\frac{E}{1-\mu}\right]\left[\frac{\alpha q_0}{K u^2}\right]\left[\frac{2}{b^2-a^2}\right]\left[\left(\frac{1+au e^{-uw}}{2}\right)(b^2-a^2)\right.$$
$$\left. + \frac{e^{-uw}}{u^2}(ub+1) - \frac{(ua+1)}{u^2} - \frac{ue^{-uw}}{3}(b^3-a^3)\right]$$

and

$$\sigma_{t(r=b)} = \sigma_{t(r=a)} - \left[\frac{E}{1-\mu}\right]\left[\frac{\alpha q_0}{K u^2}\right]\left[1 - e^{-uw}(1+uw)\right]$$

It is obvious that for reasonable values of "u" and "w" the maximum thermal stress will occur at the inner radius (r = a) of the vessel.

A similar equation could be derived for calculating the radial stress. However, as the tangential stress will always be larger than the radial stress, further derivations are not necessary.

In "Thermal Stresses in Reactor Vessels" (Ref. 22) sets of curves are presented (based on IBM 704 calculations, for determining thermal stresses in vessels with various parameters and conditions. The curves presented represent 4 cases:

(1) Equal wall temperatures at inside and outside surfaces.

(2) Inside wall insulated

(3) Outside wall insulated

(4) Equal bulk coolant temperatures in inside and outside channels

Utilization of case (3) for determining stresses in the vessel has been found to be accurate within 3% of the values determined by use of the derived equations. It is in general more conservative than the derived equations.

6.2 Thermal stress in APPR-1

For purpose of comparison of calculated values with actual values, the calculated and experimental temperature differences and thermal stresses of the APPR-1 will be presented here.

6.2.1 Calculated and measured temperature difference

As indicated on page 195, Ref. 23, the measured temperature difference between the bulk coolant temperature and the outside vessel wall temperature in the APPR-1, operating at 10 MW, was 12.6°F.

The temperature difference across the vessel wall ($T_o - T_i$) is given by:

$$(T_o - T_i) = \frac{q_o}{K u^2}\left[1 - e^{-uw}(1 + uw)\right],$$

and the temperature gradient across the film ($T_i - T_w$) is represented by:

$$(T_i - T_w) = \frac{1}{ha}\int_{r=a}^{r=b} q_o e^{-ux} r\,dr$$

or integrating and simplifying,

$$(T_i - T_w) = \frac{q_o}{u^2 a h}\left[(ua+1) - e^{-uw}(ub+1)\right]$$

where: h = heat transfer coefficient

For the APPR-1 parameters:

$T_o - T_i = 13.12^{\circ}F$

$T_i - T_w = 6.09\ ^{\circ}F$

or the total temperature difference as calculated is 19.2 $^{\circ}F$, as compared with the measured value, 12.6$^{\circ}F$.

6.2.2 Thermal stress in APPR-1

The thermal stress corresponding to the measured temperature difference (12.6 $^{\circ}F$) is 1975 psi. The stress corresponding to the calculated temperature difference (19.2$^{\circ}F$) is 2977 psi.

As may be noticed, the method of calculation yields values of temperature difference and thermal stress considerably higher than those actually existing, as evidenced by experimental measurements. It is felt that this will also be true of values calculated for the Skid-Mounted Core.

6.3 Calculated temperature difference and thermal stress at mid-plane

In designing the reactor vessel several possibilities were considered and investigated with respect to thermal stresses. Since the Skid-Mounted APPR is a package reactor, it is desirable to keep the vessel as close to the core as possible, although in doing so the thermal stress is increased. The various designs investigated in arriving at one satisfactory with respect to thermal

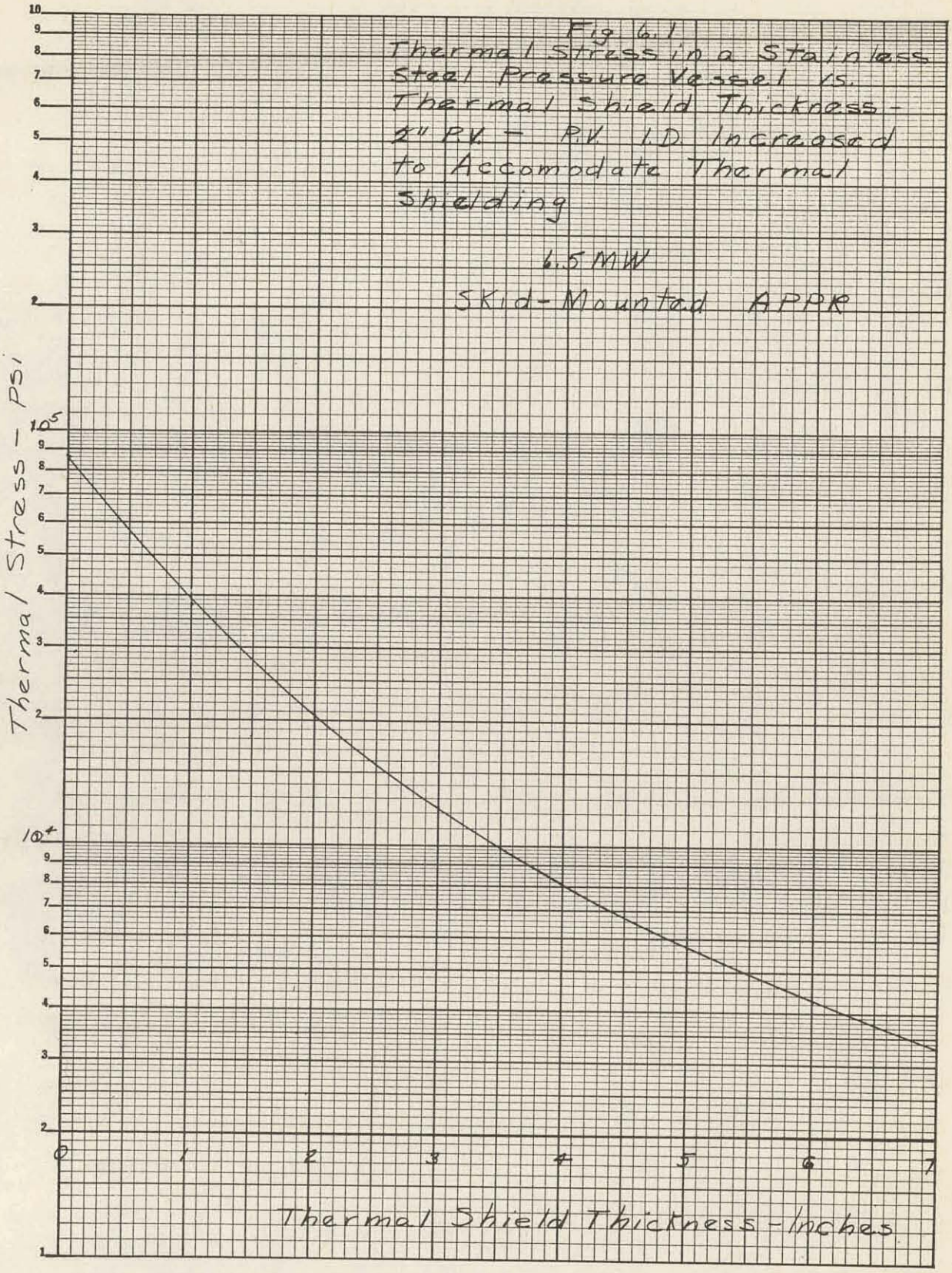
Fig 6.1
Thermal Stress in a Stainless Steel Pressure Vessel vs. Thermal Shield Thickness - 2" P.V. - P.V. I.D. Increased to Accomodate Thermal Shielding
6.5 MW
Skid-Mounted APPR
Thermal Stress - psi
10^5
10^4
0
1
2
3
4
5
6
7
Thermal Shield Thickness - Inches

stress are indicated in Table 6.1. The results of cases 3 - 7 are represented graphically in Figure 6.1.

As may be noticed from the table, the thermal stress corresponding to the final design (Case 7) is 4420 psi. The temperature difference across the wall is 30.5°F.

Table 6.1

Reactor Vessel Thermal Stresses

	Reactor Vessel			Thermal Shield			Thermal Stress
Case No.	Inside Dia.	Thickness	Material	Inside Dia.	Thickness	Material	psi
1	25"	2"	304-SS		None		85,900
2	25"	1 3/4"	304-SS		None		72,500
3	28.5"	2"	304-SS	23.5	2"	304-SS	20,000
4	30.5"	2"	304-SS	23.5"	3"	304-SS	12,200
5	30.5"	2"	304-SS	23.5"	3"	Borated 304-SS	10,670
6	37.75"	1/8"clad +2-3/8" vessel	304-SS	33"	1"	304-SS	8,060
7	37.75"	1/8"clad +2-3/8" vessel	304-SS	23.5"	2"	304-SS	4,420

6.4 Calculated thermal stress in the thermal shield

Since the data presented in Ref. 22 has been found to be accurate within 3% of values calculated from derived equations, this data was used for calculating the stress in the thermal shield. For this purpose Case 4, equal bulk coolant temperature inside and outside the channel was utilized.

The stress was calculated to be 40,300 psi. Since the thermal shield is not a structural member, however, this value is not too large.

6.5 Calculated thermal stress in vessel flange

An analytical expression for maximum thermal stress is derived on page 11 of WAPD-CE-43 (Ref. 24) and is here applied to the vessel flange of the Skid-Mounted Reactor.

For the case of a pressure vessel with the inner wall surface at Zero temperature (above some datum), the outer wallsurface perfectly insulated, and an exponential heat generation rate in the wall the maximum thermal stress occurs at the inner wall surface and is given by:

$$S_0 = \frac{E\alpha q_0}{2(1-\mu)k\beta^2}\left[2 - \frac{2}{\beta a} + \left(\frac{2}{\beta a} - \beta a\right)e^{-\beta a}\right]$$

where

S_0 =	stress at inside wall surface	psi
E =	modulus of elasticity	26.4×10^6 psi
α =	linear coefficient of thermal expansion	8.0×10^{-6}/ft ($^\circ$F)
q_0 =	volumetric heat generation rate at the inside wall	BTU/(ft)^3 (hr)
μ =	Poisson's ratio	0.3
k =	thermal conductivity	25 BTU/(hr) (ft)($^\circ$F)
β =	linear absorption coefficient	5.4408 ft^{-1}
a =	wall thickness	ft.

This equation may be safely used for the vessel flanges of the Skid-Mounted Reactor as the conditions restricing the use of the equation approximate those of the Skid. Values of the heat generation rate at the inside surface of the wall of the flange were determined and presented in Section 5.2 of the Shielding Design Analysis. The flange wall-thickness is also variable and in this case insertion of the maximum value of the thickness in the equation with the corresponding heat generation rate yields the maximum thermal stress; that is when a = 0.63333 feet and $q_0 = 1.79 \times 10^4$ BTU/(ft^3) (hr.). Then βa = (5.4408) (0.63333) = 3.4458. and

$$S_0 = \frac{(26.4\times10^6)(8.0\times10^{-6})(1.79\times10^4)}{2(1-0.3)(25)(5.4408)^2}\left\{2 - \frac{2}{3.4458} + \left[\frac{2}{3.4458} - 3.4458\right]e^{-3.4458}\right\}$$

$$= 4860 \text{ psi}$$

The allowable thermal stress in the flange is 8750 psi. This exceeds the calculated value of the maximum thermal stress, 4860 psi, by 80% which is a sufficient margin of safety.

6.6 Calculated thermal stress in integral nozzle

The same analytical expression for maximum thermal stress in a pressure vessel which was applied to the vessel flange in section 6.4 is used here to determine the maximum thermal stress in the vessel outlet nozzle.

The nozzle is so designed that it is considered an integral part of the vessel and its allowable thermal stress is that of the vessel. The volumentric heat generation rate in the inside vessel wall surface at the nozzle is 2.577 x 10^4 BTU (hr) (ft^3) as determined in Section 5.2 of the Shielding Design Analysis.

The gamma attenuation path-length through the nozzle is 0.75 feet. The linear absorption coefficient is 8.644 $(\text{feet})^{-1}$. Then $\beta a = (8.644)(0.750) = 6.483$ and the maximum thermal stress is:

$$= \frac{(26.4\times10^{6})(8.0\times10^{-6})(2.577\times10^{4})}{2(1-0.3)(25)(8.644)^{2}}\left\{2-\frac{2}{6.483}+\left[\frac{2}{6.483}-6.483\right]e^{-6.483}\right\}$$

$$= 3500 \text{ psi}$$

This stress is less than the allowable by a factor of (8750/3500) or 2.50. Since the outlet nozzle is closer to the core than the inlet nozzle (which is also integral by design) the inlet nozzle will undergo less thermal stress and a calculation is not necessary.

6.7 Conclusions

As was indicated in Section 6.3, the thermal stress in the vessel was calculated to be 4,420 psi. Since the allowable thermal stress in the vessel is 8750 psi, the vessel and thermal shield designs are satisfactory, in this respect. As was pointed out in Section 6.2, the calculated stress value is considered quite conservative.

The thermal stresses in the flange and integral nozzle are safe by factors of 1.80 and 2.50 respectively.

7.0 CORE PRESSURE DROP

The following calculations have been made for the pressure drop across the active core only, and do not include the inlet and outlet plenum chambers. All other pressure drops have been established as a separate calculation.

7.1 Comparison of calculated and experimental data

Pressure drops through the stationary fuel elements were calculated by use of the IBM 650 Digital Computer (Ref. 19). Verification of the accuracy of this program is illustrated in Fig. 7.1, where both computed pressure drops and experimental pressure drops for air flow through a fixed fuel element are plotted vs. flow. It may be noticed that the slopes of both curves are identical and that the calculated data is conservative in comparison with the experimental data, Since the method of calculation of pressure drop is the same for all fluids, the values calculated by the computer program for water flow are equally valid.

7.2 Calculation of pressure drops

Although good results were achieved in calculating the stationary fuel element pressure drops by use of the computer, it was not feasible to perform similar calculations for the control rod elements, because of the more complex geometry.

As experimental data for air flow through the control rods was available, the following method of analysis was utilized. Several cases for air flow through fixed fuel elements were calculated on the computer and plotted versus Reynold's number. The experimental data for air flow through the control rods was plotted on the same graph (Fig. 7.2). Assuming that the ratio of control rod pressure drop to fixed element pressure drop for a particular Reynolds number is constant for either air or water flow, the control rod pressure drop for water flow was determined by plotting the fixed element pressure drop for water flow versus Reynolds number and applying the ratio for that Reynolds number, as determined from Figure 7.2. This assumption was based upon the fact that friction factor

for a particular Reynold's number is independent of the fluid under consideration.

The plots for water flow are shown in Figure 7.3. From the plot of control rod pressure drop versus Reynold's number for water flow it was possible to determine the values needed for plotting Figure 7.4, "Control Rod Pressure Drop vs. Flow Per Element."

7.3 Results and conclusions

The pressure drop through a control rod element is plotted versus coolant flow in gpm in Figure 7.4. For the coolant flow required through the control rod elements in the Skid-Mounted APPR core, as established in Section 2.0, the pressure drop is 2.12 ft H_2O. This is also the total pressure drop across the core, as the control rod is the governing element with respect to pressure drop.

It may be noticed that these values are for the unmodified control rods. It is expected that the control rods to be used in the Skid-Mounted APPR will have a slightly smaller pressure drop. However, as the modifications were not completed at the time this analysis was undertaken, and as the experimental data was for an unmodified element, Figure 7.4 gives a conservative estimate of the desired values. It has been estimated that the corresponding values for the modified elements will be 10-15% lower.

The pressure drop through the fixed elements is plotted in Figure 7.5 versus coolant flow in gpm. It may be noticed from this plot that the pressure drop through a fixed element is considerably less than that through the rods. It will be necessary to orifice these elements in order to equalize all pressure

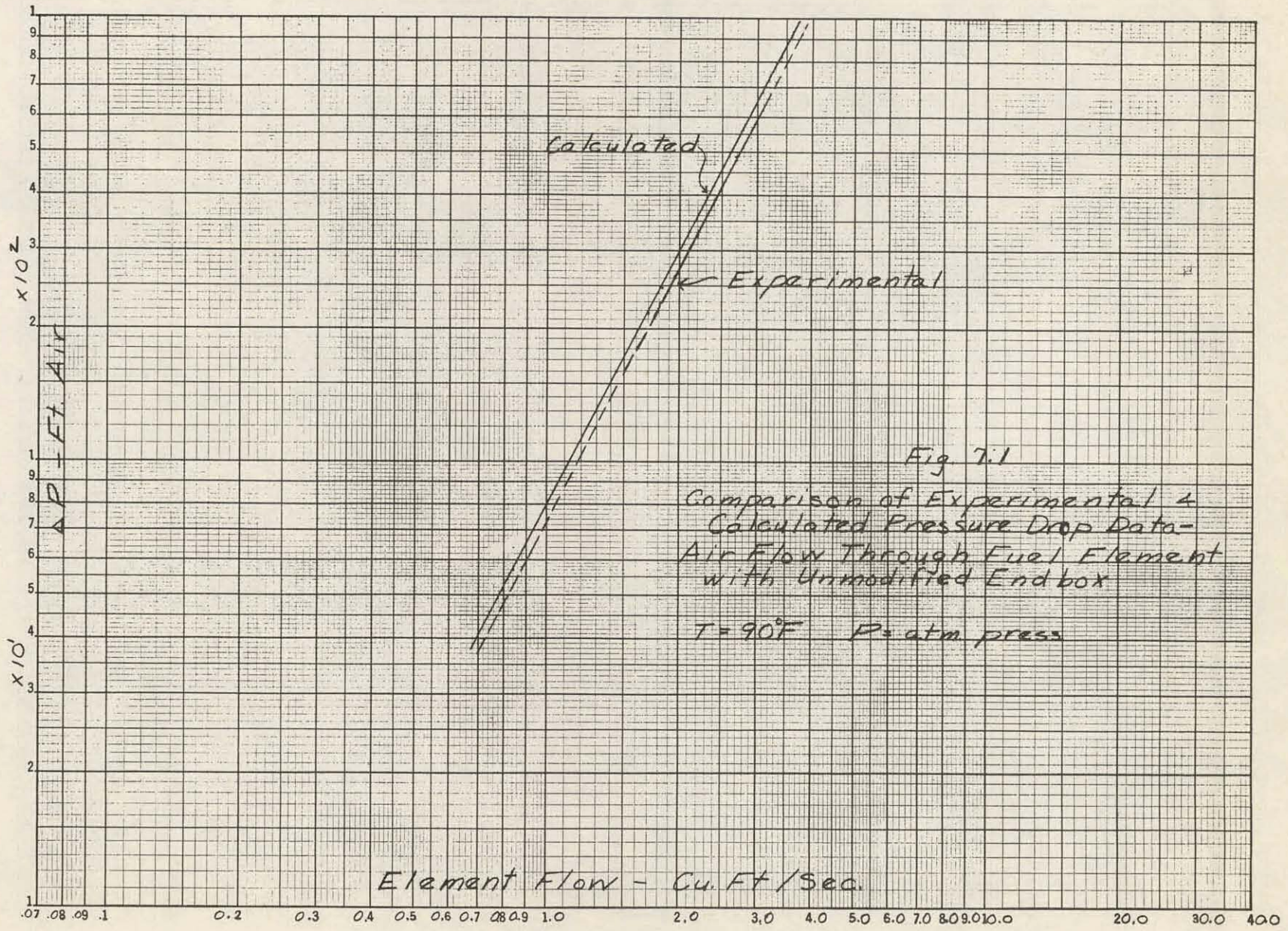

Fig. 7.1
Comparison of Experimental & Calculated Pressure Drop Data - Air Flow Through Fuel Element with Unmodified End box
T = 90°F P = atm. press

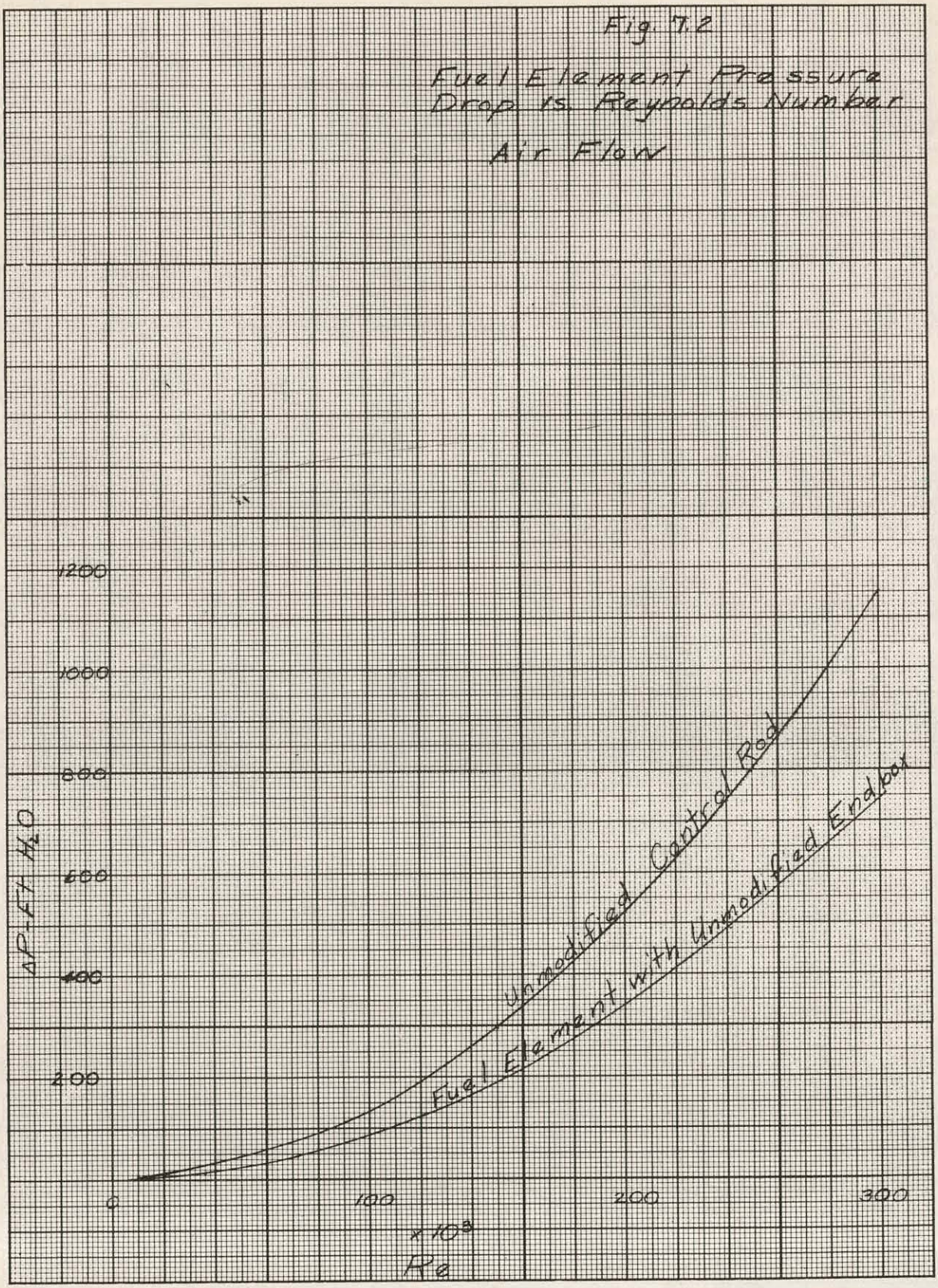
Fig. 7.2
Fuel Element Pressure Drop vs. Reynolds Number Air Flow
1200
1000
800
600
400
200
0
100
200
300
ΔP-FT H2O
x 10³
Re
Unmodified Control Rod
Fuel Element with Unmodified Endbox

Fig. 7.3

Fuel Element Pressure Drop vs. Reynolds Number

Water Flow

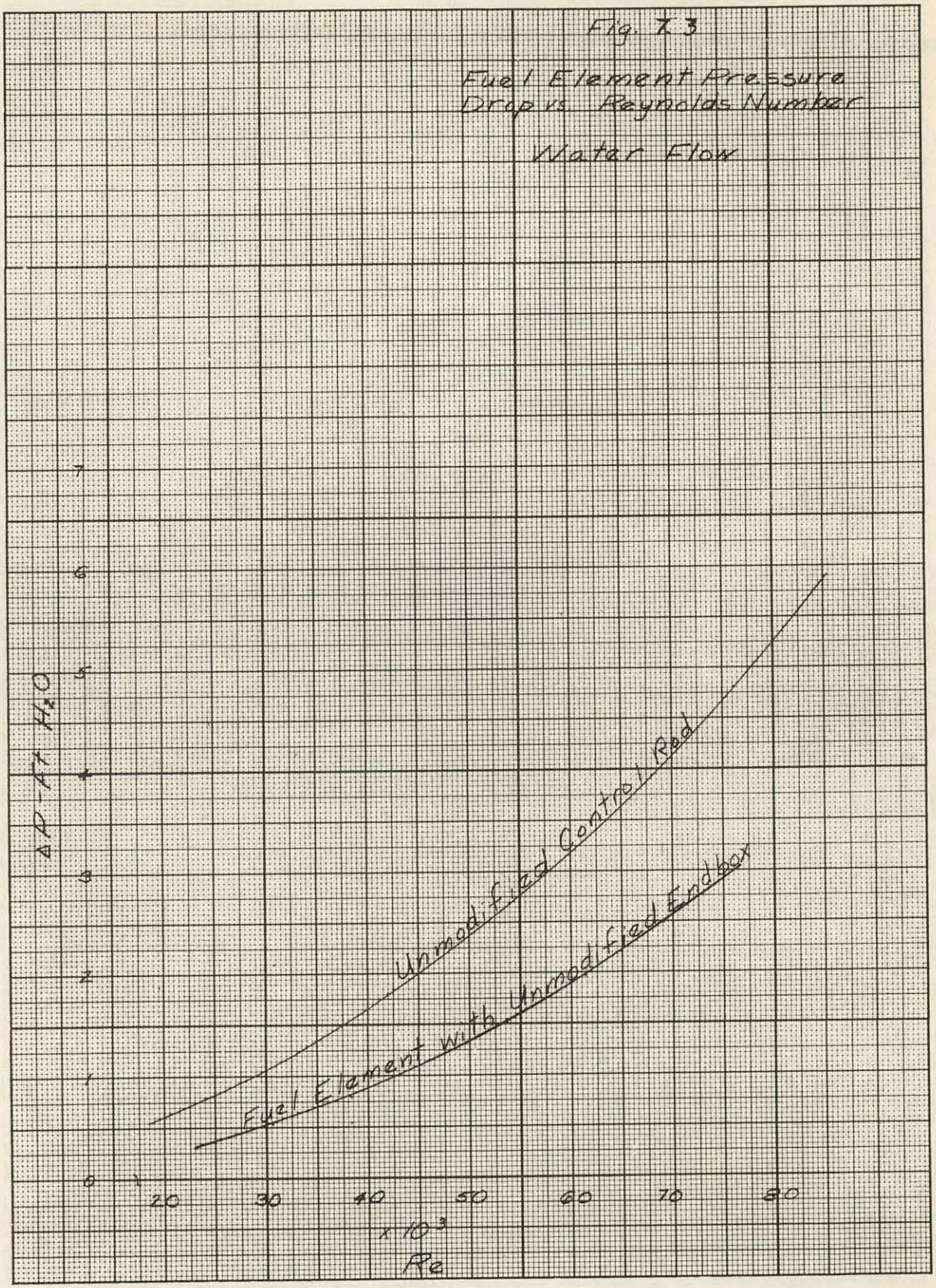

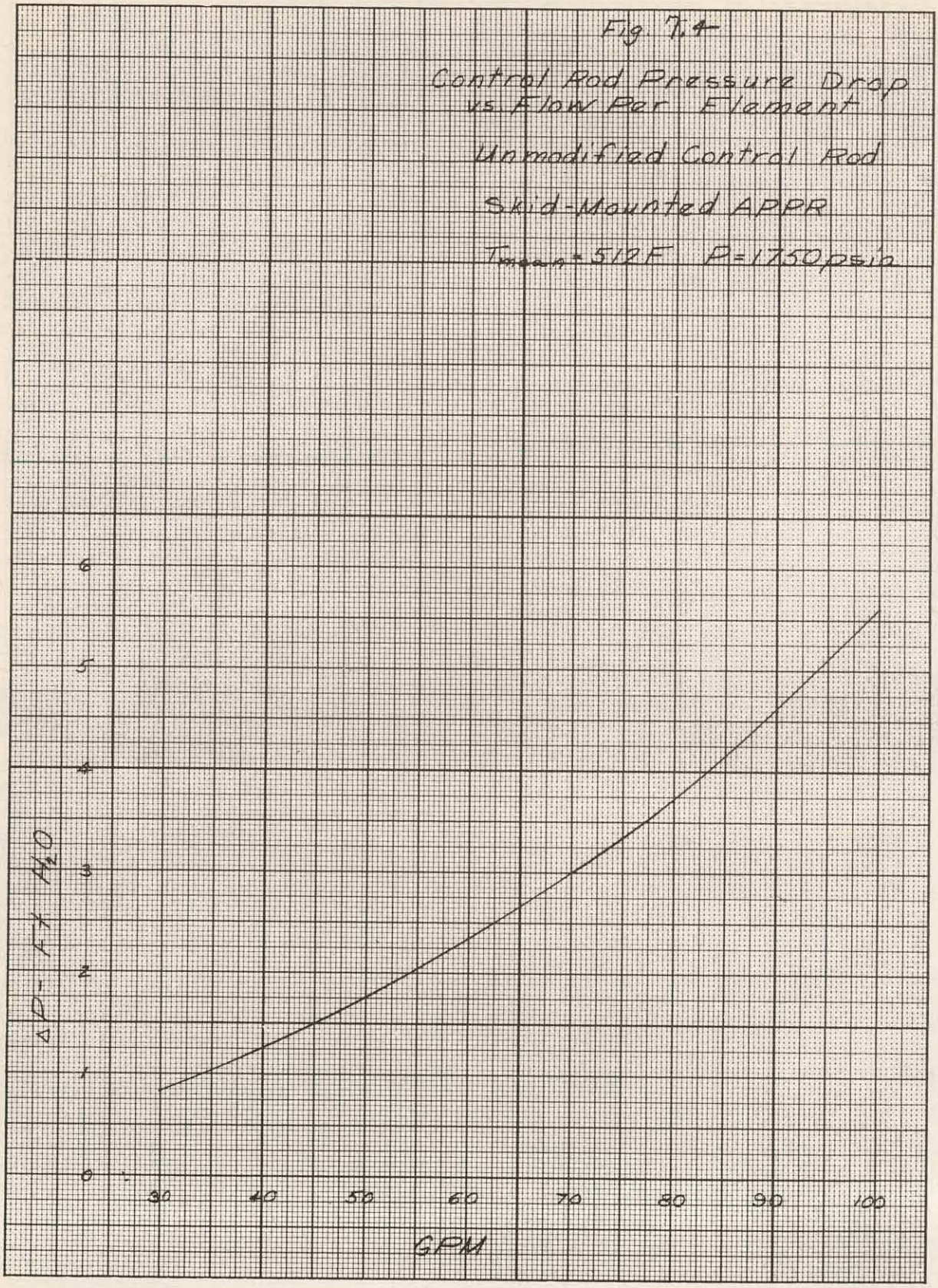
Fig. 7.4
Control Rod Pressure Drop vs. Flow Per Element
Unmodified Control Rod
Skid-Mounted APPR
T_{mean} = 512F P=1750psia
ΔP - Ft H2O
0
1
2
3
4
5
6
30
40
50
60
70
80
90
100
GPM

Fig. 7.5

Stationary Fuel Element Pressure Drop vs Flow Per Element

Skid-Mounted APPR

T_{mean} = 512F P = 1750 psia

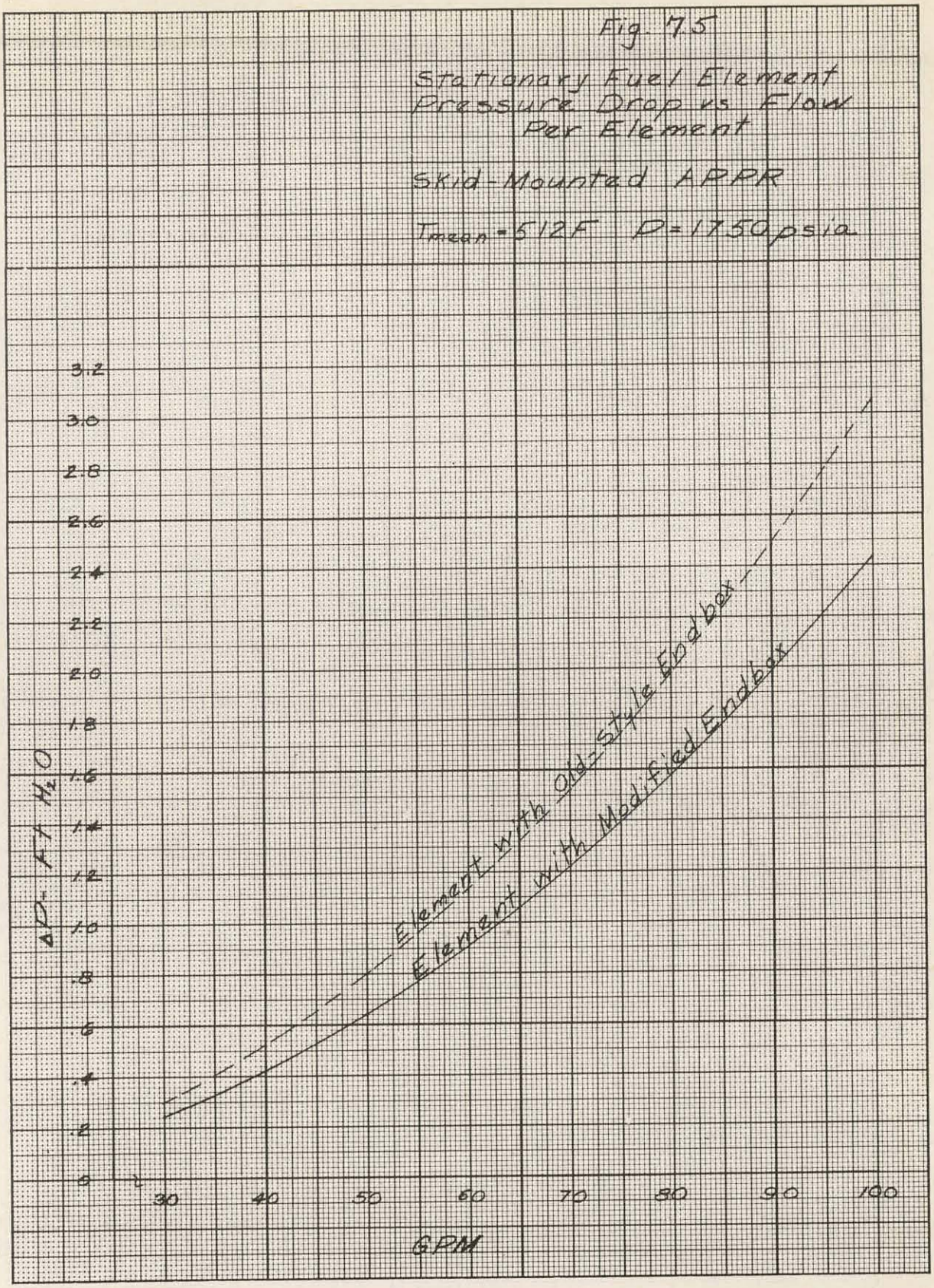

drops. Since the pressure drop through the fixed elements is 0.86 ft at the flow required for the Skid-Mounted core, the orificing required will be approximately 1.26 ft H_2O.

8.0 FUEL PLATE DEFLECTIONS

Since the internal core flow and the lattice flow through the core are in parallel, the overall pressure drop through each flow passage must be equal. However, since the geometry of the passages is not the same for both types of flow paths, and since the amount of orificing varies between flow paths, the breakdown of the overall pressure drop axially is not alike for all passages. This leads to pressure differentials across the outer fuel plates, causing deflection of the plates. If this deflection becomes greater than the allowable tolerance, burnout may result.

8.1 Calculation of pressure differential

It has been previously stated (Section 2.0) that the Skid-Mounted APPR will be a uniform flow core. However, as the worst possible conditions have been considered for both uniform and tailored flow, the results of both cases will be included.

The overall core pressure drop has been shown to be 2.12 ft H_2O. From Figure 7.5 it may be noticed that the pressure drop through a fixed element with a flow of 58.5 gpm is 0.86 ft H_2O, and that the corresponding value for a flow of 51.8 gpm (the minimum required element flow for a tailored core) is 0.694 ft H_2O. The corresponding required pressure drops across the orifice holes are 1.26 ft and 1.426 ft respectively.

The various losses through the elements, which make up the overall pressure drop across the core, are listed in Table 8.1. The notation refers to Figure 8.1.

Table 8.1

Head Loss Through Stationary Elements

Position	Type of Loss	Ft H_2O	
		51.8 gpm	58.5 gpm
h_1	sudden contraction	.0787	.0989
h_2	gradual enlargement	.0093	.0117
h_3	sudden contraction	.0139	.0175
h_4	friction loss	.3054	.3720
h_5	sudden enlargement	.0084	.0106
h_6	friction loss	.0039	.0048
h_7 *	sudden enlargement	—	—
h_8	orifice loss	1.7004	1.6045

The flow rate throughout the lattice passages is essentially equal. The breakdown of the pressure losses axially is illustrated in Table 8.2. The notation again refers to Figure 8.1.

* Since in the calculation of pressure drop across the elements, the model did not include an orifice plate, the calculations included a loss due to sudden enlargement at the outlet. For actual conditions this loss will be a part of the orifice pressure drop.

FIG. 8.1.

LOCATION OF HEAD LOSSES

THROUGH CORE

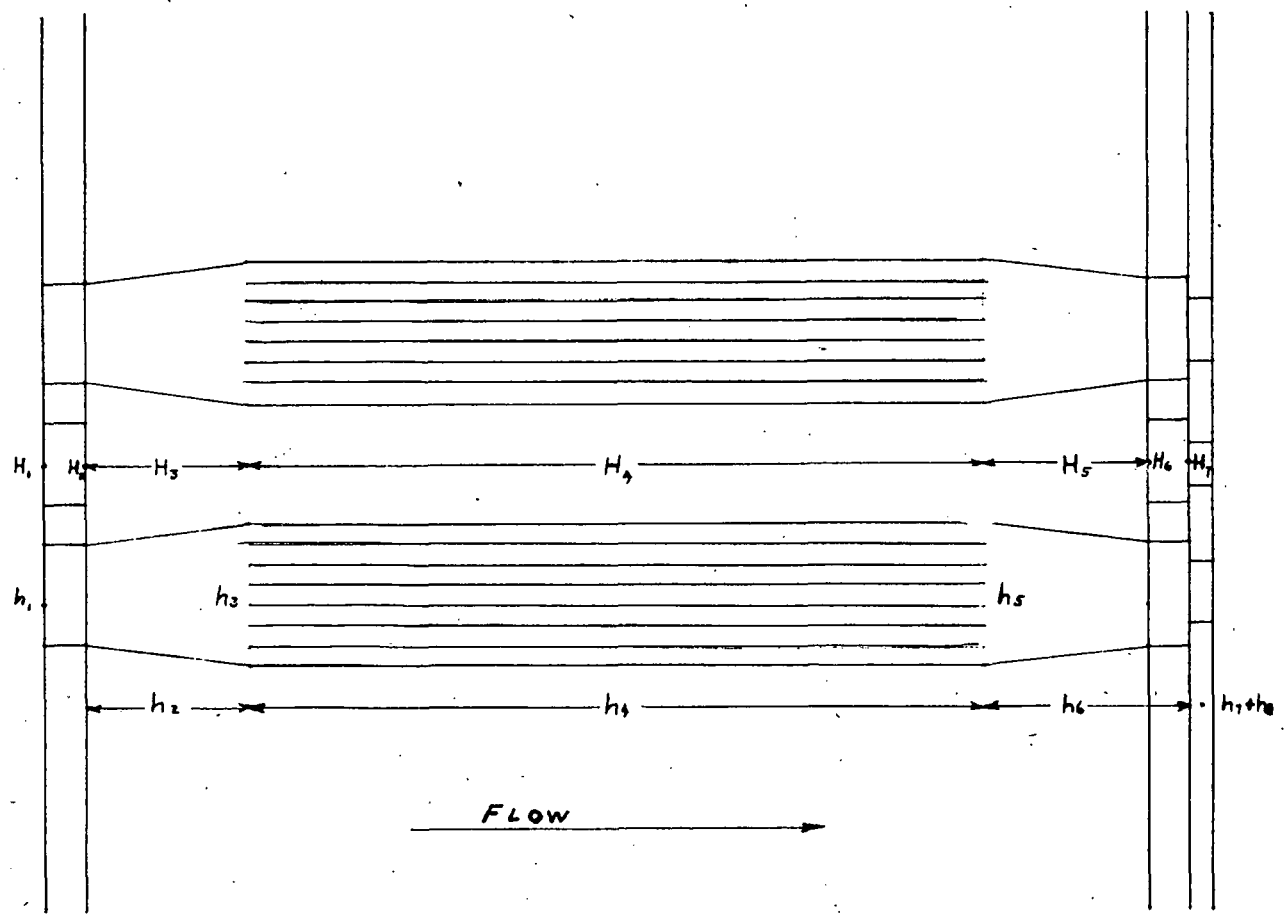

Table 8.2

Head Loss Through Lattice

Position	Type of Loss	Ft H_2O
H_1	sudden contraction	0.0467
H_2	abrupt change of shape	0.0173
H_3	gradual contraction	0.0159
H_4	friction loss	0.4750
H_5	gradual enlargement	(not needed)
H_6	abrupt contraction	"
H_7	orifice loss	"

The data in Table 8.1 and Table 8.2 is represented graphically in Figure 8.2. As may be noticed from the plot, the maximum pressure differential for a uniform flow core is 0.01 psi. The maximum differential for the core with tailored flow would have been 0.04 psi.

8.2 Experimental data

An investigation was conducted at ORNL to determine the effect of pressure differential on the outer plates of an APPR-type fuel element. The fuel elements were pressurized with air, and the deflection of the outer plates measured. (Ref. 20).

From the experimental data it becomes evident that a differential pressure exceeding 3 psi would result in a deflection of the plate which would cause the adjacent spacings between fuel elements to be beyond tolerance limits (see Ref. 20).

8.3 Conclusions

As was shown in Section 8.1, the maximum expected pressure differential across the outer fuel plates is 0.01 psi. Since the pressure differential required to deflect the plates beyond the allowable tolerance limit is 3 psi, it is apparent that further investigation of this problem is not necessary.

Figure 8.2

Head Loss Across Core

-Stationary Elements & Lattice

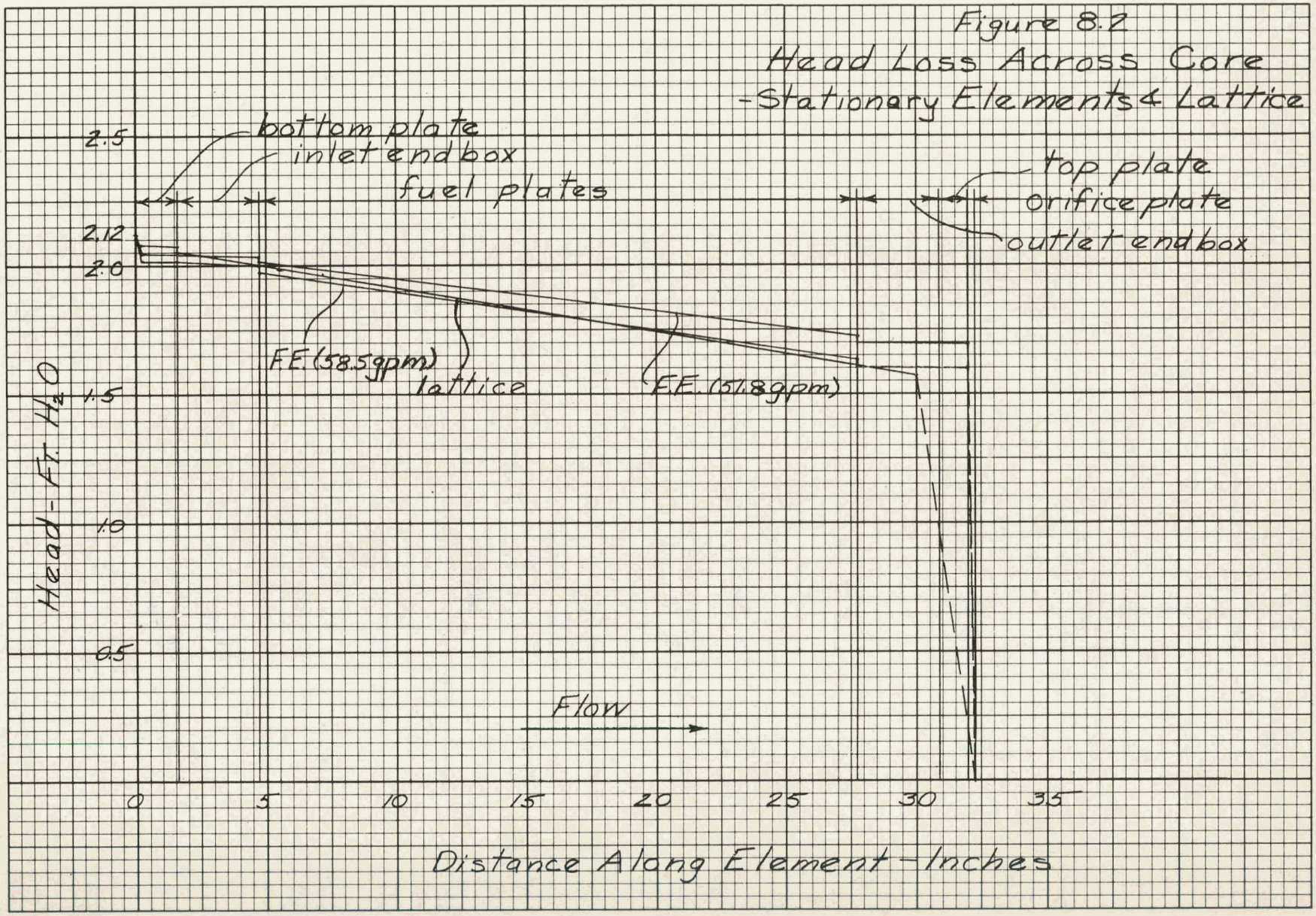

295-296

9.0 REFERENCES

1. Clark Rohsenow, "Heat Transfer and Pressure Drop Data for High Heat Flux Densities to Water at High Subcritical Pressures," Tech Rep #3, Proj. 6627, MIT

2. Epstein, Chastain, Fawcett, "Heat Transfer and Burnout to Water at High Subcritical Pressures," July 1956, BMI - 1116.

3. Jens, W.H., and Lottes, P.A., "Analysis of Heat Transfer, Burnout Pressure Drop and Density Data for High Pressure Water," May, 1951, ANL-4627.

4. Roarty, J. D.,"Application of Forced Convection Heat Transfer and Friction Correlations in Core Design," July 1954, WAPD-FE-96.

5. Roarty, Sher. "Preliminary Determination of Forced Convection Heat Transfer Coefficients for Rectangular Channels at 2000 psia, "1956, WAPD-TH-217.

6. Zerbe, Chr., "Review of Thermal Design Criteria for Pressurized Water Reactors at 2000 psia, "WAPD-SER-Ra-444.

7. APAE Memo #96, J. Brondel, May 6, 1957.

8. APAE 17 Vol. I, Thermal and Hydraulic Section.

9. AP Memo 43., Temperature Distribution and Thermal Stress in Reactor Core APPR-1.

10. Neill, F.H., and Smith, J.F. Jr., "Stainless Steel Fuel Element Test in STR," CF-54-11-13.

11. Gallagher, J. G., "Status of ORNL" - APPR Irradiation Program,"CF-55-6-124.

12. Beaver, R.J., "Present Status of Irradiation of APPR Fuel Elements," CF-55-6-167.

13. "Temperature Distribution and Thermal Stress in Reactor Core APPR-1" October 16, 1957, AP Memo 43.

14. Neill, F.H. "Irradiation of Stainless Steel Fuel Element Samples in MTR" CF55-4-153.

15. Beaver, R.J., Feldman, M.J., "MTR Test #3 of APPR Fuel Element" CF-55-4-163.

16. Beaver, R.J., "Post-Irradiation Macroscopic Examination of APPR Stainless Steel Plates removed from APPR Fuel Element Irradiated in the MTR" CF-56-1-116.

17. "Specifications for Stainless Steel MTR Irradiation Test Element" CF-55-6-31.

18. "Testing of APPR Type UO_2 Stainless Steel Element in the MTR" CF-55-6-47.

19. Bobe, Silks, Stueck, "Program No. 203, Head Loss Calculation on the IBM 650", June 10, 1958, AP Note 105.

20. Erwin, J. H., Beaver, R.J., "Effect of Pressure Differentials on Deflection of the Outer Fuel Plates of Brazed APPR Fuel Elements." February 7, 1957, CF-57-2-34.

21. Timoshenko, S., "Strength of Materials Part II Advanced Theory and Problems," D. Van Nostrand Co., Inc., March 1956.

22. Sonneman, George and Davis, Duane M. "Thermal Stresses in Reactor Vessels" WAPD-BT-1, May 1957.

23. Meem, J. L., "Initial Operation and Testing of the Army Package Power Reactor APPR-1," APAE-18, August 9, 1957.

24. Langer, B.F., "Design Basis for Reactor Vessels" WAPD-CE-43,1955.